UNCLASSIFIED

AD 273 988

Reproduced
by the

ARMED SERVICES TECHNICAL INFORMATION AGENCY
ARLINGTON HALL STATION
ARLINGTON 12, VIRGINIA

UNCLASSIFIED

CALIFORNIA INSTITUTE OF TECHNOLOGY

ANTENNA LABORATORY

Technical Report No. 27

ELECTROMAGNETIC SURFACE--WAVE PROPAGATION ALONG A DIELECTRIC CYLINDER OF ELLIPTICAL CROSS SECTION

by

Cavour W. H. Yeh

CALIFORNIA INSTITUTE OF TECHNOLOGY

Pasadena, California

Antenna Laboratory

Technical Report No. 27

ELECTROMAGNETIC SURFACE-WAVE PROPAGATION ALONG

A DIELECTRIC CYLINDER OF ELLIPTICAL CROSS SECTION

Cavour W. H. Yeh

January 1962

ACKNOWLEDGEMENTS

ABSTRACT

The problem of electromagnetic wave propagation along a dielectric rod of elliptical cross section is considered. The field components and the dispersion relations of the principal modes are obtained. The principal modes degenerate to the well known HE_{mn} modes of the circular dielectric rod as the eccentricity of the elliptical rod approaches zero. It is found that there are two non-degenerate principal modes which possess no cut off frequencies. They are called the dominant principal modes.

In contrast to the case of a circular dielectric rod, the boundary conditions for the elliptical rod cannot be satisfied by using a single product term consisting of a radial and a periodic Mathieu function of a specific order to describe the field components in both regions (the region inside the rod and the region outside the rod). It is generally believed that an infinite series of such product terms must be used to describe the field components in both regions. In the present investigation, it is shown that the boundary conditions may be fulfilled if the field components in one of the two regions are represented by a single product term consisting of a radial and a periodic Mathieu function of a specific order. The field components in the other region are then represented by an infinite series of such product terms. The problem is therefore sufficiently simplified to permit analysis.

The propagation characteristics (the propagation constant, the field distribution and the attenuation constant) of the dominant principal modes are given theoretically and experimentally. It is found that the analytic and experimental results are in very good agreement. The Q's of a dielectric rod cavity resonator supporting the dominant principal modes are also given.

TABLE OF CONTENTS

CHAPTER I - INTRODUCTION

The concept of guiding electromagnetic waves either along a single conducting wire with finite surface impedance or along a dielectric rod is not new. As early as 1899, Sommerfeld (1) conceived the idea of guiding a circularly symmetric TM wave along a conducting wire with small surface resistivity. In 1910, Hondros and Debye (2) demonstrated theoretically that it is possible to propagate a TM wave along a lossless dielectric cylinder. However, due to the large field extent outside the wire and the relatively high attenuation of this surface wave, the "open-wire" line remained a novelty for almost half a century. Recent developments in the generation and application of millimeter and sub-millimeter electromagnetic waves, the availability of very low loss dielectrics, and the development of fiber optics, have renewed interest in the surface waveguides. There have appeared numerous papers and reports concerning various forms of surface waveguides and the feasibility of these guides as practical transmission lines.

Before discussing the purpose and the scope of the present investigations, a survey of previous work on surface waveguides is in order.

1.1 Survey of the Literature

The surface wave guiding structures are capable of supporting waves intimately bounded to the surface of the structure. These waves have exponential decay characteristics in regions away from the surface and are governed by the usual propagation function $e^{i\beta z}$ along the axis of the structure, where z is the axial coordinate and β is the propagation constant. For real values of β such waves persist at arbitrarily

large distances from the source. The steady state solutions with harmonic time dependence $e^{-i\omega t}$ are the only ones considered here. Of primary interest are the values of β as a function of the frequency and of the properties of the guiding system.

The surface wave guiding system can take many forms. The one intensively studied in the past was a surface wave structure of infinite extent imbedded in an infinite uniform medium. The problem then consisted of finding the solution that satisfied the homogeneous field equations and the boundary conditions with the source at infinity.

Typical surface wave structures may be classified into three types. The first type is the dielectric coated conductor, such as dielectric coated conducting plane and wire. The second type is the interface of two dielectric media, such as dielectric rods, dielectric tubes, or dielectric strips. The third type consists of various open periodic structures, such as unbounded helix, corrugated plane or cylinder. Sketches of these three types of surface wave structures are shown in Figure I-1.

Among the various structures mentioned above, only those intimately related to the propagation of surface waves along an elliptical dielectric cylinder will be discussed further, namely, the Sommerfeld-Goubau wire, the circular dielectric rod, the dielectric tube, and the elliptical dielectric rod. Related topics such as the interaction of two surface waveguides and the problem of excitation of surface waves will also be mentioned briefly.

(a) The Sommerfeld-Goubau Wire.

The possibility of propagating a surface electromagnetic wave along a circular conducting wire was first demonstrated theoretically by
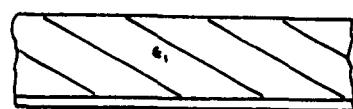
(a) dielectric coated
conducting plane
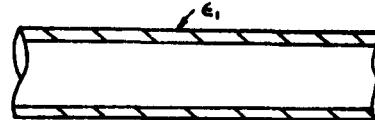
(b) dielectric coated
conducting wire
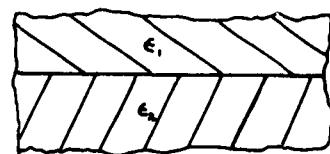
(c) dielectric slabs
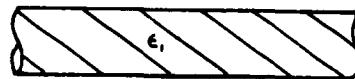
(d) dielectric rod

(e) corrugated
plane
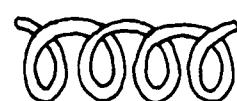
(f) unbounded helix

Fig. I-1. Typical surface wave guiding structures.
Type 1, the dielectric coated conductor, (a),(b);
Type 2, the interface of two dielectric media, (c),(d);
Type 3, the open periodic structure, (e),(f).

Sommerfeld (1) in 1899. The wave was a circularly symmetric TM mode with components H_θ, E_r, E_z and was loosely bound to the surface of the wire. In a numerical example he showed that the damping at high frequency for this type of wave was too pronounced to use as a communication wave. Consequently the practical uses of this type of transmission line were very limited. In 1909 Hondros (3), a student of Sommerfeld, showed that an asymmetric field distribution was also possible. But the wave was so strongly attenuated that it could not be observed experimentally.

Recently in 1950 Goubau (4) reinvestigated the properties of the Sommerfeld line and studied its suitability as a practical communication line. His investigation showed that a circularly symmetric surface wave might be guided by a conducting wire of small diameter with the same low attenuation as that of the conventional coaxial conductor guide. However, the field extended radially to a considerable distance outside the wire before its strength decayed to a negligible value; so that any small imperfection of the surface or any small curvature along the wire would cause radiation loss. The practical use of this surface waveguide was therefore limited. In an effort to reduce the radial extension of the field, Goubau (5) proposed the coating of the conductor with a thin sheath of dielectric, or corrugating the wire. This reduction of radial field extent was achieved with the penalty of higher attenuation due to dielectric loss or corrugation. This increased attenuation due to dielectric loss together with the original attenuation due to loss in the conductor has been calculated by Goubau (5). It should be noted, however, that the first theoretical

analysis of electromagnetic wave propagation along a conducting wire with a cylindrical insulating sheath was given by Harms (5) in 1907.

Since Goubau's report, numerous papers concerning this type of single wire line have been published. Among these are the papers by Barlow and Karbowiak (6) in 1953 on the measurement of radial field distribution; Sheibe, King and Van Zieland (7) in 1954 on the measured losses of the "Goubau Line"; and Roberts (8) on the excitation of the single wire line. Kiely (9) also reported on the effect of fog and rain drops on the attenuation characteristics of the wave propagating along a long single wire line.

(b) Circular Dielectric Rod

Hondros and Debye (2) in 1910 analyzed theoretically the guiding of a circularly symmetric TM wave along a solid lossless dielectric cylinder and thereby removed the cause of the strong attenuation due to the conductor (1). In 1915 Zahn (10) and his two students, Rüter and Schriever (11,12), confirmed the existence of such a TM wave experimentally. Carson, Mead and Schelkunoff (13) noted in their paper that Southworth in 1920 also accidentally observed such a wave in a trough of water. When the generation of high frequency electromagnetic waves (about 10 cm) became feasible, Southworth (14) described some experimental work dealing with phase velocity and attenuation of the circularly symmetric TM wave on the circular dielectric guide.

Not until 1936 were the propagation properties of asymmetric waves on a round dielectric rod considered. A rather complete mathematical analysis of this problem was given by Carson, Mead and Schelkunoff (13). It was noted in their paper that in order to satisfy the

boundary conditions, a hybrid wave (i.e., the coexistence of longitudinal electric and magnetic fields) must be assumed. In other words, asymmetric TE and TM modes were inextricably coupled to each other along a circular dielectric rod. They also showed that, 1) pure TE and TM waves could only exist in the circularly symmetric case, and 2) there existed one and only one mode, namely the lowest order hybrid wave called the HE_{11} mode, which possessed no cutoff frequency* and could propagate at all frequencies. All other circularly symmetric or non-symmetric modes had cutoff frequencies. The dispersion relations of these modes were also obtained in their paper, but no numerical results were given.

Since then the development of metal tube waveguides as transmission systems completely over-shadowed the development of dielectric waveguides. This is largely due to the fact that the field is contained entirely within the metal tube guide. For the dielectric guide, however, the field is not entirely contained which leads to greater transmission loss due to radiation when bends and discontinuities are present. A large number of papers have been published on the subject of propagation of electromagnetic waves in a hollow metal tube. Borgnis and Papas (15) gave a very comprehensive treatment on this subject.

In 1945 Mallach (16) published his results on the use of the dielectric rod as a directive radiator. He showed experimentally that the radiation pattern obtained by the use of the asymmetric HE_{11} mode produced only one lobe in the principal direction of radiation.

---

*This cutoff frequency does not have the conventional definition as that for the metal waveguide modes (see p.295 of reference 15). It is here defined that the cutoff frequency for the surface waveguide mode is the frequency below which the dielectric rod ceases to act as a binding medium and the wave is no longer guided by this surface wave structure.

Immediately after Mallach's paper, Wegener (17) presented a dissertation in which the asymmetric HE_{11} mode, together with the lowest order circularly symmetric TE and TM modes were analyzed in detail. Not only were the numerical results of the propagation constants for these waves obtained, but also their attenuation characteristics. Apparently he was not aware of Carson, Mead and Schelkunoff's work. A few experimental points were also included in his work to substantiate his theoretical results. Elsasser (18) in 1949, independent of Wegener's work, published his computation on the attenuation properties of these three lowest order waves by the perturbation method (15). In a companion paper, Chandler (19) verified experimentally Elsasser's results considering the dominant HE_{11} mode. He found that the guiding effect was retained even when the rod was only a fraction of a wavelength in diameter. Since the greater part of the guided energy was outside the dielectric, very little loss was observed. For the first time the cavity resonator technique was introduced to measure the attenuation constant of the HE_{11} mode. The resonator technique was very suitable for investigating very low loss uniform waveguides. It should be noted, however, that the formula relating the Q of the resonator and the attenuation constant α in Chandler's paper is only applicable for very small $2a/\lambda_o$, where a is the radius of the rod and λ_o is the free space wavelength (see Chapter V).

King (20) in 1952 proposed the so-called "dielectric image line" as a practical surface wave guiding device. The "dielectric image line" was made up of a semicircular dielectric rod mounted on a conducting sheet and was designed specifically for the dominant HE_{11} mode. He indicated that the conducting sheet not only could act as a supporting

device, but also as a polarization anchor for this dominant mode. A detailed study on the attenuation and the radial field decay characteristics of the HE_{11} mode guided by this image line was reported by Schlesinger and King (21) in 1953. Again the cavity resonator method, used by Chandler, was used for the attenuation constant measurement. As of now the "dielectric image line" is still the best and the most practical device for supporting the dominant dielectric mode.

(c) Circular Dielectric Tube

A natural generalization of the analysis of the propagation of electromagnetic waves on a dielectric rod would be that for the circular dielectric tube. The earliest theoretical analysis was carried out by Zachoval (22) in 1932. He considered the propagation of a circularly symmetric TM wave along a lossless circular dielectric tube. Two years later Liska (23) verified Zachoval's work experimentally. A more complete treatment on the theory of dielectric tube waveguides was given by Astraham (24) in 1949, in which both symmetric and asymmetric propagating waves were considered. He also substantiated his theoretical results by experimental data. Independently, Unger (25) in 1959 reported his investigation on the same subject and showed that a dielectric tube with a thin wall could support the dominant mode with very little loss. But the radial field extent was rather large. One of the most promising applications of dielectric tube waveguides may be found in the field of millimeter wave cavity resonator and beam coupling structure (26).

(d) Elliptical Dielectric Cylinder

The first attempt to find the dispersion relation of an electro-
magnetic wave guided by an elliptical cylinder structure was made by
Karbowiak (27) in 1954. He considered the elliptical cross-section
Sommerfeld line and the elliptical cross-section Goubau line. The wave
equation was formulated in elliptical coordinates and solutions were
obtained. However, he matched the boundary conditions only at one
point on the boundary surface; therefore his results can, at best, be
considered an approximation for very small eccentricity. Another
attempt to solve the problem of surface wave propagation along an ellip-
tical dielectric rod was made by King and Wiltse (28). Again they for-
mulated the problem in elliptical coordinates and obtained solutions of
Maxwell's equations in this coordinate system. But in matching the
fields on the boundary, similar over-simplifications of the boundary
conditions were made. The "approximation" of these two approaches can
be best illustrated by the following example. For the sake of clarity,
only the matching of the axial electric field on the boundary will be
considered.

Karbowiak's method. The expression for the axial electric field
in region 1 which is the region inside the dielectric rod is

$$E_{z_1} = A_n \, Ce_n(\xi, \gamma_1^2) \, ce_n(\eta, \gamma_1^2).^* \tag{1}$$

where A_n is an arbitrary constant. The expression for the axial elec-
tric field in the surrounding medium is

$$E_{z_0} = L_n \, Fek_n(\xi, \gamma_2^2) \, ce_n^*(\eta, \gamma_2^2) \tag{2}$$

where L_n is an arbitrary constant. It should be noted that all these

---

*The notations of the Mathieu or the modified Mathieau functions are
defined in Chapter II.

Mathieu functions and modified Mathieu functions are functions of the characteristics of the medium. The boundary condition dictates the continuity of the axial electric field, i.e., at $\xi = \xi_o$, $E_{z_1} = E_{z_o}$ we have

$$A_n Ce_n(\xi_o, \gamma_1^2) \, ce_n(\eta, \gamma_1^2) = L_n Fek_n(\xi_o, \gamma_2^2) ce_n^*(\eta, \gamma_2^2) \ . \qquad (3)$$

It should be noted that $ce_n(\eta, \gamma_1^2)$ and $ce_n^*(\eta, \gamma_2^2)$ are functions of η . The only way that equation 3 can be satisfied is by assuming $ce_n(\eta, \gamma_1^2) = ce_n^*(\eta, \gamma_2^2)$, which is not true except when the eccentricity is zero. This was the assumption made by Karbowiak.

King and Wiltse's method. King and Wiltse realized the invalidity of Karbowiak's assumption and proposed to attack the problem in a slightly different way. They assumed that the expression for the axial electric field in the dielectric rod is

$$E_{z_1} = \sum_{n=0}^{\infty} A_n Ce_n(\xi, \gamma_1^2) \, ce_n(\eta, \gamma_2^2) \qquad (4)$$

where the A_n are the arbitrary constants; and the expression for the axial electric field in the surrounding medium is

$$E_{z_o} = L_n \, Fek_n(\xi, \gamma_2^2) \, ce_n^*(\eta, \gamma_2^2) \qquad (5)$$

where L_n is an arbitrary constant. Satisfying the boundary condition at $\xi = \xi_o$, we have

$$\sum_{n=0}^{\infty} A_n Ce_n(\xi_o, \gamma_1^2) \, ce_n(\eta, \gamma_1^2) = L_n \, Fek_n(\xi_o, \gamma_2^2) \, ce_n^*(\eta, \gamma_2^2) \ . \qquad (6)$$

They then multiply both sides of the equation by $ce_\ell(\eta, \gamma_1^2)$ and

integrate with respect to η from 0 to 2π, obtaining

$$A_n Ce_n(\xi_o, r_1^2)N_n = L_n Fek_n(\xi, r_2^2)M_n , \tag{7}$$

where $N_n = \displaystyle\int_0^{2\pi} ce_n^2(\eta, r_1^2)d\eta$ and $M_n = \displaystyle\int_0^{2\pi} ce_n(\eta, r_1^2) \, ce_n^*(\eta, r_2^2)d\eta$.

This was how they eliminated the summation sign. It can be seen that an identical result, i.e., equation 7, can be obtained by the use of equations 1 and 2 . Multiplying both sides of equation 3 by $ce_n(\eta, r_1^2)$ and integrating from 0 to 2π , one obtains equation 7.

Therefore the validity of King and Wiltse's solution is also questionable.

(e) Related Topics

Unlike the waves in the metal tube waveguides, there are no evanescent modes on an open surface waveguide. It is not possible to express any arbitrary field distribution in terms of the propagating modes alone. Hence, there must exist a different type of wave, namely the radiated wave (29) if any source is present in a finite region.

As a matter of fact, it should be noted here that the presence of the surface wave was actually first postulated by Sommerfeld (30) in 1909 when he was considering the now classical problem* which bears his name. He found theoretically that there existed not only a radiated wave due to the oscillating dipole, but also a surface wave which traveled along the interface of the two dielectrics. Since then, a great number of papers and reports have been published concerning variations of this problem. The most recent investigations have been reported

---

*The Sommerfeld problem is discussed very clearly and thoroughly in Stratton (31).

by Roe (29), Whitmer (32), Tai (33), Brick (34), Wait (35), Cullen (36), and Brown (37), to mention only a few.

The problem of interaction between two parallel uniform surface waveguides is also an interesting one. Since the wave equation is not separable in the bipolar coordinates, approximate methods must be employed. Quite a few authors used the electrostatic approximation* in the earlier years. However this approximation was not satisfactory at very high frequencies. Most recently Armand (38) and Marcuse (39) treated the problem of interaction between two parallel Goubau wires without resorting to the electrostatic approximation. They formulated the problem by assuming the interaction of only one single mode on each wire, namely the circularly symmetric TM mode. They indicated the presence of space beats and the energy exchange phenomenon. Numerical examples were also given.

1.2 Purpose and Scope of the Present Investigation

In order that the dielectric rod may be a low loss surface wave device, one must choose a small value of ka where k is the free space wave number and a is the radius of the dielectric cylinder. In the millimeter wavelength range, the radius of the dielectric cylinder becomes inconveniently small. Fortunately it has been found experimentally (41) that if the circular rod is flattened, (i.e., if the circular rod is rendered to an elliptical rod of the same area), the attenuation of the dominant mode may be reduced considerably, provided that the

---

*The electrostatic approximation is as follows: In calculating the structure of the field one would neglect quantities of the order of $O(d \sqrt{k_0^2-k^2})$, where d is the distance between the wires, k_0 is the wave number for free space, and k is the propagation constant of the wave.

electric field of the dominant mode is parallel at the center of the rod to the minor axis of the elliptical rod. The use of very thin fibers of various cross-section as optical waveguides or as mode selectors in optical masers has also received considerable attention. [For example, see reference (40)]. Furthermore, it is noted that so far there exists no satisfactory way of analyzing the problem of surface wave propagation along a dielectric rod of elliptical cross-section. It is therefore the purpose of the present investigation to develop a method to analyze this problem theoretically, to examine in particular the propagation characteristics of the dominant modes, and to perform experiments to verify the analytic results.

The investigation is divided into six parts, and the results are correspondingly presented in Chapters II, III, IV, V, VI and VII. In Chapter II the fundamental theory of wave propagation along an elliptical dielectric rod is given. A method is developed to assure that the solutions of the wave equation satisfy all the boundary conditions on the surface of the dielectric rod. The characteristic equations for the principal modes are given so that the variation of guide wavelength with frequency, the dielectric constant, and the physical dimensions of the guide may be obtained. It is shown analytically that there exist two non-degenerate modes which possess no cutoff frequency. They are called the dominant modes, and it is the propagation characteristics of these that will be considered in detail in the subsequent chapters. It is also shown that all the principal modes on an elliptical dielectric rod degenerate smoothly to the well known modes on the circular dielectric guide, as the eccentricity of the elliptical rod approaches zero.

Numerical results of the characteristic equations for the dominant modes are obtained and discussed in Chapter III. Sketches of the field configurations are also given. The decay characteristic of the axial electric field is computed.

In Chapter IV the attenuation properties and the power distribution characteristics of the dominant modes are analyzed theoretically with the assumption that the dielectric loss is small. Numerical results are computed. It is found that the attenuation constant of the dominant $_e\text{HE}_{11}^{(1)}$ mode* propagating along an elliptical dielectric rod is much less than that of the dominant HE_{11} mode along a circular dielectric rod having the same cross-sectional area. Physical interpretation of these results is also presented.

The Q's of an elliptical dielectric rod cavity supporting the dominant modes are given in Chapter V. It is shown that very high Q cavity may be constructed using thin elliptical dielectric rod. Also derived is a formula relating the Q of a cavity and the attenuation constant of a transmission line supporting the same mode. This formula is more general than the one given by Davidson and Simmonds (41) in that it is also valid for the hybrid modes. This relation is very important whenever the cavity resonator method (19) is used to measure the attenuation constant.

To verify the theoretical results a systematic experimental investigation on the propagation characteristics of the two dominant modes was performed. A detailed description of the measuring apparatus and technique is presented in Chapter VI. Experimental data are then

---

*The meaning of this symbol is given in Chapter II.

compared with theoretical results, and they are in very good agreement.

Summary and conclusions are given in Chapter VII. The advantages of using a flat elliptical dielectric rod instead of a circular dielectric rod as a microwave guide are pointed out. It is also indicated that the analytic method used here may be applied to other similar problems. The problem with source present is also discussed briefly.

CHAPTER II - THEORY OF ELLIPTICAL DIELECTRIC WAVEGUIDES

The problem is formulated in terms of the elliptical cylinder
coordinates; the appropriate solutions of the wave equation in this
coordinate system are then obtained. The difficulties of satisfying
the boundary conditions on the elliptical surface are pointed out. A
method to overcome such difficulties is introduced. Various notations
and classifications of the principal propagating modes are defined.
Upon matching the boundary conditions by the indicated method, a set of
characteristic equations and explicit forms for all field components
corresponding to various modes are obtained. The existence of the
dominant modes having no cutoff frequency is demonstrated. Finally, it
will be shown that as the eccentricity approaches zero, all principal
propagating modes degenerate to the well known circular modes.

2.1 Formulation of the Problem

The surface wave propagation along an infinitely long, straight,
isotropic, and homogeneous dielectric cylinder of elliptical cross sec-
tion imbedded in an infinite dielectric medium of dielectric constant
ϵ_o and magnetic permeability μ_o , is considered. The dielectric
cylinder has a dielectric constant ϵ_1 and a magnetic permeability
μ_1 . We assume that $\mu_1 = \mu_o$, the free space magnetic permeability;
$\epsilon_1 > \epsilon_o$, and that the conductivity in both media is zero. We further
assume that the exciting source is so far away that, in the region of
interest, the surface waves dominate the radiated waves from the source.

To analyze the source-free dielectric surface waveguide of ellip-
tical cross section, the elliptical cylinder coordinates (ξ,η,z), as
shown in Figure II-1, are introduced. The elliptical cylinder coordinates

(a)

η = constant

ξ = constant = ξ_o

Semi-major axis = $q \cosh \xi_o$
Semi-minor axis = $q \sinh \xi_o$
Eccentricity, $e = 1/\cosh \xi_o$

(b)

(c)
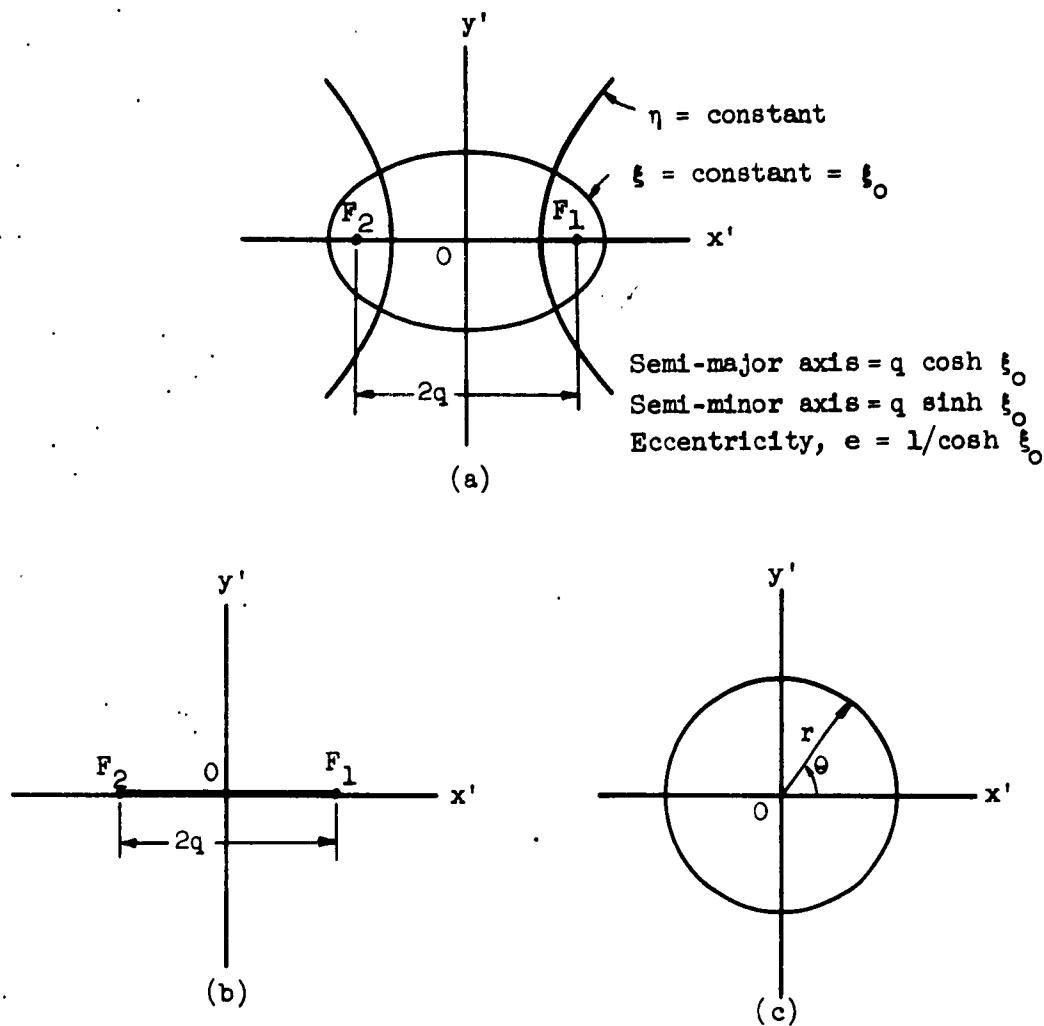
Fig.II-1 (a) Cross-section of elliptical surface waveguide.
F_1 and F_2 are the foci of the ellipse. The distance
between foci is the focal distance, $2q$.

(b) Degenerate form of ellipse when $e = 1$. As $e \to 1$
semi-minor axis $\to Q$, and semi-major axis $\to q$.

(c) Degenerate form of ellipse when $e = 0$. As $e \to 0$
$q \to 0$, $\xi_o \to \infty$, semi-major axis $\to$ semi-minor axis $\to r$.

are related to the rectangular coordinates (x',y',z') through the following,

$$x' = q \cosh \xi \cos \eta$$

$$y' = q \sinh \xi \sin \eta$$

$$z' = z$$

$$(0 \le \xi < \infty, \quad 0 \le \eta \le 2\pi)$$

where q is the semifocal length of the ellipse. The contour surfaces of constant ξ are confocal elliptic cylinders, and those of constant η are confocal hyperbolic cylinders. The elliptic cylinders and hyperbolic cylinders have foci at $x'= q$, $y'= 0$ and $x'= -q$, $y'= 0$. The semi-minor axis is equal to $q \sinh \xi_o$. The eccentricity e, defined as the ratio of the semifocal distance to the semi-major axis, is given by $e = 1/\cosh \xi_o$.

One of the confocal elliptic cylinders with $\xi = \xi_o$ is assumed to coincide with the boundary of the solid dielectric cylinder, and the z-axis coincides with its longitudinal axis.

2.2 Maxwell's Equations and Their Solutions in Elliptical Cylindrical Coordinates

It is well known that the harmonic form of Maxwell's equations in a source-free medium characterized by ϵ and μ are given by

$$\nabla \times \underline{E} = i\omega\mu \underline{H} \tag{1a}$$

$$\nabla \times \underline{H} = - i\omega\epsilon \underline{E} \tag{1b}$$

$$\nabla \cdot \underline{H} = 0 \tag{1c}$$

$$\nabla \cdot \underline{E} = 0 \tag{1d}$$

where $\underline{E}$ and $\underline{H}$ are the electric field vector and the magnetic field vector respectively. The harmonic time dependence of $e^{-i\omega t}$ for all

field quantities is assumed. The rationalized MKS system is used throughout this work. We shall now confine our treatment to waves propagating along the positive z-axis. In complex representation these assumptions result in a multiplication of all wave functions by $e^{-i\omega t} e^{i\beta z}$, i.e.,

$$\underline{E}(\xi,\eta,z,t) = \left[\underline{e}_\xi \, E_\xi(\xi,\eta) + \underline{e}_\eta \, E_\eta(\xi,\eta) + \underline{e}_z \, E_z(\xi,\eta)\right] e^{-i\omega t} e^{i\beta z} \quad (2)$$

$$\underline{H}(\xi,\eta,z,t) = \left[\underline{e}_\xi \, H_\xi(\xi,\eta) + \underline{e}_\eta \, H_\eta(\xi,\eta) + \underline{e}_z \, H_z(\xi,\eta)\right] e^{-i\omega t} e^{i\beta z} \quad (3)$$

where $\underline{e}_\xi$, $\underline{e}_\eta$ and $\underline{e}_z$ are unit vectors in the ξ,η,z directions respectively, and β, the propagation constant of the wave in the z direction, is to be determined from the boundary conditions.

In elliptical cylinder coordinates, equations 1a and 1b become

$$- i\omega\epsilon \, p^2 E_z = \frac{\partial}{\partial\xi} (p \, H_\eta) - \frac{\partial}{\partial\eta} (p \, H_\xi) \quad (4)$$

$$- i\omega\epsilon \, p \, E_\xi = \frac{\partial}{\partial\eta} (H_z) - i\beta p \, H_\eta \quad (5)$$

$$- i\omega\epsilon \, p \, E_\eta = i\beta p \, H_\xi - \frac{\partial}{\partial\xi} (H_z) \quad (6)$$

$$i\omega\mu \, p^2 H_z = \frac{\partial}{\partial\xi} (p \, E_\eta) - \frac{\partial}{\partial\eta} (p \, E_\xi) \quad (7)$$

$$i\omega\mu \, p \, H_\xi = \frac{\partial}{\partial\eta} (E_z) - i\beta \, p \, E_\eta \quad (8)$$

$$i\omega\mu \, p \, H_\eta = i\beta p \, E_\xi - \frac{\partial}{\partial\xi} (E_z) \quad (9)$$

where $p = q(\sinh^2\xi + \sin^2\eta)^{1/2}$, $k^2 = \omega^2\mu\epsilon = (\frac{2\pi}{\lambda})^2$ and λ is the wavelength of a uniform plane wave in the medium. The above equations 4 through 9 can be combined to give the field components E_ξ, E_η, H_ξ, H_η in terms of E_z and H_z only; we have,

$$E_{\xi} = \frac{1}{(k^2 - \beta^2)p} \left\{ i\beta \frac{\partial E_z}{\partial \xi} + i\omega\mu \frac{\partial H_z}{\partial \eta} \right\} \qquad (10)$$

$$E_{\eta} = \frac{1}{(k^2 - \beta^2)p} \left\{ i\beta \frac{\partial E_z}{\partial \eta} - i\omega\mu \frac{\partial H_z}{\partial \xi} \right\} \qquad (11)$$

$$H_{\xi} = \frac{1}{(k^2 - \beta^2)p} \left\{ -i\omega\epsilon \frac{\partial E_z}{\partial \eta} + i\beta \frac{\partial H_z}{\partial \xi} \right\} \qquad (12)$$

$$H_{\eta} = \frac{1}{(k^2 - \beta^2)p} \left\{ -i\omega\epsilon \frac{\partial E_z}{\partial \xi} - i\beta \frac{\partial H_z}{\partial \eta} \right\} . \qquad (13)$$

Taking the derivative of equation 12 with respect to η and the derivative of equation 13 with respect to ξ and substituting these expressions into equation 4, one obtains the equation

$$\frac{\partial^2 E_z}{\partial \xi^2} + \frac{\partial^2 E_z}{\partial \eta^2} + \left[q^2(k^2 - \beta^2)(\sinh^2\xi + \sin^2\eta) \right] E_z = 0 . \qquad (14)$$

Similarly, taking the derivative of equation 10 with respect to η and the derivative of equation 11 with respect to ξ and substituting these expressions into equation 7, one gets

$$\frac{\partial^2 H_z}{\partial \xi^2} + \frac{\partial^2 H_z}{\partial \eta^2} + \left[q^2(k^2 - \beta^2)(\sinh^2\xi + \sin^2\eta) \right] H_z = 0 . \qquad (15)$$

Equations 14 and 15 are the wave equations. It should be noted that these two wave equations are of the same form, therefore it is only necessary to solve one of them. If $H_z = 0$ a TM wave results; if $E_z = 0$ a TE wave results. The most general expressions for the electromagnetic fields consist of a linear combination of the solutions of TE and TM waves.

Consider the following partial differential equation

$$\frac{\partial^2 \Lambda}{\partial \xi^2} + \frac{\partial^2 \Lambda}{\partial \eta^2} + \left[q^2(k^2 - \beta^2)(\sinh^2\xi + \sin^2\eta) \right]\Lambda = 0 \qquad (16)$$

in which Λ may be H_z or E_z. In order to obtain the solutions of equation 16 one sets

$$\Lambda(\xi,\eta) = R(\xi)\,\Theta(\eta) \qquad (17)$$

and substitutes equation 17 into equation 16. Applying the usual separation of variables procedure, one may separate equation 16 into the following two ordinary differential equations

$$\frac{d^2\Theta(\eta)}{\partial\eta^2} + (c - 2\gamma^2\cos 2\eta)\,\Theta(\eta) = 0 \qquad (18)$$

and

$$\frac{d^2 R(\xi)}{d\xi^2} - (c - 2\gamma^2\cosh 2\xi)\,R(\xi) = 0 \qquad (19)$$

where c is the separation constant and $\gamma^2 = (k^2 - \beta^2)q^2/4$. Equation 18 is the Mathieu differential equation; equation 19, which follows from 18 by the transformation $\eta = \pm i\xi$, is the modified Mathieu differential equation (42).

For physically admissible single-valued electromagnetic fields, $\Lambda(\xi,\eta)$ must be a periodic function of η, of period π or 2π, and the separation constant c, in this case a function of γ^2, takes on an infinite set of characteristic values for every γ^2. When γ^2 is real the characteristic values are all real; since we are considering solutions in a lossless medium, only real values of c and γ^2 are of interest. Corresponding to $\gamma^2 = 0$ there are two independent periodic solutions, namely $\sin n\eta$ and $\cos n\eta$ with the separation constant $c = n^2$ where n is an integer. It can be shown (43) that when γ^2

differs from zero, a characteristic value c determines one and only one periodic solution which is either even or odd in η . The characteristic values c , giving rise to even and odd solutions are denoted here by $a_n(\gamma^2)$ and $b_n(\gamma^2)$ respectively. The subscript n identifies those sets of characteristic values which approach n^2 as γ^2 approaches zero. It is known from the Sturmian theory of second order linear differential equations that solutions associated with $a_n(\gamma^2)$ and $b_n(\gamma^2)$ have n zeros in the interval $0 \le \eta \le \pi$ (44) .

For arbitrary positive real values of γ^2, the periodic solutions of Matheiu's equation 18 are*(42,45)

$$
\theta(\eta) = \begin{cases} ce_n(\eta,\gamma^2) \\ se_n(\eta,\gamma^2) \end{cases} \quad \begin{array}{l} \text{(even)} \quad a_n(\gamma^2) \\ \text{(odd)} \quad b_n(\gamma^2) \end{array} \tag{20}
$$

and the corresponding sol·itions for the modified Mathieu's equation 19 are*

$$
R(\xi) = \begin{cases} a_1\, Ce_n(\xi,\gamma^2) + a_2 Fey_n(\xi,\gamma^2) \\ b_1\, Se_n(\xi,\gamma^2) + b_2 Gey_n(\xi,\gamma^2) \end{cases} \quad \begin{array}{l} \text{(even)} \quad a_n(\gamma^2) \\ \text{(odd)} \quad b_n(\gamma^2). \end{array} \tag{21}
$$

For arbitrary negative real values of γ^2 the periodic solutions of Mathieu's equation 18 are*

$$
\theta(\eta) = \begin{cases} ce_n^*(\eta,|\gamma^2|) \\ se_n^*(\eta,|\gamma^2|) \end{cases} \quad \begin{array}{l} \text{(even)} \quad \begin{array}{l} (a_n(|\gamma^2|) \text{ when } n \text{ even)} \\ (b_n(|\gamma^2|) \text{ when } n \text{ odd)} \end{array} \\ \text{(odd)} \quad \begin{array}{l} (b_n(|\gamma^2|) \text{ when } n \text{ even)} \\ (a_n(|\gamma^2|) \text{ when } n \text{ odd)} \end{array} \end{array} \tag{22}
$$

and the corresponding solutions for the modified Mathieu's equation 19

*See Appendix A for the definitions and series expansions of these Mathieu and modified Mathieu functions.

are*

$$R(\xi) = \begin{cases} c_1 Ce_n^*(\xi, |\gamma^2|) + c_2 Fek_n(\xi, |\gamma^2|) & \text{(even)} \\ d_1 Se_n^*(\xi, |\gamma^2|) + d_2 Gek_n(\xi, |\gamma^2|) & \text{(odd)} \end{cases} \quad \begin{array}{l} (a_n(|\gamma^2|) \text{ when } n \text{ even}) \\ (b_n(|\gamma^2|) \text{ when } n \text{ odd}) \\ (b_n(|\gamma^2|) \text{ when } n \text{ even}) \\ (a_n(|\gamma^2|) \text{ when } n \text{ odd}) \end{array}$$

(23)

$a_n(\gamma^2)$ and $b_n(\gamma^2)$ are the characteristic values and n is the order of the function. a_1, a_2, b_1, b_2, c_1, c_2, d_1 and d_2 are the arbitrary constants.

The proper choice of the above solutions to represent the electro-magnetic field of an elliptical dielectric cylinder depends upon the boundary conditions. For region 1, which is the space inside the dielectric rod, all field components must be finite. For region 0, which is the space outside the dielectric cylinder, in order that energy flow only along the axis of the cylinder, all field components, must approach zero as the radial argument approaches infinity. Consequently we must discard the functions $Fey_n(\xi, \gamma^2)$ and $Gey_n(\xi, \gamma^2)$, since they are infinite at the origin, i.e., at $\xi = 0$. The functions $Ce_n^*(\xi, |\gamma^2|)$ and $Se_n^*(\xi, |\gamma^2|)$ must also be discarded since they become infinite at infinity. Therefore the solutions of the wave equations 14 and 15 are as follows:

$$H_{z_1}(\xi, \eta, z, t) = \sum_{n=0}^{\infty} A_n Ce_n(\xi, \gamma_1^2) \, ce_n(\eta, \gamma_1^2) \, e^{-i\omega t} \, e^{i\beta_1 z}$$

$$+ \sum_{n=1}^{\infty} A_n' Se_n(\xi, \gamma_1^2) \, se_n(\eta, \gamma_1^2) e^{-i\omega t} \, e^{i\beta_1 z}, \quad (\xi_0 \geq \xi \geq 0) \quad (24)$$

$$H_{z_0}(\xi, \eta, z, t) = \sum_{n=0}^{\infty} L_n Fek_n(\xi, |\gamma_0^2|) ce_n^*(\eta, |\gamma_0^2|) \, e^{-i\omega t} \, e^{i\beta_0 z}$$

$$+ \sum_{n=1}^{\infty} L_n' Gek_n(\xi, |\gamma_0^2|) se_n^*(\eta, |\gamma_0^2|) e^{-i\omega t} \, e^{i\beta_0 z}; \quad (\infty \geq \xi \geq \xi_0) \quad (25)$$

*We follow the notation adopted by McLachlan (47) and Meixner (44).

$$E_{z_1}(\xi,\eta,z,t) = \sum_{n=0}^{\infty} B_n' Ce_n(\xi,r_1^2) \, ce_n(\eta,r_1^2) \, e^{-i\omega t} \, e^{i\beta_1 z}$$

$$+ \sum_{n=1}^{\infty} B_n Se_n(\xi,r_1^2) \, se_n(\eta,r_1^2) \, e^{-i\omega t} \, e^{i\beta_1 z}, \quad (\xi_o \geq \xi \geq 0) \quad (26)$$

$$E_{z_o}(\xi,\eta,z,t) = \sum_{n=0}^{\infty} P_n' Fek_n(\xi,|r_o^2|) \, ce_n^*(\eta,|r_o^2|) \, e^{-i\omega t} \, e^{i\beta_o z}$$

$$+ \sum_{n=1}^{\infty} P_n Gek_n(\xi,|r_o^2|) \, se_n^*(\eta,|r_o^2|) e^{-i\omega t} \, e^{i\beta_o z}, \quad (\infty \geq \xi \geq \xi_o).$$
$$(27)$$

A_n, A_n', B_n, B_n', L_n, L_n', P_n and P_n' are coefficients which are related by the boundary conditions and are functions of n, ω, r_1^2, $|r_o^2|$, and the nature of the exciting sources, but independent of the coordinates. r_1^2 and $|r_o^2|$ are respectively $(k_1^2 - \beta_1^2)q^2/4$ and $|(k_o^2 - \beta_o^2)q^2/4|$ with $k_1^2 = \omega^2 \mu \epsilon_1$ and $k_o^2 = \omega^2 \mu \epsilon_o$. ϵ_1 is the dielectric constant of the cylinder and ϵ_o is the dielectric constant of the surrounding medium. $\xi = \xi_o$ is the surface of the dielectric cylinder. All transverse field components for both regions can be derived from equations 10 through 13, using equations 24 through 27. Incidentally, the Hertz vectors π_z' and π_z'' (15) rather than E_z and H_z may be used as the scalar quantities from which the other field components may be derived.

2.3 The Boundary Conditions

The task of solving an electromagnetic wave boundary value problem is to find finite and single-valued solutions which satisfy the source-free Maxwell's equations and the boundary conditions. The boundary conditions are, that the tangential components of the electric and magnetic fields must, in general, be continuous through any surface. If

the region of interest is infinite, then the radiation condition (46)
must also be satisfied. The above conditions are necessary and suffi-
cient. In the present problem, the continuity conditions in the
elliptical cylindrical coordinates are

$$E_{z_1} = E_{z_0} \tag{1}$$

$$H_{z_1} = H_{z_0} \tag{2}$$

$$E_{\eta_1} = E_{\eta_0} \tag{3}$$

and

$$H_{\eta_1} = H_{\eta_0} \tag{4}$$

for $\xi = \xi_0$, $2\pi \geq \eta \geq 0$ and $+\infty > z > -\infty$.

In order to illustrate the difficulties encountered in satisfying
the above boundary conditions for the elliptical dielectric cylinder,
we shall first consider the case of the surface wave propagation along
a circular dielectric cylinder. The required axial electromagnetic
fields both inside and outside the circular dielectric cylinder are (13)

$$E_z^i = \sum_{n=0}^{\infty} A_n^i J_n(\zeta^i r) \cos n\theta \, e^{ikz} \, e^{-i\omega t} \qquad (0 \leq r \leq a) \tag{5}$$

$$E_z^o = \sum_{n=0}^{\infty} A_n^o K_n(\zeta^o r) \cos n\theta \, e^{ikz} \, e^{-i\omega t} \qquad (a \leq r < \infty) \tag{6}$$

$$H_z^i = \sum_{n=1}^{\infty} B_n^i J_n(\zeta^i r) \sin n\theta \, e^{ikz} \, e^{-i\omega t} \qquad (0 \leq r \leq a) \tag{7}$$

$$H_z^o = \sum_{n=1}^{\infty} B_n^o K_n(\zeta^o r) \sin n\theta \, e^{ikz} \, e^{-i\omega t} \qquad (a \leq r < \infty) \tag{8}$$

where $\zeta^i = \sqrt{k_i^2 - k^2}$ and $\zeta^o = \sqrt{k^2 - k_o^2}$ with $k_i^2 = \omega^2 \mu \epsilon_i$ and $k_o^2 = \omega^2 \mu \epsilon_o$.
ϵ_i is the dielectric constant of the cylinder, ϵ_o is the dielectric

constant of the surrounding medium, and $\epsilon_{\mathrm{\mathbb{1}}} > \epsilon_0$. A_n^1, A_n^0, B_n^1, and B_n^0 are the arbitrary constants and a is the radius of the cylinder. The boundary conditions are

$$E_z^1 = E_z^0 \tag{9}$$

$$H_z^1 = H_z^0 \tag{10}$$

$$E_\Theta^1 = E_\Theta^0 \tag{11}$$

$$H_\Theta^1 = H_\Theta^0 \tag{12}$$

at $r = a$, $0 \leq \Theta \leq 2\pi$ and $-\infty \leq z \leq \infty$. Substituting equations 5 and 6 into equation 9, one obtains

$$\sum_{n=0}^{\infty} A_n^1 J_n(\zeta^1 a)\cos n\Theta\ e^{ikz} = \sum_{n=0}^{\infty} A_n^0 K_n(\zeta^0 a)\cos n\Theta\ e^{ikz}. \tag{13}$$

Multiplying both sides of equation 13 by $\cos m\Theta$ and integrating with respect to Θ from 0 to 2π we have, due to the orthogonality of the trigonometric functions,

$$.A_n^1 J_n(\zeta^1 a) = A_n^0 K_n(\zeta^0 a) . \tag{14}$$

It should be noted that for each mode (in this case for each n) there should be only one propagation constant. Equation 14 shows that the boundary conditions may be satisfied for each n separately, due to the orthogonality in Θ of the fundamental solutions and the fact that the angular function ($\cos n\Theta$ or $\sin n\Theta$) is independent of the characteristics of the medium. Similar procedures and conclusions can be applied to the boundary conditions, equations 10, 11 and 12.

Consider the boundary condition, equation 1, for the elliptical dielectric cylinder. Substituting equations 2.2-26 and 2.2-27 into 1

one gets

$$\sum_{n=0}^{\infty} B_n' Ce_n(\xi_o, r_1^2) \, ce_n(\eta, r_1^2) \, e^{i\beta_1 z} + \sum_{n=1}^{\infty} B_n Se_n(\xi_o, r_1^2) \, se_n(\eta, r_1^2) e^{i\beta_1 z}$$

$$= \sum_{r=0}^{\infty} P_r' Fek_r(\xi_o, |r_o^2|) ce_r^*(\eta, |r_o^2|) \, e^{i\beta_o z}$$

$$+ \sum_{r=1}^{\infty} P_r Gek_r(\xi_o, |r_o^2|) se_r^*(\eta, |r_o^2|) e^{i\beta_o z} . \tag{15}$$

Equation 15 may be written as two separate equations, one corresponding to the even type modes, the other to the odd type modes. These equations are

$$\sum_{n=0}^{\infty} B_n' Ce_n(\xi_o, r_1^2) \, ce_n(\eta, r_1^2) \, e^{i\beta_1 z} =$$

$$\sum_{r=0}^{\infty} P_r' Fek_r(\xi_o, |r_o^2|) \, ce_r^*(\eta, |r_o^2|) \, e^{i\beta_o z} \tag{16}$$

and

$$\sum_{n=1}^{\infty} B_n Se_n(\xi_o, r_1^2) \, se_n(\eta, r_1^2) \, e^{i\beta_1 z} =$$

$$\sum_{r=1}^{\infty} P_r \, Gek_r(\xi_o, |r_o^2|) se_r^*(\eta, |r_o^2|) \, e^{i\beta_o z} . \tag{17}$$

Suppose one multiplies both sides of 17 by $se_m(\eta, r_1^2)$ and integrates with respect to η from 0 to 2π. Due to the orthogonality of the Mathieu functions (see Appendix A), equation 17 becomes

$$N_m B_m Se_m(\xi_o, r_1^2) e^{i\beta_1 z} = \sum_{r=1}^{\infty} P_r Gek_r(\xi_o, |r_o^2|) \, e^{i\beta_o z}$$

$$\int_0^{2\pi} se_r^*(\eta, |r_o^2|) \, se_m(\eta, r_1^2) d\eta$$

where N_m is the normalization constant, $\displaystyle\int_0^{2\pi} se_m^2(\eta, r_1^2)d\eta$. Assuming $\beta_1 = \beta_0$ one gets

$$N_m B_m Se_m(\xi_0, r_1^2) = \sum_{r=1}^{\infty} P_r Gek_r(\xi_0, |r_0^2|) \int_0^{2\pi} se_r^*(\eta, |r_0^2|)se_m(\eta, r_1^2)d\eta$$

(18)

Equation 18 involves the arbitrary constant B_m ($m = 1$, or 2, or 3, or $\cdot$ $\cdot$ $\cdot$) and an infinite number of arbitrary constants P_1, P_2, P_3 $\cdots$ P_∞. Similar procedures may be applied to the remaining boundary conditions, equations 2, 3 and 4, and each of them contributes an arbitrary constant on the left hand side of the equation and an infinite number of arbitrary constants on the right hand side of the equation. For example, using 2, an algebraic equation involving A_m ($m = 1$, or 2, or 3, or $\cdot$ $\cdot$ $\cdot$) and L_1, L_2, L_3 $\cdot$ $\cdot$ $\cdot$ L_∞ results; using 3, an algebraic equation involving A_m and B_m ($m = 1$, or 2, or 3, or $\cdot$ $\cdot$ $\cdot$), and P_1, P_2, P_3, $\cdot$ $\cdot$ $\cdot$ P_∞ and L_1, L_2, L_3 $\cdot$ $\cdot$ $\cdot$ L_∞ results; using 4, another algebraic equation involving A_m and B_m ($m = 1$, or 2, or 3, or $\cdot$ $\cdot$ $\cdot$), and P_1, P_2, P_3, $\cdot$ $\cdot$ $\cdot$ P_∞ and L_1, L_2, L_3 $\cdot$ $\cdot$ $\cdot$ L_∞ results. Since these equations involve an infinite number of arbitrary constants, an infinite set of linear algebraic equations is required. This means m must be equal to 0, then 1, then 2, $\cdot$ $\cdot$ $\cdot$, then ∞ . It can therefore be seen by the method outlined above that in matching the boundary conditions, an infinite order of Mathieu functions must be used to describe the fields in both media, i.e., both inside and outside the elliptical dielectric rod.

To overcome the above difficulties one assumes that only one term of the Mathieu function could represent the field configurations in one medium, while an infinite series of Mathieu functions in the other.

Equation 17 can be written as

$$B_n Se_n(\xi_o, \gamma_1^2) se_n(\eta, \gamma_1^2) e^{i\beta_1 z} = \sum_{r=1}^{\infty} P_r Gek_r(\xi_o, |\gamma_o^2|) se_r^*(\eta, |\gamma_o^2|) e^{i\beta_o z} \tag{19}$$

or

$$\sum_{n=1}^{\infty} B_n Se_n(\xi_o, \gamma_1^2) se_n(\eta, \gamma_1^2) e^{i\beta_1 z} = P_r Gek_r(\xi_o, |\gamma_o^2|) se_r^*(\eta, |\gamma_o^2|) e^{i\beta_o z} . \tag{20}$$

In equation 19 one **term** of the Mathieu function has been used to represent the field configuration inside the dielectric rod, and in equation 20 one term of the Mathieu function has been used to represent the field configuration outside the dielectric rod. Consider equation 19. Setting $\beta_1 = \beta_o$ and multiplying both sides of 19 by $se_m(\eta, \gamma_1^2)$ and integrating with respect to η from 0 to 2π, one obtains

$$N_{nm} B_n Se_n(\xi_o, \gamma_1^2) = \sum_{r=1}^{\infty} P_r Gek_r(\xi_o, |\gamma_o^2|) \beta_{rm} \quad (m = 0,1,2,\cdots) \tag{21}$$

where $\quad N_{nm} = \int_0^{2\pi} se_n^2(\xi_o, \gamma_1^2) d\eta$, when $n = m$

$\qquad\qquad = 0 \qquad\qquad\qquad$ when $n \neq m$

and

$$\beta_{rm} = \int_0^{2\pi} se_r^*(\xi_o, |\gamma_o^2|) \, se_m(\xi_o, \gamma_1^2) d\eta \quad .$$

For each value of n there exists an infinite set of linear algebraic equations which may be combined and simplified to give an equation involving only two arbitrary constants, B_n and P_n, i.e.,

$$N_{nn} B_n Se_n(\xi_o, \gamma_1^2) = P_n Gek_n(\xi_o, |\gamma_o^2|) F_n(\beta_{rm}) \tag{22}$$

where $F_n(\beta_{rm})$ is a function of β_{rm} .

As an example, suppose $n = 1$, equation 21 becomes

$$N_{1m}B_1Se_1(\xi_o, \gamma_1^2) = \sum_{r=1}^{\infty} P_r Gek_r(\xi_o, |\gamma_o^2|)\beta_{rm} , \qquad (m = 0,1,2,\cdots) \qquad (23)$$

with $N_{1m} = \displaystyle\int_0^{2\pi} se_1^2(\eta, \gamma_1^2)d\eta , \quad m = 1 ,$

$$= 0 \qquad\qquad m \neq 1 .$$

The infinite set of linear algebraic equations from equation 23 are

$$N_{11}B_1Se_1(\xi_o\gamma_1^2) = P_1 Gek_1(\xi_o, |\gamma_o^2|)\, \beta_{11} + P_3 Gek_3(\xi_o, |\gamma_o^2|)\beta_{31} +$$
$$+ P_5 Gek_5(\xi_o, |\gamma_o^2|)\beta_{51} + \cdots \qquad (24a)$$

$$0 = P_1 Gek_1(\xi_o, |\gamma_o^2|)\beta_{13} + P_3 Gek_3(\xi_o, |\gamma_o^2|)\beta_{33} +$$
$$+ P_5 Gek_5(\xi_o, |\gamma_o^2|)\beta_{53} + \cdots \qquad (24b)$$

$$0 = P_1 Gek_1(\xi_o, |\gamma_o^2|)\beta_{15} + P_3 Gek_3(\xi_o, |\gamma_o^2|)\beta_{35} +$$
$$+ P_5 Gek_5(\xi_o, |\gamma_o^2|)\beta_{55} + \cdots \qquad (24c)$$

Combining the above set of equations one obtains

$$N_{11}B_1Se_1(\xi_o, \gamma_1^2) = P_1 Gek_1(\xi_o, |\gamma_o^2|)\, F_1(\beta_{rm}) \qquad (25)$$

where

$$F_1(\beta_{rm}) = \frac{\begin{vmatrix} \beta_{33} & \beta_{53} & \cdots \\ \beta_{35} & \beta_{55} & \cdots \\ \cdots & \cdots & \cdots \end{vmatrix}}{\begin{vmatrix} \beta_{11} & \beta_{31} & \beta_{51} & \cdots \\ \beta_{13} & \beta_{33} & \beta_{53} & \cdots \\ \beta_{15} & \beta_{35} & \beta_{55} & \cdots \\ \cdots & \cdots & \cdots & \cdots \end{vmatrix}} . \qquad (26)$$

$P_3, P_5, \cdots P_\infty$ can all be expressed in terms of P_1 ; for example,

$$P_3 = \frac{\begin{vmatrix} \beta_{13} & \beta_{53} & \cdots \\ \beta_{15} & \beta_{55} & \cdots \\ \cdots & \cdots & \cdots \end{vmatrix}}{\begin{vmatrix} \beta_{33} & \beta_{53} & \cdots \\ \beta_{35} & \beta_{55} & \cdots \\ \cdots & \cdots & \cdots \end{vmatrix}} \cdot \frac{Gek_1(\xi_o, |r_o^2|)}{Gek_3(\xi_o, |r_o^2|)} \cdot (-P_1) \qquad (27)$$

and

$$P_5 = \frac{\begin{vmatrix} \beta_{33} & \beta_{13} & \cdots \\ \beta_{35} & \beta_{15} & \cdots \\ \cdots & \cdots & \cdots \end{vmatrix}}{\begin{vmatrix} \beta_{33} & \beta_{53} & \cdots \\ \beta_{35} & \beta_{55} & \cdots \\ \cdots & \cdots & \cdots \end{vmatrix}} \cdot \frac{Gek_1(\xi_o, |r_o^2|)}{Gek_3(\xi_o, |r_o^2|)} \cdot (-P_1) \cdot \qquad (28)$$

The above infinite determinants may be solved by the method of sucessive approximations (47). It may be shown that $P_1 > P_3 > P_5 > \cdots > P_\infty$ in this example.

The method described above will be used in a later section to satisfy the boundary conditions and to obtain the characteristic equations of the principal propagating modes. As one may anticipate, the mode classifications are much more involved in the case of the elliptical dielectric cylinder than the circular dielectric cylinder. This will be discussed in the next section.

2.4 The Notations and Classifications of the Propagating Modes

For a circular dielectric waveguide it is well known that the pure TE and TM waves can exist only if the fields are independent of the

angular coordinates. These circularly symmetric waves are designated by H_{on} for the pure TE waves and E_{on} for the pure TM waves. The subscript o signifies the angular variations and n signifies the nth root of the characteristic equation. The coexistence of E and H waves is required to satisfy the boundary conditions if the field is a function of the angular coordinate .* These asymmetric waves are then designated by HE_{mn} if the cross-sectional field pattern resembles that of an H wave and by EH_{mn} if the cross-sectional field pattern resembles that of an E wave. The subscripts m and n denote respectively the number of cyclic variations with Θ and the nth root of the characteristic equation. These hybrid asymmetric modes discussed above are doubly degenerate since an equally valid solution results if $\sin m\Theta$ is replaced by $\cos m\Theta$, and $\cos m\Theta$ by $-\sin m\Theta$.

As pointed out in the preceding section, no pure TE or TM waves can exist on an elliptical dielectric rod. All modes must be hybrid. In contrast to the case of a circular rod, the fields in one of the regions of an elliptical rod must be represented by a set of infinite series of Mathieu and modified Mathieu functions; while in the other region by a single product term of Mathieu and modified Mathieu functions. We shall be concerned only with the modes hereafter denoted as the principal modes, which will degenerate to the well-known hybrid HE_{mn} modes when the eccentricity of the ellipse is zero. The principal

---

*Physically speaking, the presence of E_z in a predominantly H wave (i.e., the HE wave) or vice versa (i.e., the EH wave) assures the return path for the electric or magnetic lines of force; in other words, the electric and magnetic field lines must form closed loops in the case of the surface wave propagation along a dielectric rod. The existence of a circularly symmetric pure E or H wave along the dielectric rod is a special case; since the electric and magnetic lines of force of the E or H wave have already formed closed loops.

modes will be denoted by $_e\text{HE}_{mn}^{(1,0)}$ or $_o\text{HE}_{mn}^{(1,0)}$ depending upon

whether the modes are even or odd. The axial magnetic and electric

fields of an even mode are represented by an even and odd Mathieu

function respectively, and those of an odd mode by an odd and even

Mathieu function respectively. The subscript m is the order of

the Mathieu function used for the single product term, and n is the

nth root of the characteristic equation. The superscript 1 or 0

indicates the region inside or outside in which a single product term

was used to represent the field configuration. The symbol HE means

that the cross-sectional field pattern of this dielectric rod mode

resembles that of an H wave in the metal guide. The symbol EH is

used if the cross-sectional field pattern of the dielectric rod mode

is similar to that of an E wave in the metal guide.

2.5 The Field Components and the Determinantal Equations of the Principal Modes

Having properly classified the modes we are now in a position to

describe the field components of the principal modes and to apply the

boundary conditions in order to obtain the characteristic equations

from which the propagation constants may be determined.

In order to simplify the notations for the Mathieu and modified

Mathieu functions without any ambiguities, the following abbreviations

are used:

$$\text{Ce}_m(\xi) = \text{Ce}_m(\xi, \gamma_1^2) \qquad\qquad \text{ce}_m(\eta) = \text{ce}_m(\eta, \gamma_1^2)$$

$$\text{Se}_m(\xi) = \text{Se}_m(\xi, \gamma_1^2) \qquad\qquad \text{se}_m(\eta) = \text{se}_m(\eta, \gamma_1^2)$$

$$\text{Fek}_r(\xi) = \text{Fek}_r(\xi, |\gamma_0^2|) \qquad\qquad \text{ce}_r^*(\eta) = \text{ce}_r^*(\eta, |\gamma_0^2|)$$

$$\text{Gek}_r(\xi) = \text{Gek}_r(\xi, |\gamma_0^2|) \qquad\qquad \text{se}_r^*(\eta) = \text{se}_r^*(\eta, |\gamma_0^2|) \ .$$

The principal modes are separated into four major types, the $_e HE_{mn}^{(1)}$ mode, the $_e HE_{mn}^{(0)}$ mode, the $_o HE_{mn}^{(1)}$ mode, and the $_o HE_{mn}^{(0)}$ mode.

(a) The $_e HE_{mn}^{(1)}$ Mode

Appropriate solutions of Maxwell's equations for both regions of the elliptical dielectric rod have been given in section 2.2. According to the definition of the $_e HE_{mn}^{(1)}$ mode, specified in section 2.4, the axial components of the magnetic and electric fields are for region 1 $(0 \leq \xi \leq \xi_o)$

$$H_{z_1} = A_m Ce_m(\xi) ce_m(\eta) e^{i\beta_1 z} \tag{1}$$

$$E_{z_1} = B_m Se_m(\xi) se_m(\eta) e^{i\beta_1 z} \tag{2}$$

and for region 0 $(\xi_o \leq \xi < \infty)$

$$H_{z_o} = \sum_{r=0}^{\infty} L_r Fek_r(\xi) ce_r^*(\eta) e^{i\beta_o z} \tag{3}$$

$$E_{z_o} = \sum_{r=1}^{\infty} P_r Gek_r(\xi) se_r^*(\eta) e^{i\beta_o z} . \tag{4}$$

A_m, B_m, L_r, and P_r are the arbitrary constants. The harmonic time dependence $e^{-i\omega t}$ has been implied in these expressions as well as in the subsequent expressions for the field intensities. Substituting 1 and 2 into 2.2-10 through 2.2-13, and carrying out the differentiation, one obtains the transverse field components for region 1 $(0 \leq \xi \leq \xi_o)$,

$$H_{\xi_1} = \frac{i\beta}{(k_1^2 - \beta^2)p} \left\{ A_m Ce_m'(\xi) ce_m(\eta) - \frac{\omega\epsilon_1}{\beta} B_m Se_m(\xi) se_m'(\eta) \right\} e^{i\beta_1 z} \tag{5}$$

$$H_{\eta_1} = \frac{i\beta}{(k_1^2 - \beta^2)p} \left\{ A_m Ce_m(\xi) ce_m'(\eta) + \frac{\omega\epsilon_1}{\beta} B_m Se_m'(\xi) se_m(\eta) \right\} e^{i\beta_1 z} \tag{6}$$

$$E_{\xi_1} = \frac{i\beta}{(k_1^2 - \beta^2)p} \left\{ \frac{\omega\mu}{\beta} A_m Ce_m(\xi) ce_m'(\eta) + B_m Se_m'(\xi) se_m(\eta) \right\} e^{i\beta_1 z} \qquad (7)$$

$$E_{\eta_1} = \frac{i\beta}{(k_1^2 - \beta^2)p} \left\{ -\frac{\omega\mu}{\beta} A_m Ce_m'(\xi) ce_m(\eta) + B_m Se_m(\xi) se_m'(\eta) \right\} e^{-\beta_1 z} \qquad (8)$$

where $k_1^2 = \omega^2\mu\epsilon_1$ and $p = q (\sin h^2\xi + \sin^2\eta)^{1/2}$. The abbreviations $Ce_m'(\xi) = \frac{d}{d\xi} Ce_m(\xi)$, $Se_m'(\xi) = \frac{d}{d\xi} Se_m(\xi)$, $ce_m'(\eta) = \frac{d}{d\eta} ce_m(\eta)$, and $se_m'(\eta) = \frac{d}{d\eta} se_m(\eta)$ have been used. Substituting equations 3 and 4 into 2.2-10 through 2.2-13, and carrying out the differentiation, one obtains the transverse field components for region 0 $(\xi_0 \leqslant \xi < \infty)$

$$H_{\xi_0} = \frac{i\beta}{(k_0^2 - \beta^2)p} \sum_{r=0}^{\infty} \left[L_r Fek_r'(\xi) ce_r^*(\eta) - \frac{\omega\epsilon_0}{\beta} P_r Gek_r(\xi) se_r^{*'}(\eta) \right] e^{i\beta_0 z} \qquad (9)$$

$$H_{\eta_0} = \frac{i\beta}{(k_0^2 - \beta^2)p} \sum_{r=1}^{\infty} \left[L_r Fek_r(\xi) ce_r'^*(\eta) + \frac{\omega\epsilon_0}{\beta} P_r Gek_r'(\xi) se_r^*(\eta) \right] e^{i\beta_0 z} \qquad (10)$$

$$E_{\xi_0} = \frac{i\beta}{(k_0^2 - \beta^2)p} \sum_{r=1}^{\infty} \left[\frac{\omega\mu}{\beta} L_r Fek_r(\xi) ce_r^{*'}(\eta) + P_r Gek_r'(\xi) se_r^*(\eta) \right] e^{i\beta_0 z} \qquad (11)$$

$$E_{\eta_0} = \frac{i\beta}{(k_0^2 - \beta^2)p} \sum_{r=0}^{\infty} \left[-\frac{\omega\mu}{\beta} L_r Fek_r'(\xi) ce_r^*(\eta) + P_r Gek_r(\xi) se_r^{*'}(\eta) \right] e^{i\beta_0 z} \qquad (12)$$

where $k_0^2 = \omega^2\mu\epsilon_0$. The prime denotes differentiation with respect to ξ or η as the case may be.

If m is odd, r must also be odd due to the orthogonality of the Mathieu functions. In other words, when m is odd the series are summed over all odd values of r; and when m is even the series are summed over all even values of r. The problem with m odd will be analyzed in detail.

Equating the tangential electric and magnetic fields H_z, E_z, H_η and E_η at the boundary surface $\xi = \xi_o$, we arrive at the following equations

$$A_m Ce_m(\xi_o) ce_m(\eta) \, e^{i\beta_1 z} = \sum_{\substack{r=1 \\ odd}}^{\infty} L_r Fek_r(\xi_o) ce_r^*(\eta) \, e^{i\beta_o z} \tag{13}$$

$$B_m Se_m(\xi_o) se_m'(\eta) \, e^{i\beta_1 z} = \sum_{\substack{r=1 \\ odd}}^{\infty} P_r Gek_r(\xi_o) se_r^*(\eta) \, e^{i\beta_o z} \tag{14}$$

$$\frac{\beta_1}{(k_1^2 - \beta_1^2)} \left[A_m Ce_m(\xi_o) ce_m'(\eta) + \frac{\omega\epsilon_1}{\beta_1} B_m Se_m'(\xi_o) se_m(\eta) \right] e^{i\beta_1 z}$$

$$= \frac{\beta_o}{(k_o^2 - \beta_o^2)} \sum_{\substack{r=1 \\ odd}}^{\infty} \left[L_r Fek_r(\xi_o) ce_r^{*'}(\eta) + \frac{\omega\epsilon_o}{\beta_o} P_r Gek_r'(\xi_o) se_r^*(\eta) \right] e^{i\beta_o z} \tag{15}$$

$$\frac{\beta_1}{(k_1^2 - \beta_1^2)} \left[-A_m \frac{\omega\mu}{\beta_1} Ce_m'(\xi_o) ce_m(\eta) + B_m Se_m(\xi_o) se_m'(\eta) \right] e^{i\beta_1 z}$$

$$= \frac{\beta_o}{(k_o^2 - \beta_o^2)} \sum_{\substack{r=1 \\ odd}}^{\infty} \left[-L_r \frac{\omega\mu}{\beta_o} Fek_r'(\xi_o) ce_r^*(\eta) + P_r Gek_r(\xi_o) se_r^{*'}(\eta) \right] e^{i\beta_o z} . \tag{16}$$

Setting $\beta = \beta_o = \beta_1$ and eliminating $ce_r^{*'}(\eta)$ and $se_r^{*'}(\eta)$ by equations 13 and 14, we obtain

$$A_m Ce_m(\xi_o) ce_m(\eta) = \sum_{\substack{r=1 \\ odd}}^{\infty} L_r Fek_r(\xi_o) ce_r^*(\eta) \tag{17}$$

$$B_m Se_m(\xi_o) se_m(\eta) = \sum_{\substack{r=1 \\ odd}}^{\infty} P_r Gek_r(\xi_o) se_r^*(\eta) , \tag{18}$$

$$A_m \left[1 - \left(\frac{k_1^2 - \beta^2}{k_o^2 - \beta^2} \right) \right] Ce_m(\xi_o) ce_m'(\eta) + \frac{\omega \epsilon_1}{\beta} B_m Se_m'(\xi_o) se_m(\eta) =$$

$$\left(\frac{k_1^2 - \beta^2}{k_o^2 - \beta^2} \right) \sum_{\substack{r=1 \\ odd}}^{\infty} \frac{\omega \epsilon_o}{\beta} P_r Gek_r'(\xi_o) se_r^*(\eta) \tag{19}$$

$$A_m \frac{\omega \mu}{\beta} Ce_m'(\xi_o) ce_m(\eta) - B_m \left[1 - \left(\frac{k_1^2 - \beta^2}{k_o^2 - \beta^2} \right) \right] Se_m(\xi_o) se_m'(\eta) =$$

$$\left(\frac{k_1^2 - \beta^2}{k_o^2 - \beta^2} \right) \sum_{\substack{r=1 \\ odd}}^{\infty} \frac{\omega \mu}{\beta} L_r Fek_r'(\xi_o) ce_r^*(\eta) \tag{20}$$

The method discussed in section 2.3 will now be used to eliminate the η dependence in the above equations. Multiplying equations 17 and 20 by $ce_s(\eta)$ and equations 18 and 19 by $se_s(\eta)$, and integrating with respect to η from 0 to 2π results in

$$A_m Ce_m(\xi_o) \epsilon_{ms} C_m = \sum_{\substack{r=1 \\ odd}}^{\infty} L_r Fek_r(\xi_o) \alpha_{rs} \tag{21}$$

$$B_m Se_m(\xi_o) \epsilon_{ms} S_m = \sum_{\substack{r=1 \\ odd}}^{\infty} P_r Gek_r(\xi_o) \beta_{rs} \tag{22}$$

$$A_m \left[1 - \left(\frac{k_1^2 - \beta^2}{k_o^2 - \beta^2} \right) \right] Ce_m(\xi_o) \chi_{ms} + \frac{\omega \epsilon_1}{\beta} B_m Se_m'(\xi_o) \epsilon_{ms} S_m =$$

$$\left(\frac{k_1^2 - \beta^2}{k_o^2 - \beta^2} \right) \frac{\omega \epsilon_1}{\beta} \sum_{\substack{r=1 \\ odd}}^{\infty} P_r Gek_r'(\xi_o) \beta_{rs} \tag{23}$$

$$A_m \frac{\omega \mu}{\beta} Ce_m'(\xi_o) \epsilon_{ms} C_m - B_m \left[1 - \left(\frac{k_1^2 - \beta^2}{k_o^2 - \beta^2} \right) \right] Se_m(\xi_o) \delta_{ms} =$$

$$\left(\frac{k_1^2 - \beta^2}{k_o^2 - \beta^2} \right) \frac{\omega \mu}{\beta} \sum_{\substack{r=1 \\ odd}}^{\infty} L_r Fek_r'(\xi_o) \alpha_{rs} \tag{24}$$

and $s = 1,3,5,7,9,\cdots$. ϵ_{ms}, C_m, S_m, α_{rs}, β_{rs}, δ_{ms} and χ_{ms} are defined as

$$\epsilon_{ms} = 1 \quad \text{when} \quad m = s$$
$$\phantom{\epsilon_{ms}} = 0 \quad \text{when} \quad m \neq s \ ;$$

$$C_m = \int_0^{2\pi} ce_m^2(\eta)d\eta \quad ;$$

$$S_m = \int_0^{2\pi} se_m^2(\eta)d\eta \quad ; \tag{25}$$

$$\alpha_{rs} = \int_0^{2\pi} ce_r^*(\eta) \ ce_s(\eta)d\eta \tag{26}$$

$$\beta_{rs} = \int_0^{2\pi} se_r^*(\eta) \ se_s(\eta)d\eta \tag{27}$$

$$\delta_{ms} = \int_0^{2\pi} se_m'(\eta) \ ce_s(\eta)d\eta \tag{28}$$

$$\chi_{ms} = \int_0^{2\pi} ce_m'(\eta) \ se_s(\eta)d\eta \ . \tag{29}$$

These integrals have been evaluated in Appendix A.4. For each value of m there exists four infinite sets of linear algebraic equations which may be combined to give the following:

$$A_m C_m Ce_m(\xi_o) = L_m Fek_m(\xi_o)M_m(\alpha_{rs}) \tag{30}$$

$$B_m Se_m(\xi_o) = P_m Gek_m(\xi_o)N_m(\beta_{rs}) \tag{31}$$

$$A_m \left[1 - \left(\frac{k_1^2 - \beta^2}{k_o^2 - \beta^2}\right)\right] Ce_m(\xi_o) \ Q_m(\beta_{rs}, \chi_{ms}) + \frac{\omega\epsilon_1}{\beta} B_m Se_m'(\xi_o) =$$
$$\left(\frac{k_1^2 - \beta^2}{k_o^2 - \beta^2}\right) \frac{\omega\epsilon_o}{\beta} P_m Gek_m'(\xi_o)N_m(\beta_{rs}) \ , \tag{32}$$

$$A_m \frac{\omega\mu}{\beta} Ce_m'(\xi_o) - B_m \left[1 - \left(\frac{k_1^2 - \beta^2}{k_o^2 - \beta^2}\right) \right] Se_m(\xi_o) R_m(\alpha_{rs}, \delta_{ms}) =$$

$$\left(\frac{k_1^2 - \beta^2}{k_o^2 - \beta^2}\right) \frac{\omega\mu}{\beta} L_m \, Fek_m'(\xi_c) M_m(\alpha_{rs}) \quad . \tag{33}$$

$M_m(\alpha_{rs})$, $N_m(\beta_{rs})$, $Q_m(\beta_{rs}, \chi_{ms})$, and $R_m(\alpha_{rs}, \delta_{ms})$ are obtained according to the technique developed in section 2.3. As an example, we choose the $m = 1$ mode. These constants are then given by

$$M_1(\alpha_{rs}) = \frac{\begin{vmatrix} \alpha_{33} & \alpha_{53} & \cdots \\ \alpha_{35} & \alpha_{55} & \cdots \\ \cdots & \cdots & \cdots \end{vmatrix}}{\begin{vmatrix} \alpha_{11} & \alpha_{31} & \alpha_{51} & \cdots \\ \alpha_{13} & \alpha_{33} & \alpha_{53} & \cdots \\ \alpha_{15} & \alpha_{35} & \alpha_{55} & \cdots \\ \cdots & \cdots & \cdots & \cdots \end{vmatrix}} \cdot \frac{1}{C_1} \quad , \tag{34}$$

$$N_1(\beta_{rs}) = \frac{\begin{vmatrix} \beta_{33} & \beta_{53} & \cdots \\ \beta_{35} & \beta_{55} & \cdots \\ \cdots & \cdots & \cdots \end{vmatrix}}{\begin{vmatrix} \beta_{11} & \beta_{31} & \beta_{51} \cdots \\ \beta_{13} & \beta_{33} & \beta_{53} \cdots \\ \beta_{15} & \beta_{35} & \beta_{55} \cdots \\ \cdots & \cdots & \cdots \cdots \end{vmatrix}} \cdot \frac{1}{S_1} \quad , \tag{35}$$

$$Q_1(\beta_{rs}, \chi_{1s}) =$$

$$\left\{ \chi_{11} - \chi_{13} \frac{\begin{vmatrix} \beta_{31} & \beta_{51} & \cdots \\ \beta_{35} & \beta_{55} & \cdots \\ \cdots & \cdots & \cdots \end{vmatrix}}{\begin{vmatrix} \beta_{33} & \beta_{53} & \cdots \\ \beta_{35} & \beta_{55} & \cdots \\ \cdots & \cdots & \cdots \end{vmatrix}} + \chi_{15} \frac{\begin{vmatrix} \beta_{31} & \beta_{51} & \cdots \\ \beta_{33} & \beta_{53} & \cdots \\ \beta_{37} & \beta_{57} & \cdots \\ \cdots & \cdots & \cdots \end{vmatrix}}{\begin{vmatrix} \beta_{33} & \beta_{53} & \cdots \\ \beta_{35} & \beta_{55} & \cdots \\ \cdots & \cdots & \cdots \end{vmatrix}} + \cdots \right\} \cdot \frac{1}{S_1} \quad (36)$$

$$R_1(\alpha_{rs}, \delta_{1s}) =$$

$$\left\{ \delta_{11} - \delta_{13} \frac{\begin{vmatrix} \alpha_{31} & \alpha_{51} & \cdots \\ \alpha_{35} & \alpha_{55} & \cdots \\ \cdots & \cdots & \cdots \end{vmatrix}}{\begin{vmatrix} \alpha_{33} & \alpha_{53} & \cdots \\ \alpha_{35} & \alpha_{55} & \cdots \\ \cdots & \cdots & \cdots \end{vmatrix}} + \delta_{15} \frac{\begin{vmatrix} \alpha_{31} & \alpha_{51} & \cdots \\ \alpha_{33} & \alpha_{53} & \cdots \\ \alpha_{37} & \alpha_{57} & \cdots \\ \cdots & \cdots & \cdots \end{vmatrix}}{\begin{vmatrix} \alpha_{33} & \alpha_{53} & \cdots \\ \alpha_{35} & \alpha_{55} & \cdots \\ \cdots & \cdots & \cdots \end{vmatrix}} + \cdots \right\} \cdot \frac{1}{C_1} \quad (37)$$

where $C_1 = \int_0^{2\pi} ce_1^2(\eta)d\eta$ and $S_1 = \int_0^{2\pi} se_1^2(\eta)d\eta$. These infinite determinants may be solved by the method of successive approximations (47).

Equations 30 through 33 are a set of four homogeneous linear algebraic equations in coefficients A_m, B_m, L_m and P_m from which only the ratios of these coefficients can be determined. These ratios provide the coupling factors between the different coefficients. For a nontrivial solution the determinant of this set of equations must vanish. Therefore we have

$$
\begin{vmatrix}
Ce_m(\xi_o) & 0 & -Fek_m(\xi_o)M_m(\alpha_{rs}) & 0 \\[2ex]
0 & Se_m(\xi_o) & 0 & -Gek_m(\xi_o)N_m(\beta_{rs}) \\[2ex]
\dfrac{\omega\varepsilon_1}{\beta}Se_m'(\xi_o) & 0 & \left(\dfrac{k_1^2-\beta^2}{k_o^2-\beta^2}\right)\dfrac{\omega\varepsilon_o}{\beta}Gek_m'(\xi_o) & \\[2ex]
-\left[1-\left(\dfrac{k_1^2-\beta^2}{k_o^2-\beta^2}\right)\right]Se_m(\xi_o) \times R_m(\alpha_{rs},\delta_{ms}) & \dfrac{k_1^2-\beta^2}{k_o^2-\beta^2}\left(\dfrac{\omega\mu}{\beta}\right)Fek_m'(\xi_o) \times M_m(\alpha_{rs}) & \times N_m(\beta_{rs}) & 0 \\
\end{vmatrix} = 0
$$

$$
\left[1-\left(\dfrac{k_1^2-\beta^2}{k_o^2-\beta^2}\right)\right]Ce_m(\xi_o) \times Q_m(\beta_{rs},\chi_{ms})
\qquad
\dfrac{\omega\mu}{\beta}Ce_m'(\xi_o)
$$

(38)

Putting

$$x^2 = q^2 \cosh^2 \xi_0 (k_1^2 - \beta^2) \tag{39}$$

$$y^2 = -q^2 \cosh^2 \xi_0 (k_0^2 - \beta^2) \tag{40}$$

after some extensive algebraic manipulation equation 38 finally yields

the transcendental characteristic equation for the $_e HE_{mn}^{(1)}$ mode

$$\left[\frac{1}{x^2} \frac{Ce_m'(\xi_0)}{Ce_m(\xi_0)} + \frac{1}{y^2} \frac{Fek_m'(\xi_0)}{Fek_m(\xi_0)} \right] \left[\frac{1}{x^2} \frac{Se_m'(\xi_0)}{Se_m(\xi_0)} + \frac{1}{y^2} \frac{\epsilon_0}{\epsilon_1} \frac{Gek_m'(\xi_0)}{Gek_m(\xi_0)} \right]$$

$$+ \frac{(x^2 + y^2)(x^2 \frac{\epsilon_0}{\epsilon_1} + y^2)}{x^4 y^4} R_m(\alpha_{rs}, \delta_{ms}) Q_m(\beta_{rs}, \chi_{ms}) = 0 . \tag{41}$$

The propagation constant β of the $_e HE_{mn}^{(1)}$ wave can be calculated from

the above characteristic equation, together with the fact that $\beta_0 = \beta_1$

or

$$x^2 + y^2 = k_0^2 q^2 \cosh^2 \xi_0 (\frac{\epsilon_1}{\epsilon_0} - 1) , \tag{42}$$

in terms of the frequency, the size of the guide , the eccentricity of

the guide and the electromagnetic constants of both regions and, of

course, the order of the mode.

The ratios between the different arbitrary constants are important

because they indicate the coupling between the amplitude and phase of

the different field components. From equations 30 through 33, expres-

sing all arbitrary constants in terms of A_m , we obtain

$$\frac{L_m}{A_m} = \frac{Ce_m(\xi_0)}{Fek_m(\xi_0) M_m(\alpha_{rs})} , \tag{43}$$

$$\frac{B_m}{A_m} = \sqrt{\frac{\mu}{\epsilon_o}} \; \frac{(\frac{x^2}{y^2}) \; Fek_m'(\xi_o) M_m(\alpha_{rs})(\frac{L_m}{A_m}) + Ce_m'(\xi_o)}{Se_m(\xi_o)\left[\frac{\sqrt{(x^2+y^2)(x^2+y^2 \frac{\epsilon_1}{\epsilon_o})}}{y^2}\right] R_m(\alpha_{rs}, \delta_{ms})} \;,$$

(44)

and

$$\frac{P_m}{A_m} = \frac{Se_m(\xi_o)}{Gek_m(\xi_o)\mathbf{N}_m(\beta_{rs})} \cdot \frac{B_m}{A_m} \;.$$

(45)

The other three types of principal modes $_e HE_{mn}^{(0)}$, $_o HE_{mn}^{(1)}$, and $_o HE_{mn}^{(0)}$, may be analyzed in a similar manner as outlined above; only their principal results will be given here.

(b) The $_e HE_{mn}^{(0)}$ Mode

The axial field components for the $_e HE_{mn}^{(0)}$ mode are, for region 1 $(0 \leqq \xi \leqq \xi_o)$,

$$H_{z_1} = \sum_{\substack{r=1 \\ odd}}^{\infty} A_r^* \; Ce_r(\xi) \; ce_r(\eta) \; e^{i\beta_1 z},$$

(46)

$$E_{z_1} = \sum_{\substack{r=1 \\ odd}}^{\infty} B_r^* \; Se_r(\xi) \; se_r(\eta) \; e^{i\beta_1 z}$$

(47)

and for region 0 $(\xi_o \leqq \xi < \infty)$,

$$H_{z_0} = L_n^* \; Fek_m(\xi) \; ce_m^*(\eta) \; e^{i\beta_o z}$$

(48)

$$E_{z_0} = P_m^* \; Gek_m(\xi) \; se_m^*(\eta) \; e^{i\beta_o z}$$

(49)

where A_r^*, B_r^*, L_m^* and P_m^* are arbitrary constants. All transverse field components can be obtained from equations 2.2-10 through 2.2-13 using equations 46 through 49.

The two determining equations for the propagation constant are

$$\left[\frac{1}{x^2}\frac{Ce_m'(\xi_o)}{Ce_m(\xi_o)} + \frac{1}{y^2}\frac{Fek_m'(\xi_c)}{Fek_m(\xi_o)}\right]\left[\frac{1}{x^2}\frac{Se_m'(\xi_o)}{Se_m(\xi_o)} + \frac{1}{y^2}\frac{\epsilon_o}{\epsilon_1}\frac{Gek_m'(\xi_o)}{Gek_m(\xi_o)}\right] +$$

$$\frac{(x^2+y^2)(x\frac{\epsilon_o}{\epsilon_1} + y^2)}{x^4 y^4} R_m^*(\alpha_{rs}^*,\delta_{ms}^*)\ Q_m^*(\beta_{rs}^*,\chi_{ms}^*)\ =\ 0 \tag{50}$$

and

$$x^2 + y^2 = k_o^2 q^2 \cosh^2 \xi_o (\frac{\epsilon_1}{\epsilon_o} - 1)\quad , \tag{51}$$

where x^2 and y^2 possess the same definition as those in equations 39 and 40 and

$$\alpha_{rs}^* = \int_0^{2\pi} ce_r(\eta)\ ce_s^*(\eta)d\eta \tag{52}$$

$$\beta_{rs}^* = \int_0^{2\pi} se_r(\eta)\ se_s^*(\eta)d\eta \tag{53}$$

$$\chi_{ms}^* = \int_0^{2\pi} ce_m^{*'}(\eta)\ se_m^*(\eta)d\eta \tag{54}$$

$$\delta_{ms}^* = \int_0^{2\pi} se_m^{*'}(\eta)\ se_m^*(\eta)\ d\eta\quad . \tag{55}$$

These integrals are evaluated in Appendix A.4. $R_m^*(\alpha_{rs}^*,\delta_{ms}^*)Q_m^*(\beta_{rs}^*,\chi_{ms}^*)$ can be obtained in the same way as outlined for $R_m(\alpha_{rs},\delta_{ms})Q_m(\beta_{rs},\chi_{ms})$ in section 2.5a.

(c) The $_o\text{HE}_{mn}^{(1)}$ Mode

The field components for region 1 $(0 \leq \xi \leq \xi_o)$ are

$$H_{z_1} = a_m Se_m(\xi)\, se_m(\eta)\, e^{i\beta z} \tag{56}$$

$$E_{z_1} = b_m Ce_m(\xi)\, ce_m(\eta)\, e^{i\beta z} \tag{57}$$

$$H_{\xi_1} = \frac{i\beta}{p(k_1^2-\beta^2)} \left\{ a_m Se_m'(\xi)\, se_m(\eta) - \frac{\omega\epsilon_1}{\beta}\, b_m Ce_m(\xi)ce_m'(\eta) \right\} e^{i\beta z} \tag{58}$$

$$H_{\eta_1} = \frac{i\beta}{p(k_1^2-\beta^2)} \left\{ a_m Se_m(\xi)\, se_m'(\eta) + \frac{\omega\epsilon_1}{\beta}\, b_m Ce_m'(\xi)ce_m(\eta) \right\} e^{i\beta z} \tag{59}$$

$$E_{\xi_1} = \frac{i\beta}{p(k_1^2-\beta^2)} \left\{ a_m \frac{\omega\mu}{\beta}\, Se_m(\xi)se_m'(\eta) + b_m Ce_m'(\xi)ce_m(\eta) \right\} e^{i\beta z} \tag{60}$$

$$E_{\eta_1} = \frac{i\beta}{p(k_1^2-\beta^2)} \left\{ - a_m \frac{\omega\mu}{\beta}\, Se_m'(\xi)se_m(\eta) + b_m Ce_m(\xi)ce_m'(\eta) \right\} e^{i\beta z}. \tag{61}$$

The field components for region 0 $(\xi_o \leq \xi < \infty)$ are

$$H_{z_o} = \sum_{\substack{r=1 \\ odd}}^{\infty} g_r Gek_r(\xi)\, se_r^*(\eta)\, e^{i\beta z} \tag{62}$$

$$E_{z_o} = \sum_{\substack{r=1 \\ odd}}^{\infty} h_r Fek_r(\xi)ce_r^*(\eta)\, e^{i\beta z} \tag{63}$$

$$H_{\xi_o} = \frac{i\beta}{p(k_o^2-\beta^2)} \sum_{\substack{r=1 \\ odd}}^{\infty} \left\{ g_r Gek_r'(\xi)se_r^*(\eta) - \frac{\omega\epsilon_o}{\beta}\, h_r Fek_r(\xi)ce_r^{*\prime}(\eta) \right\} e^{i\beta z} \tag{64}$$

$$H_{\eta_o} = \frac{i\beta}{p(k_o^2-\beta^2)} \sum_{\substack{r=1 \\ odd}}^{\infty} \left\{ g_r Gek_r(\xi)se_r^{*\prime}(\eta) + \frac{\omega\epsilon_o}{\beta}\, h_r Fek_r'(\xi)ce_r^*(\eta) \right\} e^{i\beta z} \tag{65}$$

$$E_{\xi_o} = \frac{i\beta}{p(k_o^2-\beta^2)} \sum_{\substack{r=1 \\ odd}}^{\infty} \left\{ g_r \frac{\omega\mu}{\beta} Gek_r(\xi) se_r^{*'}(\eta) + h_r Fek_r'(\xi) ce_r^*(\eta) \right\} e^{i\beta z} \quad (66)$$

$$E_{\eta_o} = \frac{i\beta}{p(k_o^2-\beta^2)} \sum_{\substack{r=1 \\ odd}}^{\infty} \left\{ - g_r \frac{\omega\mu}{\beta} Gek_r'(\xi) se_r^*(\eta) + h_r Fek_r(\xi) ce_r^{*'}(\eta) \right\} e^{i\beta z} \quad (67)$$

a_m, b_m, g_r, and h_r are the arbitrary constants. Upon matching the
boundary conditions, one obtains the dispersion relations for the propa-
gation constant

$$\left[\frac{1}{x^2} \frac{Se_m'(\xi_o)}{Se_m(\xi_o)} + \frac{1}{y^2} \frac{Gek_m'(\xi_o)}{Gek_m(\xi_o)} \right] \left[\frac{1}{x^2} \frac{Ce_m'(\xi_o)}{Ce_m(\xi_o)} + \frac{1}{y^2} \frac{\epsilon_o}{\epsilon_1} \frac{Fek_m'(\xi_o)}{Fek_m(\xi_o)} \right]$$

$$+ \frac{(x^2+y^2)(x^2 \frac{\epsilon_o}{\epsilon_1} + y^2)}{x^4 y^4} Q_m(\beta_{rs},\chi_{ms}) R_m(\alpha_{rs},\delta_{ms}) = 0 \quad (68)$$

and

$$x^2 + y^2 = k_o^2 q^2 \cosh^2\xi_o (\frac{\epsilon_1}{\epsilon_o} - 1) , \quad (69)$$

where x^2, y^2, α_{rs}, β_{rs}, χ_{ms}, δ_{ms}, $Q_m(\beta_{rs},\chi_{ms})$ and $R_m(\alpha_{rs},\delta_{ms})$ have
been defined in section 2.5A.

Expressing all arbitrary constants in terms of a_m, we have

$$\frac{g_m}{a_m} = \frac{Se_m(\xi_o)}{Gek_m(\xi_o) N_m(\beta_{rs})} \quad (70)$$

and

$$\frac{b_m}{a_m} = \sqrt{\frac{\mu}{\epsilon_o}} \frac{(\frac{x^2}{y^2})Gek_m'(\xi_o) N_m(\beta_{rs}) (\frac{g_m}{a_m}) + Se_m'(\xi_o)}{Ce_m(\xi_o)\left[\frac{\sqrt{(x^2+y^2)(x^2+y^2 \frac{\epsilon_1}{\epsilon_o})}}{y^2} \right] Q_m(\beta_{rs},\chi_{ms})} \quad (71)$$

and

$$\frac{h_m}{a_m} = \frac{Ce_m(\xi_o)}{Fek_m(\xi_o)M_m(\alpha_{rs})} \frac{b_m}{a_m} \quad , \tag{72}$$

where $N_m(\beta_{rs})$ and $M_m(\alpha_{rs})$ have been defined in section 2.5a .

(d) The $_oHE_{mn}^{(0)}$ Mode

The axial field components for region 1 $(0 \leq \xi \leq \xi_o)$ are

$$H_{z_1} = \sum_{r=1}^{\infty} a_r^* \, Se_r(\xi) \, se_r(\eta) \, e^{i\beta z} \tag{73}$$

$$E_{z_1} = \sum_{r=1}^{\infty} b_r^* \, Ce_r(\xi) \, ce_r(\eta) \, e^{i\beta z} \quad . \tag{74}$$

And the axial field components for region 0 $(\xi_o \leq \xi < \infty)$ are

$$H_{z_o} = g_m^* \, Gek_m(\xi) \, se_m^*(\eta) \, e^{i\beta z} \tag{75}$$

$$E_{z_o} = h_m^* \, Fek_m(\xi) \, ce_m^*(\eta) \, e^{i\beta z} \quad . \tag{76}$$

a_r^*, b_r^*, g_m^* and h_m^* are the arbitrary constants.

The dispersion relations for the propagation constant are

$$\left[\frac{1}{x^2} \frac{Se_m'(\xi_o)}{Se_m(\xi_o)} + \frac{1}{y^2} \frac{Gek_m'(\xi_o)}{Gek_m(\xi_o)} \right] \left[\frac{1}{x^2} \frac{Ce_m'(\xi_o)}{Ce_m(\xi_o)} + \frac{1}{y^2} \frac{\epsilon_o}{\epsilon_1} \frac{Fek_m'(\xi_o)}{Fek_m(\xi_o)} \right]$$

$$+ \frac{(x^2 + y^2)(x^2 \frac{\epsilon_o}{\epsilon_1} + y^2)}{x^4 y^4} Q_m^*(\beta_{rs}^*, \chi_{ms}^*) R_m^*(\alpha_{rs}^*, \delta_{ms}^*) = 0 \tag{77}$$

and

$$x^2 + y^2 = k_o^2 \, q^2 \, \cosh^2 \xi_o \left(\frac{\epsilon_1}{\epsilon_o} - 1 \right) \quad . \tag{78}$$

where x^2, y^2, α_{rs}^*, β_{rs}^*, χ_{ms}^*, δ_{ms}^*, $R_m^*(\alpha_{rs}^*, \delta_{ms}^*)$ and $Q_m^*(\beta_{rs}^*, \chi_{ms}^*)$ are

given in section 2.5b.

Some interesting observations concerning these dispersion relations for the principal modes can be made:

The presence of the factor $R_m(\alpha_{rs}, \delta_{ms}) \, Q_m(\beta_{rs}, \chi_{ms})$ or $R_m^*(\alpha_{rs}^*, \delta_{ms}^*) \, Q_m^*(\beta_{rs}^*, \chi_{ms}^*)$ in the dispersion relations is the result of using an infinite series to represent the field components in one of the two regions. According to Karbowiak's approximations (27), i.e., $ce_m(\eta) = ce_m^*(\eta)$, $se_m(\eta) = se_m^*(\eta)$, $ce_m'(\eta) = -se_m(\eta)m$, and $se_m'(\eta) = ce_m(\eta)m$, one obtains for these principal modes the dispersion relations that are the same as those given above except that the factor $R_m(\alpha_{rs}, \delta_{ms}) \, Q_m(\beta_{rs}, \chi_{ms})$ or $R_m^*(\alpha_{rs}^*, \beta_{ms}^*) \, Q_m^*(\beta_{rs}^*, \chi_{ms}^*)$ is replaced by $-m^2$.

The differences between the dispersion relations for the $_eHE_{mn}^{(1)}$ mode and the $_eHE_{mn}^{(0)}$ mode or the $_oHE_{mn}^{(1)}$ mode and the $_oHE_{mn}^{(0)}$ mode are the factors $R_m(\alpha_{rs}, \delta_{ms}) \, Q_m(\beta_{rs}, \chi_{ms})$ and $R_m^*(\alpha_{rs}^*, \delta_{ms}^*) \, Q_m^*(\beta_{rs}^*, \chi_{ms}^*)$. Numerically speaking, these factors are in general not identical except when $\xi_o = \infty$. It is therefore expected that these modes are not degenerate modes, in general. However, it was found numerically in the next chapter that when $m = 1$ and $n = 1$ within a certain arbitrary region in the x-y plane* $R_1(\alpha_{rs}, \delta_{1s}) \, Q_1(\alpha_{rs}, \chi_{1s}) \approx$ $R_1^*(\alpha_{rs}^*, \delta_{1s}^*) \, Q_1^*(\alpha_{rs}^*, \chi_{1s}^*)$. Thus the $_eHE_{11}^{(1)}$ mode and the $_eHE_{11}^{(0)}$ mode, or the $_oHE_{11}^{(1)}$ mode and the $_oHE_{11}^{(0)}$ mode may be considered degenerate within this region. One may generalize the above

---

*Here x and y are not the components in the rectangular coordinates. x^2 and y^2 are defined by equations 2.5a-39 and 2.5a-40 respectively.
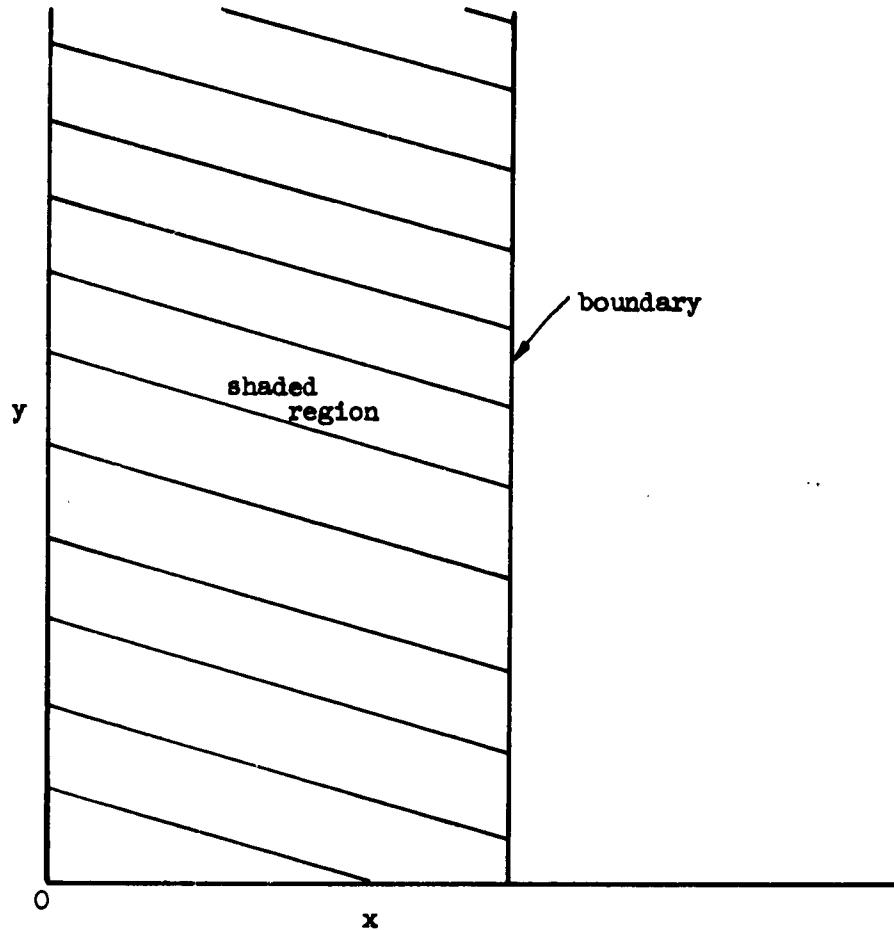
Fig. II-3. The $_e\text{HE}_{mn}^{(1)}$ mode and the $_e\text{HE}_{mn}^{(0)}$ mode, or the $_o\text{HE}_{mn}^{(1)}$ mode and the $_o\text{HE}_{mn}^{(0)}$ mode are almost degenerate within the shaded region. The boundary of the shaded region is quite arbitrary. It is determined according to the allowable differences of $R_m(\alpha_{rs},\delta_{ms})Q_m(\beta_{rs},\chi_{ms})$ and $R_m^*(\alpha_{rs}^*,\delta_{ms}^*)Q_m^*(\beta_{rs}^*, \chi_{ms}^*)$.

observation by stating that in the x-y plane there exists a certain region (shaded in Figure II-2) in which the $_e\text{HE}_{mn}^{(1)}$ and the $_e\text{HE}_{mn}^{(0)}$ mode or the $_o\text{HE}_{mn}^{(1)}$ and the $_o\text{HE}_{mn}^{(0)}$ mode may be considered degenerate. The boundary of this certain region is determined according to the allowable differences between the factor $R_m(\alpha_{rs}, \delta_{ms}) \; Q_m(\beta_{rs}, \cancel{Y}_{ms})$ and the factor $R_m^*(\alpha_{rs}^*, \delta_{ms}^*) \; Q_m^*(\beta_{rs}^*, \cancel{Y}_{ms}^*)$.

2.6 Cutoff Frequencies of the Principal Dominant Modes

It is known that x and y are the roots of the dispersion relations. Combining equations 2.5-39 and 2.5-40 we arrive at the propagation constant

$$\beta = \frac{1}{q \cosh \xi_0} \left[q^2 \cosh^2 \xi_0 k_1^2 - x^2 \right]^{1/2} = \frac{1}{q \cosh \xi_0} \left[q^2 \cosh^2 \xi_0 k_0^2 + y^2 \right]$$

$$= \frac{1}{q \cosh \xi_0} \left[\frac{x^2 + \frac{\epsilon_1}{\epsilon_0} y^2}{\frac{\epsilon_1}{\epsilon_0} - 1} \right]^{1/2} \quad . \tag{1}$$

In order to have a guided wave, β^2, x^2 and y^2 must all be real and positive*. One recalls that the positive and real values of y^2 indicate that the field intensities outside the dielectric rod decay with increasing distance from the surface of the guide. If y^2 is negative and real, the expressions for the field components will indicate the presence of an outgoing radial wave at a large distance from the surface of the dielectric rod, which can only come from an infinitely long

---

*The fact that x^2 and y^2 must all be real and positive offers a way to determine the upper and lower bounds of the propagation constant β. According to equations 2.5-39 and 2.5-40, $\beta^2 \leqq k_1^2$ and $\beta^2 \geqq k_0^2$. Thus $k_0 \leqq \beta \leqq k_1$.

(in the z direction) line type source located at some finite ξ . Such sources have not been postulated in the assumptions. In fact, the concern here is with the source-free problem. Thus y^2 must be positive real for all surface guided waves and consequently the lowest permissible value of y^2 is zero. The propagation constant and the frequency corresponding to this value of y^2 are

$$\beta_{(y^2=0)} = \frac{x}{q \cosh \xi_o \sqrt{(\frac{1}{\epsilon_o} - 1)}} \tag{2}$$

and

$$\omega_{(y^2=0)} = \frac{x}{q \cosh \xi_o \sqrt{(\frac{\epsilon_1}{\epsilon_o} - 1)\mu\epsilon_o}} \tag{3}$$

respectively. x corresponds to the root of the characteristic equation with $y^2 = 0$. The frequency defined by equation 3 is called the cutoff frequency of the wave, since below such frequency the mode can no longer exist on the dielectric guide. Physically it means that below this cutoff frequency the structure can no longer support such a wave and thereby ceases to be a binding medium.

The approximate expressions of the modified Mathieu functions for small x and y are derived in Appendix A.2. For small values of y we have

$$\frac{1}{y^2} \frac{Fek'_m(\xi_o)}{Fek_m(\xi_o)} = \frac{1}{y^2} \left\{ -m - \frac{y^2}{8(m^2-1)} \cdot \frac{e^{2\xi_o}}{\cosh^2\xi_o} [(m+1) + (m-1)e^{-4\xi_o}] + 0(y^4) \right\} ,$$

$$[\text{for } m \geq 3 \ (m \text{ odd})] \tag{4}$$

$$\frac{1}{y^2} \frac{Fek_1'(\xi_0)}{Fek_1(\xi_0)} = \frac{1}{y^2} \left\{ -1 + \frac{y^2 e^{2\xi_0}}{8 \cosh^2 \xi_0} \ln(\frac{e^\alpha y e^{\xi_0}}{4 \cosh \xi_0})[3 - 2e^{-2\xi_0}] + 0(y^4) \right\} \qquad (5)$$

and

$$\frac{1}{y^2} \frac{Gek_m'(\xi_0)}{Gek_m(\xi_0)} = \frac{1}{y^2} \left\{ -m - \frac{y^2}{8(m^2-1)} \cdot \frac{e^{2\xi_0}}{\cosh^2 \xi_0} [(m+1) + (m-1)e^{-4\xi_0}] + 0(y^4) \right\},$$

$$[\text{for } m \geq 3 \quad (m \text{ odd})] \qquad (6)$$

$$\frac{1}{y^2} \frac{Gek_1'(\xi_0)}{Gek_1(\xi_0)} = \frac{1}{y^2} \left\{ -1 + \frac{y^2 e^{2\xi_0}}{8 \cosh^2 \xi_0} \ln(\frac{e^\alpha y e^{\xi_0}}{4 \cosh \xi_0}) [3 + 2e^{-2\xi_0}] + 0(y^4) \right\} \qquad (7)$$

where α is the Euler's constant. For small values of x, we have

$$\frac{1}{x^2} \frac{Ce_m'(\xi_0)}{Ce_m(\xi_0)} = \frac{1}{x^2} \left[\tanh \xi_0 \, G_1 + 0(x^2) \right] , \qquad [\text{for } m \geq 1 \quad (m \text{ odd})] \qquad (8)$$

and

$$\frac{1}{x^2} \frac{Se_m'(\xi_0)}{Se_m(\xi_0)} = \frac{1}{x^2} \left[\coth \xi_0 \, G_2 + 0(x^2) \right] , \qquad [\text{for } m \geq 1 \quad (m \text{ odd})] \qquad (9)$$

where

$$G_1 = \frac{\displaystyle\sum_{r=0}^{\frac{m-1}{2}} (-1)^r \frac{(\frac{m-1}{2} + r)!}{(\frac{m-1}{2} - r)!} \frac{(\cosh \xi_0)^{2r}}{4^{(\frac{m-1}{2} - r)} (2r)!}}{\displaystyle\sum_{r=0}^{\frac{m-1}{2}} (-1)^r \frac{(\frac{m-1}{2} + r)!}{(\frac{m-1}{2} - r)!} \frac{(\cosh \xi_0)^{2r}}{4^{(\frac{m-1}{2} - r)} (2r+1)!}}$$

and

$$G_2 = \cfrac{\displaystyle\sum_{r=0}^{\frac{m-1}{2}} (-1)^r \frac{(\frac{m-1}{2} + r)!}{(\frac{m-1}{2} - r)!} \cfrac{(\sinh \xi_o)^{2r}}{4^{(\frac{m-1}{2} - r)}(2r)!}}{\displaystyle\sum_{r=0}^{\frac{m-1}{2}} (-1)^r \frac{(\frac{m-1}{2} + r)!}{(\frac{m-1}{2} - r)!} \cfrac{(\sinh \xi_o)^{2r}}{4^{(\frac{m-1}{2} - r)}(2r+1)!}} .$$

It can be shown that for small values of x and y to the first order approximation,

$$R_m(\alpha_{rs}, \delta_{ms}) \; Q_m(\beta_{rs}, \mathcal{Y}_{ms}) \approx R_m^*(\alpha_{rs}^*, \delta_{ms}^*) \; Q_m^*(\beta_{rs}^*, \mathcal{Y}_{ms}^*) \approx -m^2 . \tag{10}$$

Substituting the above approximations into the characteristic equation 2.5-41 or 2.5-50, one obtains for the even principal waves

$$x^2 \approx \cfrac{[m(1 + \frac{\epsilon_o}{\epsilon_1}) + (\frac{\epsilon_o}{\epsilon_1} \tanh \xi_o \, G_1 + \coth \xi_o \, G_2)] \, 4(m^2-1)}{\cfrac{e^{2\xi_o}}{\cosh^2 \xi_o} [(m+1) + (m-1) \, e^{-4\xi_o}]} , \tag{11}$$

$$[\text{for} \quad m \ge 3 \; (m \text{ odd})]$$

and

$$x^2 \approx \cfrac{[(1 + \frac{\epsilon_o}{\epsilon_1}) + (\frac{\epsilon_o}{\epsilon_1} \tanh \xi_o + \coth \xi_o)] \, 8}{-\frac{\epsilon_o}{\epsilon_1} \cfrac{e^{2\xi_o}}{\cosh^2 \xi_o} \ell n \, (e^\alpha \cfrac{y \, e^{\xi_o}}{2 \cosh \xi_o})[3 - 2e^{-2\xi_o}]} , \tag{12}$$

$$[\text{for} \quad m = 1].$$

Upon inspection of equation 11 we may immediately conclude that the right hand side of the equation is always positive and non-zero and is not necessarily small for all values of ξ_o and ϵ_o/ϵ_1 , thus x is not zero and is not necessarily small. In other words, the imposed

small x approximation is not valid and x must be determined from
the original characteristic equation 2.5-41 or 2.5-50 with y = 0 .
The same conclusion may be reached for m ≥ 2 (m even) even princi-
pal modes.

From equation 12 it is noted that as y approaches zero
$\ell n(e^{\alpha} \frac{y \, e^{\xi_0}}{2 \cosh \xi_0})$ approaches -∞ , thus the right hand side of this
equation approaches +0 . In other words, as y approaches zero, x
also approaches zero and the imposed small x approximation is valid.
Therefore the cutoff frequency of the $_e HE_{11}^{(1)}$ mode or the $_e HE_{11}^{(0)}$ mode is
zero (refer to equation 3). It should further be noted that the
$_e HE_{11}^{(1)}$ mode and the $_e HE_{11}^{(0)}$ mode are degenerate at zero frequency.

Substituting the above approximate expressions 4, 5, 6, 7, 8, 9
and 10 into the characteristic equation 2.5-68 or 2.5-77, we arrive at
the following expressions for the odd principal waves:

$$x^2 \approx \frac{.4(m^2-1) \, [m(1 + \frac{\epsilon_0}{\epsilon_1}) + (\tanh \xi_0 \, G_1 + \frac{\epsilon_0}{\epsilon_1} \coth \xi_0 \, G_2)]}{\frac{e^{2\xi_0}}{\cosh^2 \xi_0} \, [(m+1) + (m-1) \, e^{-4\xi_0}]} , \qquad (13)$$

$$[\text{for } m \ge 3 \text{ (m odd)}],$$

and

$$x^2 \approx \frac{0[(1 + \frac{\epsilon_0}{\epsilon_1}) + (\tanh \xi_0 + \frac{\epsilon_0}{\epsilon_1} \coth \xi_0)]}{-\frac{\epsilon_0}{\epsilon_1} \frac{e^{2\xi_0}}{\cosh^2 \xi_0} \, \ell n(e^{\alpha} \frac{y \, e^{\xi_0}}{2 \cosh \xi_0})[3 - 2e^{-2\xi_0}]} , \qquad (\text{for } m = 1) . \qquad (14)$$

Similar conclusions as those for the even principal waves are
reached. For the m ≥ 3 (m odd) odd principal waves, the right hand
side of equation 13 is always positive and non-zero, thus x is also

positive and non-zero. It can be shown that the same conclusion applies for the $m \geq 2$ (m even) odd principal waves. However, for the $m = 1$ odd principal wave, according to equation 14, as y approaches zero x must also approach zero. There exists no cutoff frequency for the $_o\text{HE}_{11}^{(1)}$ or $_o\text{HE}_{11}^{(0)}$ mode (refer to equation 3). And at zero frequency the $_o\text{HE}_{11}^{(1)}$ and $_o\text{HE}_{11}^{(0)}$ modes are degenerate.

The results of the analysis in this section are summarized as follows.

i. Along an elliptical dielectric rod there are only two non-degenerate modes, namely the $_e\text{HE}_{11}^{(1)}$ mode and the $_o\text{HE}_{11}^{(1)}$ mode, which possess no cutoff frequencies.

ii. It can be observed from equations 12 and 14 that as the elliptical cross section of the dielectric rod gets flatter, x approaches zero more slowly since $\coth \xi_o$ is very large if ξ_o is very small. This fact has been verified in the next chapter (see Figures III-1 and III-6).

iii. The cutoff frequencies of all the other modes are higher for flatter elliptical cross section rod.

2.7 Transition to Circular Cross Section

As an ellipse degenerates to a circle its semifocal length q tends to zero while ξ_o approaches infinity so that the product $q \cosh \xi_o$ or $q \sinh \xi_o$ or qe^{ξ_o} tends to a constant r_o which is the radius of the degenerated circle. The degenerate forms of the Mathieu and modified Mathieu functions are given in Appendix A.3.

Using these degenerate expressions one obtains the following degenerate forms for the factors appearing in the characteristic equations:

$$\frac{Ce_m'(\xi_o)}{Ce_m(\xi_o)} \rightarrow \frac{x\,J_m'(x)}{J_m(x)} \quad , \tag{1}$$

$$\frac{Se_m'(\xi_o)}{Se_m(\xi_o)} \rightarrow \frac{x\,J_m'(x)}{J_m(x)} \quad , \tag{2}$$

$$\frac{Fek_m'(\xi_o)}{Fek_m(\xi_o)} \rightarrow \frac{y\,K_m'(y)}{K_m(y)} \quad , \tag{3}$$

$$\frac{Gek_m'(\xi_o)}{Gek_m(\xi_o)} \rightarrow \frac{y\,K_m'(y)}{K_m(y)} \quad , \tag{4}$$

$$\alpha_{rs} \approx \alpha_{rs}^* \approx \beta_{rs} \approx \beta_{rs}^* \rightarrow 1 \qquad \text{when } r = s \tag{5}$$
$$\rightarrow 0 \qquad \text{when } r \neq s$$

$$\delta_{ms} \approx \delta_{ms}^* \approx -\gamma_{ms} \approx -\gamma_{ms}^* \rightarrow m \qquad \text{when } m = s \tag{6}$$
$$\rightarrow 0 \qquad \text{when } m \neq s$$

$$R_m(\alpha_{rs},\gamma_{ms})\,Q_m(\beta_{rs},\gamma_{ms}) \approx R_m^*(\alpha_{rs}^*,\gamma_{ms}^*)\,Q_m^*(\beta_{rs}^*,\gamma_{ms}^*) \rightarrow -m^2 \tag{7}$$

with $x^2 = r_o^2(k_1^2 - \beta^2)$ and $y^2 = r_o^2(\beta^2 - k_o^2)$. Putting these degenerate expressions into any one of the characteristic equations for the four types of principal modes yields

$$\left[\frac{1}{x}\frac{J_m'(x)}{J_m(x)} + \frac{1}{y}\frac{K_m'(y)}{K_m(y)}\right]\left[\frac{1}{x}\frac{J_m'(x)}{J_m(x)} + \frac{\epsilon_o}{\epsilon_1}\frac{1}{y}\frac{K_m'(y)}{K_m(y)}\right]$$

$$= m^2\frac{(x^2+y^2)(x^2\frac{\epsilon_o}{\epsilon_1} + y^2)}{x^4\,y^4} \tag{8}$$

which is the characteristic equation for the hybrid HE_{mn} mode on a circular dielectric rod. (Compare with equation III-40 in reference (13)).

One can easily show that only one term of the infinite product
series used to represent the field configurations in one of the two
regions remains. The order of this remaining term corresponds to the
order of the single product term representing the field configurations
in the other region. In other words,

$$L_r \rightarrow L_m \qquad \text{when} \quad r = m \qquad\qquad (9)$$
$$\rightarrow 0 \qquad \text{when} \quad r \neq m \; ,$$

$$P_r \rightarrow P_m \qquad \text{when} \quad r = m \qquad\qquad (10)$$
$$\rightarrow 0 \qquad \text{when} \quad r \neq m \; ,$$

$$A_r^* \rightarrow A_m^* \qquad \text{when} \quad r = m \qquad\qquad (11)$$
$$\rightarrow 0 \qquad \text{when} \quad r \neq m \; ,$$

$$B_r^* \rightarrow B_m^* \qquad \text{when} \quad r = m \qquad\qquad (12)$$
$$\rightarrow 0 \qquad \text{when} \quad r \neq m \; ,$$

$$g_r \rightarrow g_m \qquad \text{when} \quad r = m \qquad\qquad (13)$$
$$\rightarrow 0 \qquad \text{when} \quad r \neq m \; ,$$

$$h_r \rightarrow h_m \qquad \text{when} \quad r = m \qquad\qquad (14)$$
$$\rightarrow 0 \qquad \text{when} \quad r \neq m \; ,$$

$$a_r^* \rightarrow a_m^* \qquad \text{when} \quad r = m \qquad\qquad (15)$$
$$\rightarrow 0 \qquad \text{when} \quad r \neq m \; ,$$

$$b_r^* \rightarrow b_m^* \qquad \text{when} \quad r = m \qquad\qquad (16)$$
$$\rightarrow 0 \qquad \text{when} \quad r \neq m \; .$$

It thus appears that the $_e\text{HE}_{mn}^{(1)}$, $_e\text{HE}_{mn}^{(0)}$, $_o\text{HE}_{mn}^{(1)}$, and $_o\text{HE}_{mn}^{(0)}$ modes are
degenerate when the elliptical cross section degenerates to the

circular cross section.

CHAPTER III - NUMERICAL ANALYSIS OF THE DOMINANT MODES

It is the purpose of this chapter to investigate in detail the propagation characteristics of the dominant modes on a lossless elliptical dielectric rod.

After a brief review of the method for computing the numerical values of the Mathieu and modified Mathieu functions, the transcendental characteristic equations derived in the previous chapter for the $_e\text{HE}_{11}^{(1)}$ mode and the $_o\text{HE}_{11}^{(1)}$ mode are solved. Several graphs showing how the propagation constants vary with parameters are given. Interpretations of the results are given. The field configurations and the axial electric field extent of these waves are also considered.

3.1 Computation of the Mathieu and Modified Mathieu Functions

It is known that the periodic Mathieu functions may be expanded in terms of an infinite series of trigonometric functions, and that the corresponding modified Mathieu functions can be expanded in terms of an infinite series of products of Bessel functions (see Appendix A.1). These Bessel function product series converge very rapidly [see McLachlan (45), p.257]. As has been pointed out on page 21, Chapter II, in order that the solutions of the Mathieu differential equation be periodic, the characteristic number c or the separation constant of the wave equation must satisfy a certain transcendental infinite continued-fraction equation which is a function of γ^2.[*] Furthermore, the coefficients of these infinite series are functions of γ^2 and c (42, 45).

---

[*]The infinite continued-fraction equation was first used by Ince (48) in calculating the characteristic numbers; c and γ^2 are defined in equations 2.2-18 and 2.2-19.

Supposing one is interested in obtaining the numerical value of a certain modified Mathieu function of order m , he must first determine the value of the characteristic number which is the root of an infinite continued-fraction transcendental equation and then find the coefficients from the three-term recurrence relations which are functions of γ^2 and c . Substituting these coefficients into the infinite Bessel function product series and carrying out the computations, he then finally obtains the result.

According to the above description, it is quite evident that the task of computing the numerical values for a great number of Mathieu and modified Mathieu functions is very time consuming and laborious. Fortunately it is found that the characteristic numbers and the coefficients for a certain finite range of γ^2 , which is the range of interest for this present problem, have been tabulated and published by the National Applied Mathematics Laboratories of the National Bureau of Standards (49). These tabulated values are used in our computations.

3.2 Solutions of the Characteristic Equations

The solutions of the characteristic equations for the dominant $_e\text{HE}_{11}^{(1)}$ mode and the $_o\text{HE}_{11}^{(1)}$ mode will now be considered. It can be seen that all these transcendental characteristic equations are of the form

$$f(\xi_o, \frac{\epsilon_o}{\epsilon_1}, y, x) = 0 \quad . \tag{1}$$

Knowing ξ_o which determines the eccentricity of the elliptical cross-section and ϵ_o/ϵ_1 which is the relative dielectric constant of the surrounding medium and the medium of the rod, equation 1 reduces to

$$g(y,x) \Big|_{\substack{\xi_o = \text{const.} \\ \epsilon_o/\epsilon_1 = \text{const.}}} = 0 \tag{2}$$

y and x are related to the major axis of the rod, the frequency, the propagation constant and the characteristics of the medium by the relations

$$y^2 = - q^2 \cosh^2 \xi_0 (k_0^2 - \beta^2)$$

and

$$x^2 = q^2 \cosh^2 \xi_0 (k_1^2 - \beta^2) \ ,$$

respectively. In order to have propagating waves on the dielectric rod x and y must both be positive and real. Furthermore, for these dominant modes as y varies from 0 to $+\infty$, x varies from 0 to some finite positive constant which is a function of ϵ_0/ϵ_1 and ξ_0. Equation 2 can most readily be solved by the "cut and try" method. Assuming y to be some finite constant, say y_0, the first root of x can be found by plotting the function $g_{\substack{\xi_0=\text{const.} \\ \epsilon_0/\epsilon_1=\text{const.}}} (y_0, x)$ versus x as x varies from zero and up, and obtaining the first value x_0 where the function is equal to zero. Then by setting y to be another constant, the above process is repeated.

The above method of solution will now be applied to the characteristic equations for the even and odd dominant modes.

(a) The Even Dominant Mode, the $_e HE_{11}^{(1)}$ Mode.

From equation 2.5a-41 setting m = 1 and n = 1, the characteristic equation for the $_e HE_{11}^{(1)}$ mode is

$$\left[\frac{1}{x^2}\frac{Ce_1'(\xi_o)}{Ce_1(\xi_o)} + \frac{1}{y^2}\frac{Fek_1'(\xi_o)}{Fek_1(\xi_o)}\right]\left[\frac{1}{x^2}\frac{Se_1'(\xi_o)}{Se_1(\xi_o)} + \frac{1}{y^2}\frac{\epsilon_o}{\epsilon_1}\frac{Gek'_1(\xi_o)}{Gek_1(\xi_o)}\right]$$

$$+ \frac{(x^2+y^2)(x^2\frac{\epsilon_o}{\epsilon_1}+y^2)}{x^4 y^4}\cdot R_1(\alpha_{rs},\delta_{1s})\ Q_1(\beta_{rs},\chi_{1s}) = 0\ .\quad (3)$$

$R_1(\alpha_{rs},\delta_{1s})$ and $Q_1(\beta_{rs},\chi_{1s})$ are given by (see equations 2.5-36 and 2.5-37)

$R_1(\alpha_{rs},\delta_{1s})\ =$

$$\left\{\delta_{11}-\delta_{13}\frac{\begin{vmatrix}\alpha_{31} & \alpha_{51} & \cdots\\ \alpha_{35} & \alpha_{55} & \cdots\\ \cdots & \cdots & \cdots\end{vmatrix}}{\begin{vmatrix}\alpha_{33} & \alpha_{53} & \cdots\\ \alpha_{35} & \alpha_{55} & \cdots\\ \cdots & \cdots & \cdots\end{vmatrix}} + \delta_{15}\frac{\begin{vmatrix}\alpha_{31} & \alpha_{51} & \cdots\\ \alpha_{33} & \alpha_{53} & \cdots\\ \cdots & \cdots & \cdots\end{vmatrix}}{\begin{vmatrix}\alpha_{33} & \alpha_{53} & \cdots\\ \alpha_{35} & \alpha_{55} & \cdots\\ \cdots & \cdots & \cdots\end{vmatrix}} + \cdots\right\}\frac{1}{C_1}\ ,\quad (4)$$

and

$Q_1(\beta_{rs},\chi_{1s})\ =$

$$\left\{\chi_{11}-\chi_{13}\frac{\begin{vmatrix}\beta_{31} & \beta_{51} & \cdots\\ \beta_{35} & \beta_{55} & \cdots\\ \cdots & \cdots & \cdots\end{vmatrix}}{\begin{vmatrix}\beta_{33} & \beta_{53} & \cdots\\ \beta_{35} & \beta_{55} & \cdots\\ \cdots & \cdots & \cdots\end{vmatrix}} + \chi_{15}\frac{\begin{vmatrix}\beta_{31} & \beta_{51} & \cdots\\ \beta_{33} & \beta_{53} & \cdots\\ \cdots & \cdots & \cdots\end{vmatrix}}{\begin{vmatrix}\beta_{33} & \beta_{53} & \cdots\\ \beta_{35} & \beta_{55} & \cdots\\ \cdots & \cdots & \cdots\end{vmatrix}} + \cdots\right\}\frac{1}{S_1}\ ,\quad (5)$$

where

$$\delta_{1s} = \int_0^{2\pi} se_1'(\eta) \, ce_s(\eta) d\eta \quad , \tag{6}$$

$$\varkappa_{1s} = \int_0^{2\pi} ce_1'(\eta) \, se_s(\eta) d\eta \quad , \tag{7}$$

$$\alpha_{rs} = \int_0^{2\pi} ce_r^*(\eta) \, ce_s(\eta) d\eta \quad , \tag{8}$$

$$\beta_{rs} = \int_0^{2\pi} se_r^*(\eta) \, se_s(\eta) d\eta \quad , \tag{9}$$

$$C_1 = \int_0^{2\pi} ce_1^2(\eta) d\eta \quad , \tag{10}$$

$$S_1 = \int_0^{2\pi} se_1^2(\eta) d\eta \quad . \tag{11}$$

Upon examining the solutions of equations 6 through 11, the following deductions can be made:

(i) $\quad |\delta_{11}| > |\delta_{13}| > |\delta_{15}| > \cdots > |\delta_{1s}|$

(ii) $\quad |\varkappa_{11}| > |\varkappa_{13}| > |\varkappa_{15}| > \cdots > |\varkappa_{1s}|$

(iii) $\quad |\alpha_{11}| > |\alpha_{13}| > |\alpha_{15}| > \cdots > |\alpha_{1s}|$

$$|\alpha_{33}| > \begin{matrix} |\alpha_{13}| \\ \text{or} \\ |\alpha_{31}| \end{matrix} > |\alpha_{35}| > \cdots > |\alpha_{3s}|$$

$$|\alpha_{55}| > \begin{matrix} |\alpha_{15}| \\ \text{or} \\ |\alpha_{51}| \end{matrix} > \begin{matrix} |\alpha_{35}| \\ \text{or} \\ |\alpha_{53}| \end{matrix} > |\alpha_{57}| > \cdots > |\alpha_{5s}|$$

$$\cdots \quad \cdots \quad \cdots \quad \cdots \quad \cdots \quad \cdots$$

(iv) $\quad |\beta_{11}| > |\beta_{13}| > |\beta_{15}| > \cdots > |\beta_{1s}|$

$$|\beta_{33}| > \begin{matrix} |\beta_{13}| \\ \text{or} \\ |\beta_{31}| \end{matrix} > |\beta_{35}| > \cdots > |\beta_{3s}|$$

$$|\beta_{55}| > \begin{matrix} |\beta_{15}| \\ \text{or} \\ |\beta_{51}| \end{matrix} > \begin{matrix} |\beta_{35}| \\ \text{or} \\ |\beta_{53}| \end{matrix} > |\beta_{57}| > \cdots > |\beta_{58}|$$

$$\cdots \qquad \cdots \qquad \cdots \qquad \cdots \qquad \cdots \qquad \cdots$$

It is found that three terms (i.e., $s = 1,3,5$ and $r = 1,3,5$) of the expansion are sufficient to approximate the value $R_1(\alpha_{rs},\delta_{1s})$ $Q_1(\beta_{rs},\chi_{1s})$ in the region of interest $(0 \leqslant x \leqslant 5 , 0 \leqslant y \leqslant 3)$. The validity of the "3-term" approximation can best be illustrated by the numerical values in the following table:

ξ_o	x	y	Exact* $R_1(\alpha_{rs},\delta_{1s})Q_1(\beta_{rs},\chi_{1s})$	3-Term Approx. $R_1(\alpha_{rs},\delta_{1s})Q_1(\beta_{rs},\chi_{1s})$
3.0	1.1	0.1	-0.9999	-0.9999
	2.1	2.9	-0.9999	-0.9999
0.7	1.4	0.1	-0.9999	-0,9999
	2.7	2.9	-0.8979	-0.8984
0.2	2.8	0.1	-0.9991	-1.0002
	4.7	1.7	-0.7533	-0.7781

$\xi_o = 3.0$ corresponds to an ellipse with eccentricity = 0.0932 (or the ratio of semi-minor to semi-major = 0.995) which is very close to a circle. The value of $R_1(\alpha_{rs},\delta_{1s})Q_1(\beta_{rs},\chi_{1s})$ for a circular rod is exactly 1.00000 for all values of x and y . As ξ_o gets smaller, i.e., as the ellipse gets flatter , the dependence of $R_1(\alpha_{rs},\delta_{1s})$ $Q_1(\beta_{rs},\chi_{1s})$ with x and y becomes more pronounced, and for large

---

*By the exact value we mean the value obtained by using five terms, (i.e., $s = 1,3,5,7,9$ and $r = 1,3,5,7,9$.) of the expansions (equations 6 through 11).

values of x or y the value of $R_1(\alpha_{rs}, \delta_{ls})Q_1(\beta_{rs}, \chi_{ls})$ gets quite

small. It means that more terms of the expansions (equations 6 through

11) are required to obtain the value of $R_1(\alpha_{rs}, \delta_{ls})Q_1(\beta_{rs}, \chi_{ls})$ and

the field components of the mode, as the ellipse becomes flatter and

approaches a strip. Consequently, the computations become more involved.

However, if we limit our interest to only the region $\infty \leq \xi_0 \leq 0.2$,

$0 \leq x \leq 5$ and $0 \leq y \leq 3$, the "three-term approximation" is sufficient

for our computations.

According to the discussion in section 2.5 it is known that the

$_e HE_{11}^{(1)}$ and $_e HE_{11}^{(0)}$ modes cannot in general be considered degenerate

except in a certain region. It can be seen from the following table

that our region of interest is within this region.

ξ_0	x	y	3-Term Approx. $R_1(\alpha_{rs}, \delta_{ls})(Q_1(\beta_{rs}, \chi_{ls})$	3-Term Approx. $R_1^*(\alpha_{rs}^*, \delta_{ls}^*)Q_1^*(\beta_{rs}^*, \chi_{ls}^*)$
3.0	1.1	0.1	-0.9999	-0.9999
	2.1	2.9	-0.9999	-0.9999
0.7	1.4	0.1	-0.9999	-0.9999
	2.7	2.9	-0.8984	-0.8990
0.2	2.8	0.1	-1.0002	-1.0004
	4.7	1.7	-0.7781	-0.7805

Since in this region $R_1(\alpha_{rs}, \delta_{ls})Q_1(\beta_{rs}, \chi_{ls}) \approx R_1^*(\alpha_{rs}^*, \delta_{ls}^*)Q_1^*(\beta_{rs}^*, \chi_{ls}^*)$,

one may assume that the $_e HE_{11}^{(1)}$ and $_e HE_{11}^{(0)}$ modes are almost degenerate

and only one of the modes, the $_e HE_{11}^{(1)}$ mode, needs to be considered.

Now we are in a position to compute the roots of the characteristic

equation 3 for the $_e HE_{11}^{(1)}$ mode.

The computations were carried out on a high speed electronic computer, the IBM 7090*. The coefficients $A_r^{(m)}$ and $B_r^{(m)}$ prepared by NBS (49) were stored in the computer's memory cells. A three-point Lagrangian interpolation (50) sub-routine was used to interpolate the coefficients $A_r^{(m)}$ and $B_r^{(m)}$ from the stored values. The number of decimals for the various coefficients obtainable with a maximum error of 2.5 uni·s in the last place by this interpolation method have been tabulated in the NBS Table. It was found that the values of the Mathieu functions or the modified Mathieu functions obtained using these interpolated coefficients were correct at least to the third significant figure. The roots of the characteristic equation were found according to the method outlined on page 60 of this chapter. The results are shown in Figure III-1 for the case of $\epsilon_1/\epsilon_0 = 2.5$ and for various values of ξ_0 ranging from $\xi_0 = 3.0$ to $\xi_0 = 0.2$.

It is required that the propagation constant inside the rod be the same as that outside the rod, i.e., from equations 2.5-39 and 2.5-40 ,

$$x^2 + y^2 = \left(\frac{2q \cosh \xi_0}{\lambda_0}\right)^2 \pi^2 \left(\frac{\epsilon_1}{\epsilon_0} - 1\right) . \tag{12}$$

The intersection of the function in Figure III-1 with the circle, determined by equation 12, gives the values of x and y required. The propagation constant β of the wave is related to x and y by

$$x^2 = \left(\frac{2q \cosh \xi_0}{\lambda_0}\right)^2 \pi^2 \left[\frac{\epsilon_1}{\epsilon_0} - \left(\frac{\lambda_0 \beta}{2\pi}\right)^2\right] \tag{13}$$

and

$$y^2 = \left(\frac{2q \cosh \xi_0}{\lambda_0}\right)^2 \pi^2 \left[\left(\frac{\lambda_0 \beta}{2\pi}\right)^2 - 1\right] \tag{14}$$

---

*The facilities of IBM 7090 were provided by Western Data Processing Center at UCLA.
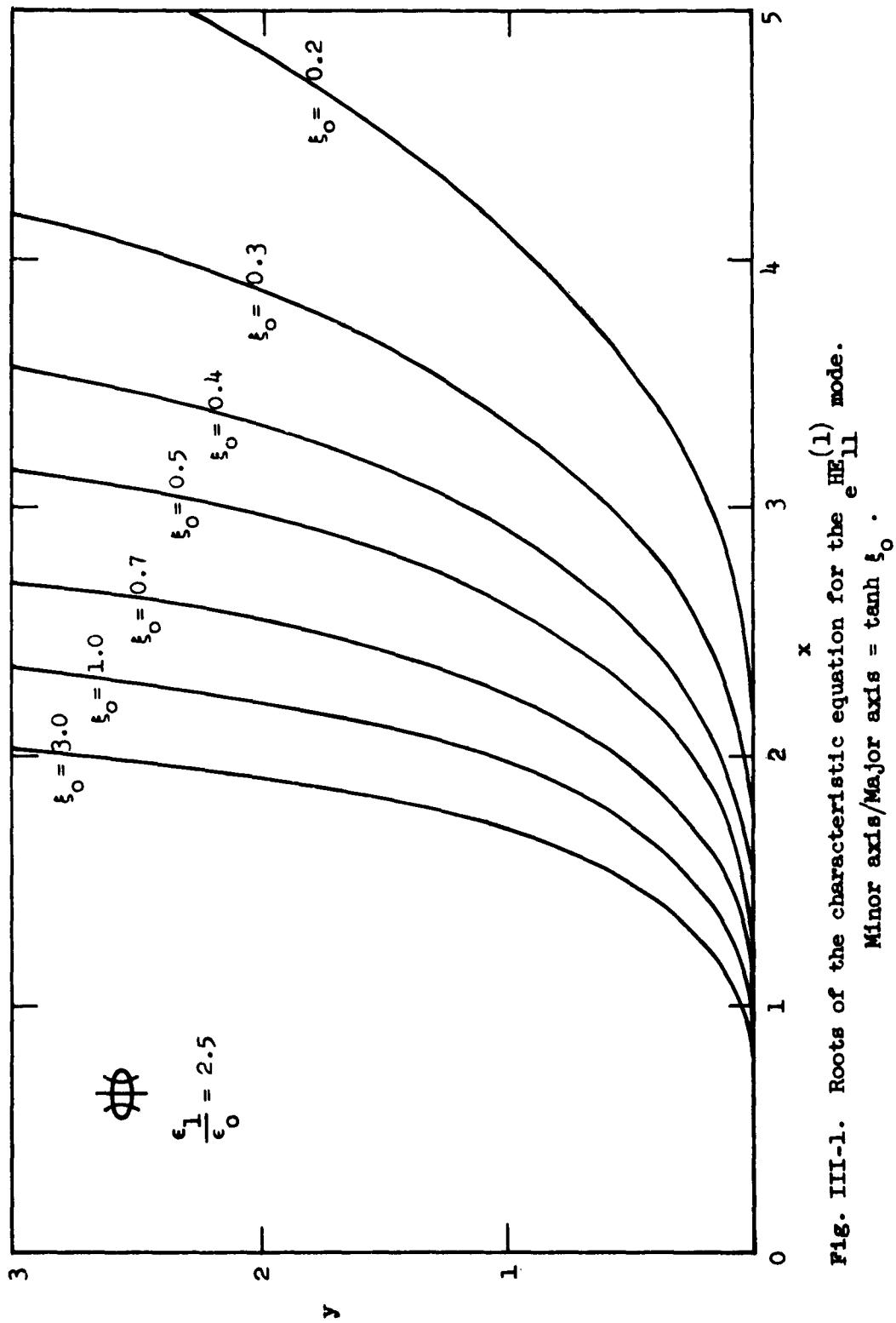
Fig. III-1. Roots of the characteristic equation for the $_e\mathrm{HE}_{11}^{(1)}$ mode. Minor axis/Major axis = $\tanh \xi_o$.
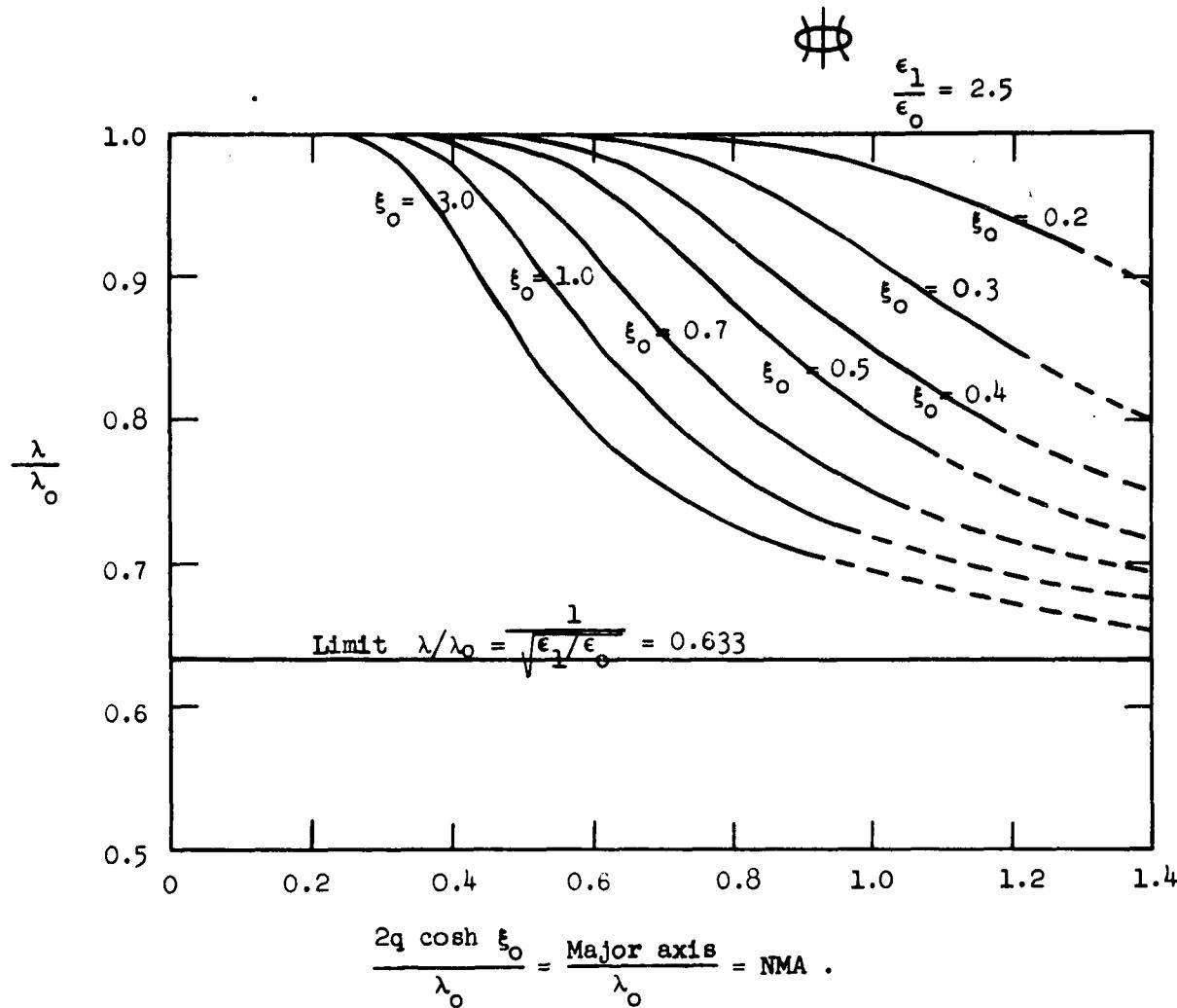
Fig. III-2. Normalized guide wavelength λ/λ_o of the $_e\text{HE}_{11}^{(1)}$ mode as a function of normalized major axis.

respectively, where λ_o is the free-space wavelength. Carrying out

the method outlined above graphically, the results are given in Figure

III-2. The normalized guide wavelength λ/λ_o is plotted against the

normalized major axis $2q \cosh \xi_o / \lambda_o$ for various values of ξ_o in

Figure III-2. It is noted that the guide wavelength λ is related to

the propagation constant β by the relation $\beta = 2\pi/\lambda$ and $2q \cosh \xi_o$

is the major axis of the ellipse. As expected, no cutoff frequency

exists for this dominant $_e\text{HE}_{11}^{(1)}$ mode. For small values of $2q \cosh \xi_o/\lambda_o$

(i.e., the size of the major axis $2q \cosh \xi_o$ compared with the free

space wavelength λ_o is small) the guide wavelength approaches that of

the free space wavelength; for large values of $2q \cosh \xi_o/\lambda_o$, it

approaches asymptotically to the characteristic wavelength of the rod

material, $\lambda_M = \dfrac{\lambda_o}{\sqrt{\epsilon_1/\epsilon_o}}$. For small values of y which correspond to

the small values of $2q \cosh \xi_o/\lambda_o$ the modified Mathieu functions

describing the field outside the dielectric rod decay very slowly;

physically it means that the field strength of the wave falls off very

slowly away from the rod and only a small part of the energy is trans-

ported within the dielectric cylinder. The guide wavelength of this

hybrid $_e\text{HE}_{11}^{(1)}$ mode actually becomes that of a transverse electromag-

netic plane wave* as the size of the dielectric rod becomes vanishingly

small. For very large values of y which correspond to very large

values of $2q \cosh \xi_o/\lambda_o$, the modified Mathieu functions describing

the field outside the dielectric rod disappear very quickly, so the field

strength of the wave outside the rod vanishes very fast and almost all

*Although the wave is propagating at the plane-wave velocity of a medium
it does not follow that the wave is entirely transverse. See reference
(51).

the energy is transported within the dielectric cylinder. The guide

wavelength of the hybrid $_e HE_{11}^{(1)}$ mode approaches that of a TEM plane

wave propagating in a uniform medium filled with a dielectric of

dielectric constant ϵ_1 . The above discussion concerning the field

decay properties of the wave will be substantiated later in this chap-

ter with numerical results.

It may be further observed that for a fixed value of $2q \cosh \xi_o / \lambda_o$

as the ellipse becomes flatter, i.e., as ξ_o becomes smaller, the

guide wavelength becomes closer to the free space wavelength. This

effect can best be illustrated by Figure III-3 in which λ / λ_o is

plotted against ξ_o for various fixed values of $2q \cosh \xi_o / \lambda_o$

The fact that the variation of the curve becomes gentler as

$2q \cosh \xi_o / \lambda_o$ gets smaller is expected, since at very low frequencies

most of the energy is outside the dielectric rod thus the geometry of

the cross-section is not important as far as the guide wavelength is

concerned.

It is also noted that for a fixed value of $2q \cosh \xi_o / \lambda_o$ there

is more binding dielectric material in a circular rod $(\xi_o = \infty)$ than

in a flatter elliptical rod, therefore, (λ / λ_o) is smaller for larger

ξ_o . However, this is not the only reason. Supposing we plotted

λ / λ_o against the normalized cross-sectional area, $(\dfrac{2q \cosh \xi_o}{\lambda_o})^2 \tanh \xi_o$

for various fixed values of ξ_o in Figure III-4. It can be seen for

very small values of $(\dfrac{2q \cosh \xi_o}{\lambda_o})^2 \tanh \xi_o$, say < 0.05 , that $\lambda / \lambda_o \approx 1$

for all values of ξ_o . As $(\dfrac{2q \cosh \xi_o}{\lambda_o})^2 \tanh \xi_o$ gets larger, the

effect of varying ξ_o becomes more noticeable. For a fixed value of

$(\dfrac{2q \cosh \xi_o}{\lambda_o})^2 \tanh \xi_o$, λ / λ_o is smaller for smaller ξ_o . This behavior
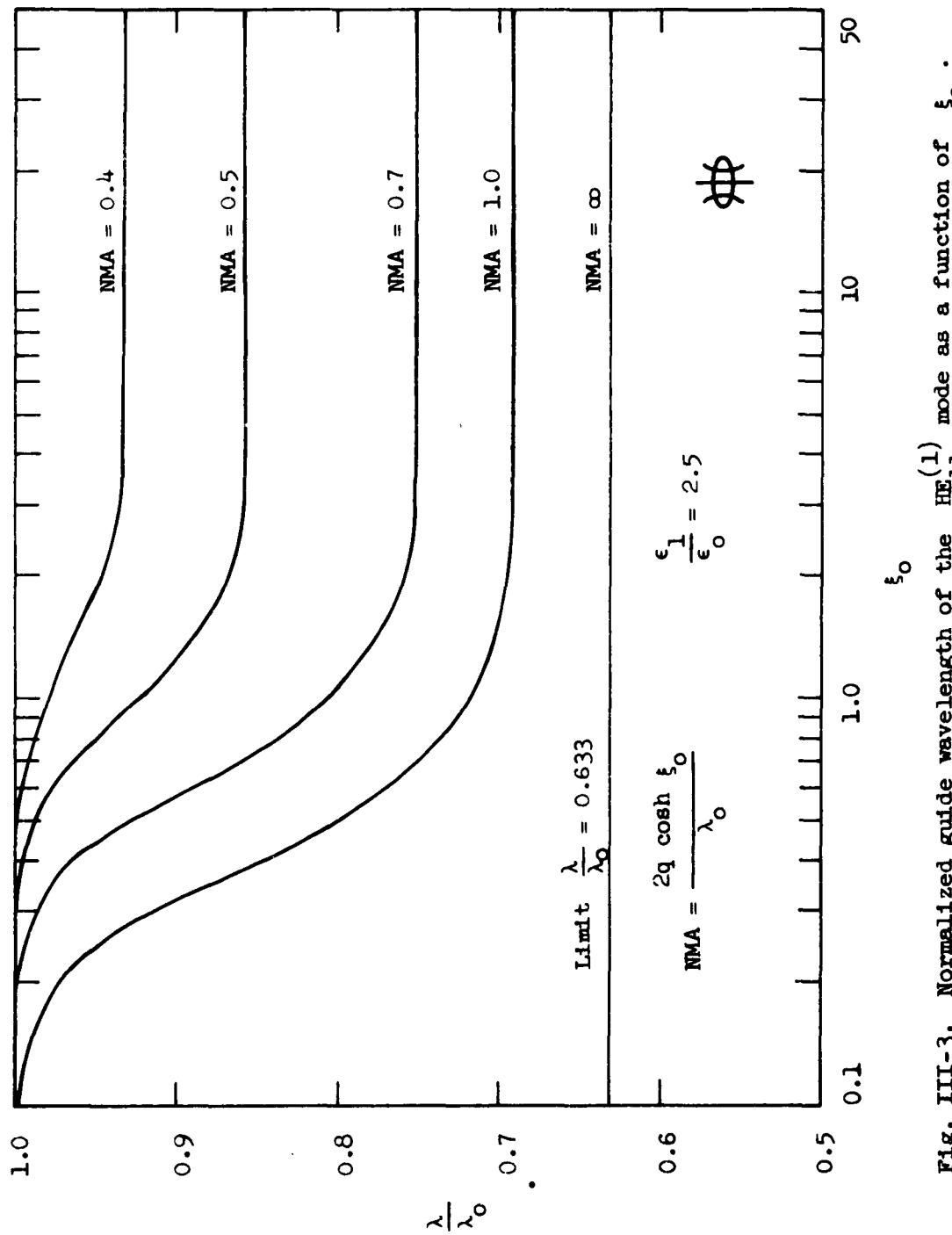
Fig. III-3. Normalized guide wavelength of the $_e\text{HE}_{11}^{(1)}$ mode as a function of ξ_o .
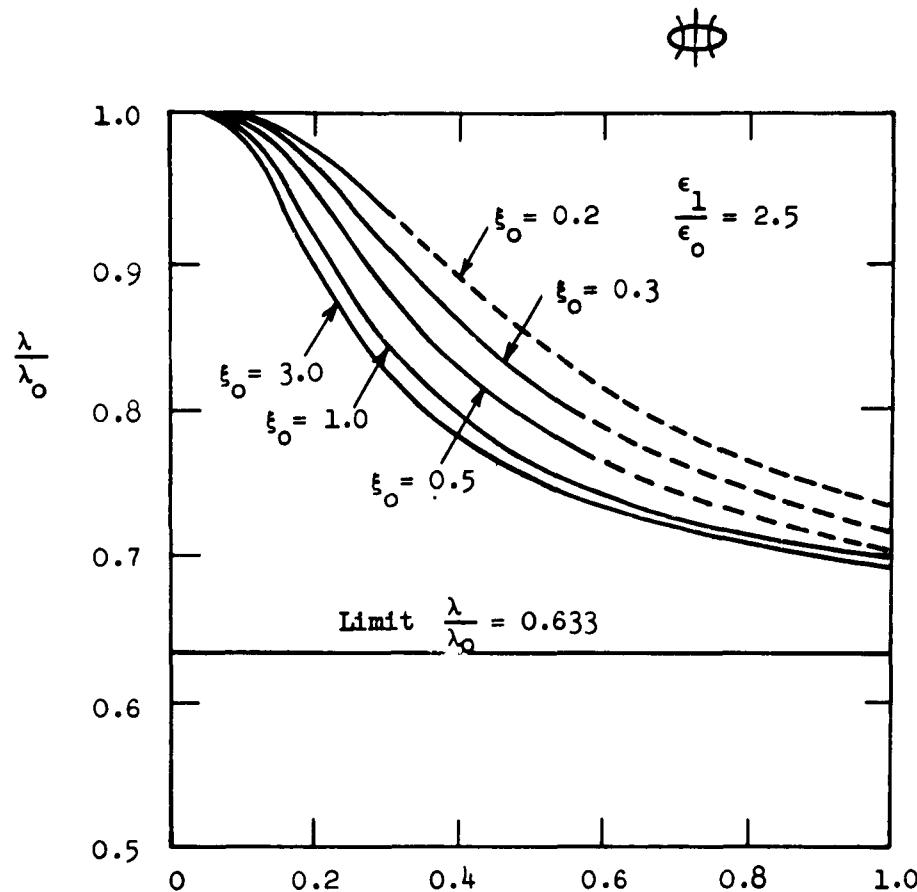
$$\left(\frac{2q \ \cosh \ \xi_o}{\lambda_o}\right)^2 \tanh \xi_o = \frac{4}{\pi} \frac{area}{\lambda_o^2} = NCSA$$

Fig. III-4. Normalized guide wavelength of the $_e HE_{11}^{(1)}$ mode as a function of normalized cross-sectional area.

suggests that the field intensity is more concentrated in a circular rod than in an elliptical rod with the same cross-sectional area, and that more energy is transmitted inside the circular rod. We conclude that the circular dielectric rod is a better binding medium for the $_e\text{HE}_{11}^{(1)}$ mode than an elliptical rod. As $(\frac{2q\ \cosh\ \xi_0}{\lambda_o})^2\tanh\ \xi_0$ becomes very large, the effect of varying ξ_0 on λ/λ_o again becomes quite small, since most of the energy is carried inside the dielectric rod; therefore, the geometry of the cross section is not important. When $\xi_0 \to 0$ and $(\frac{2q\ \cosh\ \xi_0}{\lambda_o})^2\tanh\ \xi_1 \to \infty$, the problem can best be handled by considering the case of a TM wave propagating along a thin sheet of dielectric slab in space. Due to the simple geometry of this equivalent problem, it can be easily analyzed (52). The results will not be given here.

It can be seen from the above numerical results that the $_e\text{HE}_{11}^{(1)}$ mode passes smoothly to the circular HE_{11} mode as $\xi_0 \to \infty$. The $\xi_0 = 3.0$ curve in Figure III-2 is almost identical with that given by Wegener (17).

The effect of the variation of relative dielectric constant ϵ_1/ϵ_o on the propagation constant can be seen readily from Figure III-5. As a representative example, $\xi_0 = 0.7$ is chosen to illustrate the effect. For large values of ϵ_1/ϵ_o, λ approaches to the characteristic wavelength of the rod material, $\lambda_M = \lambda_o/\sqrt{\epsilon_1/\epsilon_o}$ very quickly; and for quite small values of ϵ_1/ϵ_o, i.e., $\epsilon_1/\epsilon_o \to 1$, λ/λ_o varies very slowly with respect to $\frac{2q\ \cosh\ \xi_0}{\lambda_o}$. One may therefore deduce that for constant $\frac{2q\ \cosh\ \xi_0}{\lambda_o}$ and constant ξ_0 more energy is carried within a rod with higher relative dielectric constant and that the field outside the rod also decays faster for the higher dielectric constant rod.
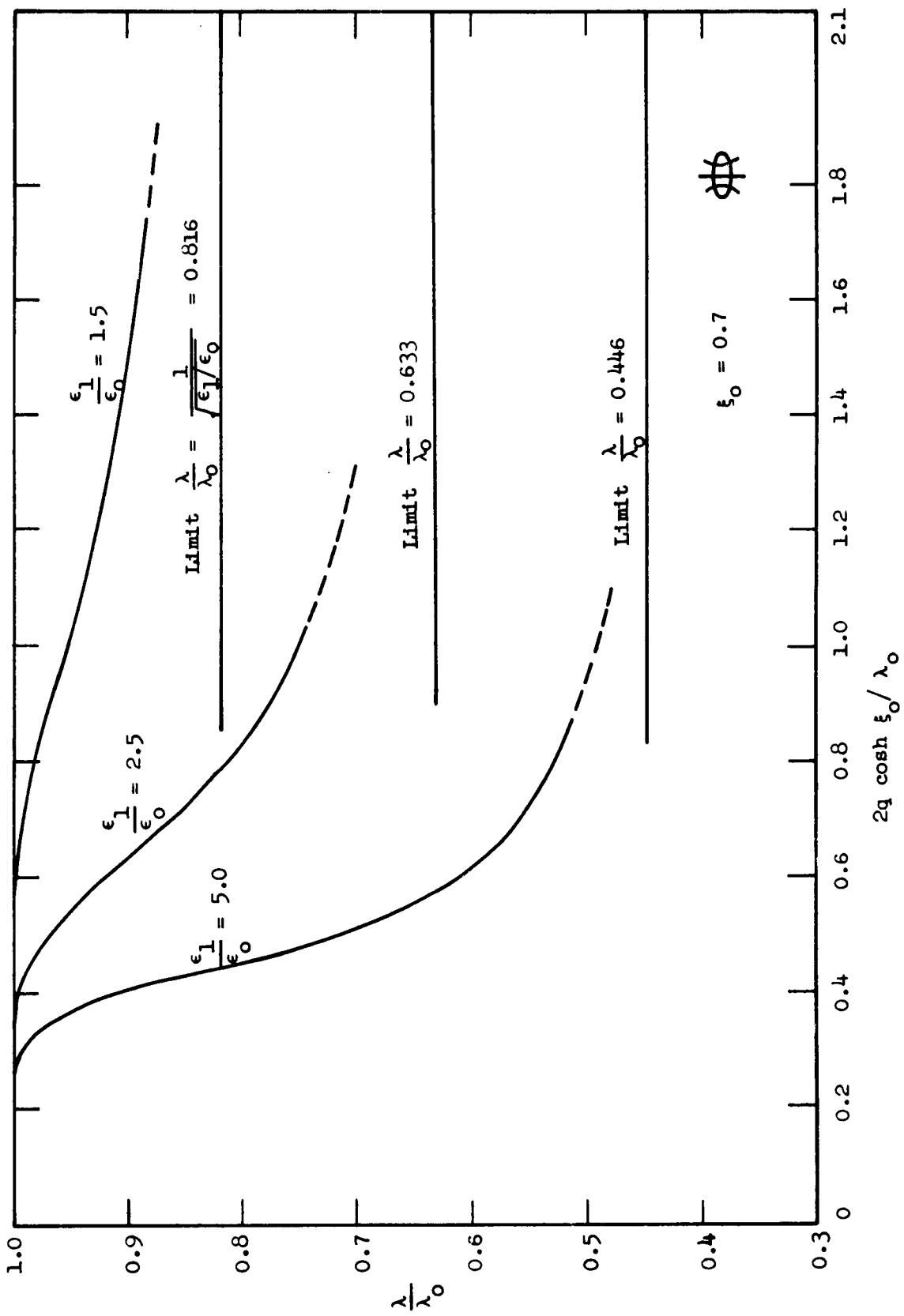
Fig. III-5. Normalized guide wavelength of the $_e\text{HE}_{11}^{(1)}$ mode as a function of normalized major axis for various values of ϵ_1/ϵ_o.

It may then seem that the higher dielectric constant rod is more desirable as a transmission waveguide. Unfortunately the high dielectric constant material usually is associated with a large loss factor (63).

(b) The Odd Dominant Mode, the $_o\text{HE}_{11}^{(1)}$ Mode

Similar procedures as those used for the $_e\text{HE}_{11}^{(1)}$ mode can be applied here to analyze numerically the characteristic equation for the $_o\text{HE}_{11}^{(1)}$ mode. From equation 2.5c-68, setting $m = 1$ and $n = 1$, the characteristic equation for the $_o\text{HE}_{11}^{(1)}$ mode is

$$\left[\frac{1}{x^2} \frac{\text{Se}_1'(\xi_o)}{\text{Se}_1(\xi_o)} + \frac{1}{y^2} \frac{\text{Gek}_1'(\xi_o)}{\text{Gek}_1(\xi_o)} \right] \left[\frac{1}{x^2} \frac{\text{Ce}_1'(\xi_o)}{\text{Ce}_1(\xi_o)} + \frac{1}{y^2} \frac{\epsilon_o}{\epsilon_1} \frac{\text{Fek}_1'(\xi_o)}{\text{Fek}_1(\xi_o)} \right]$$

$$+ \frac{(x^2 + y^2)(x^2 \frac{\epsilon_o}{\epsilon_1} + y^2)}{x^4 y^4} Q_1(\beta_{rs}, \lambda_{1s}) R_1(\alpha_{rs}, \delta_{1s}) \qquad (15)$$

where $R_1(\alpha_{rs}, \delta_{1s})$ and $Q_1(\beta_{rs}, \lambda_{1s})$ have been defined by equations 4 and 5 respectively. The discussion given in section 3.2a concerning the validity of "3-term" approximation for $R_1(\alpha_{rs}, \delta_{1s}) \, Q_1(\beta_{rs}, \lambda_{1s})$ also applies here. Furthermore, since $R_1(\alpha_{rs}, \delta_{1s}) \, Q_1(\beta_{rs}, \lambda_{1s}) \approx R_1^*(\alpha_{rs}^*, \delta_{1s}^*) \, Q_1^*(\beta_{rs}^*, \lambda_{1s}^*)$ within the region of interest (i.e., $0 \leqslant x \leqslant 5$, $0 \leqslant y \leqslant 3$), the $_o\text{HE}_{11}^{(1)}$ mode and the $_o\text{HE}_{11}^{(0)}$ mode are also considered to be degenerate.

Equation 15 is now solved according to the method outlined in section 3.1. Figure III-6 shows the results of this extensive computation. Again y is plotted against x for various values of ξ_o, and a constant value of ϵ_1/ϵ_o which equals 2.5. Combining the results shown in Figure III-6 with equations 12, 13 and 14, the guide wavelength
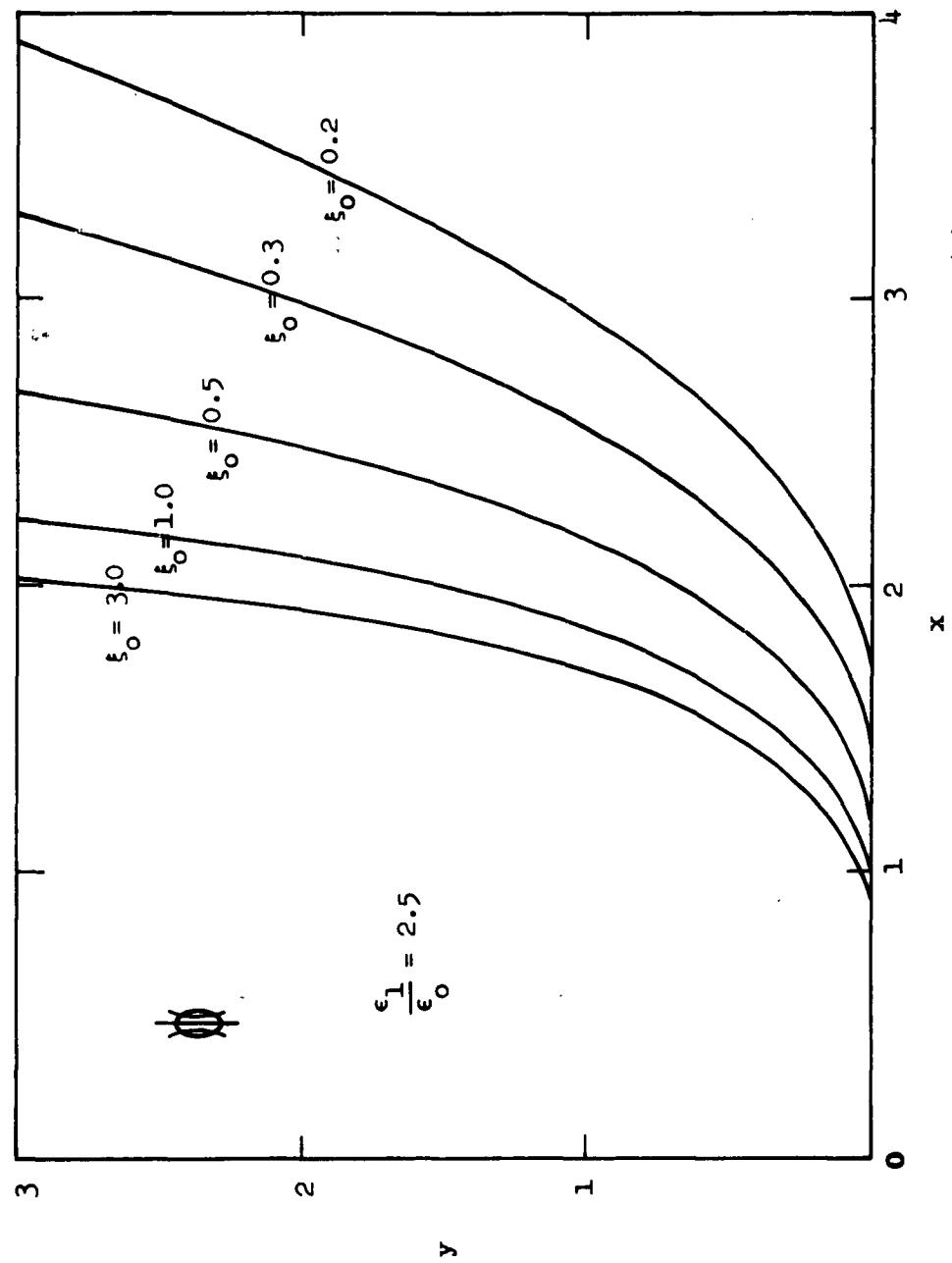
Fig. III-6. Roots of the characteristic equation for the $_{o}HE_{11}^{(1)}$ mode. Minor axis/Major axis = tanh ξ_{o} .

which is a function of ξ_o , ω , the size of the guide, and ϵ_1/ϵ_o can

be obtained. The normalized guide wavelength λ/λ_o versus the nor-

malized major axis $\dfrac{2q \cosh \xi_o}{\lambda_o}$ for various values of ξ_o , and a

constant ϵ_1/ϵ_o is given in Figure III-7. The pattern of the curves

is very similar to that of the $_eHE_{11}^{(1)}$ mode. Again as expected, no cut-

off frequency is observed. When the frequency is low, i.e., $\dfrac{2q \cosh \xi_o}{\lambda_o}$

is small, the guide wavelength becomes that of the free-space wavelength

and most of the energy is being transported outside the dielectric rod;

a small value of $\dfrac{2q \cosh \xi_o}{\lambda_o}$ implies a small value of y , which means

that the field outside the rod decays at a rather low rate. For a large

value of $\dfrac{2q \cosh \xi_o}{\lambda_o}$ the guide wavelength approaches asymptotically the

characteristic wavelength of the rod material $\lambda_M = \lambda_o/\sqrt{\epsilon_1/\epsilon_o}$, almost

all the energy is being transported inside, and the field outside the

rod decays very rapidly.

By comparing Figure III-7 with III-2, it is noted that the dif-

ference between the guide wavelength curves for the $_oHE_{11}^{(1)}$ mode and the

$_eHE_{11}^{(1)}$ mode is more pronounced as ξ_o gets smaller. The normalized

guide wavelength of the $_oHE_{11}^{(1)}$ mode approaches to the limit, $\lambda/\lambda_o =$

$1/\sqrt{\epsilon_1/\epsilon_o}$, faster. For example, when $\xi_o = 0.2$ and $\dfrac{2q \cosh \xi_o}{\lambda_o} = 0.9$,

λ/λ_o for the $_oHE_{11}^{(1)}$ mode is 0.895, while λ/λ_o for the $_eHE_{11}^{(1)}$ mode is

0.987. We conclude that the $_oHE_{11}^{(1)}$ mode binds closer to the dielectric

rod than the $_eHE_{11}^{(1)}$ mode. When ξ_o is larger than 3, the guide wave-

length for the $_oHE_{11}^{(1)}$ mode is almost identical with that for the $_eHE_{11}^{(1)}$

mode, since these modes are degenerate on a circular dielectric guide.

To show the effect of the variation of ξ_o with respect to λ/λ_o

for a fixed value of $\dfrac{2q \cosh \xi_o}{\lambda_o}$, Figure III-8 is introduced. For a

fixed value of $\dfrac{2q \cosh \xi_o}{\lambda_o}$ the curve for the $_oHE_{11}^{(1)}$ mode is smoother

than that for the $_eHE_{11}^{(1)}$ mode. It is again quite evident that when
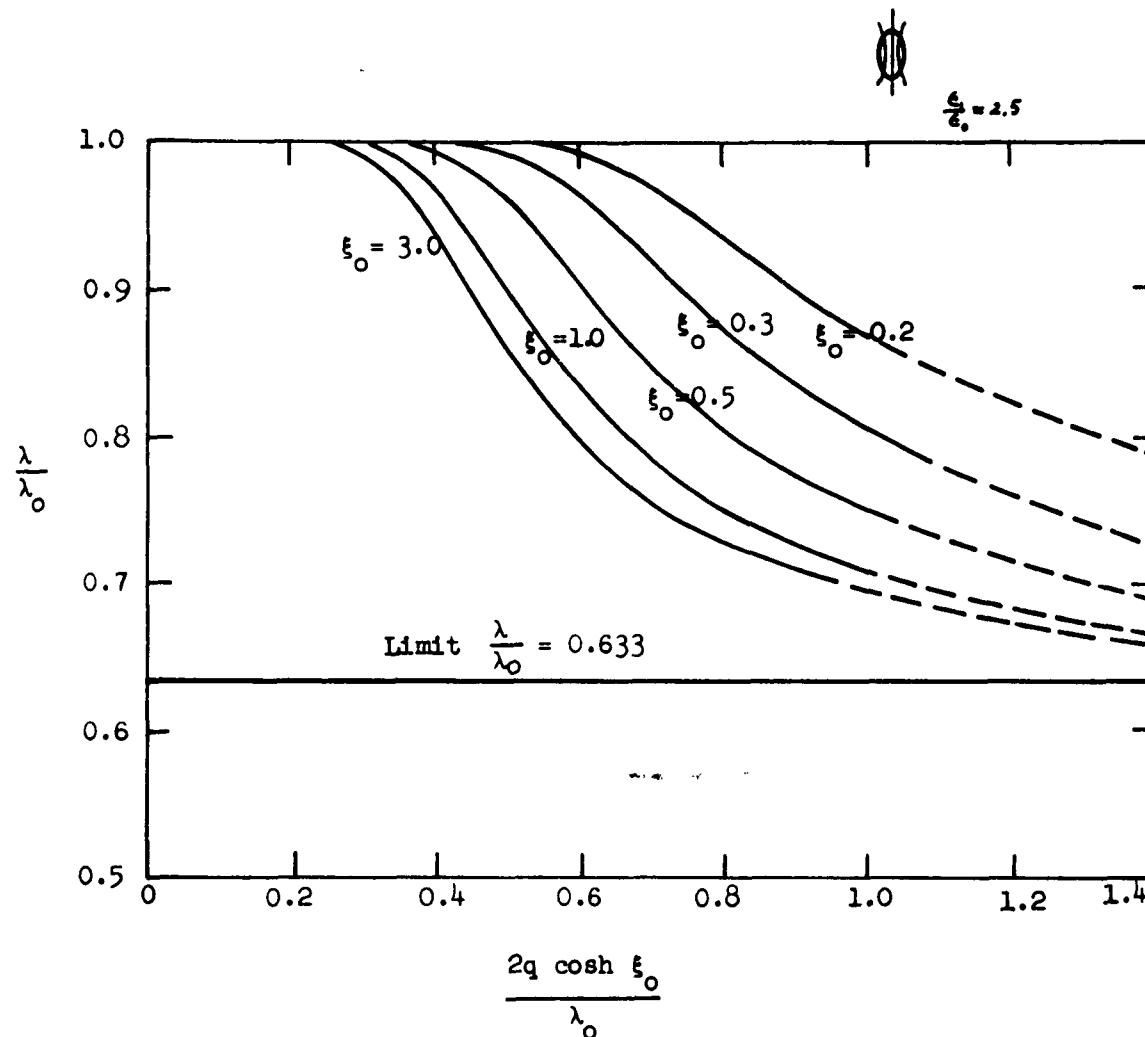
Fig. III-7. Normalized guide wavelength of the $_o\text{HE}_{11}^{(1)}$ mode as a function of normalized major axis.
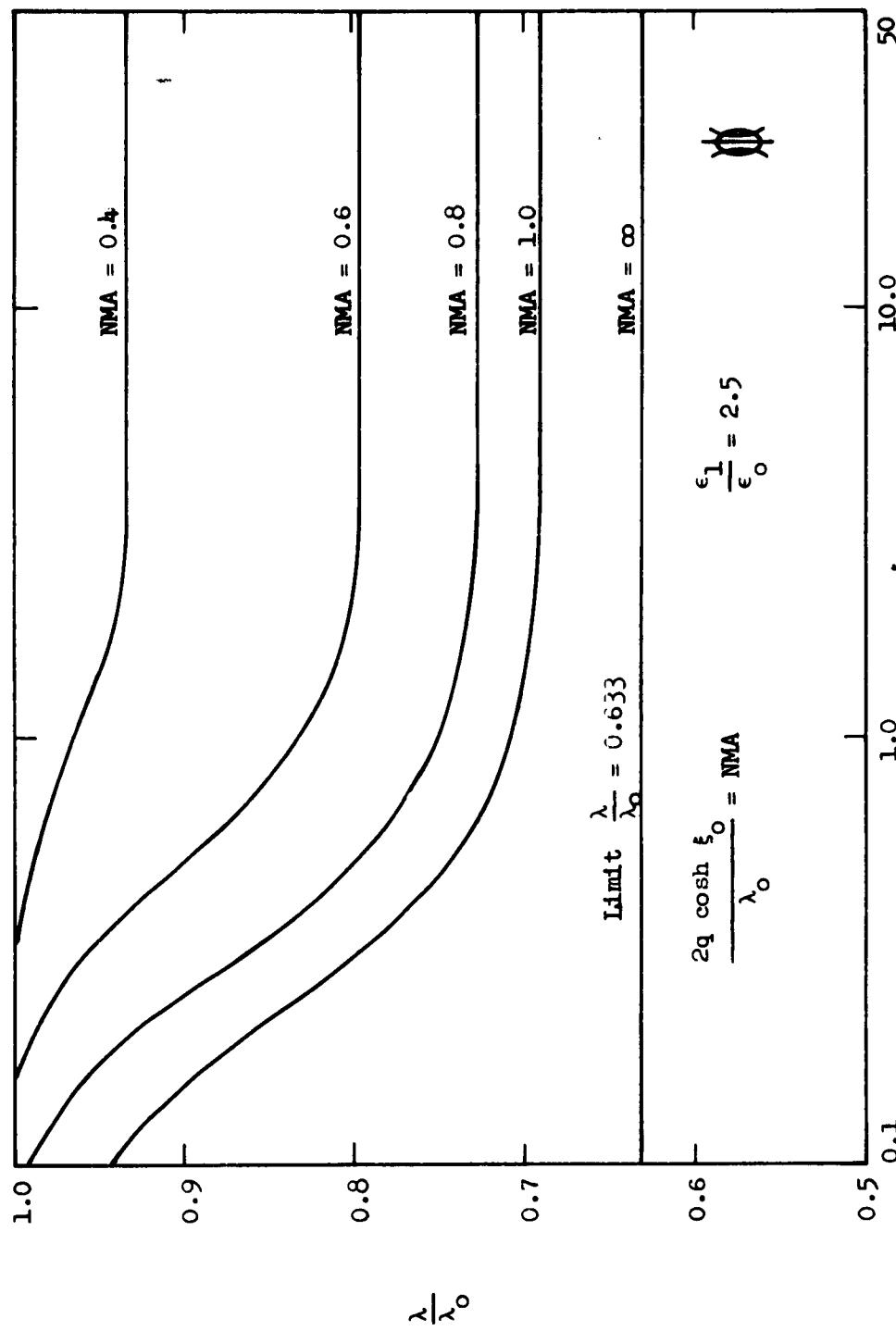
Fig. III-8. Normalized guide wavelength of the $_oHE_{11}^{(1)}$ mode as a function of ξ_o.

$\dfrac{2q \cosh \xi_O}{\lambda_O}$ is very small, λ/λ_O is a constant with respect to the variation of ξ_O . For very large values of $\dfrac{2q \cosh \xi_O}{\lambda_O}$ the geometry of the rod is not important as far as λ/λ_O is concerned.

In Figure III-9 the normalized guide wavelength is plotted against the normalized cross-sectional area, $(\dfrac{2q \cosh \xi_O}{\lambda_O})^2 \tanh \xi_O$ for various values of ξ_O . Unlike the case for the $_e HE_{11}^{(1)}$ mode, it seems that the elliptical rod is a better binding geometry for the $_o HE_{11}^{(1)}$ mode than a circular rod. These curves for various values of ξ_O are quite close to each other, which means physically that the field lines are quite uniform for this $_o HE_{11}^{(1)}$ mode. The slight differences between these curves may be explained by the fact that as a circular rod deforms into an elliptical rod, the electric lines of force are being squeezed together so that the field density is more concentrated. For a very flat elliptical rod, the electric lines of force are almost uniform (the field density is also almost uniform) and any further flattening of the rod would not change the field density too much. Figure III-10 shows the variation of the λ/λ_O versus $\dfrac{2q \cosh \xi_O}{\lambda_O}$ (with ξ_O = const.) curve with respect to the various values of ϵ_1/ϵ_O . The behavior of these curves for the $_o HE_{11}^{(1)}$ mode is very similar to those for the $_e HE_{11}^{(1)}$ mode. It is interesting to note that as ϵ_1/ϵ_O approaches unity, or as ϵ_1/ϵ_O approaches infinity, the λ/λ_O versus $\dfrac{2q \cosh \xi_O}{\lambda_O}$ curve for the $_o HE_{11}^{(1)}$ mode becomes identical with that for the $_e HE_{11}^{(1)}$ mode.

As $\dfrac{2q \cosh \xi_O}{\lambda_O} \to \infty$ and $\xi_O \to 0$, this problem degenerates to the problem of TE wave propagation along a thin sheet of dielectric slab in space (52).

$$\frac{\epsilon_1}{\epsilon_o} = 2.5$$
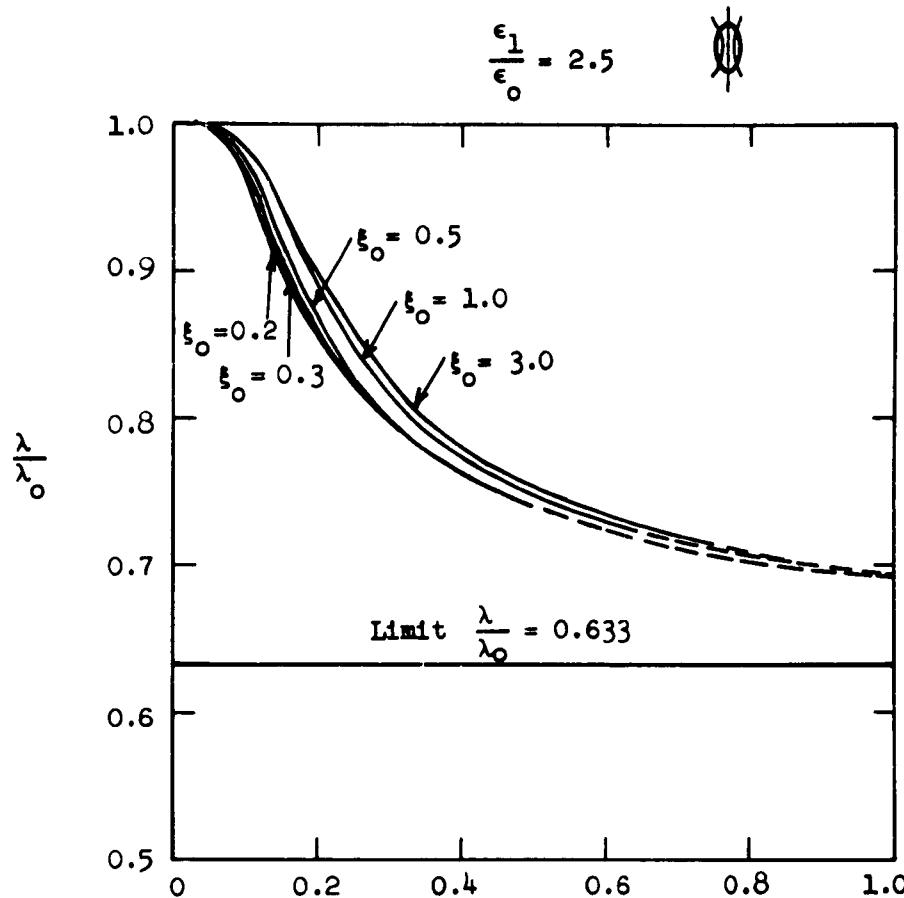
$$\left(\frac{2q \cosh \xi_o}{\lambda_o}\right)^2 \tanh \xi_o = \frac{4}{\pi} \frac{area}{\lambda_o^2} = NCSA$$

Fig. III-9. Normalized guide wavelength of the $_oHE_{11}^{(1)}$ mode as a function of normalized cross-sectional area.
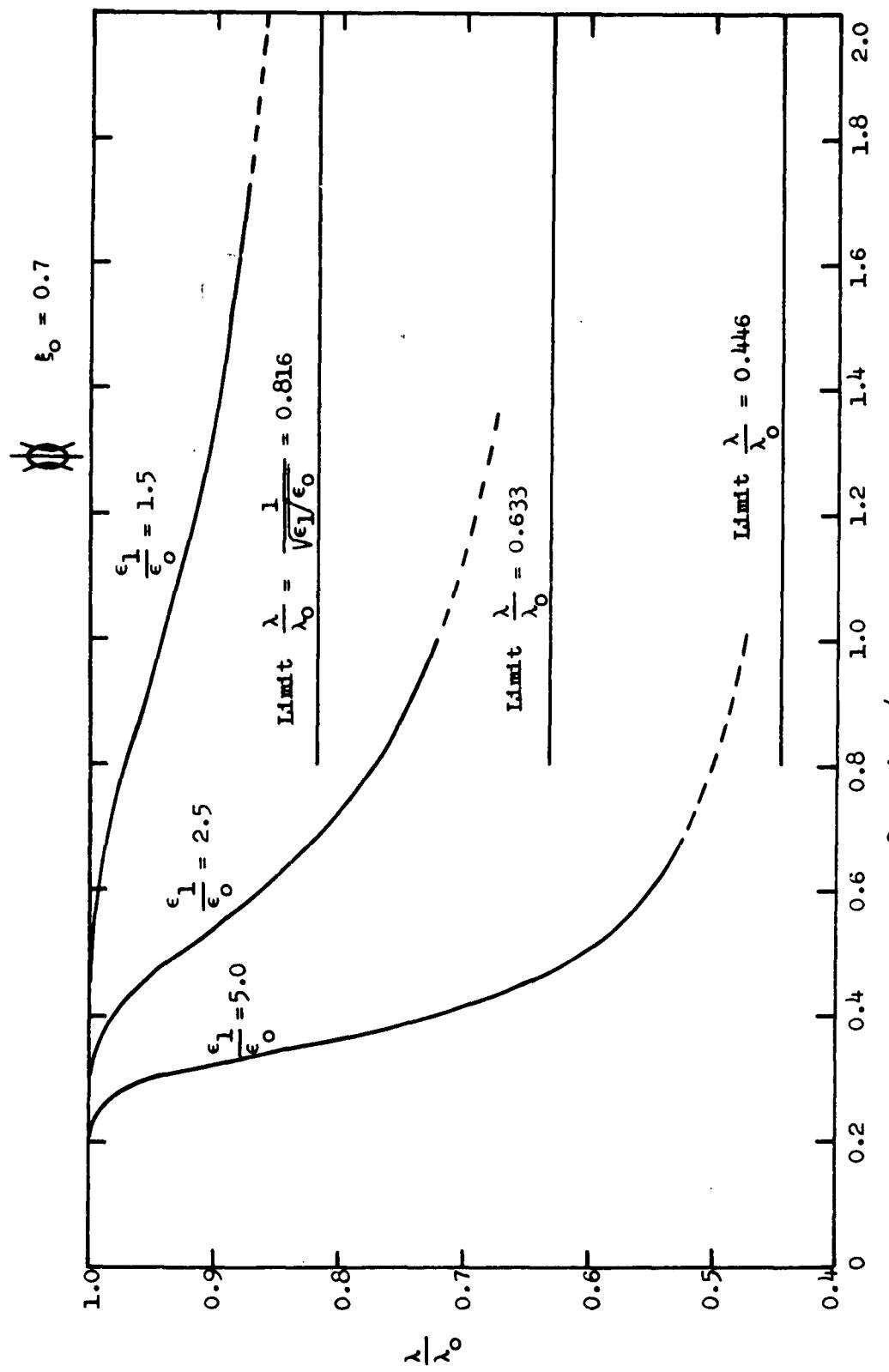
Fig. III-10. Normalized guide wavelength of the $_oHE_{11}^{(1)}$ mode as a function of normalized major axis for various values of ϵ_1/ϵ_o.

3.3 Field Configurations

In practice the field configurations are most quickly found by inspection of the mode functions. It is found that the patterns of the electric and magnetic field lines are quite similar to those known in a hollow metallic guide. However, owing to the absence of the metallic shield around the dielectric, the field is no longer confined to the inner space. Furthermore, due to the absence of conducting walls and therefore the absence of the conduction current, all the electric and magnetic field lines must form closed loops.

Figures III-11a and III-12a show the transverse cross-sectional field distributions of the $_e\mathrm{HE}_{11}^{(1)}$ mode and the $_o\mathrm{HE}_{11}^{(1)}$ mode respectively. The longitudinal cross-sectional views of the field distributions of the $_e\mathrm{HE}_{11}^{(1)}$ mode and the $_o\mathrm{HE}_{11}^{(1)}$ mode are given by Figures III-11b and III-12b. The traveling wave patterns are shown in these figures. Solid lines indicate the electric lines of force; dotted lines represent the magnetic lines of force. Three dimensional sketches of the field configurations for these two dominant modes are shown in Figures III-13 and III-14. The field configurations of these modes are quite similar to the corresponding dominant modes in the metal tube waveguide, as mentioned above; a simple method of excitation is thus available.   The method of excitation of the $_e\mathrm{HE}_{11}^{(1)}$ mode and the $_o\mathrm{HE}_{11}^{(1)}$ mode will be discussed in greater detail in Chapter VI.

3.4 Rate of Field Decay

The dielectric rod waveguide is an open structure and hence the field is not confined within the dielectric rod. Therefore, the guide is susceptible to considerable radiation loss when it is mismatched at

electric lines of force ———
magnetic lines of force — — — —

(a)   (b)
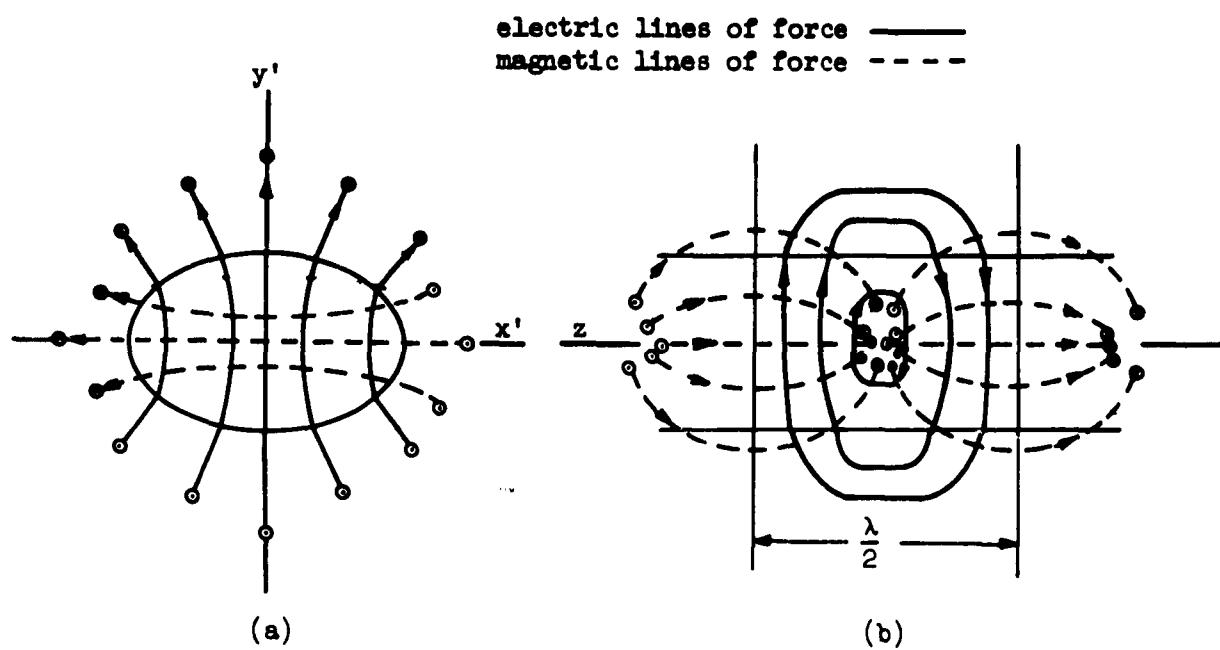
Fig. III-11. Field configuration of the $_e\mathrm{HE}_{11}^{(1)}$ mode.
(a) cross section
(b) longitudinal section


(a)   (b)
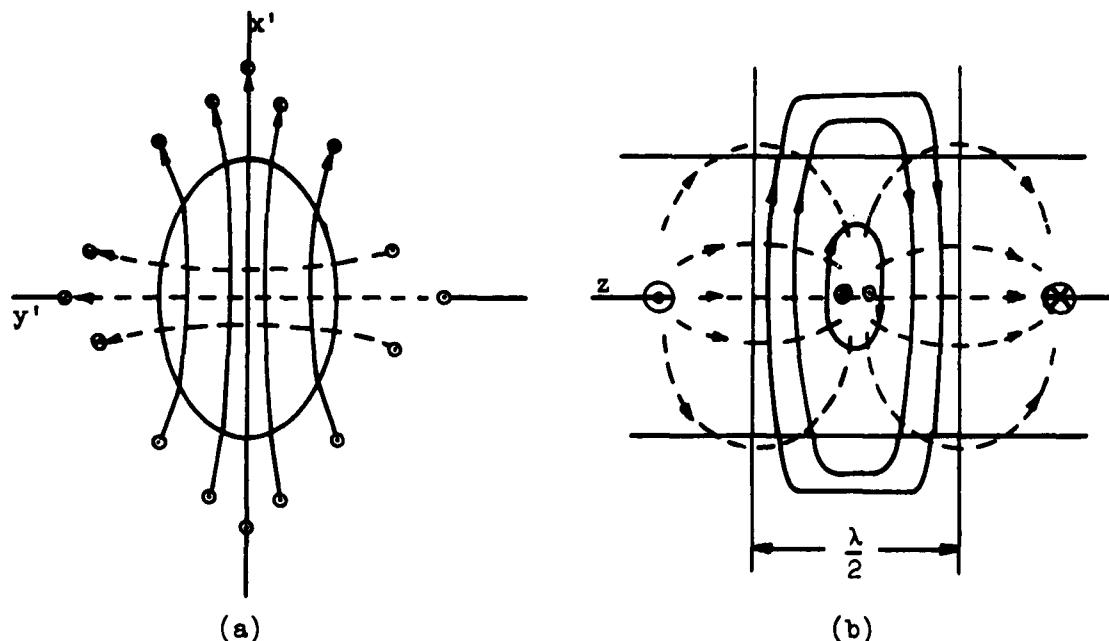
Fig. III-12. Field configuration of the $_o\mathrm{HE}_{11}^{(1)}$ mode
(a) cross section
(b) longitudinal section
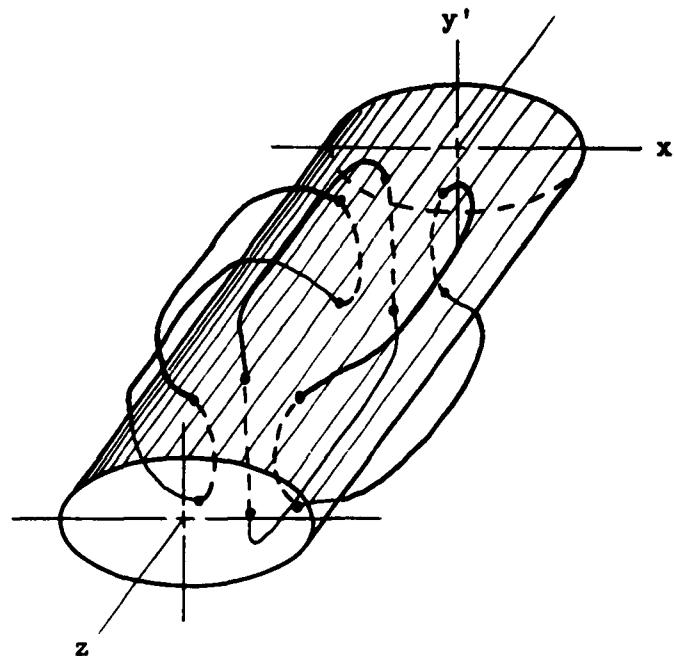
Fig. III-13. A sketch of the electric lines of force for the $_e\text{HE}_{11}^{(1)}$ mode
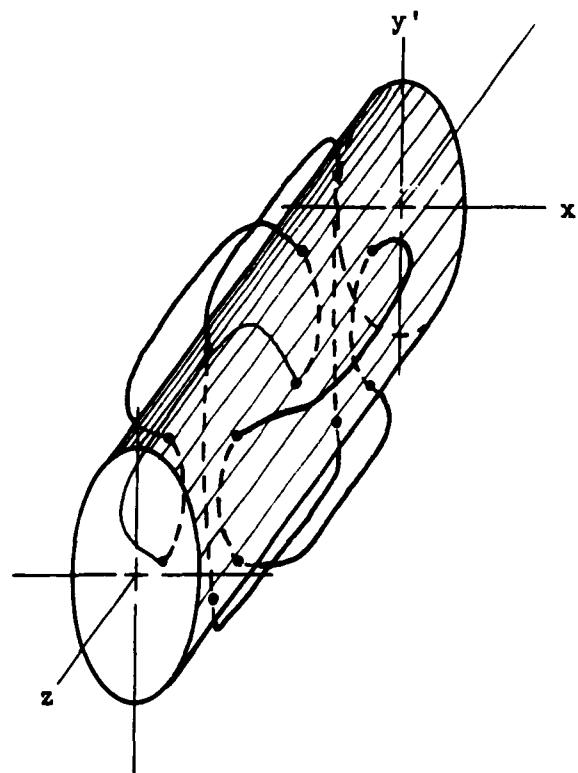

Fig. III-14. A sketch of the electric lines of force for the $_o\text{HE}_{11}^{(1)}$ mode

input and output ends, when it is curved, or when extraneous objects are near it. The knowledge of the external field extent and the rate of field decay outside the rod is very important. It is known from the discussion in section 3.2 that for small values of $\dfrac{2q \cosh \xi_o}{\lambda_o}$ most of the energy is transported outside the dielectric rod, thereby we may expect to have a large field extent and a slow rate of field decay. For large values of $\dfrac{2q \cosh \xi_o}{\lambda_o}$ most of the energy is being carried inside the rod so that the field extent is quite moderate and the rate of field decay is fast. To get an idea of the variation in the rate of field decay and the field extent with respect to the change in $\dfrac{2q \cosh \xi_o}{\lambda_o}$ and ξ_o, numerical results for the longitudinal electric field will be obtained.

(a) The $_e\text{HE}_{11}^{(1)}$ Mode

According to section 2.5a, setting $m = 1$ and $n = 1$, the equation for the external longitudinal electric field of the $_e\text{HE}_{11}^{(1)}$ mode is

$$E_z = \sum_{r=1}^{\infty} P_r \text{Gek}_r(\xi) \; se_r^*(\eta) \; e^{i\beta z} \tag{1}$$

where

$$\frac{P_3}{P_1} = \frac{\text{Gek}_1(\xi_o)}{\text{Gek}_3(\xi_o)} \; \frac{\begin{vmatrix} \beta_{13} & \beta_{53} & \beta_{73} & \cdots \\ \beta_{15} & \beta_{55} & \beta_{75} & \cdots \\ \beta_{17} & \beta_{57} & \beta_{77} & \cdots \\ \cdots & \cdots & \cdots & \cdots \end{vmatrix}}{\begin{vmatrix} \beta_{33} & \beta_{53} & \cdots \\ \beta_{35} & \beta_{55} & \cdots \\ \cdots & \cdots & \cdots \end{vmatrix}} \; , \tag{2}$$

$$\frac{P_5}{P_1} = - \frac{Gek_1(\xi_o)}{Gek_5(\xi_o)} \frac{\begin{vmatrix} \beta_{33} & \beta_{13} & \beta_{73} \\ \beta_{35} & \beta_{15} & \beta_{75} \\ \cdots & \cdots & \cdots \end{vmatrix}}{\begin{vmatrix} \beta_{33} & \beta_{53} & \cdots \\ \beta_{35} & \beta_{55} & \cdots \\ \cdots & \cdots & \cdots \end{vmatrix}} \quad , \tag{3}$$

The above infinite determinants may be solved by the method of successive approximations (47). It is found that

$$P_1 > P_3 \gg P_5 \gg P_7 \cdots \quad . \tag{4}$$

Therefore the external E_z may be approximated by only considering a few terms of the expansion. The normalized external longitudinal electric field is given by

$$\frac{E_z}{E_{z_o}} = \frac{Gek_1(\xi) \; se_1^*(\eta) + \frac{P_3}{P_1} Gek_3(\xi) \; se_3^*(\eta) + \cdots}{Gek_1(\xi_o) \; se_1^*(\eta) + \frac{P_3}{P_1} Gek_3(\xi_o) \; se_3^*(\eta) + \cdots} \quad , \tag{5}$$

where E_z is the axial electric field intensity at ξ and E_{z_o} is the intensity of the axial electric field at $\xi = \xi_o$. Equation 5 is computed for various values of ξ_o and $\frac{2q \cosh \xi_o}{\lambda_o}$ with $\epsilon_1/\epsilon_o = 2.5$ and $\eta = \pi/2$. The results are shown in Figures III-15, 16, 17, 18 and 19 for $\dot{\xi}_o = 3.0$, 1.0, 0.75, 0.5 and 0.3 respectively. A family of

Fig. III-15.

Fig. III-16.

Fig. III-17.

B/B$_o$

Fig. III-18.

$_e\text{HE}_{11}^{(1)}$ mode
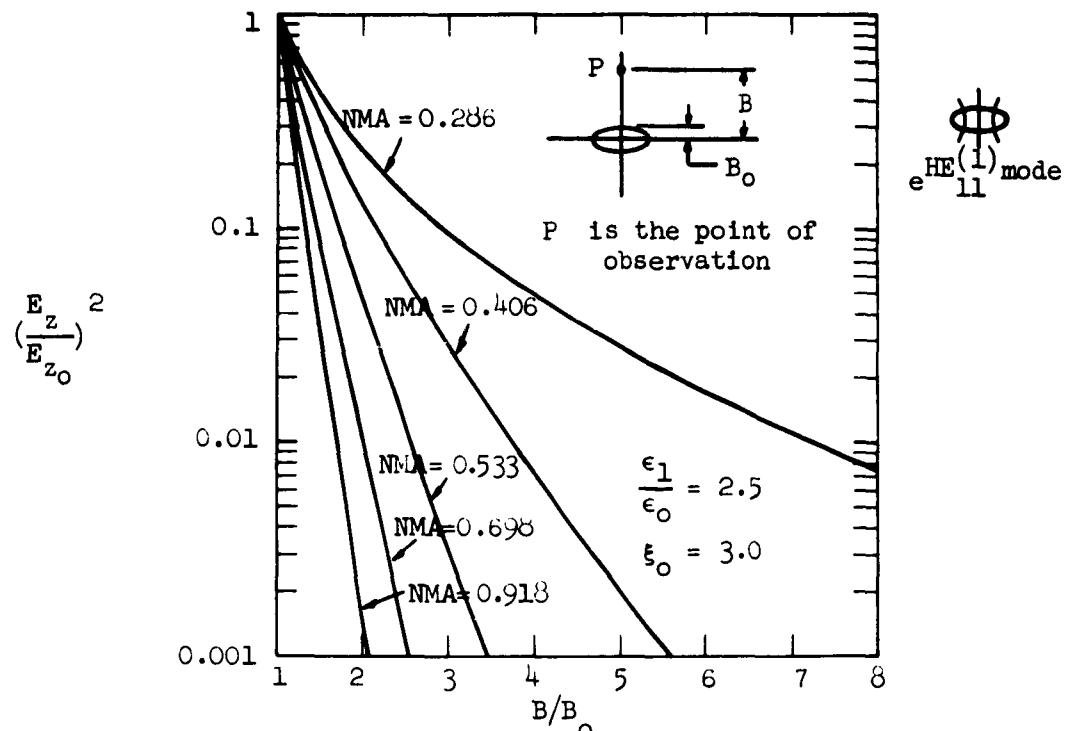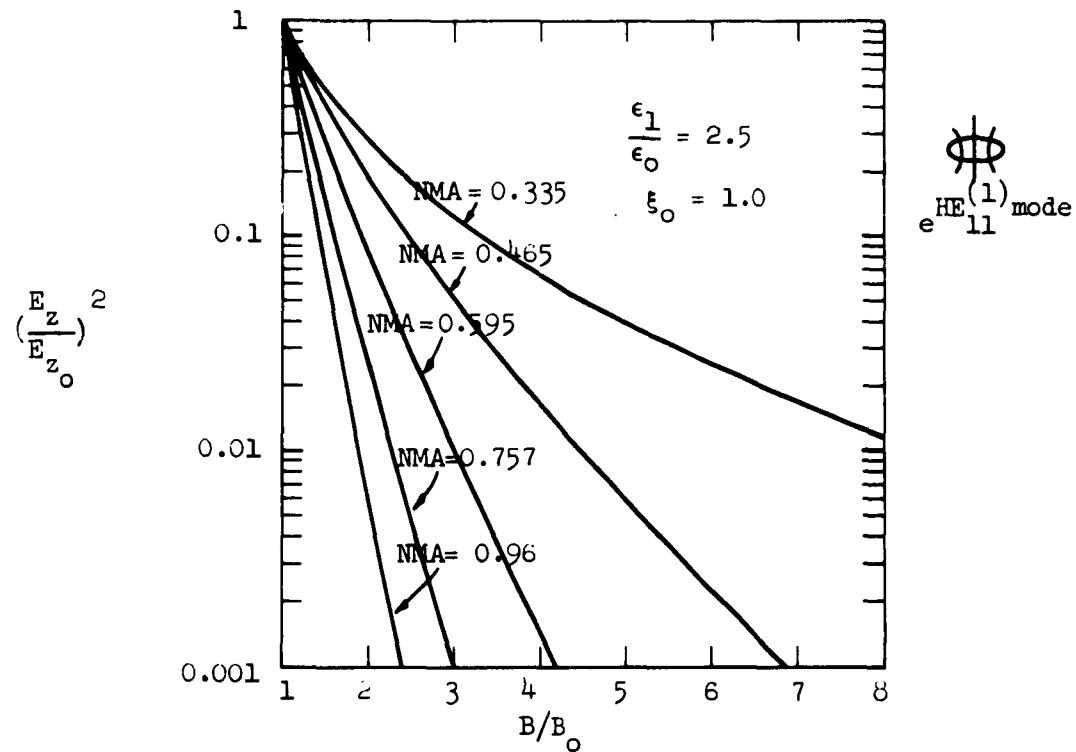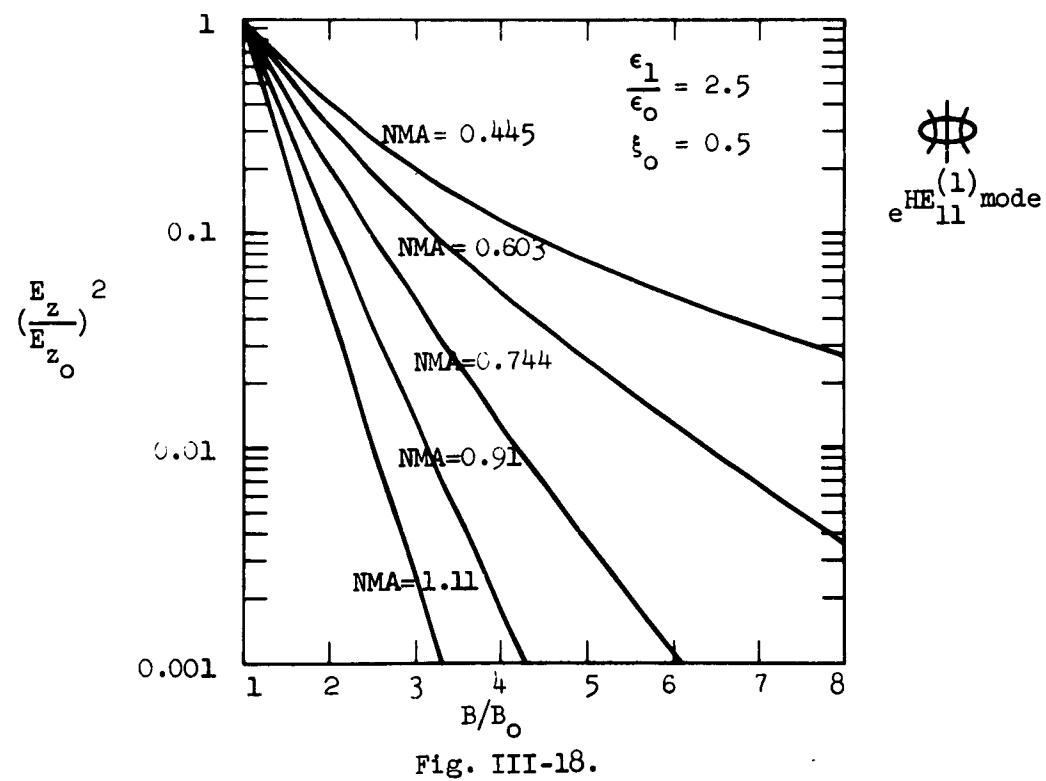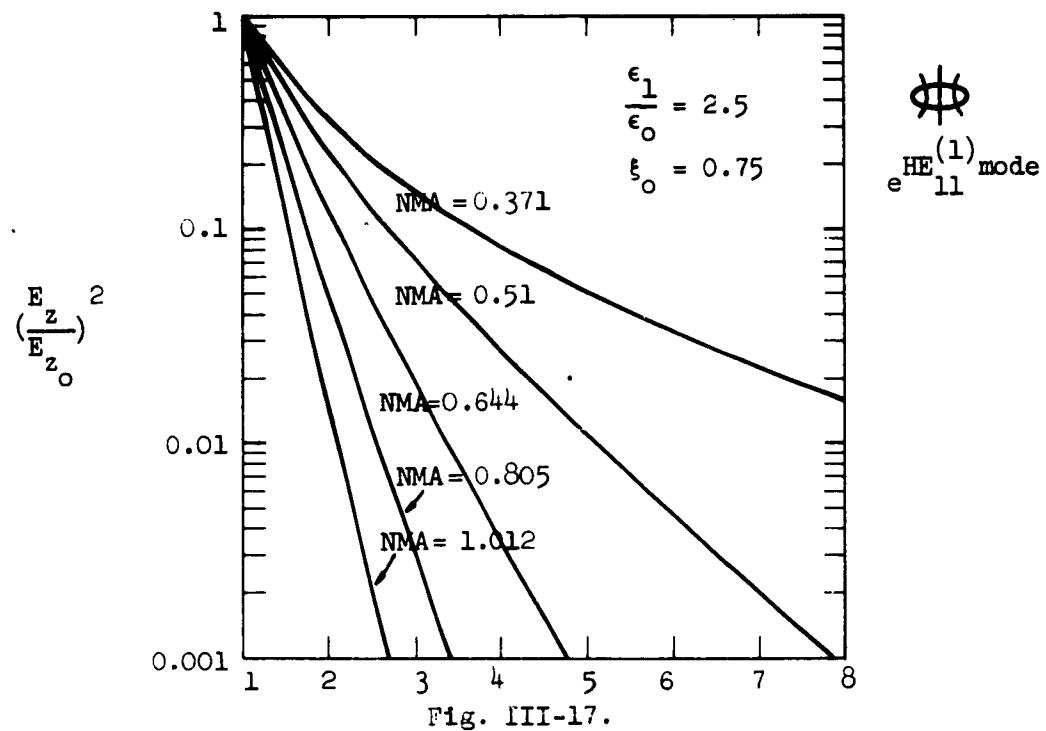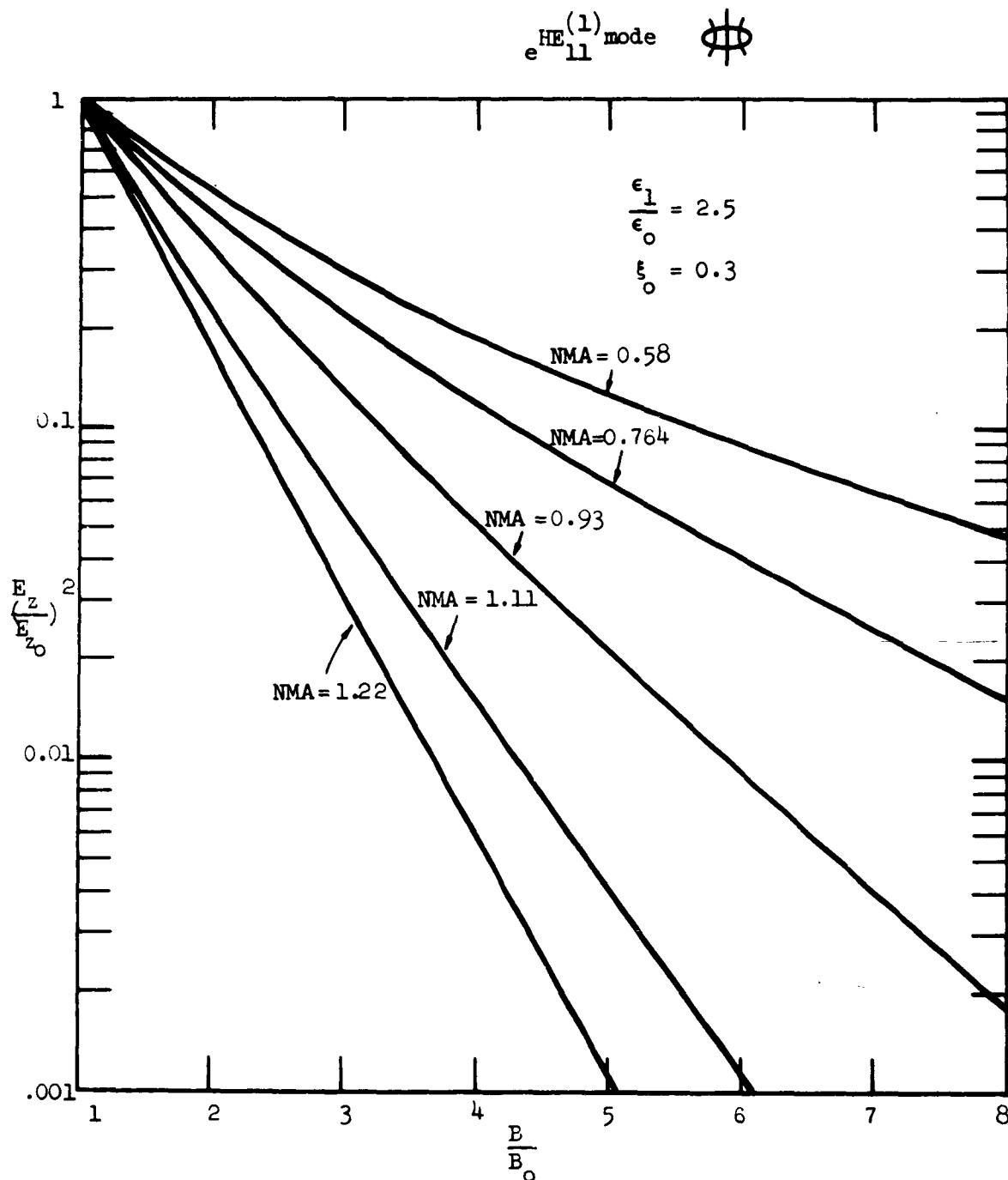

Figure III-19

curves for various values of $\dfrac{2q \cosh \xi_0}{\lambda_0}$ are shown in each figure.*

These figures possess similar characteristics as far as the variation of $\dfrac{2q \cosh \xi_0}{\lambda_0}$ is concerned. The axial electric field decays (not exponentially) much slower and extends much farther for smaller values of $\dfrac{2q \cosh \xi_0}{\lambda_0}$. For large values of $\dfrac{2q \cosh \xi_0}{\lambda_0}$ the field decays exponentially quite rapidly and its extent is quite small. Physically it means more energy is being carried outside the guide for smaller values of $\dfrac{2q \cosh \xi_0}{\lambda_0}$. The same conclusion was reached in the discussion in section 3.2

To observe the effect of axial electric field extent as a function of frequency for various values of eccentricities, we introduce Figure III-20. The field extent, B/B_0 , at which point $(E_z/E_{z_0})^2 = 0.1$ is plotted against the normalized frequency $(\dfrac{2q \cosh \xi_0}{\lambda_0})^2 \tanh \xi_0$ for various ξ_0 . It is quite evident that B/B_0 is larger for the flatter elliptical cross-section rod. As frequency becomes very high the normalized field extent B/B_0 approaches to unity and for low frequencies B/B_0 can get very large. Since B_0 is a function of ξ_0 , it is somewhat difficult to compare the absolute axial electric field extent of a circular rod and that of an elliptical rod having the same cross-sectional area using Figure III-20. Thus Figure III-21 is introduced. B/λ_0 , the normalized absolute field extent, is plotted against the normalized cross-sectional area, $(\dfrac{2q \cosh \xi_0}{\lambda_0})^2 \tanh \xi_0$ for various ξ_0 .

*In each figure $(E_z/E_{z_0})^2$ is plotted against B/B_0 for various values of $2q \cosh \xi_0/\lambda_0$ and for a fixed value of ξ_0 . B is the distance from the axis to the point of observation; B_0 is the semi-minor axis. (See the sketch in Figure III-15). E_{z_0} is the axial electric field strength at the point of observation.

$$\frac{\epsilon_1}{\epsilon_0} = 2.5$$
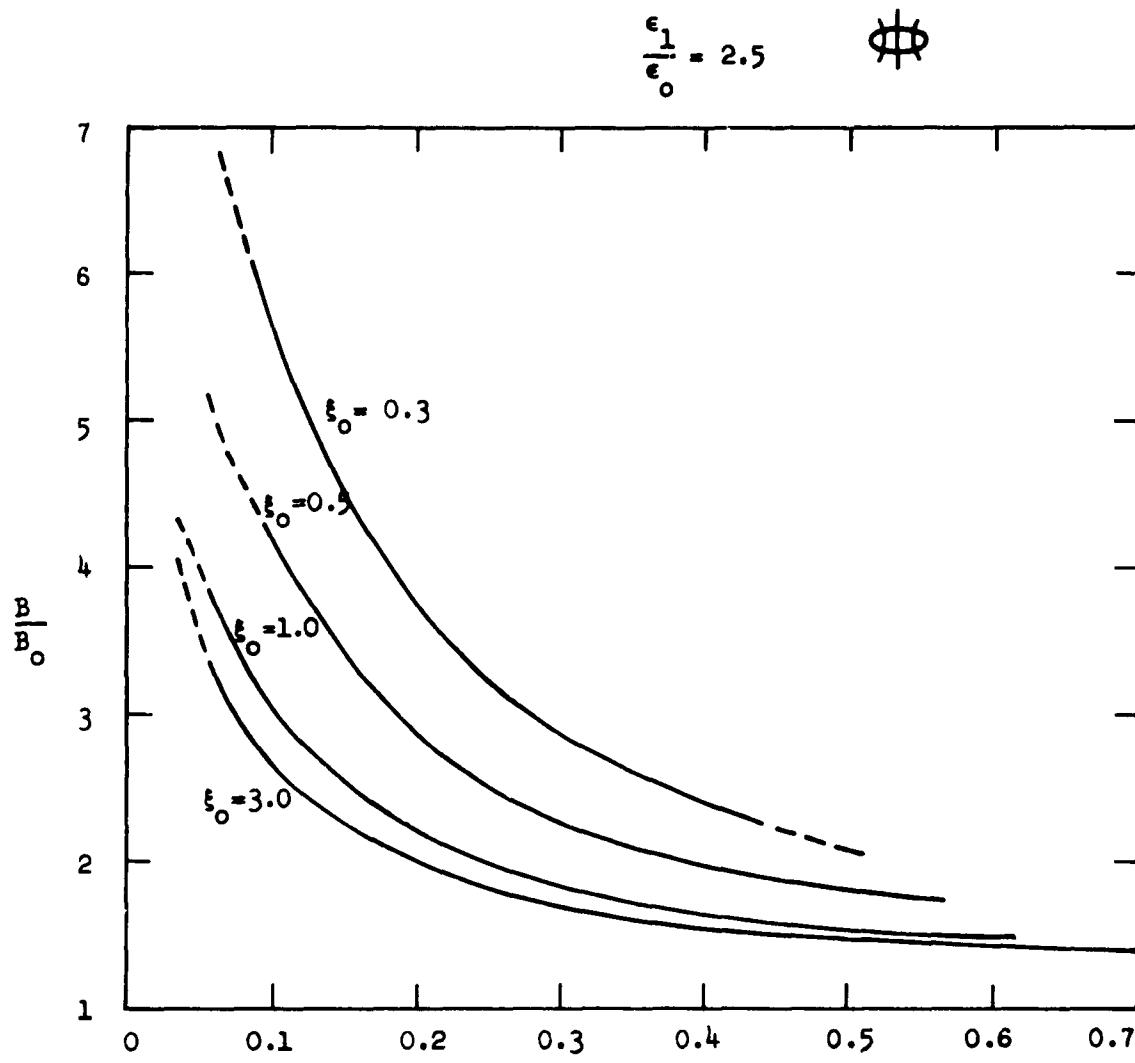
$$\left(\frac{2q \cosh \xi_0}{\lambda_0}\right)^2 \tanh \xi_0 = NCSA$$

Fig. III-20. Field extent B/B_0 where $(E_z/E_{z_0})^2 = 0.1$ as a function of normalized cross sectional area for the $_e HE_{11}^{(1)}$ mode.

$$\frac{\epsilon_1}{\epsilon_0} = 2.5$$
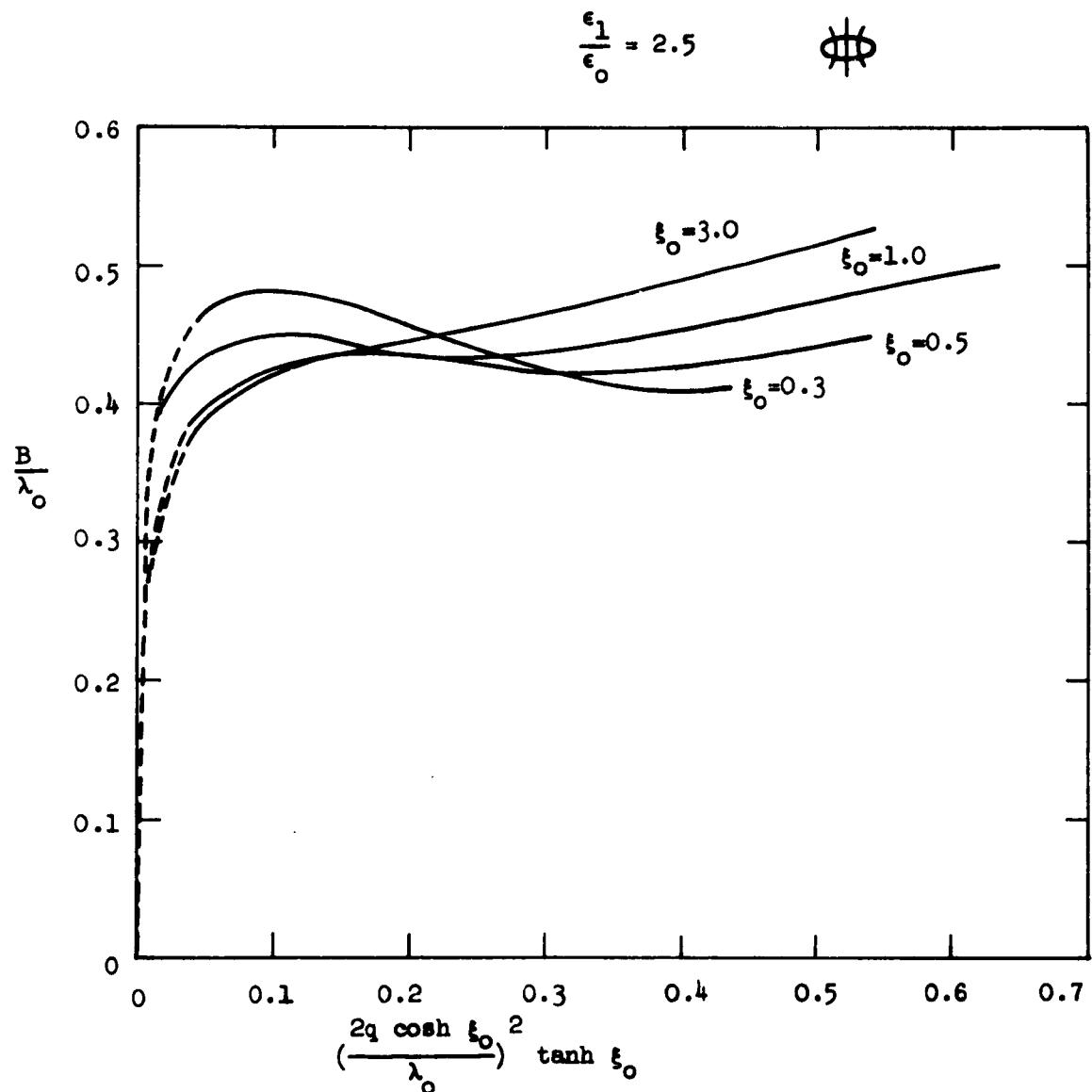
Fig. III-21. Normalized axial electric field extent B/λ_0 as a
function of normalized cross-sectional area for the
$_e HE_{11}^{(1)}$ mode . B is the distance measured from the
origin to the point of observation where $(E_z/E_{z_0})^2 = 0.1$

Some very interesting features are noted in this figure. For the

region $0.05 = (\frac{2q \cosh \xi_0}{\lambda_0})^2 \tanh \xi_0 \leq 0.5$ and $0.2 \leq \xi_0 < \infty$, the

variation of B/λ_0 is quite small; it varies between 0.35 and 0.55.

As $(\frac{2q \cosh \xi_0}{\lambda_0})^2 \tanh \xi_0$ approaches infinity so does B/λ_0; at

very low frequencies, B/λ_0 approaches zero. As the cross section of

the rod gets flatter, i.e., as ξ_0 gets smaller, the peaks and the

valleys of the curves become more pronounced. The fact that within a

certain frequency range the absolute axial electric field extent of a

flatter elliptical rod is actually smaller than that of a circular rod

of the same cross-sectional area is worth mentioning. As a typical

numerical example, we choose $\lambda_0 = 3$ cm . According to Figure III-21

the absolute field extent B for $(E_z/E_{z_0})^2 = 0.1$ is 1.37 cm for a

circular rod with a 1.5 cm diameter, while it is 1.28 cm for $\xi_0 = 0.5$

elliptical rod with the same cross-sectional area.

Similar curves for smaller values of $(E_z/E_{z_0})^2$ may be plotted.

The general shapes of these curves remain the same, only the peaks and

valleys of these curves are more pronounced.

Figures III-15 through III-19 also offer a convenient way of

verifying the purity of the mode on the dielectric guide. (Experiments

on the field decay properties of the $_e\mathrm{HE}_{11}^{(1)}$ mode have been carried out

and the results are reported in Chapter VI.)

Although only the E_z field is discussed above, it may be shown

that the other electric field components also possess similar though not

identical behaviors.

(b) The $_o\text{HE}_{11}^{(1)}$ Mode

Setting $m = 1$ and $n = 1$ in equation 2.5-63, one obtains the expression representing the external axial electric field for the $_o\text{HE}_{11}^{(1)}$ mode:

$$E_z = \sum_{\substack{r = 1 \\ \text{odd}}}^{\infty} h_r \text{Fek}_r(\xi) \, ce_r^*(\eta) \, e^{i\beta_o z} \, , \tag{6}$$

where

$$\frac{h_3}{h_1} = \frac{\text{Fek}_1(\xi_o)}{\text{Fek}_3(\xi_o)} \cdot \frac{\begin{vmatrix} \alpha_{13} & \alpha_{53} & \alpha_{73} \\ \alpha_{15} & \alpha_{55} & \alpha_{75} \\ \cdots & \cdots & \cdots \end{vmatrix}}{\begin{vmatrix} \alpha_{33} & \alpha_{53} & \cdots \\ \alpha_{35} & \alpha_{55} & \cdots \\ \cdots & \cdots & \cdots \end{vmatrix}} \tag{7}$$

$$\frac{h_5}{h_1} = \frac{\text{Fek}_1(\xi_o)}{\text{Fek}_5(\xi_o)} \cdot \frac{\begin{vmatrix} \alpha_{33} & \alpha_{13} & \alpha_{73} & \cdots \\ \alpha_{35} & \alpha_{15} & \alpha_{75} & \cdots \\ \alpha_{37} & \alpha_{17} & \alpha_{77} & \cdots \\ \cdots & \cdots & \cdots & \cdots \end{vmatrix}}{\begin{vmatrix} \alpha_{33} & \alpha_{53} & \cdots \\ \alpha_{35} & \alpha_{55} & \cdots \\ \cdots & \cdots & \cdots \end{vmatrix}} \tag{8}$$

. . . .

The above infinite determinants may be solved by the method of successive approximation. It can be shown that $h_1 < h_3 \ll h_5 \ll h_7 \cdots \ll h_\infty$. Therefore the value of the external axial electric field can be approximated by using only a few terms of the expansion, 6. The normalized external axial electric field is

$$\frac{E_z}{E_{z_o}} = \frac{Fek_1(\xi)\, ce_1^*(\eta) + \frac{h_3}{h_1} Fek_3(\xi)\, ce_3^*(\eta) + \cdots}{Fek_1(\xi_o)ce_1^*(\eta) + \frac{h_3}{h_1} Fek_3(\xi_o)ce_3^*(\eta) + \cdots} \,. \qquad (9)$$

Numerical computations are carried out assuming $\eta = 0$. The results are shown in Figures III-22 through III-25.for ξ_o ranging from $\xi_o = 3.0$ to $\xi_o = 0.2$. In each of these figures $(E_z/E_{z_o})^2$ is plotted against A/A_o for various values of $\frac{2q \cosh \xi_o}{\lambda_o}$. $2A_o$ is the major axis of the ellipse while A is the distance measured from the origin to the point of observation in the $\eta = 0$ plane (see the sketch in Figure III-22). The decay characteristics are as expected. At lower frequencies the field decays slower since a larger portion of the energy is carried outside the rod, and at higher frequencies the field decays faster and the field extent is less, since more energy is carried inside the rod.

Figure III-26 which is similar to Figure III-21 is introduced. In this figure the normalized absolute axial electric field extent $2A/\lambda_o$ is plotted against the normalized cross-sectional area $(\frac{2q \cosh \xi_o}{\lambda_o})^2$. tanh ξ_o, for various values of ξ_o; the point of observation is taken to be the point where $(E_z/E_{z_o})^2 = 0.1$. Again as $\omega \to 0$, $2A/\lambda_o$ approaches to zero; and as $(\frac{2q \cosh \xi_o}{\lambda_o})^2$ tanh $\xi_o \to \infty$, so does $2A/\lambda_o$. However, it is interesting to note the variation of these curves with respect to the change in eccentricity. Unlike the $_eHE_{11}^{(1)}$ mode, $2A/\lambda_o$ is always larger for flatter elliptical cross section rod. This is because the major axis of a flatter ellipse is always longer than a rounder one having the same area.

Figures III-22 through III-25 may also be used to check the purity
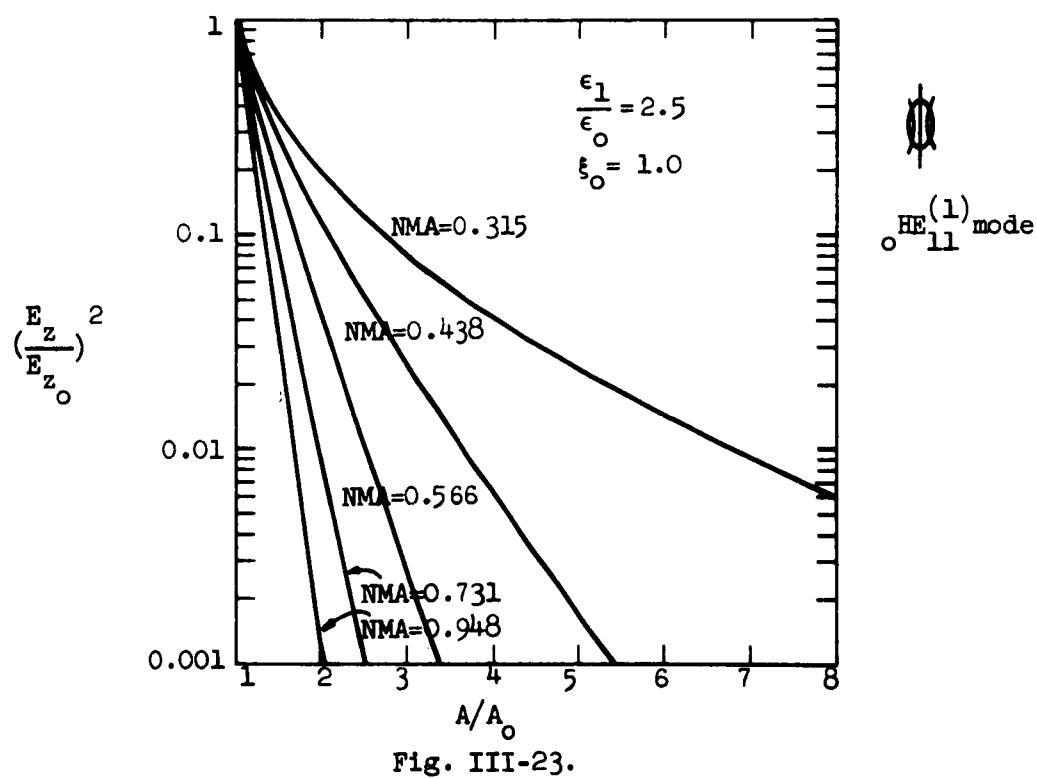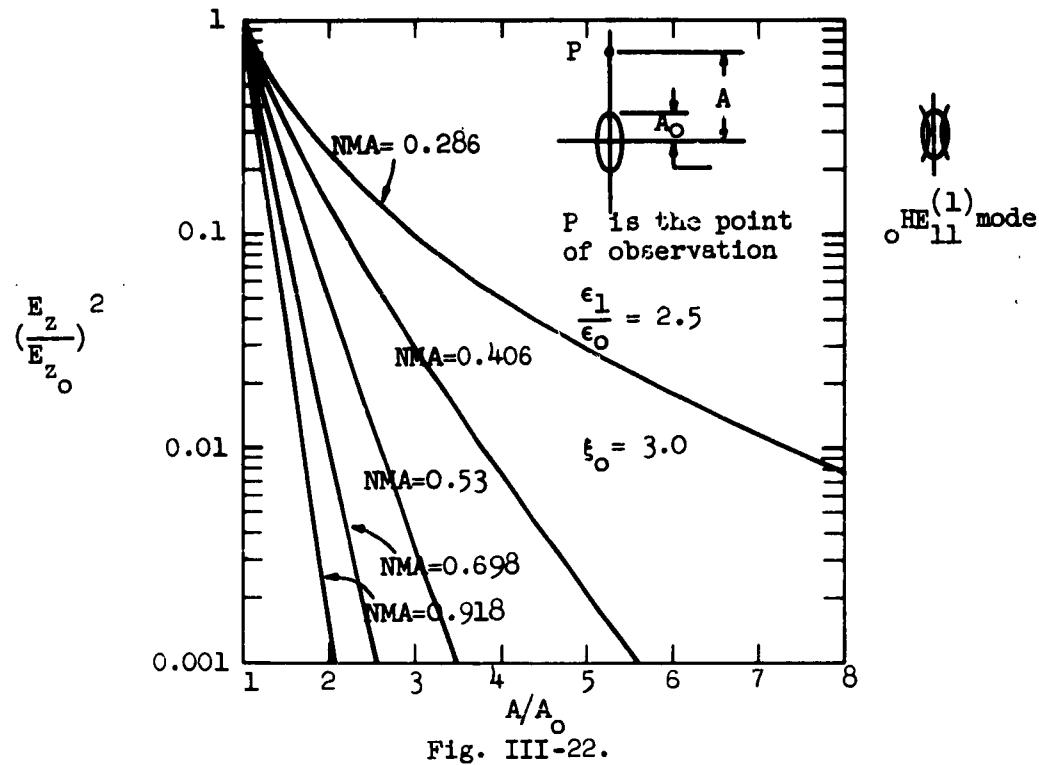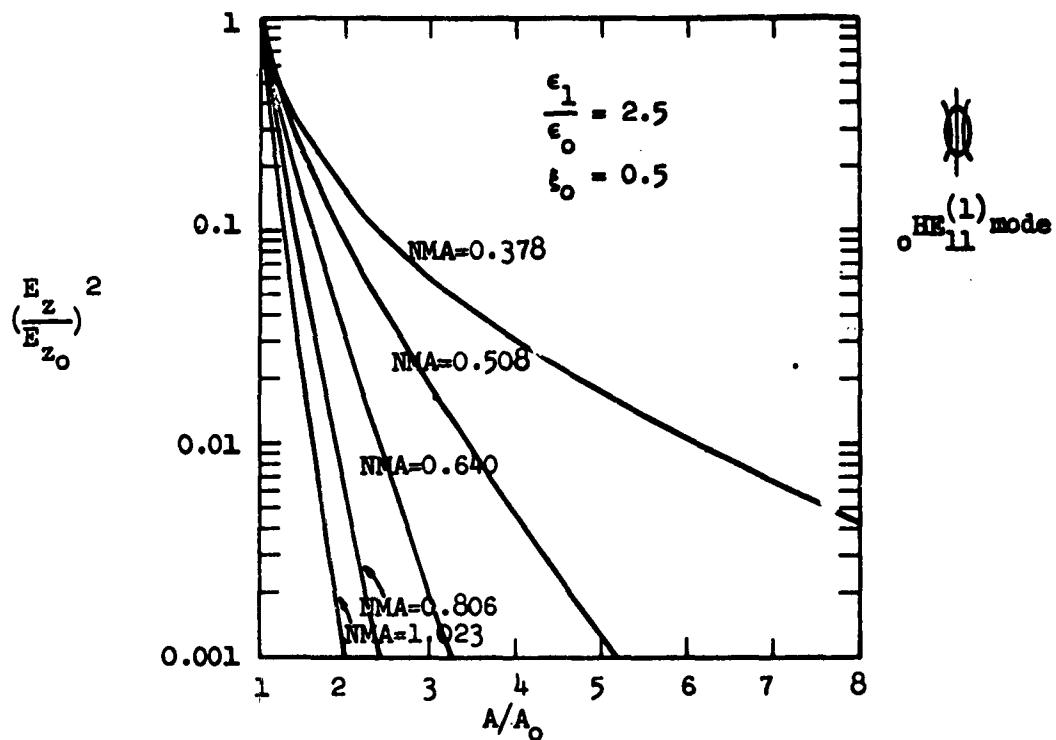
Fig. III-22.

Fig. III-23.
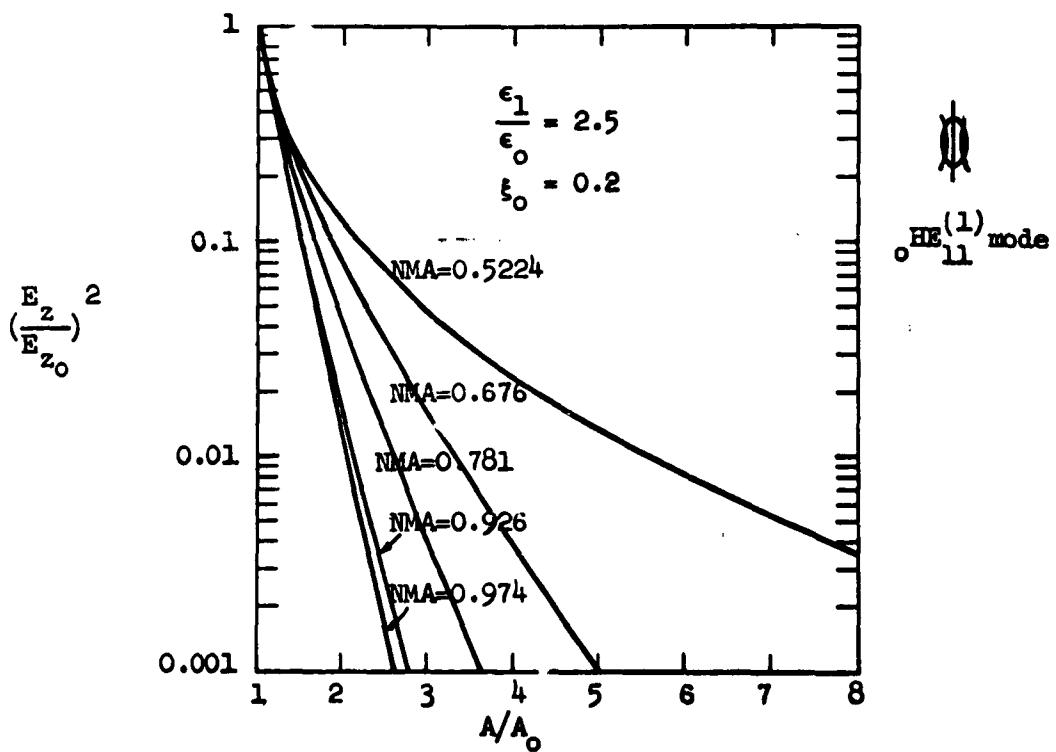
Fig. III-24.

Fig. III-25.

$$\frac{\epsilon_1}{\epsilon_0} = 2.5$$
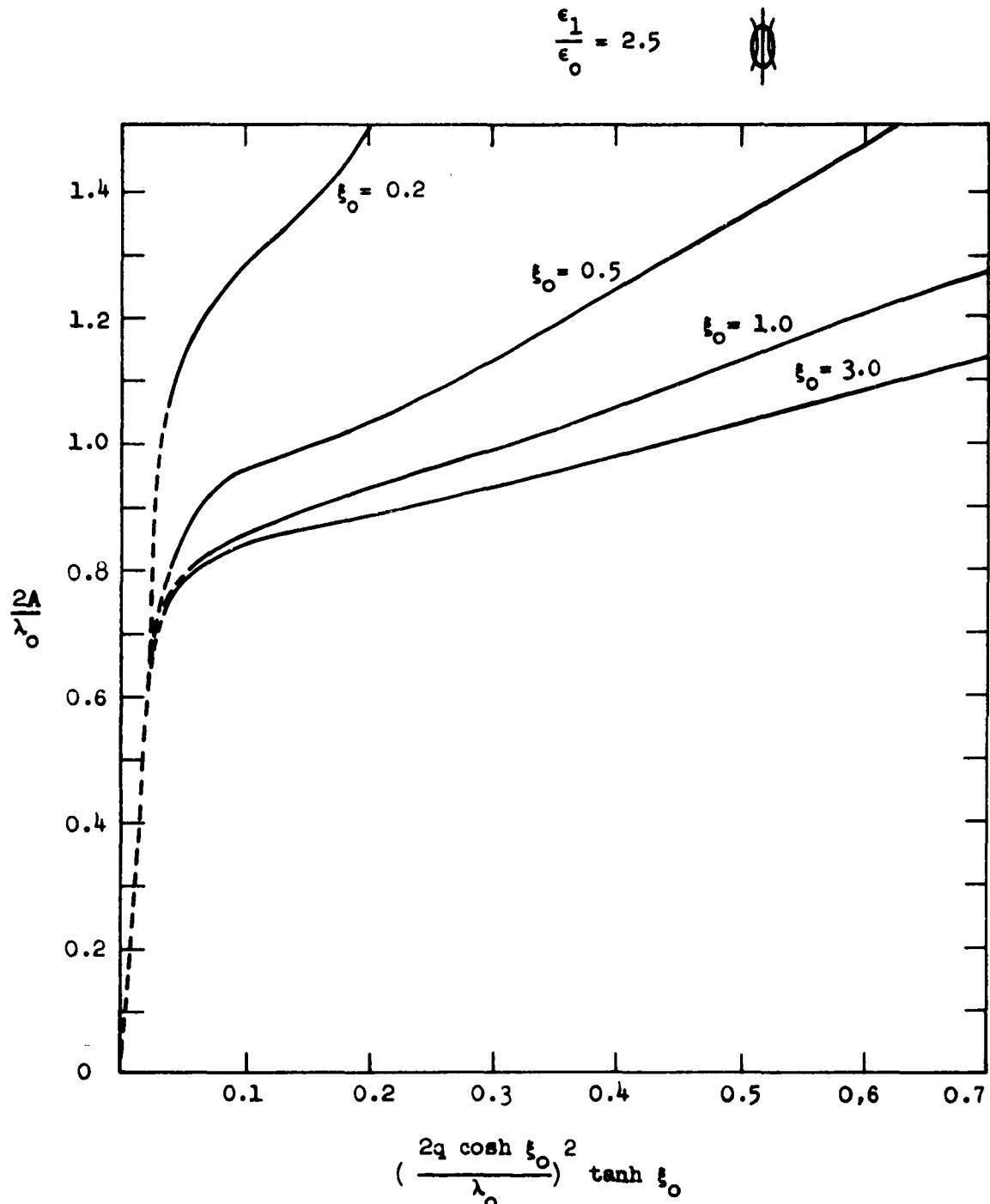
Fig. III-26. Normalized axial electric field extent $2A/\lambda_0$ as a function of the normalized cross-sectional area for the $_0HE_{11}^{(1)}$ mode. A is the distance measured from the origin to the point of observation where $(E_z/E_{z_0})^2 = 0.1$

of the $_o\text{HE}_{11}^{(1)}$ mode on the elliptical dielectric rod.

3.5 Summary

The numerical results of the characteristic equations for the two dominant modes are obtained. It is found that for the $_e\text{HE}_{11}^{(1)}$ mode the guide wavelength becomes longer as the elliptical cross-section becomes flatter, and for the $_o\text{HE}_{11}^{(1)}$ mode the opposite is true, although not as pronounced. As expected, there is no cutoff frequency for these two dominant modes. The fact that these two modes are degenerate when $\xi_o \rightarrow \infty$ is also demonstrated numerically.

Sketches of the field configurations for these modes are obtained. It is observed that the cross-sectional views of these modes are similar to the cross-sectional field pattern of the dominant mode in the metal waveguide. The possibility of launching these dominant dielectric rod modes by means of the metal waveguide is also discussed.

The field extent of these modes outside the dielectric rod is considered. It is found that the electric field extent of the $_o\text{HE}_{11}^{(1)}$ mode is much greater than that of the $_e\text{HE}_{11}^{(1)}$ mode, and the flatter the cross section, the larger the contrast.

CHAPTER IV - ATTENUATION AND POWER FLOW CHARACTERISTICS OF THE DOMINANT MODES

Having obtained the guide wavelength from the transcendental

equation and investigated the field decay characteristics, it would

seem appropriate to consider the attenuation and power flow properties

of these dominant modes. Attenuation is caused by imperfection of the

dielectric material. It is possible to include the lossy characteristics

of the dielectric material by assuming a complex dielectric constant to

represent the permittivity of the material. The effective complex

dielectric constant is given by

$$\epsilon_e = \epsilon_{1e} + i\epsilon'_{1e} \,. \tag{1}$$

Replacing the lossless dielectric constant ϵ_1 (as used in Chapters II

and III) by the effective complex dielectric constant ϵ_e and substitut-

ing ϵ_e into the equations in Chapters II and III where applicable, one

notes that since the arguments of the Mathieu and modified Mathieu func-

tions are complex, the roots of the characteristic equations can no

longer be real and must be complex. Therefore the propagation constant

β is also complex and must be represented by

$$\beta = \beta' + i\alpha \tag{2}$$

where β' is the new real propagation constant of the wave on the lossy

dielectric guide and α is the attenuation factor of the wave. Of

course the new real propagation constant β' does not necessarily equal

the propagation constant of the wave along the lossless dielectric guide.

The numerical solutions of these complex characteristic equations are

extremely complicated and involved. Even the analytic properties of the

Mathieu and modified Mathieu functions with complex argument have not been well investigated and understood (45,49).

However, when the conductivity of the imperfect dielectric is very low, in other words, when the imaginary part of the effective dielectric constant given by equation 1 is very small, i.e., $\epsilon'_{1e} \ll \epsilon_{1e}$, it can be assumed (15) that to the first order approximation the dissipation has no effect on the field configuration of the wave, which simply remains the same as that of the lossless case. Thus the propagation constant β is unchanged by the presence of small dielectric loss and therefore the analyses carried out in the previous chapters still apply. The mode functions in the case of small dielectric loss differ from those of the lossless case only by a multiplicative attenuation factor $e^{-\alpha z}$, where α is the attenuation constant and can be calculated by a perturbation method which will be described later.

The approximate formula for the attenuation constant α will be derived by the Poynting's vector theorem. The problem of attenuation of the $_e\mathrm{HE}_{11}^{(1)}$ mode along a slightly lossy dielectric rod will then be analyzed analytically and numerically. The results will be exhibited graphically. Similar considerations concerning the problem of attenuation of the $_o\mathrm{HE}_{11}^{(1)}$ mode along a slightly lossy dielectric rod will also be made. The results on the attenuation properties of these two dominant modes will be discussed and compared in detail. The power flow characteristics of these modes will be calculated.

4.1 The Attenuation Constant

The attenuation constant α can be calculated by a perturbation method, provided that the power loss per wavelength along the rod is small compared to the power flowing along the rod. Since there is no radiation perpendicular to the rod at large distances, the power flow is only in the z-direction, i.e., only along the axis of the rod. It has been pointed out earlier that the fields are damped exponentially as they propagate along the rod, and if their attenuation factor is α, that of the Poynting's vector is 2α. Therefore the attenuation constant can be calculated from the following relation:

$$2\alpha = \left| \frac{1}{P} \frac{\partial P}{\partial z} \right| \quad , \tag{1}$$

where P is the time average transmitted power and $\frac{\partial P}{\partial z}$ is the time average power loss per unit length. According to Poynting's theorem (15) we have*

$$\frac{\partial}{\partial z} S_z + \nabla_t \cdot \underline{S}_t = - \underline{J} \cdot \underline{E}^* + i\omega \left(\mu \underline{H} \cdot \underline{H}^* - \epsilon \underline{E} \cdot \underline{E}^* \right) \tag{2}$$

where S_z is the longitudinal component of the Poynting's vector $\underline{S}$, and $\underline{S}_t$ is the transverse part of $\underline{S}$. Integrating this expression over a cross-section A of the guide (this A includes the cross-section A_i of the dielectric guide and the cross-section A_o outside the dielectric rod) we get

$$\frac{\partial P}{\partial z} + \oint_c \underline{n} \cdot (\underline{E} \times \underline{H}^*) d\ell = - \sigma_d \int_{A_i} \underline{E} \cdot \underline{E}^* \, dA + 4i\omega \left[W_m - W_e \right] \tag{3}$$

---

* $\underline{E}^*$ or $\underline{H}^*$ signifies the complex conjugate of $\underline{E}$ or $\underline{H}$ respectively.

where $\frac{\partial}{\partial z} P$ is the time-average power loss per unit length; W_m and W_e are the time-average magnetic energy and electric energy per unit length of the guide respectively. It has been assumed that $\sigma_d = 0$ outside the rod and $\underline{J} = \sigma_d \underline{E}$ inside the rod. The value of the second integral on the left hand side of equation 3 is zero, since power flows along the rod only. For the undisturbed field, $W_m = W_e$, thus we have

$$\frac{\partial}{\partial z} P = - \sigma_d \int_{A_1} \underline{E} \cdot \underline{E}^* \, dA \ . \tag{4}$$

The time-average transmitted power is given by

$$P = \int_A \underline{e}_z \cdot (\underline{E}_t \times \underline{H}_t^*) \, dA \ . \tag{5}$$

$\underline{E}_t$ and $\underline{H}_t$ are the transverse components of the electric and magnetic field of the mode under consideration, and A is the total cross-sectional area of the guide. Substituting equations 4 and 5 into 1 we get the expression for the attenuation factor

$$2\alpha = \left| \frac{\sigma_d \int_{A_1} \underline{E} \cdot \underline{E}^* \, dA}{\int_A \underline{e}_z \cdot (\underline{E}_t \times \underline{H}_t^*) \, dA} \right| \tag{6}$$

where the unit of α is nepers/meter. Changing into practical units we have

$$\alpha = \frac{1}{2} \cdot 8.686 \cdot \sigma_d \cdot \sqrt{\frac{\mu_o}{\epsilon_o}} \left| \frac{\int_{A_1} \underline{E} \cdot \underline{E}^* \, dA}{\frac{\mu_o}{\epsilon_o} \int_A \underline{e}_z \cdot (\underline{E}_t \times \underline{H}_t^*) \, dA} \right| \text{(db/meter)} \tag{7}$$

where $\sigma_d = \omega \epsilon_1 \phi_d$. ϵ_1 and ϕ_d are respectively the dielectric

constant and the loss tangent of the rod. It may be noted that for a plane wave propagating in an infinite homogeneous medium of conductivity σ_d , the expression within the absolute value signs becomes $1/\sqrt{\epsilon_1/\epsilon_o}$ where ϵ_o is the dielectric constant of the surrounding medium.

Let us now consider the integrals within the absolute value signs. In elliptic cylinder coordinates these integrals can be expressed as follows:

$$\int_{A_i} \underline{E} \cdot \underline{E}^* \, dA = \int_0^{\xi_o} \int_0^{2\pi} (E_{\xi_1} E^*_{\xi_1} + E_{\eta_1} E^*_{\eta_1} + E_{z_1} E^*_{z_1}) q^2 (\sinh^2\xi + \sin^2\eta) \, d\eta d\xi \quad (8)$$

and

$$\int_A \underline{e}_z \cdot (\underline{E}_t \times \underline{H}^*_t) dA = \int_{A_i} \underline{e}_z \cdot (\underline{E}_{t_1} \times \underline{H}^*_{t_1}) dA + \int_{A_o} \underline{e}_z \cdot (\underline{E}_{t_o} \times \underline{H}^*_{t_o}) dA$$

$$= \int_0^{\xi_o} \int_0^{2\pi} (E_{\xi_1} H^*_{\eta_1} - E_{\eta_1} H^*_{\xi_1}) q^2 (\sinh^2\xi + \sin^2\eta) d\eta d\xi$$

$$+ \int_{\xi_o}^{\infty} \int_0^{2\pi} (E_{\xi_o} H^*_{\eta_o} - E_{\eta_o} H^*_{\xi_o}) q^2 (\sinh^2\xi + \sin^2\eta) d\eta d\xi , \quad (9)$$

where the subscript 1 and the subscript 0 represent the inside and outside regions of the dielectric rod respectively, and q is the semifocal length of the ellipse. ξ_o is the boundary surface of the elliptical rod.

4.2 The Attenuation Factor and the Power Distribution Characteristics of the $_e HE^{(1)}_{11}$ Mode

The field components of the $_e HE^{(1)}_{11}$ mode can be obtained from section 2.5a by setting m = 1 and n = 1. They are, for region 1, $(0 \leq \xi \leq \xi_o)$,

$$H_{z_1} = A_1 Ce_1(\xi)\, ce_1(\eta)\, e^{i\beta z} \tag{1}$$

$$E_{z_1} = B_1 Se_1(\xi)\, se_1(\eta)\, e^{i\beta z} \tag{2}$$

$$H_{\xi_1} = \frac{i\beta}{(k_1^2-\beta^2)p} \left\{ A_1 Ce_1'(\xi)\, ce_1(\eta) - \frac{\omega\epsilon_1}{\beta} B_1 Se_1(\xi)\, se_1'(\eta)\right\} e^{i\beta z} \tag{3}$$

$$H_{\eta_1} = \frac{i\beta}{(k_1^2-\beta^2)p} \left\{ A_1 Ce_1(\xi)\, ce_1'(\eta) + \frac{\omega\epsilon_1}{\beta} B_1 Se_1'(\xi)\, se_1(\eta)\right\} e^{i\beta z} \tag{4}$$

$$E_{\xi_1} = \frac{i\beta}{(k_1^2-\beta^2)p} \left\{ \frac{\omega\mu}{\beta} A_1 Ce_1(\xi)\, ce_1'(\eta) + B_1 Se_1'(\xi)\, se_1(\eta)\right\} e^{i\beta z} \tag{5}$$

$$E_{\eta_1} = \frac{i\beta}{(k_1^2-\beta^2)p} \left\{ -\frac{\omega\mu}{\beta} A_1 Ce_1'(\xi)\, ce_1(\eta) + B_1 Se_1(\xi)\, se_1'(\eta)\right\} e^{i\beta z} \tag{6}$$

and for region 0 $(\xi_0 \le \xi < \infty)$

$$H_{z_0} = \sum_{\substack{r=1\\ \text{odd}}}^{\infty} L_r\, Fek_r(\xi)\, ce_r^*(\eta)\, e^{i\beta z} \tag{7}$$

$$E_{z_0} = \sum_{\substack{r=1\\ \text{odd}}}^{\infty} P_r\, Gek_r(\xi)\, se_r^*(\eta)\, e^{i\beta z} \tag{8}$$

$$H_{\xi_0} = \frac{i\beta}{(k_0^2-\beta^2)p} \sum_{\substack{r=1\\ \text{odd}}}^{\infty} \left[L_r Fek_r'(\xi)ce_r^*(\eta) - \frac{\omega\epsilon_0}{\beta} P_r Gek_r(\xi)se_r^{*\prime}(\eta)\right] e^{i\beta z} \tag{9}$$

$$H_{\eta_0} = \frac{i\beta}{(k_0^2-\beta^2)p} \sum_{\substack{r=1\\ \text{odd}}}^{\infty} \left[L_r Fek_r(\xi)ce_r^{*\prime}(\eta) + \frac{\omega\epsilon_0}{\beta} P_r Gek_r'(\xi)se_r^*(\eta)\right] e^{i\beta z} \tag{10}$$

$$E_{\xi_0} = \frac{i\beta}{(k_0^2-\beta^2)p} \sum_{\substack{r=1\\ \text{odd}}}^{\infty} \left[\frac{\omega\mu}{\beta} L_r Fek_r(\xi)ce_r^{\prime*}(\eta) + P_r Gek_r'(\xi)se_r^*(\eta)\right] e^{i\beta z} \tag{11}$$

$$E_{\eta_0} = \frac{i\beta}{(k_0^2-\beta^2)p} \sum_{\substack{r=1\\ \text{odd}}}^{\infty} \left[-\frac{\omega\mu}{\beta} L_r Fek_r'(\xi)ce_r^*(\eta) + P_r Gek_r(\xi)se_r^{*\prime}(\eta)\right] e^{i\beta z} \tag{12}$$

where $k_0^2 = \omega^2\mu\epsilon_0$, $k_1^2 = \omega^2\mu\epsilon_1$, and $p = q(\sinh^2\xi + \sin^2\eta)^{1/2}$. A_1, B_1, L_r and P_r are the arbitrary constants which are related by the boundary

conditions and are given by (see section 2.5a, equations 43 through 45)

$$\frac{L_1}{A_1} = \frac{Ce_1(\xi_o)}{Fek_1(\xi_o)} \cdot \frac{1}{M_1(\alpha_{rs})} \quad , \tag{13}$$

$$\frac{L_3}{A_1} = \frac{L_3}{L_1}\frac{L_1}{A_1} = -\frac{Fek_1(\xi_o)}{Fek_3(\xi_o)} \cdot \frac{\begin{vmatrix} \alpha_{13} & \alpha_{53} & \alpha_{73} \\ \alpha_{15} & \alpha_{55} & \alpha_{75} \\ \alpha_{17} & \alpha_{57} & \alpha_{77} \\ \cdots & \cdots & \cdots \end{vmatrix}}{\begin{vmatrix} \alpha_{33} & \alpha_{53} & \cdots \\ \alpha_{35} & \alpha_{55} & \cdots \\ \cdots & \cdots & \cdots \end{vmatrix}} \cdot \frac{L_1}{A_1} \quad , \tag{14}$$

$$\frac{L_5}{A_1} = \frac{L_5}{L_1}\frac{L_1}{A_1} = -\frac{Fek_1(\xi_o)}{Fek_5(\xi_o)} \cdot \frac{\begin{vmatrix} \alpha_{33} & \alpha_{13} & \alpha_{73} & \cdots \\ \alpha_{35} & \alpha_{15} & \alpha_{75} & \cdots \\ \alpha_{37} & \alpha_{17} & \alpha_{77} & \cdots \\ \cdots & \cdots & \cdots & \cdots \end{vmatrix}}{\begin{vmatrix} \alpha_{33} & \alpha_{53} & \cdots \\ \alpha_{35} & \alpha_{55} & \cdots \\ \cdots & \cdots & \cdots \end{vmatrix}} \cdot \frac{L_1}{A_1} \quad , \tag{15}$$

$$\frac{B_1}{A_1} = \sqrt{\frac{\mu}{\epsilon_o}} \ \frac{x^2 Fek_1'(\xi_o)\frac{L_1}{A_1}M_1(\alpha_{rs}) - Ce_1'(\xi_o)y^2}{Se_1(\xi_o)\left[(x^2+ y^2)(x^2+ y^2 \frac{\epsilon_1}{\epsilon_o})\right]^{1/2}R_1(\alpha_{rs},\delta_{1s})} \quad , \tag{16}$$

$$\frac{P_1}{A_1} = \frac{P_1}{B_1} \cdot \frac{B_1}{A_1} = \frac{Se_1(\xi_o)}{Gek_1(\xi_o)} \cdot \frac{1}{N_1(\beta_{rs})} \cdot \frac{B_1}{A_1} \quad , \tag{17}$$

$$\frac{P_3}{A_1} = \frac{P_3}{P_1} \cdot \frac{P_1}{A_1} = - \frac{Gek_1(\xi_o)}{Gek_3(\xi_o)} \frac{\begin{vmatrix} \beta_{13} & \beta_{53} & \cdots \\ \beta_{15} & \beta_{55} & \cdots \\ \cdots & \cdots & \cdots \end{vmatrix}}{\begin{vmatrix} \beta_{33} & \beta_{53} & \cdots \\ \beta_{35} & \beta_{55} & \cdots \\ \cdots & \cdots & \cdots \end{vmatrix}} \cdot \frac{P_1}{A_1} \, , \tag{18}$$

$$\frac{P_5}{A_1} = \frac{P_5}{P_1} \cdot \frac{P_1}{A_1} = - \frac{Gek_1(\xi_o)}{Gek_5(\xi_o)} \frac{\begin{vmatrix} \beta_{33} & \beta_{13} & \cdots \\ \beta_{35} & \beta_{15} & \cdots \\ \cdots & \cdots & \cdots \end{vmatrix}}{\begin{vmatrix} \beta_{33} & \beta_{53} & \cdots \\ \beta_{35} & \beta_{55} & \cdots \\ \cdots & \cdots & \cdots \end{vmatrix}} \cdot \frac{P_1}{A_1} \, , \tag{19}$$

and   . . . .

The symbols used in the above expressions have all been defined in
Chapter II.

Upon examining the second integral in equation 4.1-9, it can be
seen that it would be extremely laborious to carry out this integral if
many terms of the expansions representing the field components outside
the guide are required. Fortunately it is found that, within the region
of our interest, i.e., for $\xi_o \geq 0.2$, $x \leq 5$, and $0.1 \leq y \leq 3$,
$\left| \frac{L_1}{A_1} \right| \gg \left| \frac{L_3}{A_1} \right| \gg \left| \frac{L_5}{A_1} \right| \gg \cdots \gg \left| \frac{L_\infty}{A_1} \right|$, and $\left| \frac{P_1}{A_1} \right| \gg \left| \frac{P_3}{A_1} \right| \gg \left| \frac{P_5}{A_1} \right| \gg \cdots$
$\gg \left| \frac{P_\infty}{A_1} \right|$, so that the expressions representing the field components
outside the guide can be approximated by only two terms of the infinite
series expansion. In other words, the infinite series, representing the

field components in region 0, converge rather rapidly, providing that ξ_o is not too small. For instance, it is found numerically that when $\xi_o \gtrsim 1.0$, the value of H_{z_o} (see equation 7) computed from the first two terms of the infinite series, is accurate to the fifth significant figure at the worst; when $1.0 \gtrsim \xi_o \gtrsim 0.5$, it is accurate to the fourth significant figure at the worst; and when $0.5 \gtrsim \xi_o \gtrsim 0.2$, it is accurate to the second significant figure at the worst. It can be seen that the accuracy gets better as ξ_o gets larger, assuming that the same number of terms is used.

We are now in a position to consider the integrals in equations 4.1-8 and 4.1-9. Substituting equations 2, 5 and 6 into 4.1-8, one obtains

$$\int_0^{\xi_o} \int_0^{2\pi} (E_{\xi_1} E_{\xi_1}^* + E_{\eta_1} E_{\eta_1}^* + E_{z_1} E_{z_1}^*)q^2(\sinh^2\xi + \sin^2\eta)d\eta\, d\xi$$

$$= \int_0^{\xi_o} \int_0^{2\pi} \left\{ \frac{\beta^2(\frac{\mu}{\epsilon_o})A_1^2}{(k_1^2 - \beta^2)^2} \left[\frac{\omega^2\mu\epsilon_o}{\beta^2}(Ce_1^2(\xi)ce_1'^2(\eta) + Ce_1'^2(\xi)ce_1^2(\eta) + \right.\right.$$

$$+ (\frac{B_1}{A_1})^2(\frac{\epsilon_o}{\mu})(Se_1'^2(\xi)se_1^2(\eta) + Se_1^2(\xi)se_1'^2(\eta) + 2\frac{\omega\sqrt{\mu\epsilon_o}}{\beta}\sqrt{\frac{\epsilon_o}{\mu}}(\frac{B_1}{A_1})$$

$$\left.\left(Ce_1(\xi)Se_1'(\xi)ce_1'(\eta)se_1(\eta) - Ce_1'(\xi)Se_1(\xi)ce_1(\eta)se_1'(\eta)\right)\right]$$

$$+ \frac{\epsilon_o}{\mu}(\frac{B_1}{A_1})^2 Se_1^2(\xi)se_1^2(\eta)\ (\sinh^2\xi + \sin^2\eta) \Bigg\}\ d\eta d\xi\ . \tag{20}$$

Separating the angular and radial integrals and simplifying, one gets

$$\frac{\int_{A_1} (\underline{E}_1 \cdot \underline{E}_1^*) dA}{\cosh^2 \xi_0 q^2 A_1^2 \frac{\mu}{\epsilon_0}} = C_1 \left[C_2 (I_8 I_1 + I_9 I_2) + \left(\frac{B_1}{A_1}\right)^2 \left(\frac{\epsilon_0}{\mu}\right)(I_{10}I_3 + I_{11}I_4) \right.$$

$$\left. + 2\sqrt{C_2} \left(\frac{B_1}{A_1}\right)\sqrt{\frac{\epsilon_0}{\mu}} \ (I_{12}I_5 - I_{13}I_6) \right] + \left(\frac{B_1}{A_1}\right)^2 \left(\frac{\epsilon_0}{\mu}\right)\left[I_{14}I_3 + \frac{1}{2} \frac{I_{11}(I_3 - I_7)}{\cosh^2 \xi_0} \right]$$

$$(21)$$

where $C_1 = \dfrac{x^2 + y^2 \frac{\epsilon_1}{\epsilon_0}}{x^4 (\frac{\epsilon_1}{\epsilon_0} - 1)}$, $C_2 = \dfrac{x^2 + y^2}{x^2 + \frac{\epsilon_1}{\epsilon_0} y^2}$, $x^2 = q^2 \cosh \xi_0 (k_1^2 - \beta^2)$, and

$y = -q^2 \cosh^2 \xi_0 (k_0^2 - \beta^2)$. I_1 through I_7 are the angular integrals which

can be integrated analytically and are given in Appendix B.1; I_8 through

I_{14} are the radial integrals which must be evaluated numerically and are

defined in Appendix B.2.

Substituting equations 3 through 6 into the first integral in equa-

tion 4.1-9 gives

$$\int_0^{\xi_0} \int_0^{2\pi} (E_{\xi_1} H_{\eta_1}^* - E_{\eta_1} H_{\xi_1}^*) q^2 (\sinh^2 \xi + \sin^2 \eta) d\eta d\xi$$

$$= \frac{\beta^2 A_1^2 \sqrt{\frac{\mu}{\epsilon_0}}}{(k_1^2 - \beta^2)^2} \int_0^{\xi_0} \int_0^{2\pi} \left[\frac{\omega \sqrt{\mu \epsilon_0}}{\beta} \left(Ce_1^2(\xi) ce_1^{'2}(\eta) + Ce_1^{2'}(\xi) ce_1^2(\eta) \right) \right.$$

$$+ \frac{\epsilon_1}{\epsilon_0} \frac{\omega \sqrt{\mu \epsilon_0}}{\beta} \left(\frac{\epsilon_0}{\mu}\right)\left(\frac{B_1}{A_1}\right)^2 \left(Se_1^{'2}(\xi) se_1^2(\eta) + Se_1^2(\xi) se_1^{'2}(\eta) \right)$$

$$+ \left(\frac{B_1}{A_1}\right) \sqrt{\frac{\epsilon_0}{\mu}} \left(1 + \frac{\omega^2 \mu \epsilon_1}{\beta^2}\right) \left(Ce_1(\xi) Se_1'(\xi) ce_1'(\eta) se_1(\eta) \right.$$

$$\left. - Ce_1'(\xi) Se_1(\xi) ce_1(\eta) se_1'(\eta) \right) \Bigg] d\eta \ d\xi \ . \quad (22)$$

Simplifying this expression we have

$$\frac{\int_{A_1} \underline{e}_z \cdot (\underline{E}_{1t} \times \underline{H}_{1t})dA}{\cosh^2 \xi_o q^2 A_1^2 \sqrt{\frac{\mu}{\epsilon_o}}} = C_1 \left[\sqrt{C_2} \, (I_8 I_1 + I_9 I_2) + \frac{\epsilon_1}{\epsilon_o} \sqrt{C_2} \, \frac{\epsilon_o}{\mu} \, (\frac{B_1}{A_1})^2 (I_{10} I_3 + I_{11} I_4) \right.$$

$$\left. + \sqrt{\frac{\epsilon_o}{\mu}} \, \frac{B_1}{A_1} \, (1 + \frac{\epsilon_1}{\epsilon_o} C_2)(I_{12} I_5 - I_{13} I_6) \right] \quad , \qquad (23)$$

where C_1, C_2, x and y have been defined earlier. The angular integrals I_1 through I_6 and the radial integrals I_8 through I_{13} are all given in Appendix B.1 and Appendix B.2 respectively. The above expression 23 also represents the portion of the total transmitted power being carried inside the dielectric rod. The other part of the transmitted power which is carried outside the rod is represented by the second integral in equation 4.1-9. Substituting the "two-term-approximation" of equations 9 through 12 into the second integral in equation 4.1-9, one gets

$$\int_{\xi_o}^{\infty} \int_0^{2\pi} (E_{\xi_o} H^*_{\eta_o} - E_{\eta_o} H^*_{\xi_o}) q^2 (\sinh^2 \xi + \sin^2 \eta) d\eta \, d\xi$$

$$= \frac{\beta^2}{(k_o^2 - \beta^2)^2} \int_{\xi_o}^{\infty} \int_0^{2\pi} \left\{ L_1^2 \frac{\omega\mu}{\beta} \, (B1) + P_1^2 \frac{\omega\epsilon_o}{\beta} \, (B2) \right.$$

$$\left. + P_1 L_1 (1 + \frac{\omega^2 \mu \epsilon_o}{\beta^2})(B3) \right\} \, d\eta \, d\xi \, , \qquad (24)$$

in which

$$(B1) = Fek_1^2(\xi)ce_1^{*'2}(\eta) + (\frac{L_3}{L_1})^2 Fek_3^2(\xi)ce_3^{*'2}(\eta) + 2(\frac{L_3}{L_1})Fek_1(\xi)Fek_3(\xi)ce_1^{*'}(\eta)\,ce_3^{*'}(\eta)$$

$$+ Fek_1'^2(\xi)\,ce_1^{*2}(\eta) + (\frac{L_3}{L_1})^2 Fek_3'^2(\xi)ce_3^{*2}(\eta) + 2(\frac{L_3}{L_1})Fek_1'(\xi)Fek_3'(\xi)ce_1^*(\eta)ce_3^*(\eta),$$

$$(B2) = Gek_1^2(\xi)se_1^{*'2}(\eta) + (\frac{P_3}{P_1})^2 Gek_3^2(\xi)se_3^{*'2}(\eta) + 2(\frac{P_3}{P_1})Gek_1(\xi)Gek_3(\xi)se_1^{*'}(\eta)se_3^{*'}(\eta)$$

$$+ Gek_1'^2(\xi)se_1^{*2}(\eta) + (\frac{P_3}{P_1})^2 Gek_3'^2(\xi)se_3^{*2}(\eta) + 2(\frac{P_3}{P_1})Gek_1'(\xi)Gek_3'(\xi)se_1^*(\eta)se_3^*(\eta),$$

and

$$(B3) = Fek_1(\xi)Gek_1'(\xi)ce_1^*(\eta)se_1^*(\eta) - Fek_1'(\xi)Gek_1(\xi)ce_1^*(\eta)se_1^*(\eta)$$

$$+ \frac{L_3}{L_1}\left[Fek_3(\xi)Gek_1'(\xi)ce_3^{*'}(\eta)se_1^*(\eta) - Fek_3'(\xi)Gek_1(\xi)se_1^{*'}(\eta)ce_3^*(\eta) \right]$$

$$+ \frac{P_3}{P_1}\left[Fek_1(\xi)Gek_3'(\xi)ce_1^*(\eta)se_3^*(\eta) - Fek_1'(\xi)Gek_3(\xi)ce_1^*(\eta)se_3^{*'}(\eta) \right]$$

$$+ (\frac{L_3}{L_1})(\frac{P_3}{P_1})\left[Fek_3(\xi)Gek_3'(\xi)ce_3^{*'}(\eta)se_3^*(\eta) - Fek_3'(\xi)Gek_3(\xi)se_3^{*'}(\eta)ce_3^*(\eta) \right] .$$

Simplifying equation 24 results in

$$\frac{\int_{A_o} \underline{e}_z \cdot (\underline{E}_{to} \times \underline{H}_{to}^*)dA}{\cosh^2\xi_o q^2 A_1^2 \frac{\mu_o}{\epsilon_o}} = \frac{x^4}{y^4} C_1 \left\{ (\frac{L_1}{A_1})^2 \sqrt{C_2} \cdot (BI) + (\frac{P_1}{A_1})^2 \sqrt{C_2} \frac{\epsilon_o}{\mu} (BII) \right.$$

$$\left. + \sqrt{\frac{\epsilon_o}{\mu}} (\frac{L_1}{A_1})(\frac{P_1}{A_1})(1 + C_2) (BIII) \right\} , \qquad (25)$$

where

$$(BI) = (I_1'I_{21}' + I_2'I_{22}') + (\frac{L_3}{L_1})^2 (I_3'I_{23}' + I_{24}'I_4') + 2(\frac{L_3}{L_1})(I_{25}'I_5' + I_{26}'I_6') ,$$

$$(BII) = (I_{27}'I_7' + I_{28}'I_8') + (\frac{P_3}{P_1})^2 (I_{29}'I_9' + I_{30}'I_{10}') + 2(\frac{P_3}{P_1})(I_{31}'I_{11}' + I_{32}'I_{12}') ,$$

$$(BIII) = (I'_{33}I'_{13} - I'_{34}I'_{14}) + (\frac{L_3}{L_1})(I'_{35}I'_{15} - I'_{36}I'_{16}) + (\frac{P_3}{P_1})(I'_{37}I'_{17} - I'_{38}I'_{18})$$

$$+ (\frac{P_3}{P_1})(\frac{L_3}{L_1})(I'_{39}I'_{19} - I'_{40}I'_{20}) \ ,$$

and C_1, C_2, x and y have been defined earlier. Again the angular integrals I'_1 through I'_{20} which can be integrated analytically, and the radial integrals I'_{21} through I'_{40} which must be evaluated numerically, are tabulated in Appendix B.1 and Appendix B.2. It should be noted that the numerical values of the higher order terms, neglected in the above expressions (BI), (BII), and (BIII) are of the order of P_5/P_1 or L_5/L_1. Expression 25 represents the portion of the power being transmitted outside the rod.

Substituting equations 21, 23, and 25 into the expression within the absolute value signs of equation 4.1-7, we get

$$R = \left| \frac{\displaystyle\int_{A_1} (\underline{E}_1 \cdot \underline{E}_1^*) dA}{\displaystyle\int_{A_1 + A_0} (\underline{E}_t \times \underline{H}_t^*) \cdot \underline{e}_z dA} \right| \sqrt{\frac{\epsilon_o}{\mu}} = \frac{f_1}{f_2 + f_3} \ , \tag{26}$$

where

$$f_1 = C_1 \left[C_2(I_8I_1 + I_9I_2) + (\frac{B_1}{A_1})^2 \frac{\epsilon_o}{\mu} (I_{10}I_3 + I_{11}I_4) + 2\sqrt{C_2} (\frac{B_1}{A_1}) \right.$$

$$\left. \sqrt{\frac{\epsilon_o}{\mu}} (I_{12}I_5 - I_{13}I_6) \right] + (\frac{B_1}{A_1})^2 \frac{\epsilon_o}{\mu} (I_{14}I_3 + \frac{I_{11}(I_3 - I_7)}{\cosh^2 \xi_o \, 2})$$

$$f_2 = C_1 \left[\sqrt{C_2}(I_8I_1 + I_9I_2) + \frac{\epsilon_1}{\epsilon_o} \sqrt{C_2} \, \frac{\epsilon_o}{\mu} (\frac{B_1}{A_1})^2 (I_{10}I_3 + I_{11}I_4) \right.$$

$$\left. + \sqrt{\frac{\epsilon_o}{\mu}} \frac{B_1}{A_1} (1 + \frac{\epsilon_1}{\epsilon_o} C_2)(I_{12}I_5 - I_{13}I_6) \right] \ ,$$

and

$$f_3 = \frac{x^4}{y^4} C_1 \left[\left(\frac{L_1}{A_1}\right)^2 \sqrt{C_2} \text{ (BI)} + \left(\frac{P_1}{A_1}\right)^2 \sqrt{C_2} \frac{\epsilon_0}{\mu} \text{ (BII)} + \sqrt{\frac{\epsilon_0}{\mu}} \left(\frac{L_1}{A_1}\right)\left(\frac{P_1}{A_1}\right)(1+C_2) \text{ (BIII)} \right].$$

R is related to the attenuation constant α in db/meter by the following relation

$$\alpha = \frac{8.686}{2} \sigma_d \sqrt{\frac{\mu}{\epsilon_0}} R \qquad (27)$$

where σ_d is the conductivity of the dielectric rod.

Using the results given in Chapter III regarding the relationship between x and y for various values of ξ_0 and ϵ_1/ϵ_0, numerical computation of R can now be carried out. All radial integrals, I_8 through I_{13} and I'_{21} through I'_{40}, are evaluated numerically using Simpson's rule (50). Results of this very lengthy computation are shown in Figure IV-1*. In this figure the value R , which is directly proportional to the attenuation constant (see equation 27) is plotted against the normalized major axis (NMA), $\dfrac{2q \cosh \xi_0}{\lambda_0}$, for various values of ξ_0 ranging from $\xi_0 = 3.0$ to $\xi_0 = 0.2$. It is assumed that $\epsilon_1/\epsilon_0 = 2.5$. For sufficiently large values of NMA, R tends toward the plane-wave value $1/\sqrt{\epsilon_1/\epsilon_0}$ for all values of ξ_0 ; for small enough values of NMA R can be chosen as small as desired. This behavior is attributed to the fact that, when NMA is sufficiently large, almost all of the energy of the wave is transmitted inside the rod**; and for small values of NMA almost all of the energy is outside the rod. (It has been assumed that the dielectric surrounding the rod is perfect.) It is also clear

---

*It takes almost 20 minutes of continuous computation by the IBM7090 computer to obtain each curve.

**It is noted that when NMA is very large the attenuation factor R is numerically identical with the attenuation factor of a certain waveguide mode propagating in a perfectly conducting metal tube waveguide filled with the same dielectric material as that of the dielectric rod under consideration.
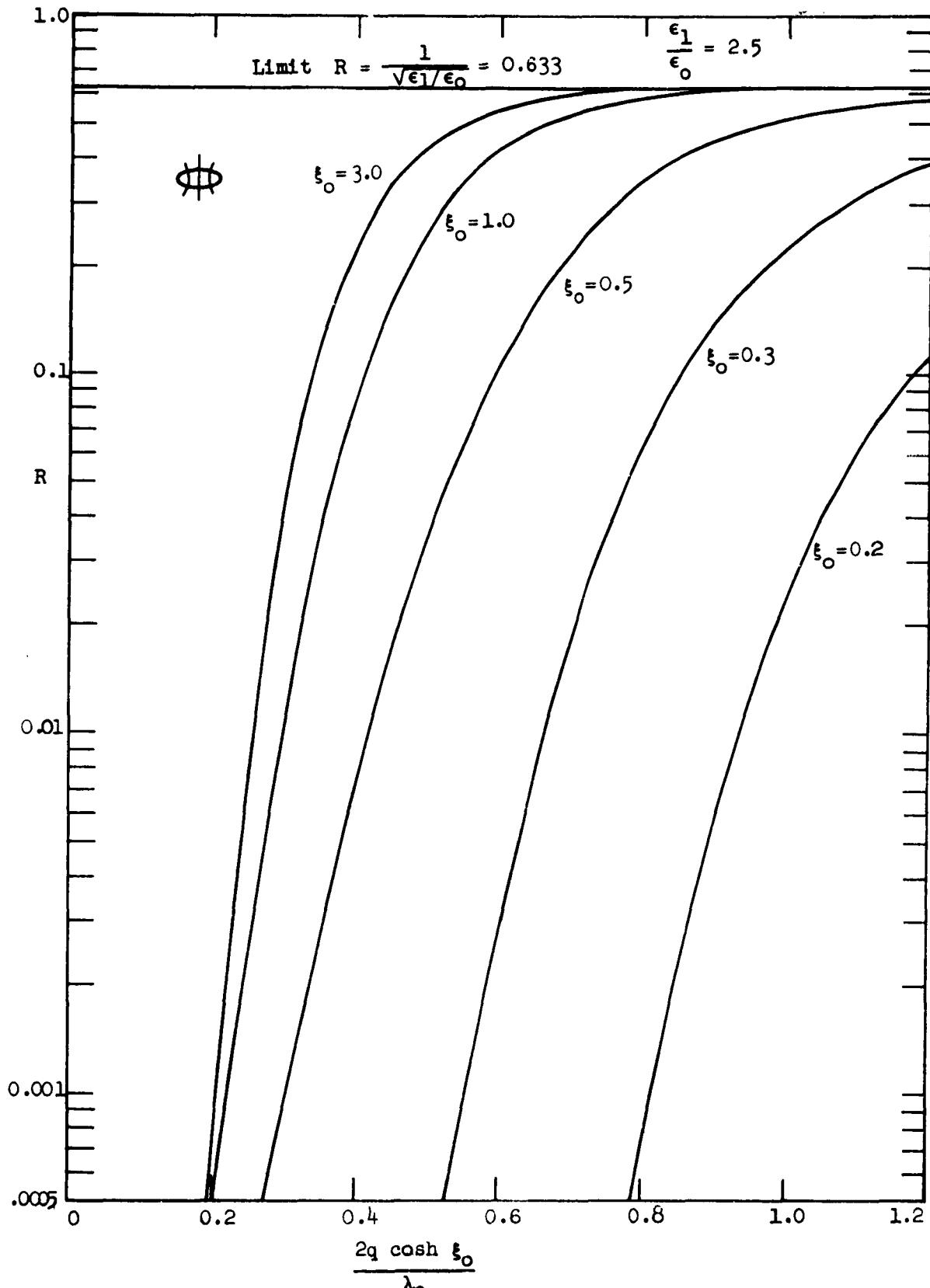
Fig. IV-1. Attenuation factor R for the $_e\text{HE}_{11}^{(1)}$ mode as a function of normalized major axis.

that R tends to the limit $1/\sqrt{\epsilon_1/\epsilon_0}$ much slower as ξ_0 gets smaller and that flatter elliptical dielectric guide possesses lower loss characteristics. This may be explained by the fact that, according to Figure IV-1, for a constant value of NMA, smaller ξ_0 rod has less volume of dielectric material and therefore lower dielectric loss. However, this is not the only reason. If we plot R against the normalized cross-sectional area (NCSA), $\left(\dfrac{2q \cosh \xi_0}{\lambda_0}\right)^2 \tanh \xi_0$, for various values of ξ_0 with $\epsilon_1/\epsilon_0 = 2.5$, as in Figure IV-2, the same effect (i.e., lower loss for smaller ξ_0) of a lesser degree can still be observed. As the elliptical cross-section gets flatter, the field of the $_e\mathrm{HE}_{11}^{(1)}$ wave spreads out more so that the total integrated effect on the attenuation indicates that this type of field distribution offers less loss. The shape of these curves in Figure IV-2 shows that the attenuation factor can be made extremely small if a very flat strip is used. For example, when NCSA = 0.15 the attenuation constant α of the $_e\mathrm{HE}_{11}^{(1)}$ mode can be made ten times smaller if $\xi_0 = 0.3$ elliptical rod is used rather than a circular rod, and α may be almost 90 times smaller if $\xi_0 = 0.2$ elliptical rod is used. It is interesting to compare the axial electric field extent of these rods corresponding to the above example. According to Figure III-21, when NCSA = 0.15 the axial electric field extent B/λ_0 where $(E_z/E_{z_0})^2 = 0.1$ for $\xi_0 = 0.3$ elliptical rod, is 0.47, and for $\xi_0 = 3.0$ elliptical rod it is 0.435.

The fact that the variation of slopes with respect to NCSA in Figure IV-2 is smaller for flatter rods in the low loss region, is quite significant. It means that a small imperfection in the dimensions of a flatter rod would induce a smaller change in the attenuation factor R .
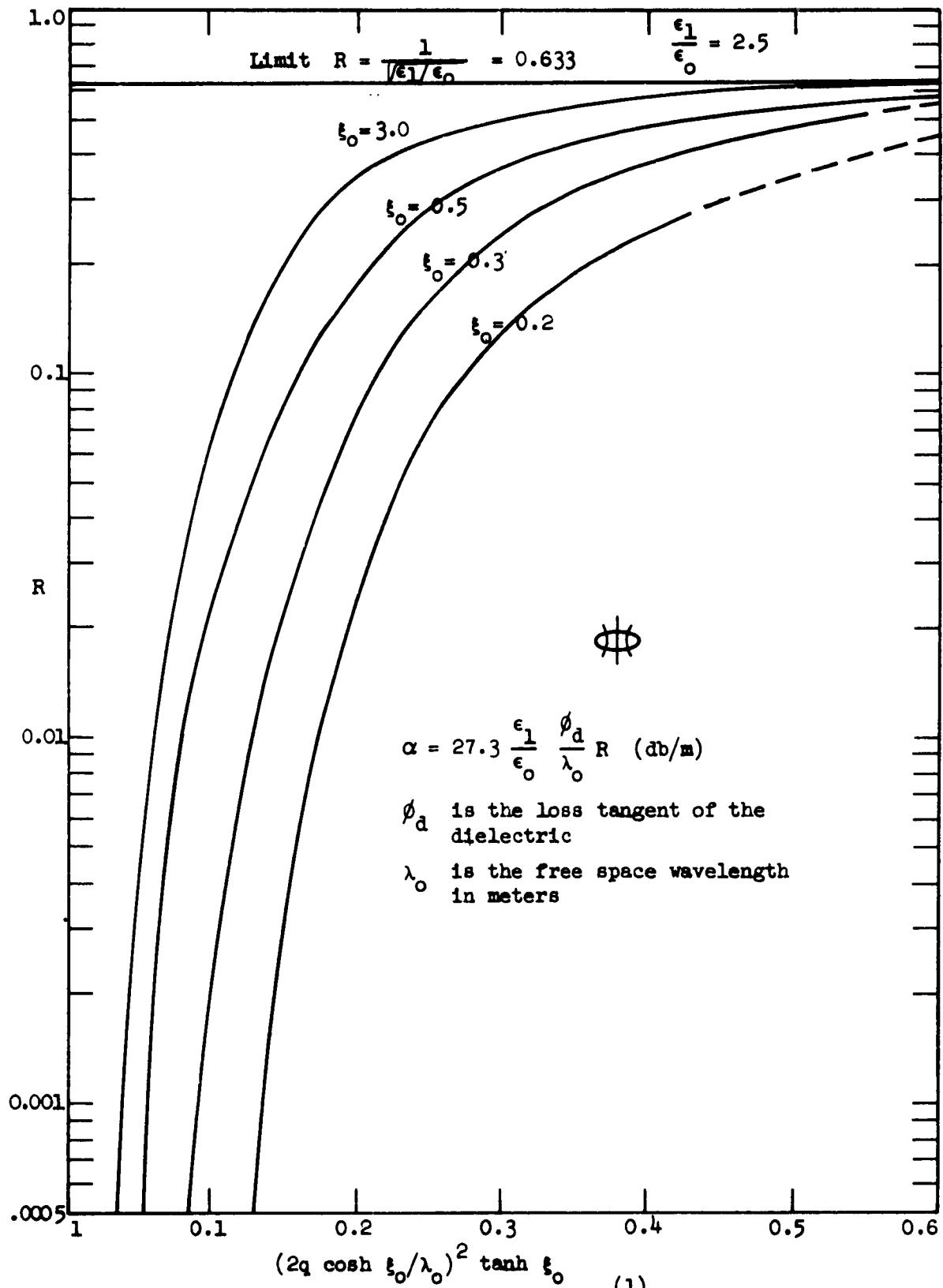
Fig. IV-2. Attenuation factor R for the $_e\text{HE}_{11}^{(1)}$ mode as a function of normalized cross sectional area.

It is interesting to note the distribution of the transmitted power. There is a very close correlation between the percentage of power carried inside the rod and the loss factor of the wave. With the help of Poynting's vector theorem, one can easily calculate the percentage of power transmitted inside the dielectric rod. It is

$$\frac{P_i}{P_t} = \frac{f_2}{f_2 + f_3} \quad , \tag{28}$$

where f_2 and f_3 are given in equation 26. Numerical results of equation 28 are given in Figure IV-3 in which P_i/P_t is plotted against NMA for various values of ξ_o ; ϵ_1/ϵ_o is assumed to be constant and is equal to 2.5 . It is observed from Figures IV-2 and IV-3 that a higher percentage of power transmitted inside the rod corresponds to a higher attenuation factor and more power is carried inside the circular rod than an elliptical rod of identical cross-sectional area. Figure IV-3 also confirms the fact that more power is carried inside the rod as the frequency gets higher.

The ξ_o = 3.0 curve in Figure IV-1 corresponds very well with the published results for the circular dielectric rod (18). The analytic expression of the loss factor R for the degenerate circular dielectric rod can easily be derived from equation 26. Noting that as $\xi_o \to \infty$, $q \to 0$, $q \cosh \xi_o \to a$ and $q e^{\xi}/2 \to \rho$, where a is the radius of the circule and ρ is the radial component in the polar coordinates, one gets,

$$\frac{L_3}{A_1} \to \frac{L_5}{A_1} \to \frac{L_7}{A_1} \to \cdots \frac{L_\infty}{A_1} \to 0$$
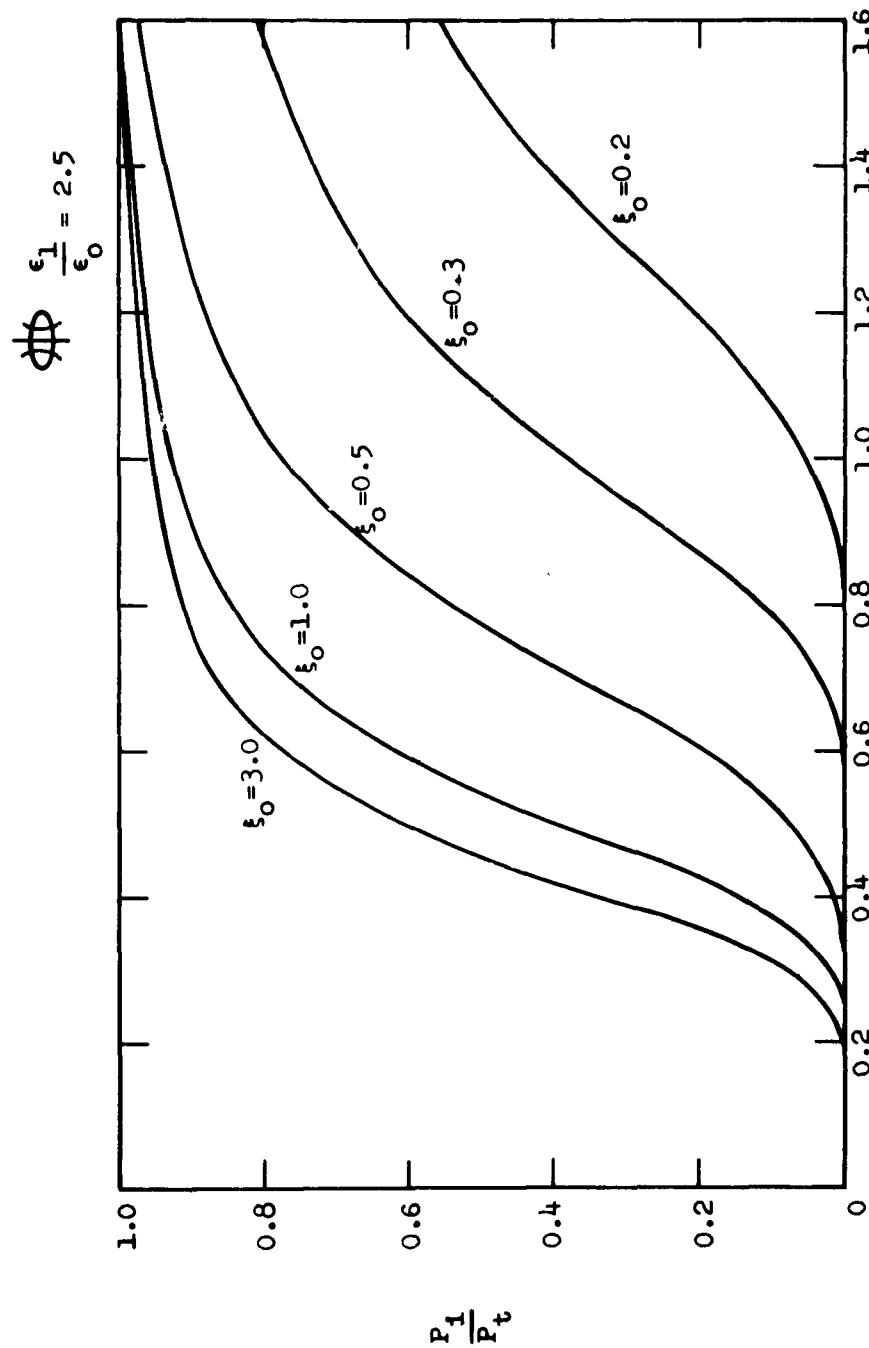
Fig. IV-3. The fraction of total power carried inside a dielectric rod supporting the $_e\text{HE}_{11}^{(1)}$ mode as a function of the normalized major axis

$$\frac{P_3}{A_1} \rightarrow \frac{P_5}{A_1} \rightarrow \frac{P_7}{A_1} \rightarrow \cdots \frac{P_\infty}{A_1} \rightarrow 0$$

$$\frac{B_1}{A_1} \rightarrow \sqrt{\frac{\mu}{\epsilon_o}} \; \frac{\frac{x^2}{y^2} \; y \; K_1'(y) \; \frac{L_1}{A_1} + x \; J_1'(x)}{J_1(x)\left[\frac{\sqrt{x^2+y^2}\,(x^2+y^2\frac{\epsilon_1}{\epsilon_o})}{y^2}\right]}$$

$$\frac{L_1}{A_1} \rightarrow \frac{J_1(x)}{K_1(y)} \; , \qquad \frac{P_1}{A_1} \rightarrow \frac{J_1(x)}{K_1(y)} \; (\frac{B_1}{A_1})$$

and

$$x^2 = a^2(k_1^2 - \beta^2) \; , \qquad y^2 = -a^2(k_o^2 - \beta^2) \; ,$$

since

$$\alpha_{rs} = 0 \quad \text{when} \quad r \neq s$$
$$= 1 \quad \text{when} \quad r = s$$

$$\beta_{rs} = 0 \quad \text{when} \quad r \neq s$$
$$= 1 \quad \text{when} \quad r = s$$

$$R(\alpha_{rs}, \delta_{1s}) \rightarrow 1$$
$$Q(\beta_{rs}, \gamma_{1s}) \rightarrow 1 \; .$$

Equations 21, 23 and 25 degenerate to the known expressions associated
with the loss factor of the dominant mode propagating along a circular
dielectric rod (21); they are, respectively,

$$\frac{\int_{A_1} (\underline{E}_1 \cdot \underline{E}_1^*) dA}{a^2 A_1^2 \; \frac{\mu_o}{\epsilon_o}} \rightarrow C_1\left[C_2(I_8 + I_9) + (\frac{B_1}{A_1})^2 \; \frac{\epsilon_o}{\mu_o} \; (I_{10} + I_{11})\right.$$
$$\left. - 2\sqrt{C_2} \; \sqrt{\frac{\epsilon_o}{\mu_o}} \; \frac{B_1}{A_1} \; (I_{12} + I_{13})\right] + (\frac{\epsilon_o}{\mu_o})\frac{B_1}{A_1} \; I_{14} \; ,$$

$$\frac{\displaystyle\int_{A_1} (\underline{E}_{t1} \times \underline{H}^*_{t1}) \cdot \underline{e}_z dA}{a^2 A_1^2 \sqrt{\frac{\mu_o}{\epsilon_o}}} \rightarrow C_1 \left[\sqrt{C_2}(I_8 + I_9) + \frac{\epsilon_1}{\epsilon_o}\sqrt{C_2} \frac{\epsilon_o}{\mu} (\frac{B_1}{A_1})^2 (I_{10} + I_{11}) \right.$$

$$\left. -\sqrt{\frac{\epsilon_o}{\mu}} \frac{B_1}{A_1} (1 + \frac{\epsilon_1}{\epsilon_o} C_2)(I_{12} + I_{13}) \right] \qquad ,$$

and

$$\frac{\displaystyle\int_{A_o} (\underline{E}_{to} \times \underline{H}^*_{to}) \cdot \underline{e}_z dA}{a^2 A_1^2 \sqrt{\frac{\mu_o}{\epsilon_o}}} \rightarrow \frac{x^4}{y^4} C_1 \left[(\frac{L_1}{A_1})^2 \sqrt{C_2}(I'_{21} + I'_{22}) + (\frac{P_1}{A_1})^2 \frac{\epsilon_o}{\mu}\sqrt{C_2}(I'_{27} + I'_{28}) \right.$$

$$\left. - (\frac{L_1}{A_1})(\frac{P_1}{A_1})\sqrt{\frac{\epsilon_1}{\mu}} (1 + C_2)(I'_{33} + I'_{34}) \right] \qquad ,$$

where $\qquad C_1 = \dfrac{x^2 + y^2 \frac{\epsilon_1}{\epsilon_o}}{x^4 (\frac{\epsilon_1}{\epsilon_o} - 1)} \quad , \quad C_2 = \dfrac{x^2 + y^2}{x^2 + \frac{\epsilon_1}{\epsilon_o} y^2} \qquad ,$

$$I_8 = I_{11} = \int_0^x J_1^2(p) \frac{dp}{p} , \qquad I_9 = I_{10} = \int_0^x J_1'^2(p) p \, dp ,$$

$$I_{12} = I_{13} = \int_0^x J_1(p) J_1'(p) dp, \qquad I_{14} = \int_0^x J_1^2(p) \frac{p}{x^2} dp \qquad ,$$

$$I'_{21} = I'_{27} = \int_y^\infty K_1^2(n) \frac{dn}{n} \qquad , \qquad I'_{20} = I'_{28} = \int_y^\infty K_1'^2(n) n \, dn \qquad ,$$

and $\quad I'_{33} = I'_{34} = \displaystyle\int_y^\infty K_1(n) K_1'(n) dn$

in which $p = x \frac{\rho}{a}$ and $n = y \frac{\rho}{a}$. The attenuation constant of the HE_{11} wave on a circular dielectric rod can easily be obtained by substituting the above expressions into equation 4.1-7.

4.3 The Attenuation Factor and Power Distribution Characteristics of the $_o HE_{11}^{(1)}$ Mode

The case of the $_o HE_{11}^{(1)}$ wave can be analyzed in a similar manner to that of the $_e HE_{11}^{(1)}$ wave. From section 2.5c one obtains the field components of the $_o HE_{11}^{(1)}$ mode. They are, for region 1 $(0 \leqslant \xi \leqslant \xi_o)$,

$$H_{z_1} = a_1 Se_1(\xi) se_1(\eta) e^{i\beta z} \tag{1}$$

$$E_{z_1} = b_1 Ce_1(\xi) ce_1(\eta) e^{i\beta z} \tag{2}$$

$$H_{\xi_1} = \frac{i\beta}{p(k_1^2 - \beta^2)} \left\{ a_1 Se_1'(\xi) se_1(\eta) - \frac{\omega\epsilon_1}{\beta} b_1 Ce_1(\xi) ce_1'(\eta) \right\} e^{i\beta z} \tag{3}$$

$$H_{\eta_1} = \frac{i\beta}{p(k_1^2 - \beta^2)} \left\{ a_1 Se_1(\xi) se_1'(\eta) + \frac{\omega\epsilon_1}{\beta} b_1 Ce_1'(\xi) ce_1(\eta) \right\} e^{i\beta z} \tag{4}$$

$$E_{\xi_1} = \frac{i\beta}{p(k_1^2 - \beta^2)} \left\{ a_1 \frac{\omega\mu}{\beta} Se_1(\xi) se_1'(\eta) + b_1 Ce_1'(\xi) ce_1(\eta) \right\} e^{i\beta z} \tag{5}$$

$$E_{\eta_1} = \frac{i\beta}{p(k_1^2 - \beta^2)} \left\{ - a_1 \frac{\omega\mu}{\beta} Se_1'(\xi) se_1(\eta) + b_1 Ce_1(\xi) ce_1'(\eta) \right\} e^{i\beta z} \tag{6}$$

and for region 0 $(\xi_o \leqslant \xi < \infty)$.

$$H_{z_o} = \sum_{\substack{r=1 \\ odd}}^{\infty} g_r Gek_r(\xi) se_r^*(\eta) e^{i\beta z} \tag{7}$$

$$E_{z_o} = \sum_{\substack{r=1 \\ odd}}^{\infty} h_r Fek_r(\xi) ce_r^*(\eta) e^{i\beta z} \tag{8}$$

$$H_{\xi_o} = \frac{i\beta}{p(k_o^2 - \beta^2)} \sum_{\substack{r=1 \\ odd}}^{\infty} \left\{ g_r Gek_r'(\xi) se_r^*(\eta) - \frac{\omega\epsilon_o}{\beta} h_r Fek_r(\xi) ce_r^{*'}(\eta) \right\} e^{i\beta z} \tag{9}$$

$$H_{\eta_o} = \frac{i\beta}{p(k_o^2-\beta^2)} \sum_{\substack{r=1 \\ odd}}^{\infty} \left\{ g_r \dot{Gek}_r(\xi) se_r^{*\prime}(\eta) + \frac{\omega\epsilon_o}{\beta} h_r Fek_r^{\prime}(\xi) ce_r^{*}(\eta) \right\} e^{i\beta z} \qquad (10)$$

$$E_{\xi_o} = \frac{i\beta}{p(k_o^2-\beta^2)} \sum_{\substack{r=1 \\ odd}}^{\infty} \left\{ g_r \frac{\omega\mu}{\beta} Gek_r(\xi) se_r^{*\prime}(\eta) + h_r Fek_r^{\prime}(\xi) ce_r^{*}(\eta) \right\} e^{i\beta z} \qquad (11)$$

$$E_{\eta_o} = \frac{i\beta}{p(k_o^2-\beta^2)} \sum_{\substack{r=1 \\ odd}}^{\infty} \left\{ - g_r \frac{\omega\mu}{\beta} Gek_r^{\prime}(\xi) se_r^{*}(\eta) + h_r Fek_r(\xi) ce_r^{*\prime}(\eta) \right\} e^{i\beta z} \qquad (12)$$

where $k_o^2 = \omega^2\mu\epsilon_o$, $k_1^2 = \omega^2\mu\epsilon_1$ and $p = q(\sinh^2\xi + \sin^2\eta)^{1/2}$. a_1, b_1, g_r and h_r are arbitrary constants which are related by the boundary conditions and are given by (see section 2.5c equations 70, 71 and 72,)

$$\frac{g_1}{a_1} = \frac{Se_1(\xi_o)}{Gek_1(\xi_o)N_1(\beta_{rs})} \qquad (13)$$

$$\frac{g_3}{a_1} = \frac{g_3}{g_1}\frac{g_1}{a_1} = - \frac{Gek_1(\xi_o)}{Gek_3(\xi_o)} \frac{\begin{vmatrix} \beta_{13} & \beta_{53} & \cdots \\ \beta_{15} & \beta_{55} & \cdots \\ \cdots & \cdots & \cdots \end{vmatrix}}{\begin{vmatrix} \beta_{33} & \beta_{53} & \cdots \\ \beta_{35} & \beta_{55} & \cdots \\ \cdots & \cdots & \cdots \end{vmatrix}} \cdot \frac{g_1}{a_1} , \qquad (14)$$

$$\frac{g_5}{a_1} = \frac{g_5}{g_1}\frac{g_1}{a_1} = - \frac{Gek_1(\xi_o)}{Gek_5(\xi_o)} \frac{\begin{vmatrix} \beta_{33} & \beta_{13} & \cdots \\ \beta_{35} & \beta_{15} & \cdots \\ \cdots & \cdots & \cdots \end{vmatrix}}{\begin{vmatrix} \beta_{33} & \beta_{53} & \cdots \\ \beta_{35} & \beta_{55} & \cdots \\ \cdots & \cdots & \cdots \end{vmatrix}} \cdot \frac{g_1}{a_1} \qquad (15)$$

· ·

$$\frac{b_1}{a_1} = \sqrt{\frac{\mu}{\epsilon_o}} \; \frac{\frac{x^2}{y^2} \mathrm{Gek}_1'(\xi_o) N_1(\beta_{rs}) \frac{g_1}{a_1} + \mathrm{Se}_1'(\xi_o)}{\mathrm{Ce}_1(\xi_o) \; \dfrac{\sqrt{(x^2+y^2)(x^2+y^2\frac{\epsilon_1}{\epsilon_o})}}{y^2} \; Q_1(\beta_{rs},\chi_{1s})} \quad , \qquad (16)$$

$$\frac{h_1}{a_1} = \frac{\mathrm{Ce}_1(\xi_o)}{\mathrm{Fek}_1(\xi_o) M_1(\alpha_{rs})} \cdot \frac{b_1}{a_1} \qquad\qquad (17)$$

$$\frac{h_3}{a_1} = \frac{h_3}{h_1}\frac{h_1}{a_1} = -\frac{\mathrm{Fek}_1(\xi_o)}{\mathrm{Fek}_3(\xi_o)} \frac{\begin{vmatrix} \alpha_{13} & \alpha_{53} & \cdots \\ \alpha_{15} & \alpha_{55} & \cdots \\ \cdots & \cdots & \cdots \end{vmatrix}}{\begin{vmatrix} \alpha_{33} & \alpha_{53} & \cdots \\ \alpha_{35} & \alpha_{55} & \cdots \\ \cdots & \cdots & \cdots \end{vmatrix}} \cdot \frac{h_1}{a_1} \qquad (18)$$

$$\frac{h_5}{a_1} = \frac{h_5}{h_1}\frac{h_1}{a_1} = -\frac{\mathrm{Fek}_1(\xi_o)}{\mathrm{Fek}_3(\xi_o)} \frac{\begin{vmatrix} \alpha_{33} & \alpha_{13} & \cdots \\ \alpha_{35} & \alpha_{15} & \cdots \\ \cdots & \cdots & \cdots \end{vmatrix}}{\begin{vmatrix} \alpha_{33} & \alpha_{53} & \cdots \\ \alpha_{35} & \alpha_{55} & \cdots \\ \cdots & \cdots & \cdots \end{vmatrix}} \cdot \frac{h_1}{a_1} \qquad (19)$$

and . . . .

The attenuation factor of the $_o\mathrm{HE}_{11}^{(1)}$ mode can be calculated in a similar manner as that of the $_e\mathrm{HE}_{11}^{(1)}$ mode. It can be shown that $g_1/a_1 > g_3/a_1 \gg g_5/a_1 \gg \cdots \gg g_\infty/a_1$, and $h_1/a_1 > h_3/a_1 \gg h_5/a_1 \gg \cdots \gg h_\infty/a_1$, provided that $\xi_o \geq 0.2$, $0 \leq x \leq 5$, and $y \leq 3.0$. The first two terms of the infinite series are sufficient to represent

the field components in region 0 .

Substituting the appropriate field expressions 1 through 12 into 4.1-7 one finds after some manipulation that

$$\alpha = \frac{8.686}{2} \sigma_d \sqrt{\frac{\mu}{\epsilon_o}} \ R' \ , \quad (\mathrm{db/m}) \tag{20}$$

in which $R' = F_1 / F_2 + F_3$,

where

$$F_1 = \frac{\int_{A_1}(\underline{E}_1 \cdot \underline{E}_1^*)dA}{\cosh^2\xi_o q^2 a_1^2 \frac{\mu}{\epsilon_o}} = C_1\left[C_2(I_{11}I_4 + I_{10}I_3) + \left(\frac{b_1}{a_1}\right)^2 \frac{\epsilon_o}{\mu}(I_9I_2 + I_8I_1) \right.$$

$$\left. + 2\sqrt{C_2}\left(\frac{b_1}{a_1}\right)\sqrt{\frac{\epsilon_o}{\mu}}(I_{13}I_6 - I_{12}I_5)\right] + \left(\frac{b_1}{a_1}\right)^2 \frac{\epsilon_o}{\mu}\left[I_{14_{NN}}I_2 + \frac{1}{2}\frac{I_8(I_2 - I_{7c})}{\cosh^2\xi_o}\right] ,$$

$$\tag{21}$$

$$F_2 = \frac{\int_{A_1}(\underline{E}_{t1} \times \underline{H}_{t1}^*)\cdot \underline{e}_z dA}{\cosh^2\xi_o q^2 a_1^2 \sqrt{\frac{\mu}{\epsilon_o}}} = C_1\left[\sqrt{C_2}(I_{11}I_4 + I_{10}I_3) + \frac{\epsilon_1}{\epsilon_o}\sqrt{C_2}\left(\frac{b_1}{a_1}\right)^2 \frac{\epsilon_o}{\mu}(I_9I_2 + I_8I_1)\right.$$

$$\left. + \left(\frac{b_1}{a_1}\right)\sqrt{\frac{\epsilon_o}{\mu}}\left(1 + \frac{\epsilon_1}{\epsilon_o}\sqrt{C_2}\right)(I_{13}I_6 - I_{12}I_5)\right] , \quad (22)$$

and

$$F_3 = \frac{\int_{A_o}(\underline{E}_{to} \times \underline{H}_{to}^*)\cdot \underline{e}_z dA}{\cosh^2\xi_o q^2 a_1^2 \sqrt{\frac{\mu}{\epsilon_o}}} = \frac{x^4}{y^4} C_1\left[\left(\frac{g_1}{a_1}\right)^2 \sqrt{C_2}(BI)' + \left(\frac{h_1}{a_1}\right)^2 \frac{\epsilon_o}{\mu}\sqrt{C_2}(BII)'\right.$$

$$\left. + \left(\frac{g_1}{a_1}\right)\left(\frac{h_1}{a_1}\right)\sqrt{\frac{\epsilon_o}{\mu}}(1 + C_2)(BIII)'\right] . \tag{23}$$

(BI)', (BII)', and (BIII)' are respectively

$$(I_7'I_{27}' + I_8'I_{28}') + \left(\frac{g_3}{g_1}\right)^2 (I_9'I_{29}' + I_{30}'I_{10}') + 2\left(\frac{g_3}{g_1}\right)(I_{31}'I_{11}' + I_{32}'I_{12}') \ ,$$

$$(I_1'I_{21}' + I_2'I_{22}') + \left(\frac{h_3}{h_1}\right)^2 (I_3'I_{23}' + I_{24}'I_4') + 2\left(\frac{h_3}{h_1}\right)(I_{25}'I_5' + I_{26}'I_{61}') \ ,$$

and

$$(I_{34}'I_{14}' - I_{33}'I_{13}') + \left(\frac{g_3}{g_1}\right)^2 (I_{36}'I_{16}' - I_{35}'I_{15}') + \left(\frac{h_3}{h_1}\right)^2 (I_{38}'I_{18}' - I_{37}'I_{17}')$$

$$+ \left(\frac{g_3}{g_1}\right)\left(\frac{h_3}{h_1}\right)(I_{40}'I_{20}' - I_{39}'I_{19}') \ ,$$

where I_1 through I_6 , I_8 through I_{13} , I_1' through I_{40}' , I_{7c} and I_{14NN} are given in Appendix B . The loss factor R' for the $_0HE_{11}^{(1)}$ mode as a function of NMA is computed for various values of ξ_0 ranging from $\xi_0 = 0.2$ to $\xi_0 = 3.0$. The relative dielectric constant ϵ_1/ϵ_0 is assumed to be constant and equals 2.5. The results are plotted in Figure IV-4. The attenuation factor R' for the $_0HE_{11}^{(1)}$ mode varies with frequency in a similar way as that for the $_eHE_{11}^{(1)}$ mode, viz., the attenuation factor R' approaches $1/\sqrt{\epsilon_1/\epsilon_0}$ as frequency approaches infinity and R' can be made arbitrarily small by lowering the frequency. It should be noted that the slope of the curve for the elliptical rod in the low loss region is quite steep, i.e., a small variation in NMA would cause a rather significant fluctuation in R'. It is quite obvious that the $_eHE_{11}^{(1)}$ mode is more suitable than the $_0HE_{11}^{(1)}$ mode as a transmission mode.

The distribution of the transmitted power as a function of frequency can easily be computed. The percentage of power carried inside the dielectric rod is
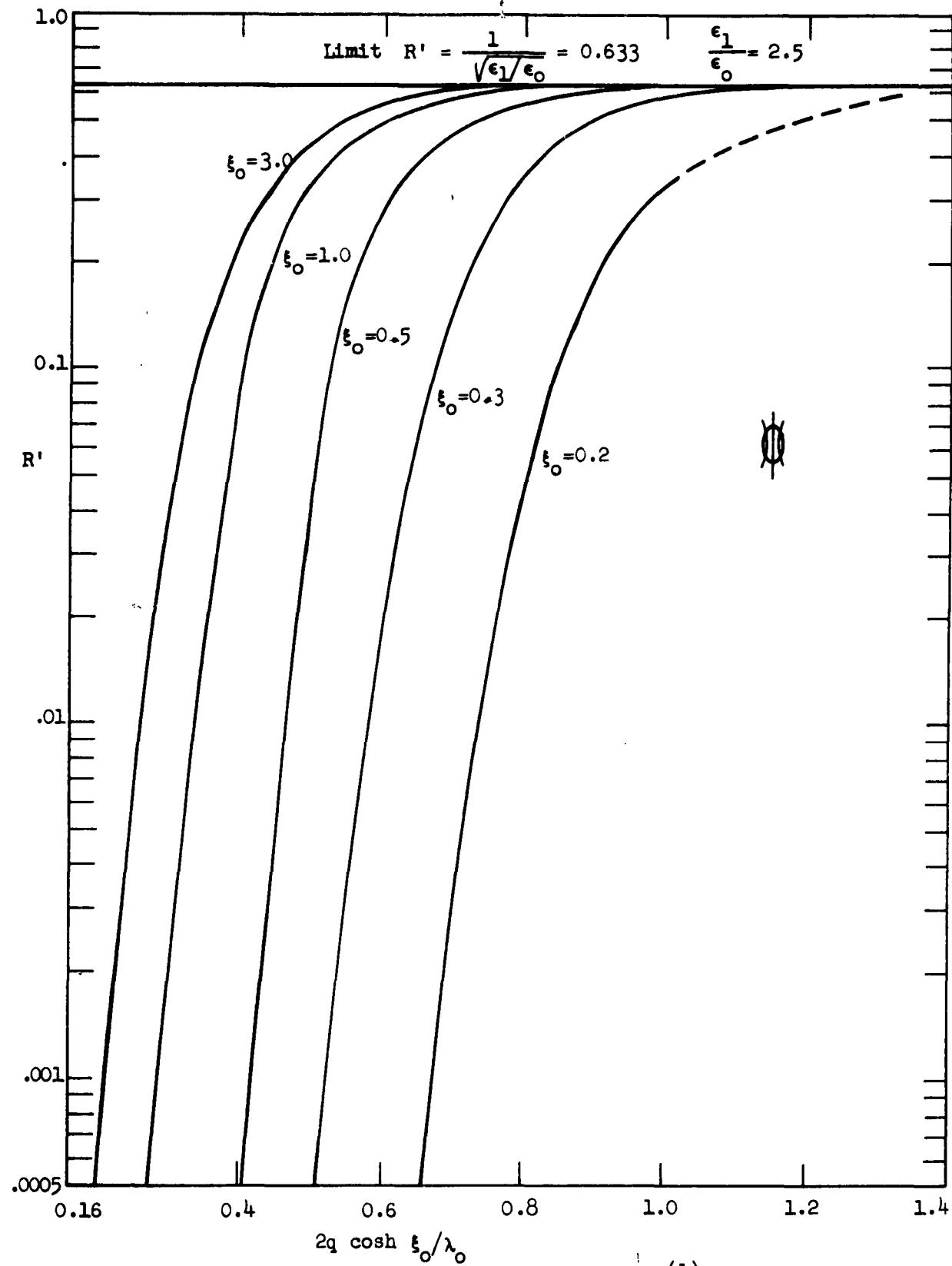
Fig. IV-4. The attenuation factor R' for the $_o HE_{11}^{(1)}$ mode as a function of the normalized major axis.
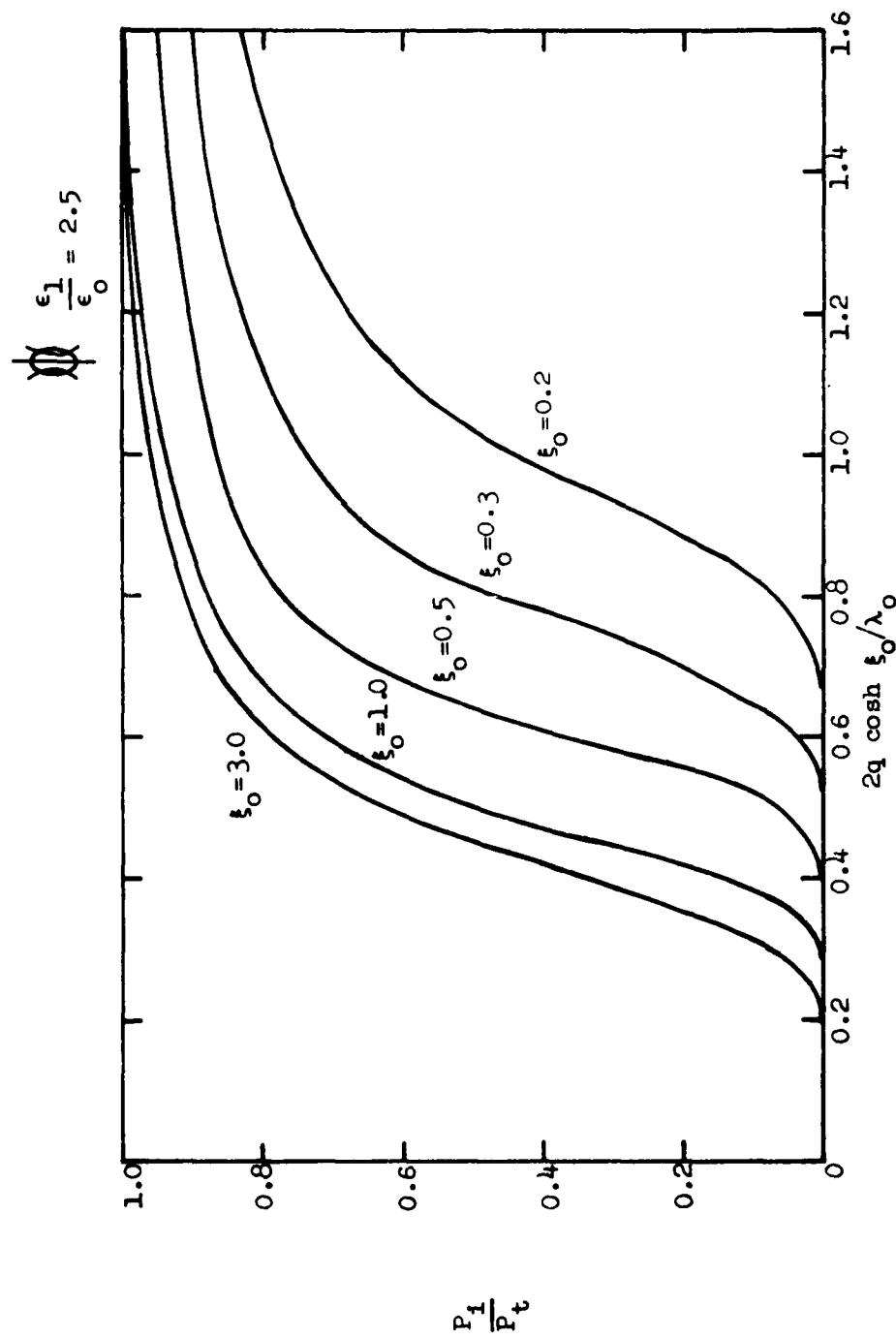
Fig. IV-5. The fraction of total power carried inside a dielectric rod supporting the $_o HE_{11}^{(1)}$ mode as a function of the normalized major axis.

$$\frac{P_i'}{P_t'} = \frac{F_2}{F_2 + F_3} \qquad (24)$$

where F_2 and F_3 are given by equations 22 and 23 respectively.

Figure IV-5 shows the variation of P_i'/P_t' as a function of NMA for

various values of ξ_o ; ϵ_1/ϵ_o equals 2.5 . The behavior of these curves

is as expected. More power is carried inside the rod as the frequency

gets higher. Again there is a very close correlation between the

amount of power carried inside the rod and the value of the attenuation

factor.

4.4 Summary

A detailed analysis on the attenuation characteristics of the

$_e\mathrm{HE}_{11}^{(1)}$ mode and the $_o\mathrm{HE}_{11}^{(1)}$ mode propagating along an elliptical dielec-

tric rod are carried out in this chapter. Numerical results are obtained.

It is found that a thin elliptical dielectric rod operating in the

dominant $_e\mathrm{HE}_{11}^{(1)}$ mode is a better guiding structure than a circular

dielectric rod operating in the dominant HE_{11} mode, because the $_e\mathrm{HE}_{11}^{(1)}$

mode has much lower loss on a flat elliptical rod than on a circular rod

of identical cross-sectional area.

It would be interesting to compare the attenuation constant of the

$_e\mathrm{HE}_{11}^{(1)}$ mode with the attenuation constants of some well known metallic

waveguide modes in the millimeter wavelength region. The values of the

attenuation constants for various kinds of waves are tabulated in the

following table.

Type of Waveguide	Type of Propagating Mode	Frequency	Dimensions of the Waveguide	Attenuation Constant α (db/100 ft)
Rectangular Metal Wave-guide (RG98/u)	The Dominant TE_{10} Mode	60 kmc.		60
Circular Metal Wave-guide	The Circular Symmetric TE_{01} Mode	60 kmc.	7/10" I.D.*	4
			7/3" I.D.**	0.4
Polystyrene*** Elliptical Dielectric Waveguide	The Dominant $eHE_{11}^{(1)}$ Mode	60 kmc.	$2A \times 2B \ (mm)^2$	
			$2.24 \times 2.24 \ (\xi_0 = 3.0)$	141
			$3.3 \times 1.52 \ (\xi_0 = 0.5)$	70
			$4.14 \times 1.2 \ (\xi_0 = 0.3)$	35
			$5.01 \times 1.0 \ (\xi_0 = 0.2)$	11
			$\frac{4}{\pi} \frac{area}{\lambda_0^2} = 0.2$	
			$1.94 \times 1.94 \ (\xi_0 = 3.0)$	83
			$2.85 \times 1.31 \ (\xi_0 = 0.5)$	34
			$3.59 \times 1.05 \ (\xi_0 = 0.3)$	9.6
			$4.06 \times 0.863 \ (\xi_0 = 0.2)$	1.3
			$\frac{4}{\pi} \frac{area}{\lambda_0^2} = 0.15$	

* This waveguide can support 11 other asymmetric modes at this frequency.

** This waveguide can support 49 other modes at this frequency.

*** The Polystyrene has a dielectric constant of 2.5 and a loss tangent ϕ_d of 0.001.

CHAPTER V - ELLIPTICAL DIELECTRIC ROD RESONATOR

To conclude the theoretical analysis of surface wave propagation along an elliptical dielectric rod, we include here the analysis of the Q factor of the elliptical dielectric rod cavity. The earliest work on dielectric resonators was carried out by Richtmyer (53) in 1939. He developed the theory of operation for several interesting dielectric resonators of simple shapes, such as the spherical dielectric cavity and the "doughnut" shape dielectric cavity. The dielectric tube resonator was first used by the group in the Northwestern University (54). Later in 1959 Becker and Coleman (26) made use of the dielectric tube resonator to generate millimeter and submillimeter waves and to operate as a frequency meter. Most recently Snitzer (40) proposed the use of dielectric rod cavity as a mode selector in laser operation.

In the present problem the dielectric rod cavity consists of an elliptical dielectric rod suitably terminated at its ends by sufficiently large flat metal plates which are perpendicular to the axis of the rod (see Figure V-1). At resonance, the length of the cavity L must
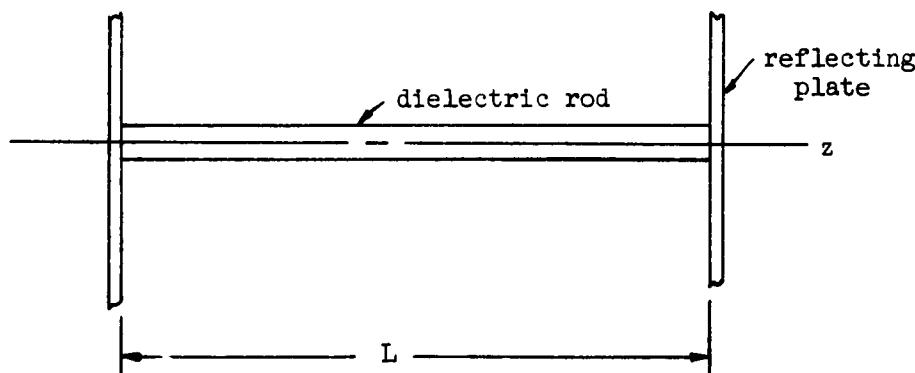

Figure V-1. The Elliptical Dielectric Rod Resonator

be $n \frac{\lambda_g}{2}$ (n, an integer), where λ_g is the guide wavelength of the particular mode under consideration and is a function of λ_o, ϵ_1/ϵ_o, and the size and shape of the dielectric rod. The relations between λ_g and the mentioned physical constants are determined by the boundary conditions. Only the $_e\text{HE}_{11n}^{(1)}$ and the $_o\text{HE}_{11n}^{(1)}$ modes of the dielectric rod resonator will be considered in this chapter.

The Q factor of a resonator is indicative of the energy storage capability of a structure relative to the associated energy dissipation arising from various loss mechanisms, such as those due to the imperfection of the dielectric material and the finite conductivity of the end plates. The common definition for Q is applicable to the dielectric rod resonator, and is given by (15)

$$Q = \omega_o \frac{\text{total time-average energy stored}}{\text{average power loss}} = \omega_o \frac{\overline{W}}{\overline{P}} , \tag{1}$$

where ω_o is the frequency of oscillation. The above approximate expression is valid when $Q \gg 1$.

In our case the time-average power dissipation $\overline{P}$ consists of two parts, the power loss due to the dielectric rod and that due to the metal end walls

$$\overline{P} = \overline{P}_{\text{dielectric}} + \overline{P}_{\text{wall}} . \tag{2}$$

The power dissipation due to the dielectric rod is given by (15)

$$\overline{P}_{\text{dielectric}} = -\sigma_d \int_0^L \int_{A_1} (\underline{E}_1 \cdot \underline{E}_1^*) \, dA \, dz \tag{3}$$

while the loss due to the end wall is (15)

$$\bar{P}_{wall} = \frac{1}{2} \sqrt{\frac{\omega\mu}{2\sigma_M}} \int_{\substack{A_{end} \\ wall}} \underline{H}_{t_{wall}} \cdot \underline{H}^*_{t_{wall}} \, dA \, , \tag{4}$$

where $\sqrt{\frac{\omega\mu}{2\sigma_M}}$ is the surface resistance, R_s . The total time-average energy stored is given by (15)

$$\bar{W} = 2\bar{W}_m = 2\bar{W}_e = \frac{\mu}{2} \int_{V_{i+o}} \underline{H} \cdot \underline{H}^* \, dV = \frac{\epsilon}{2} \int_{V_{i+o}} \underline{E} \cdot \underline{E}^* dV \tag{5}$$

where V_{i+o} is the total volume of the cavity.

5.1 Q of a Cavity Supporting the $_e HE_{11n}^{(1)}$ Mode

By a linear superposition of the mode functions 4.2-1 through 4.2-12 for the $_e HE_{11}^{(1)}$ wave traveling in the positive and negative z-direction, the normal modes of the cavity may be constructed. The resultant axial fields of an $_e HE_{11}^{(1)}$ wave traveling in the positive z-direction and a superposed $_e HE_{11}^{(1)}$ wave of the same amplitude traveling in the opposite direction are as follows for region 1 $(0 \leqq \xi \leqq \xi_o)$

$$H_{z_1} = A \, Ce_1(\xi) ce_1(\eta) \sin \beta z \tag{1}$$

$$E_{z_1} = - B \, Se_1(\xi) se_1(\eta) \cos \beta z \tag{2}$$

and for region 0 $(\xi_o \leqq \xi < \infty)$

$$H_{z_o} = \sum_{\substack{r=1 \\ odd}}^{\infty} L_r Fek_r(\xi) ce_r^*(\eta) \sin \beta z \tag{3}$$

$$E_{z_o} = -\sum_{\substack{r=1 \\ odd}}^{\infty} P_r Gek_r(\xi) se_r^*(\eta) \cos \beta z \tag{4}$$

All the symbols in the above expressions have the same meaning as those defined in the previous chapters. The arbitrary constants A_1, B_1, L_r and P_r which are related by the boundary conditions are given by equations 4.2-13 through 4.2-19. Expressions 1 through 4 satisfy the boundary conditions on the surface of the dielectric rod and at the end $z = 0$. To make them also satisfy the boundary conditions at the other end, $z = L$, we restrict β in such a way that $\beta L = n\pi$ where n is an integer, (i.e., $L = n\lambda_g/2$).

Substituting the proper field expressions into 5-5, carrying out the integrations where possible and retaining enough terms of the expansion to give the same order of approximation as obtained in Chapter IV, one finally arrives at (after some rather lengthy algebraic manipulations) the expression for the energy stored in the cavity for the $_e\text{HE}_{11n}^{(1)}$ mode,

$$\bar{W} = \frac{\epsilon_1}{2} \int_{V_1} (\underline{E}_1 \cdot \underline{E}_1^*)dV + \frac{\epsilon_o}{2} \int_{V_o} (\underline{E}_o \cdot \underline{E}_o^*)dV$$

$$= \cosh^2\xi_o \; q^2 A_1^2 \; \frac{L\epsilon_o}{4} \; \frac{\mu_o}{\epsilon_o} \; C_T \tag{5}$$

where
$$C_T = \frac{\epsilon_1}{\epsilon_o} \left(\frac{B_1}{A_1}\right)^2 \frac{\epsilon_o}{\mu_o} \left[I_{14}I_3 + \frac{I_{11}(I_3 - I_7)}{2\cosh^2\xi_o} \right] + \frac{\epsilon_1}{\epsilon_o} C_1 \left[C_2(I_8 I_1 + I_9 I_2) \right.$$

$$+ \left(\frac{B_1}{A_1}\right)^2 \frac{\epsilon_o}{\mu_o} (I_{10}I_3 + I_{11}I_4) + 2\sqrt{C_2} \left(\frac{B_1}{A_1}\right)\sqrt{\frac{\epsilon_o}{\mu_o}} (I_{12}I_5 - I_{13}I_6) \Big]$$

$$+ \left(\frac{P_1}{A_1}\right)^2 \left(\frac{\epsilon_o}{\mu_o}\right) \left\{ \left[I_{41}' I_8' + \frac{I_{27}'(I_8' - I_a')}{2\cosh^2\xi_o} \right] + \left(\frac{P_3}{P_1}\right)^2 \left[I_{42}' I_{10}' + \frac{I_{29}'(I_{10}' - I_b')}{2\cosh^2\xi_o} \right] \right.$$

$$+ 2\left(\frac{P_3}{P_1}\right) \left[I_{43}' I_{12}' + \frac{I_{31}'(I_{12}' - I_c')}{2\cosh^2\xi_o} \right] \Big\} + \frac{x^4}{y^4} C_1 \left[\left(\frac{L_1}{A_1}\right)^2 (\text{BI})C_2 \right.$$

$$+ \left(\frac{P_1}{A_1}\right)^2 \left(\frac{\epsilon_o}{\mu_o}\right)(\text{BII}) + 2\sqrt{C_2}\left(\frac{L_1}{A_1}\right)\left(\frac{P_1}{A_1}\right) \sqrt{\frac{\epsilon_o}{\mu_o}} (\text{BIII}) \Big].$$

C_1, C_2, BI, BII, BIII, x^2 and y^2 are given in Chapter IV. The integrals, i.e., I's or I''s, are defined in Appendix B.

The power dissipation due to the dielectric loss is

$$\bar{P}_{dielectric} = -\frac{\sigma_d L}{2} \int_0^{\xi_0} \int_0^{2\pi} (\underline{E}_1 \cdot \underline{E}_1^*) p^2 d\eta d\xi$$

$$= -\frac{\sigma_d L}{2} A_1^2 q^2 \cosh^2 \xi_0 \frac{\mu_o}{\epsilon_o} C_d \qquad (6)$$

where

$$C_d = \left(\frac{B_1}{A_1}\right)^2 \left(\frac{\epsilon_o}{\mu_o}\right) \left[I_{14}I_3 + \frac{I_{11}(I_3 - I_7)}{2 \cosh^2 \xi_0} \right] + C_1 \left[C_2(I_8I_1 + I_9I_2) \cdot \right.$$

$$\left. + \left(\frac{B_1}{A_1}\right)^2 \frac{\epsilon_o}{\mu_o} (I_{10}I_3 + I_{11}I_4) + 2\sqrt{C_2} \left(\frac{B_1}{A_1}\right) \sqrt{\frac{\epsilon_o}{\mu_o}} (I_{12}I_5 - I_{13}I_6) \right] .$$

Again the integrals are defined in Appendix B.

Another source of power loss in this cavity is caused by the finite surface conductivity of the reflecting end plates. This loss may be computed from equation 5-4,

$$\bar{P}_{wall} = 2 \left[\frac{1}{2} R_s \int_{A_{i+o}} (\underline{H}_t \cdot \underline{H}_t^*)_{at\ z=0} dA \right] = R_s A_1^2 \cosh^2 \xi_0 q^2 C_w \qquad (7)$$

where

$$C_w = C_1 \left[(I_8I_1 + I_9I_2) + \frac{\epsilon_1}{\epsilon_o} C_2 \left(\frac{B_1}{A_1}\right)^2 \frac{\epsilon_o}{\mu_o} (I_{10}I_3 + I_{11}I_4) \right.$$

$$\left. + 2 \left(\frac{B_1}{A_1}\right) \sqrt{\frac{\epsilon_o}{\mu_o}} \sqrt{C_2} \sqrt{\frac{\epsilon_1}{\epsilon_o}} (I_{12}I_5 - I_{13}I_6) \right]$$

$$+ \frac{x^4}{y^4} C_1 \left[\left(\frac{L_1}{A_1}\right)^2 (BI) + C_2 \left(\frac{P_1}{A_1}\right)^2 \frac{\epsilon_o}{\mu_o} (BII) + 2 \left(\frac{L_1}{A_1}\right) \left(\frac{P_1}{A_1}\right) \sqrt{\frac{\epsilon_o}{\mu_o}} \sqrt{C_2} (BIII) \right] .$$

Rearranging expression 5-1, we get

$_e HE_{11n}^{(1)}$ mode

$\dfrac{\epsilon_1}{\epsilon_o} = 2.5$

$$Q_d = \frac{1}{2\phi_d \frac{\epsilon_1}{\epsilon_o}} \frac{C_T}{C_d}$$

$$Q_w = \frac{L}{2\delta} \frac{C_T}{C_w}$$

$(2q \cosh \xi_o/\lambda_o)^2 \tanh \xi_o$
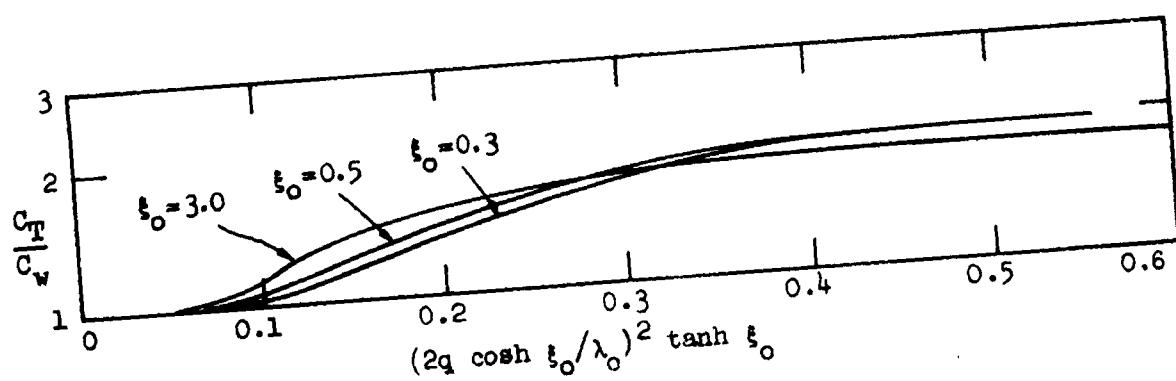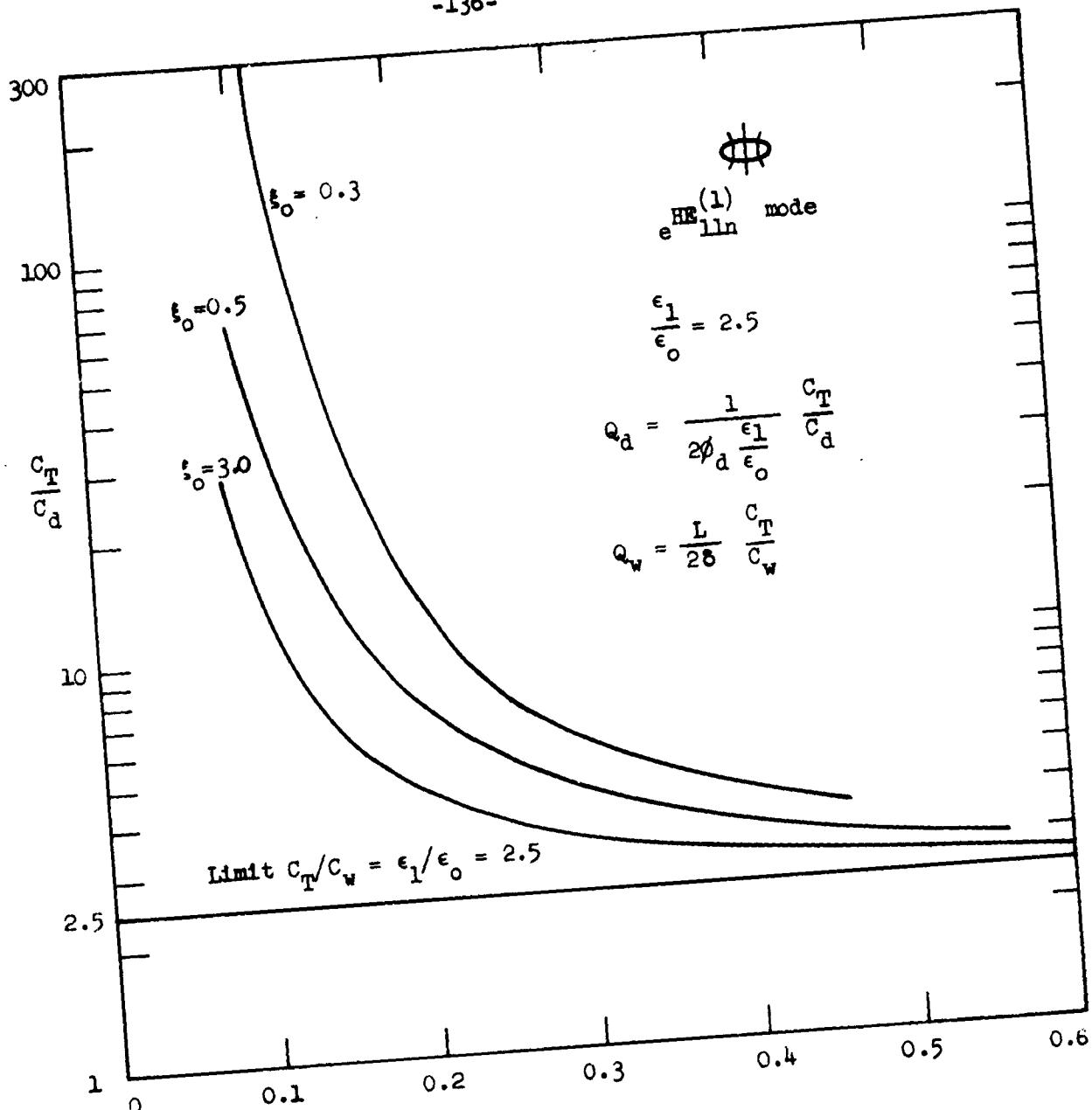
Fig. V-2.

$$\frac{1}{Q} = \frac{\bar{P}}{\omega \bar{W}} = \frac{\bar{P}_{dielectric}}{\omega \bar{W}} + \frac{\bar{P}_{wall}}{\omega \bar{W}} = \frac{1}{Q_d} + \frac{1}{Q_w} \qquad . \qquad (8)$$

Q_d is the Q factor of the cavity if the end plates are perfectly con-ducting, and Q_w is the Q factor of the cavity if the dielectric is perfect. According to equation 8 we have

$$Q_d = \frac{\omega \bar{W}}{\bar{P}_{dielectric}} = \frac{1}{2\phi_d \frac{\epsilon_1}{\epsilon_o}} \frac{C_T}{C_d} \qquad (9)$$

and

$$Q_w = \frac{\omega \bar{W}}{\bar{P}_{wall}} = \frac{L}{2\delta} \frac{C_T}{C_w} \qquad (10)$$

where ϕ_d is the loss tangent of the dielectric rod and δ is the skin depth of the end plates.

The expressions C_T/C_d and C_T/C_w are evaluated numerically and the results are shown in Figure V-2 in which C_T/C_d and C_T/C_w are plotted against the normalized cross-sectional area (NCSA) for various values of ξ_o with $\epsilon_1/\epsilon_o = 2.5$. For small values of NCSA, C_T/C_d can be very large, thus Q_d can also be very large. This is because most of the energy is outside the rod. As NCSA approaches infinity, C_T/C_d approaches ϵ_1/ϵ_o and Q_d approaches $1/2\phi_d$[*]. Again one notes that the flatter the elliptical cross section, the higher the Q_d factor.

It is worthwhile to take notice of the behavior of C_T/C_w as a function of NCSA. For an ordinary cylindrical metallic waveguide of simple cross-sectional shape, terminated at both ends by short-circuiting

---

[*]Incidentally, the Q of a section of perfectly conducting metallic wave-guide, terminated at both ends by perfectly conducting end walls and filled with a dielectric material with a loss factor of ϕ_d is also $1/2\phi_d$.

plates, the Q factor resulting from the imperfection of the end plates is $L/2\delta$. L is the length of the guide and δ is the skin depth of the end plates. This Q factor is independent of the type and order of the mode under consideration as long as the mode is either of TE, TM or TEM type and not of a hybrid type. It means that for this type of cavity, C_T/C_W is always unity. However, C_T/C_W is no longer a constant (see Figure V-2) if a hybrid wave is present. This characteristic is probably due to the fact that the TE and TM waves are inextricably coupled to each other on a dielectric rod except for the circularly symmetric waves.

It is also noted that Q_d is independent of the length of the cavity and Q_w is directly proportional to the length of the cavity. The total Q of the cavity can be computed from the knowledge of Q_w and Q_d using equation 8. For a very long cavity, $Q_w \gg Q_d$, therefore $Q_{total} \approx Q_d$.

5.2 The Q of a Cavity Supporting the $_o HE_{11n}^{(1)}$ Mode

For the sake of completeness, we include here the analysis of the $_o HE_{11n}^{(1)}$ mode. The geometry of the cavity is the same as the one shown in Figure V-1. The analysis in this section follows very closely that in the previous section, therefore only the results will be given here.

The power dissipations due to the dielectric loss and the end walls loss are respectively,

$$\overline{P}'_{dielectric} = -\frac{\sigma_d L}{2} \int_0^{\xi_0} \int_0^{2\pi} (\underline{E}_1 \cdot \underline{E}_1^*) p^2 d\eta d\xi$$

$$= -\frac{\sigma_d L}{2} A_1^2 q^2 \cosh^2 \xi_0 \frac{\mu_o}{\epsilon_o} C_d' \tag{1}$$

and

$$\overline{P}'_{wall} = 2 \cdot \left[\frac{R_s}{2} \int_{A_{1+o}} (\underline{H}_t \cdot \underline{H}_t^*)_{at\ z=0}\ dA \right]$$

$$= R_s A_1^2 \cosh^2 \xi_o q^2 C'_w \tag{2}$$

where

$$C'_d = \left(\frac{B_1}{A_1}\right)^2 \frac{\epsilon_o}{\mu_o} \left[I_{14_{NN}} I_2 + \frac{I_8(I_2 - I_{7c})}{2\cosh^2\xi_o} \right] + C_1 \left[C_2(I_{11}I_4 + I_{10}I_3) \right.$$

$$\left. + \left(\frac{B_1}{A_1}\right)^2 \frac{\epsilon_o}{\mu_o} (I_8 I_1 + I_9 I_2) + 2\sqrt{C_2} \left(\frac{B_1}{A_1}\right) \sqrt{\frac{\epsilon_o}{\mu_o}} (I_{13}I_6 - I_{12}I_5) \right]$$

and

$$C'_w = C_1 \left[(I_{10}I_3 + I_{11}I_4) + \frac{\epsilon_1}{\epsilon_o} C_2 \left(\frac{B_1}{A_1}\right)^2 \frac{\epsilon_o}{\mu_o} (I_8 I_1 + I_9 I_2) \right.$$

$$\left. + 2\left(\frac{B_1}{A_1}\right)\sqrt{\frac{\epsilon_o}{\mu_o}}\sqrt{C_2}\sqrt{\frac{\epsilon_1}{\epsilon_o}} (I_{13}I_6 - I_{12}I_5) \right]$$

$$+ \frac{x^4}{y^4} C_1 \left[\left(\frac{L_1}{A_1}\right)^2 (BI)' + C_2\left(\frac{P_1}{A_1}\right)^2 \frac{\epsilon_o}{\mu_o} (BII)' + 2\left(\frac{L_1}{A_1}\right)\left(\frac{P_1}{A_1}\right)\sqrt{\frac{\epsilon_o}{\mu_o}}\sqrt{C_2}(BIII)' \right]$$

All the symbols in the above expressions have been defined either in Chapter IV or in Appendix B. The total time average energy stored in the cavity is given by

$$\overline{W}'_T = 2W_E = 2W_H = \frac{1}{2}\epsilon_1 \int_{V_1} (\underline{E}_1 \cdot \underline{E}_1^*)dV + \frac{1}{2}\epsilon_o \int_{V_o} (\underline{E}_o \cdot \underline{E}_o^*)dV$$

$$= \cosh^2\xi_o\ q^2 A_1^2\ \frac{L\epsilon_o}{4}\ \frac{\mu_o}{\epsilon_o}\ C'_T \tag{3}$$

where

$$
C_T' = \frac{\epsilon_1}{\epsilon_0} \left(\frac{B_1}{A_1}\right)^2 \frac{\epsilon_0}{\mu_0} \left[I_{14_{NN}} I_2 + \frac{I_8(I_2 - I_{7c})}{2\cosh^2 \xi_0} \right] + \frac{\epsilon_1}{\epsilon_0} C_1 \left[C_2(I_{11}I_4 + I_{10}I_3) \right.
$$

$$
+ \left(\frac{B_1}{A_1}\right)^2 \frac{\epsilon_0}{\mu_0} (I_8 I_1 + I_9 I_2) + 2\sqrt{C_2} \left(\frac{B_1}{A_1}\right) \sqrt{\frac{\epsilon_0}{\mu_0}} (I_{13}I_6 - I_{12}I_5) \left. \right]
$$

$$
+ \left(\frac{P_1}{A_1}\right)^2 \frac{\epsilon_0}{\mu_0} \left\{ \left[I_{44}'I_2' + \frac{I_{21}'(I_2' - I_a')}{2\cosh^2 \xi_0} \right] + \left(\frac{P_3}{P_1}\right)^2 \left[I_{45}'I_4' + \frac{I_{23}'(I_4' - I_b')}{2\cosh^2 \xi_0} \right] \right.
$$

$$
+ 2\left(\frac{P_3}{P_1}\right) \left[I_{46}'I_6' + \frac{I_{25}'(I_6' - I_c')}{2\cosh^2 \xi_0} \right] \left. \right\}
$$

$$
+ \frac{x^4}{y^4} C_1 \left[\left(\frac{L_1}{A_1}\right)^2 (BI)' \, C_2 + \left(\frac{P_1}{A_1}\right)^2 \left(\frac{\epsilon_0}{\mu_0}\right)(BII)' + 2\sqrt{C_2} \left(\frac{L_1}{A_1}\right)\left(\frac{P_1}{A_1}\right) \sqrt{\frac{\epsilon_0}{\mu_0}} (BIII)' \right]
$$

$\overline{P}_d'$, $\overline{P}_w'$ and $\overline{W}_T'$ are related to the Q factor by the following relation

$$
\frac{1}{Q'} = \frac{\overline{P}}{\omega \overline{W}_T'} = \frac{\overline{P}_{dielectric}'}{\omega \, \overline{W}_T'} + \frac{\overline{P}_{wall}'}{\omega \, \overline{W}_T'} = \frac{1}{Q_d'} + \frac{1}{Q_w'} \tag{4}
$$

where

$$
Q_d' = \frac{\omega \, \overline{W}_T'}{\overline{P}_{dielectric}} = \frac{1}{2\phi_d \frac{\epsilon_1}{\epsilon_0}} \frac{C_T'}{C_d'}
$$

and

$$
Q_w' = \frac{\omega \, \overline{W}_T'}{\overline{P}_{wall}} = \frac{L}{2\delta} \frac{C_T'}{C_w'} \quad .
$$

ϕ_d is the loss tangent of the dielectric and δ is the skin depth of the reflecting end plates.

The expressions C_T'/C_d' and C_T'/C_w' are evaluated numerically. Results are given in Figure V-3 in which C_T'/C_d' and C_T'/C_w' are plotted against the normalized major axis (NMA) for various values of ξ_0 with $\epsilon_1/\epsilon_0 = 2.5$. The characteristics are similar to those of the
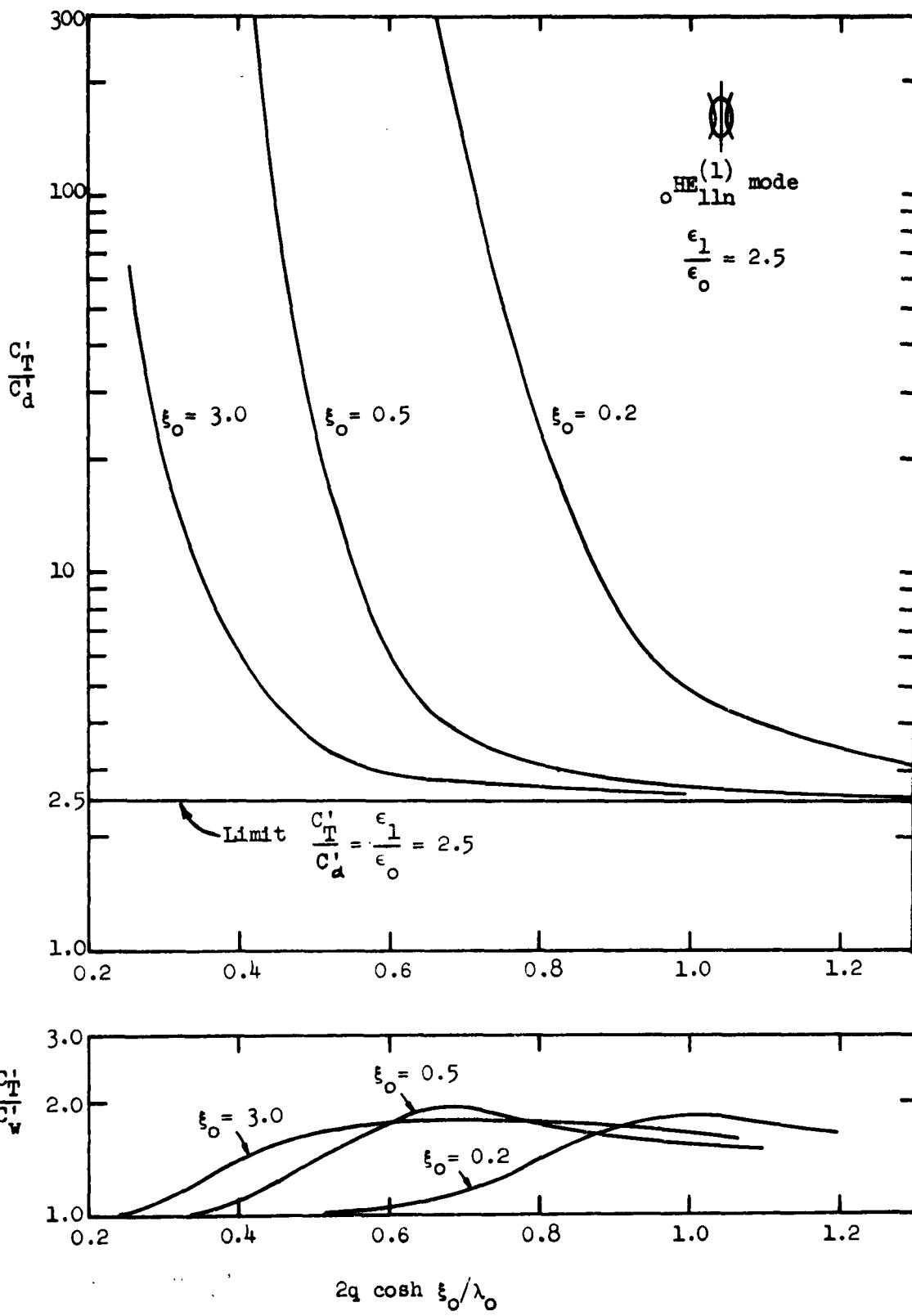
Figure V-3

$_e\text{HE}_{11n}^{(1)}$ mode. C_T'/C_d' can be made as large as desired by choosing suitable values of NMA. As NMA approaches infinity, C_T'/C_d' approaches ϵ_1/ϵ_0 for all ξ_0. In the region where C_T'/C_d' is large, the slopes of these curves are very large; in other words, a small variation in NMA can cause a rather larger variation in C_T'/C_d', thus a large variation in Q_d. The behavior of C_T'/C_w' is similar to that of the $_e\text{HE}_{11n}^{(1)}$ mode. Similar deductions as those given in section 5.1 can be made and will not be repeated here.

5.3 Relation between Q and α

In 1944 Davidson and Simmonds (41) derived a relation between the Q of a cavity composed of a uniform transmission line with short-circuiting ends and the attenuation constant α of such a transmission line. Later in 1950, Barlow and Cullen (55) rederived this relation. These authors showed that this relation is quite general and is applicable to arbitrary cross-section, uniform metal tube waveguides. Since then one of the standard techniques for the measurement of the attenuation constant α is the use of the cavity method*. This method offers an excellent way of measuring the attenuation constant of the guide when the loss is quite small. Later on this method is generalized and applied to open waveguides, such as the single wire line, the dielectric cylinder guide and associated guides, by various authors (6,7,19,21).

However, it should be remembered that the formula by Davidson, Simmonds and Barlow is derived under the assumption that there exists a single equivalent transmission line for the mode under consideration.

---

*The procedures of this method in general are the following. Short the uniform transmission line under consideration at both ends and measure the Q of such a resonator. From the knowledge of the measured Q and other constants such as the cut-off frequency of the guide, the frequency of oscillation, etc., it is an easy matter to obtain α from the formula derived by these authors.

This assumption is true for a pure TE, TM or TEM mode, but it is not clear that such a single equivalent transmission line exists for the hybrid waves. This suspicion originates from the fact that a) the TE and TM waves are intimately coupled to each other, and b) the characteristic impedance defined by Schelkunoff (56) is not constant with respect to the transverse coordinates. It is, therefore, very difficult to conceive the possibility that there exists a single equivalent transmission line for this hybrid mode; at best the hybrid wave may be represented by a set of transmission lines coupled tightly with one another. Hence the formula by Davidson, Simmonds and Barlow is not applicable to the hybrid wave.*

A more general relation between Q and α can be obtained without using the transmission line equivalent circuit, provided that α is very small compared with β (57). The propagation constant of a guided wave with small attenuation constant at ω_o is

$$\Gamma(\omega_o) = \alpha(\omega_o) + i\beta(\omega_o) \quad . \tag{1}$$

At resonance**, the following relation is true

$$\Gamma(\omega_o) + \frac{\partial\Gamma}{\partial\omega} \Delta\omega \approx i\beta(\omega_o) \quad . \tag{2}$$

Combining equations 1 and 2 we have

$$\alpha(\omega_o) = - \frac{\partial\Gamma}{\partial\omega} \Delta\omega = - i \frac{\partial\beta}{\partial\omega} \Delta\omega \quad . \tag{3}$$

According to the definition of group velocity v_g which is $\frac{\partial\omega}{\partial\beta}$ and the definition of the Q factor which is $\omega_o/2(\frac{\Delta\omega}{1})$, we finally arrive

---

*But several investigators (19,21) apparently unaware of this restriction, used this formula in their investigations of the hybrid wave.
**The resonant cavity is made by shorting both ends of the guide under consideration.

at the relation

$$\alpha = \frac{\omega_o}{2Q v_g} = \frac{v_p}{v_g} \frac{\beta}{2Q} \quad . \tag{4}$$

This is the general relation that we are seeking. Substituting the values of v_p/v_g* for TE, TM or TEM into equation 4, one gets the relations derived by Davidson, etc. For the TM or TE mode,

$$\frac{v_p}{v_g} = \frac{1}{1 - (\frac{\lambda}{\lambda_c})^2} \quad , \quad \therefore \quad \alpha = \frac{1}{1 - (\frac{\lambda}{\lambda_c})^2} \frac{\beta}{2Q} \quad , \quad \text{and for the TEM mode,}$$

$v_p/v_g = 1$, $\therefore \alpha = \beta/2Q$. λ_c is the cut-off wavelength.

The group and phase velocity of the dominant modes can be obtained easily from the ω-β diagram. A sketch of the ω-β diagram for the dominant modes is shown in Figure V-4. It can be seen that at low frequencies or small β's, $v_{ph} \approx v_g$ and again at very high frequencies or large β's, $v_{ph} \approx v_p$. Therefore, the relation $\alpha = \beta/2Q$ is applicable only at very low frequencies or at very high frequencies.

* $v_p = v_{ph} =$ the phase velocity of the wave.
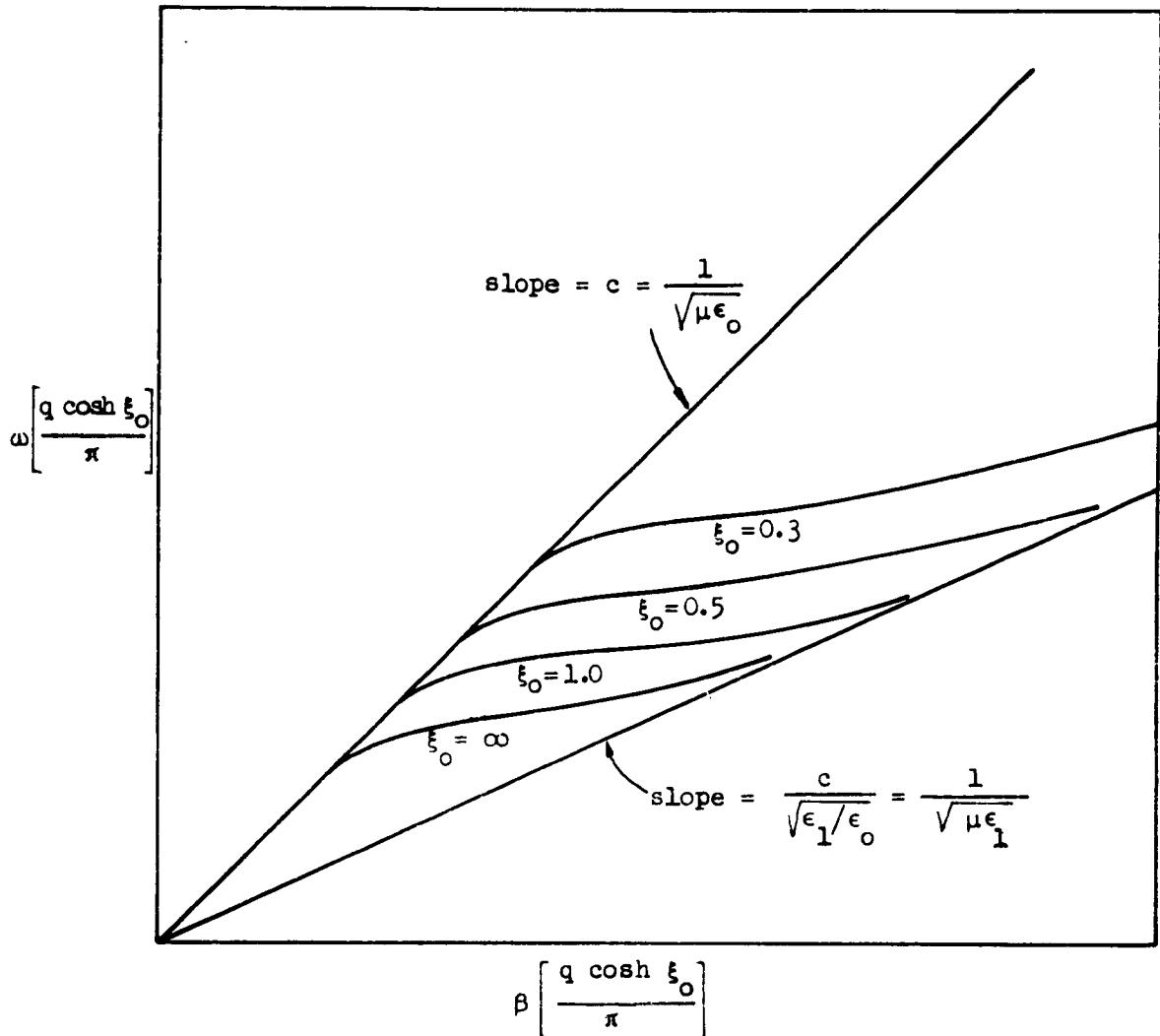
Fig. V-4. A sketch of the ω-β diagram for the dominant dielectric rod mode.

CHAPTER VI - EXPERIMENTAL INVESTIGATIONS

It is the purpose of this chapter to investigate and verify the analytic results experimentally. The properties of a certain propagating mode along an infinitely long uniform waveguide are usually specified by three characteristics[*], (a) the guide wavelength which is directly related to the propagation constant of the wave, (b) the field configurations or the field distributions, (c) the power loss or the attenuation

---

[*]In order that a good matching condition may be obtained so that in coupling energy into and out of a dielectric rod guide without the presence of high standing-wave ratio which is a measure of the relative intensities of reflected and incident waves, the knowledge of the characteristic impedance or the wave impedance is very important. As we have pointed out earlier the characteristic impedance defined in the usual manner (i.e., the Schelkunoff definition) is not meaningful, since it is a function of the transverse coordinate system. A mean value impedance, which takes into account the energy distribution over a cross-section of the rod was first suggested by Wegener. He divided the (circular) dielectric rod into four sections and in each of these four sections he assumed the field to be independent of ϕ, the angular variation, so that in regions I and III, ϕ is assumed to be zero and in regions II and IV, ϕ is assumed to be $\pi/2$. [See Figure 9, ref. (17)]. The approximate expression for mean impedance is therefore

$$Z = \frac{\int_{I+III} \left(\frac{E_\phi}{H_\rho}\right)_{\phi=0} (\underline{E} \times \underline{H}^*) \cdot \underline{e}_z \, dA + \int_{II+IV} \left(\frac{E_\rho}{H_\phi}\right)_{\phi=\pi/2} (\underline{E} \times \underline{H}^*) \underline{e}_z \, dA}{\int (\underline{E} \times \underline{H}^*) \cdot \underline{e}_z \, dA} \quad .$$

He showed that $Z/Z_o \approx \lambda_g/\lambda_o$. Similar approximate mean impedance as defined above may be obtained for the elliptical dielectric rod.

The fact that the characteristic impedance of the hybrid waveguide is not well defined shows that the single transmission line analog is at best an approximation. Any measurements assuming the single transmission analog of this guide are therefore approximate, and should not be considered as precision measurements.

Since at present we are only concerned with the problems of wave propagation along an infinitely long uniform dielectric rod, the "characteristic impedance" or the equivalent circuit network of this guide will not be considered.

constant of the wave. Experiments will therefore be specifically designed to measure these three quantities.

After a detailed description of the experimental apparatus, the methods of measurement for these various quantities are discussed. The experimental results are then compared with the theoretical results. A discussion will be given.

6.1 Experimental Apparatus

Figure VI-1 is a photograph of the general physical appearance of the experimental set-up. A block diagram is shown in Figure VI-2. For the sake of convenience and simplicity, measurements were performed in the X-band frequency range. The microwave X-band power was obtained from an X-13 Varian reflex klystron which offered a maximum power output of five milliwatts and was powered by the Hewlett-Packard power supply. The microwave signal was modulated with a 1000 cps square wave. The output of the klystron was connected to an isolator followed by an attenuator, a cavity resonator, a slotted line section, and a section of standard X-band rectangular metallic waveguide. These were standard X-band components. The other end of the rectangular metallic waveguide was connected to the special apparatus specifically designed for the present experimental investigation; see Figure VI-2.

The following sections are devoted to a detailed description of the special apparatus.

A. The Launching Device

The method of transferring microwave energy from an ordinary metallic waveguide into a dielectric rod was not very difficult or complicated. Since a rectangular metal guide operating in the dominant TE_{10} mode had
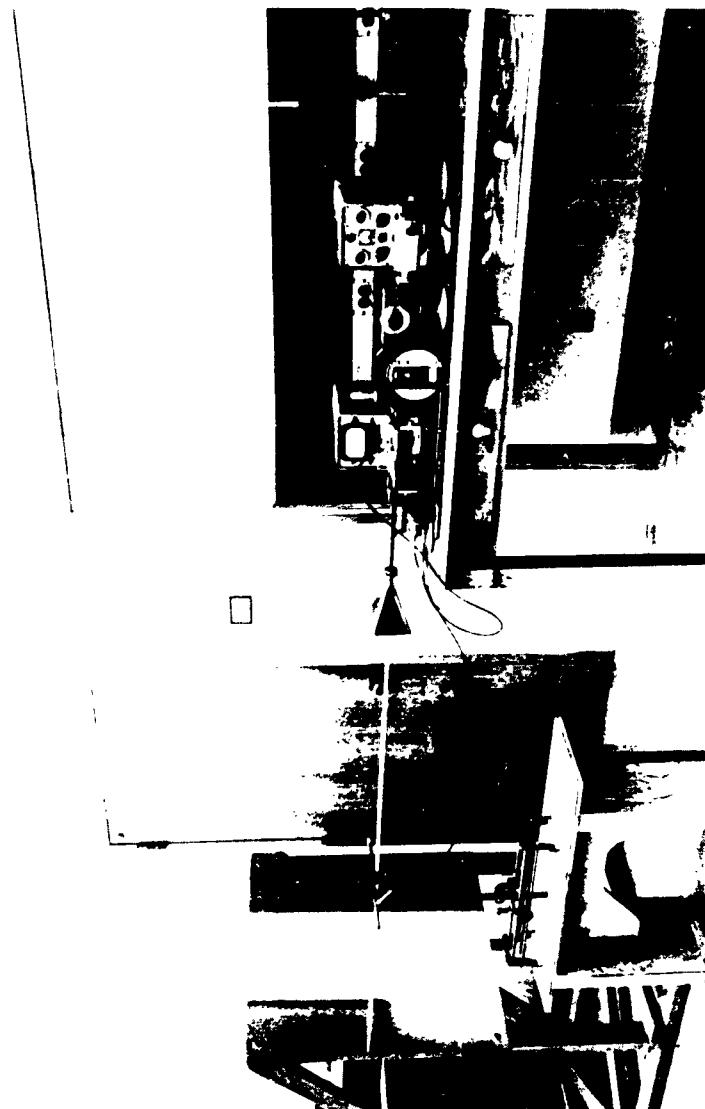
Fig. VI-1. Experimental Apparatus
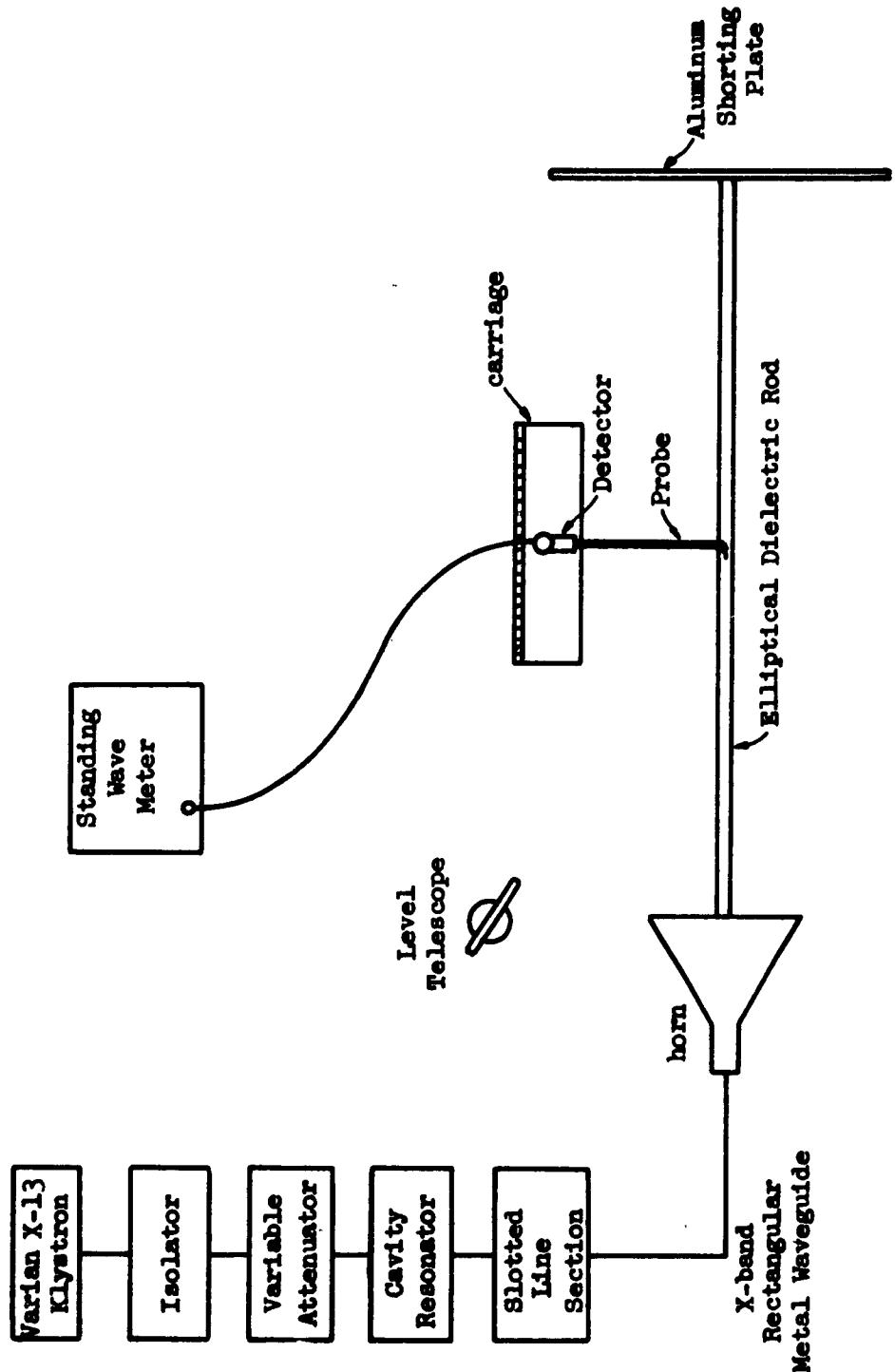
Fig. VI-2. Block diagram showing arrangement of components for determining guide wavelength, field extent and attenuation factor of the elliptical dielectric waveguide.

an electric field whose configuration was roughly similar to the transverse component of the electric field of the $_e\mathrm{HE}_{11}^{(1)}$ mode or the $_o\mathrm{HE}_{11}^{(1)}$ mode on the dielectric guide, the transfer could be made simply by inserting the dielectric rod longitudinally into the metal guide for a short distance. The orientation of the cross-section depended upon whether the $_e\mathrm{HE}_{11}^{(1)}$ mode or the $_o\mathrm{HE}_{11}^{(1)}$ mode was desired. To improve the matching and to minimize reflection the dielectric rod was tapered to a point within the guide and after emerging from the metal guide the rod was tapered to whatever size was required for a given test. Furthermore a flare pyramidal horn whose flare angle was adjusted for best energy transfer was connected to the rectangular metal guide. (See Figure VI-3).


rectangular
metal waveguide   horn   elliptical dielectric rod
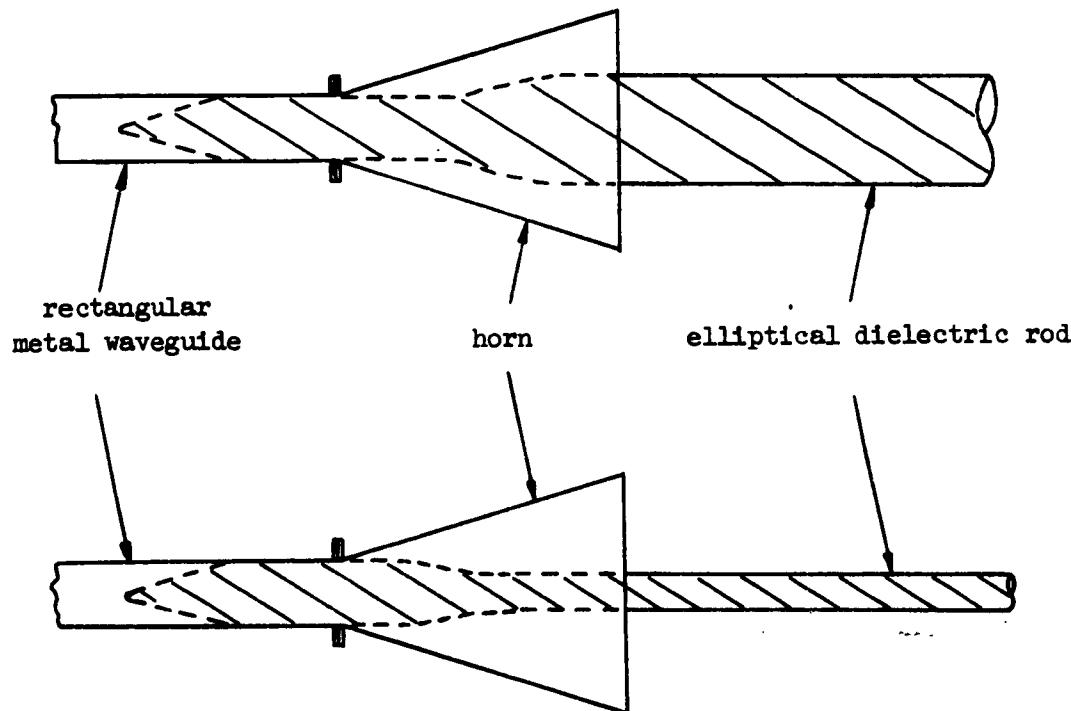
Figure VI-3.   The Launching Device.

B. The Elliptical Dielectric Rod

Since dielectric rods of elliptical cross-section were not com-
mercially available, they were machined from available rectangular
lucite strips which were at least five and half feet long. A total
of twelve rods of different sizes and ellipticities were made, in
order that the experimental data would cover a wide range of $\frac{2q \cosh \xi_0}{\lambda_0}$
and ξ_0 values. A picture of these rods is shown in Figure VI-4. One
end of each rod was machined very flat while the other end was tapered
as described in section 6.1A to fit into the metal guide. A small chunk
of lucite was taken from each rod in order to measure the electrical
properties of each rod individually by Von Hippel's method (58). It was
found that the dielectric constant of these rods varied between ϵ = 2.5
to ϵ = 2.6 and the loss tangent varied from tan δ = 0.005 to
tan δ = 0.003. It should be noted that due to the resilient property
of lucite it was very difficult to machine such a required length uni-
formly. A special and rather expensive technique was developed and used.
Although extreme care was taken in making these rods, some small non-
uniformities which might attribute to experimental errors were unavoid-
able. The major axis and ξ_0 of these elliptical rods ranged from
2A = 1.5 in. to 2A = 0.5 in. and ξ_0 = ∞ to ξ_0 = 0.37 .

C. The Shorting Plate

In order that the plate could be a good shorting device, its sur-
face had to be very flat and large enough to intercept practically all
of the energy outside the dielectric rod and the plate had to be made
of good conducting material. A 1/4"x36"x36" aluminum plate was used.
One side of the aluminum plate was machined flat and its surface was

Fig. VI-4.   Elliptical Dielectric Rods
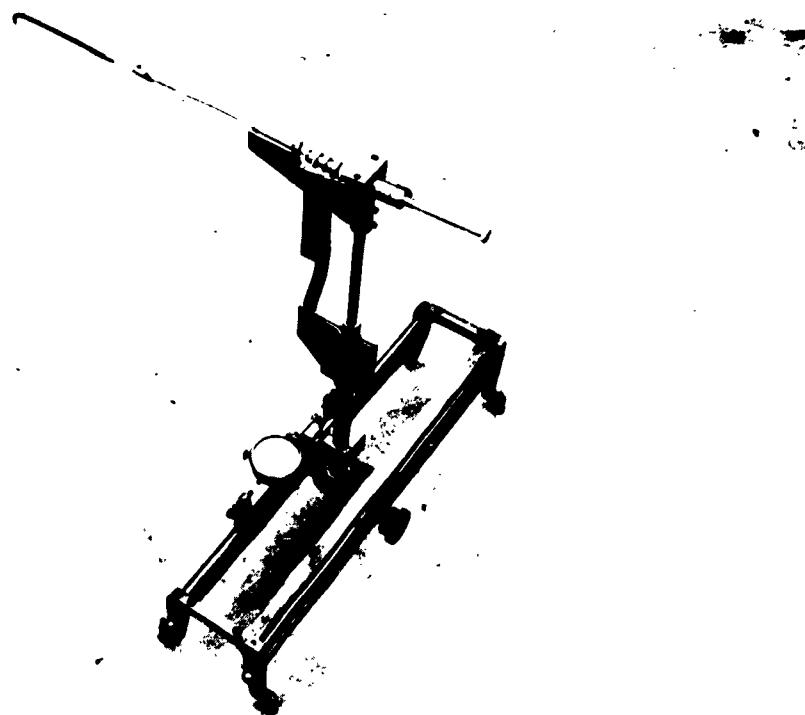
Fig. VI-5.   Probe and Its Carriage

cleaned and polished in order to assure maximum conductivity. The plate and its support can be seen clearly in Figure VI-1.

D. The Probe and Its Carriage

To detect and measure the electromagnetic field on the dielectric rod, a small electric probe was designed and used. The probe consisted of a section of rigid coaxial cable whose outside diameter was about 1/8" and whose length was about 1'3". An inch from one end of the cable was formed into a gradual 90° bend and the center conductor protruded about 1/8". The other end was connected to a crystal detector which was calibrated, and the output of this detector was connected to the HP standing wave indicator. The L bend was introduced to reduce the amount of metal conductors parallel to the electric field indicator. The probe and the detector were supported by a stand which was fastened to a HP carriage. A picture of the probe and its support is shown in Figure VI-5. The whole instrument was so designed that the probe might be moved up and down radially with respect to the center axis of the dielectric rod and longitudinally along the center axis of the rod. Furthermore, the probe could be adjusted to detect either E_{ξ} or E_z field. The longitudinal movement of the probe could be measured from a scale on the carriage; and a dial indicator was used to obtain accurate measurements of small longitudinal movements of the probe. The radial movement of the probe was measured by a level telescope whose movement had been calibrated.

With the help of a transit and a level this whole experimental set-up was aligned carefully. The dielectric rod had to be very straight

and its axis perpendicular to the shorting plate. To insure a good contact between the polished shorting plate and the flat end of the dielectric rod, a slight pressure was asserted on both ends of the system. To minimize sagging of some small or flat rods, very thin nylon threads were used along the rod to provide support. Although disturbances due to these threads were unavoidable, because of the sizes of the rods used at this frequency range very little perturbation was observed.

6.2 Method of Measurement

In general there are two most commonly used methods for measuring the propagation characteristics of a certain mode along a uniform low loss waveguide. The first one is the so-called resonator technique. The guide under consideration is placed between two parallel plates with proper coupling holes. Resonance occurs when the length of the cavity is $n \frac{\lambda_g}{2}$ where n is an integer and λ_g is the guide wavelength of the mode on the guide. λ_g can be measured easily either by counting the number of minima within the cavity length with a small probe or by moving one of the reflector plates and measuring the displacement of the plate for each resonant peak. By measuring the Q of this cavity, the attenuation constant α can readily be calculated*. This method is particularly useful and accurate for very low loss transmission lines**. The second method is the standing wave measurement technique. The guide is terminated by a perfectly reflecting plate acting as a short-circuit device. The propagating wave is perfectly reflected by the termination and a standing

---

*See equations 5.3-4
**This method was first used by Chandler (19) on the measurement of attenuation factor for the HE_{11} mode on a very small circular dielectric rod.

wave pattern is formed along the guide. A probe, such as the one des-
cribed earlier in section 6.1D, can be used to detect the microwave
signal along an open waveguide. By measuring the distance between two
adjacent minima of the standing wave pattern, and the standing wave
ratio, it is an easy matter to calculate the guide wavelength and the
attenuation factor of the mode on the guide*.

---

*The formula relating the attenuation factor α with the standing wave
ratio can be derived as follows: It is well known that

$$A = 5 \log_{10} \frac{P_1}{P_3} \text{ db}$$

where P_1 and P_3 are respectively the input and reflected power of
the guide; and

$$\frac{P_1}{P_3} = \left(\frac{r-1}{r+1}\right)^2,$$ where r is the standing wave ratio

at the probe. Therefore, we have $\alpha = \frac{10}{\ell} \log_{10}\left(\frac{r-1}{r+1}\right)^2 \text{ db/m}$ in which ℓ
is the length of the guide as indicated in Figure VI-6.
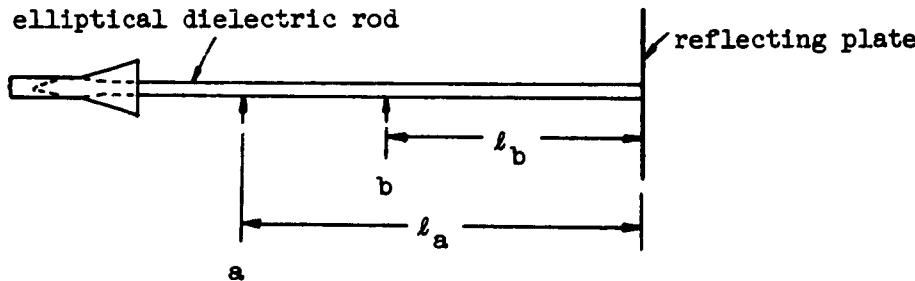
Figure VI-6.

To take into account the loss due to imperfection of the shorting plate
one notes that the attenuation measured at point a is $A_a = \alpha \ell_a + D$,
and similarly the measured attenuation at point b is
$A_b = \alpha \ell_b + D$ where D is the loss of the reflecting plate. Combining
these two equations and eliminating D one gets

$$\alpha = \frac{(A_a - A_b)}{(\ell_a - \ell_b)} \quad \text{(db/meter)}$$

The latter method was used for our measurements since it presented a simple and expedient way of measuring the desired quantities with reasonably good accuracy. To avoid perturbation by the launching device or by end effects, measurements were made in the middle section of the rod. It should also be mentioned that throughout this whole experiment the coupling between the probe and the field was kept at a minimum in order to avoid interference with the propagating wave.

6.3 Comparison of the Theoretical and Experimental Results

The results are separated into three general categories.

A. Guide Wavelength

Guide wavelength was measured according to the procedures described earlier. The distance between adjacent minima of the standing wave pattern was measured at several sections along the guide and the average value was calculated and recorded as the measured $\lambda_g/2$. The maximum difference between these measurements was about 3%. Wavelength measurements were taken from nine different sizes of elliptical dielectric rod for the $_e\text{HE}_{11}^{(1)}$ mode and the $_o\text{HE}_{11}^{(1)}$ mode. Normalized experimental results, together with their corresponding theoretical results, are given in Figures VI-7 through VI-15. The physical size of each dielectric rod used and its measured dielectric constant are indicated in each figure. Excellent agreement was obtained.

To illustrate the agreement between the analytic and experimental results, we introduce the following table:

Fig. VI-7.

(Circles are experimental points)

Fig. VI-8.

Fig. VI-9.

$\xi_0 = 0.775$

$\dfrac{\epsilon_1}{\epsilon_0} = 2.5$

$_e HE_{11}^{(1)}$ mode

(Circles are experimental points)

	ξ_0	$\dfrac{\epsilon_1}{\epsilon_0}$
a	0.848	2.5
b	0.376	2.5

$_e HE_{11}^{(1)}$ mode

Fig. VI-10.

$2q \cosh \xi_0 / \lambda_0$

$\xi_o = 0.368$

$\dfrac{\epsilon_1}{\epsilon_o} = 2.5$

$_e HE_{11}^{(1)}$ mode

$2q \cosh \xi_o / \lambda_o$
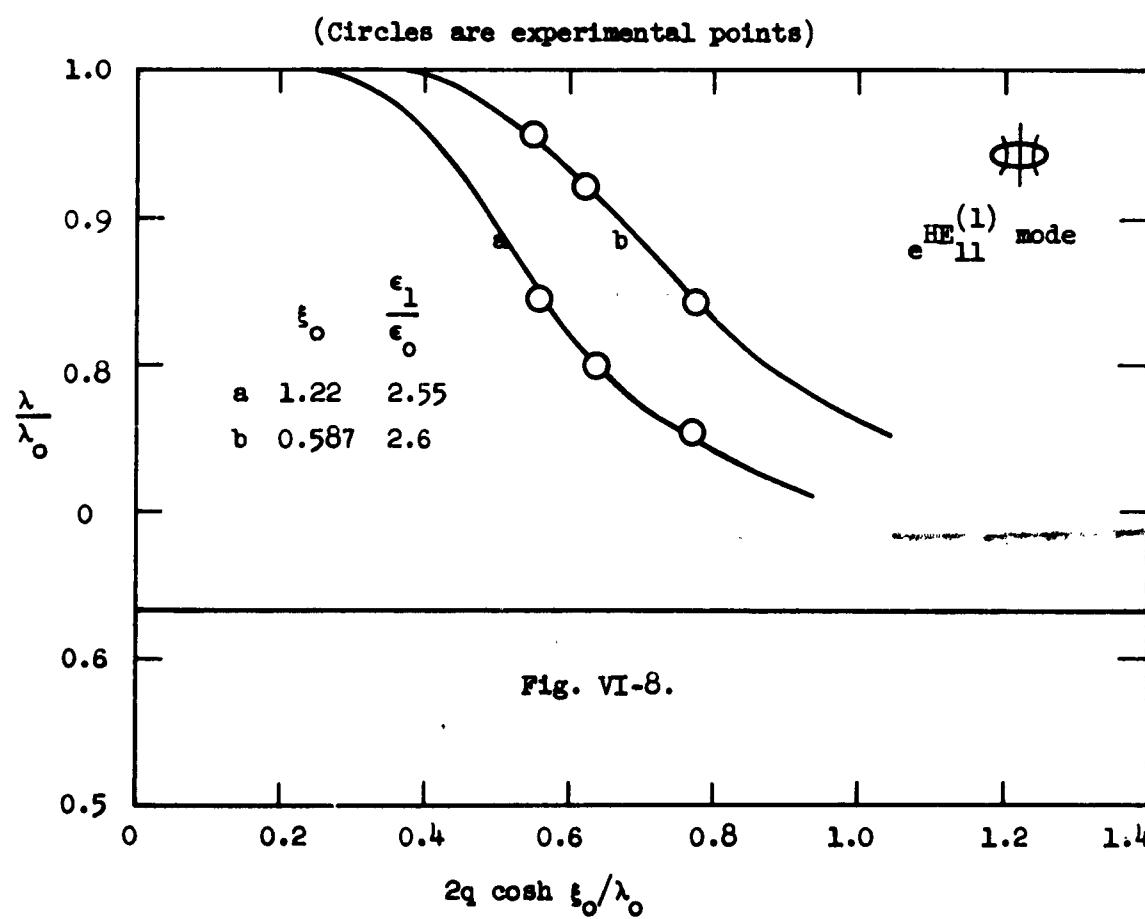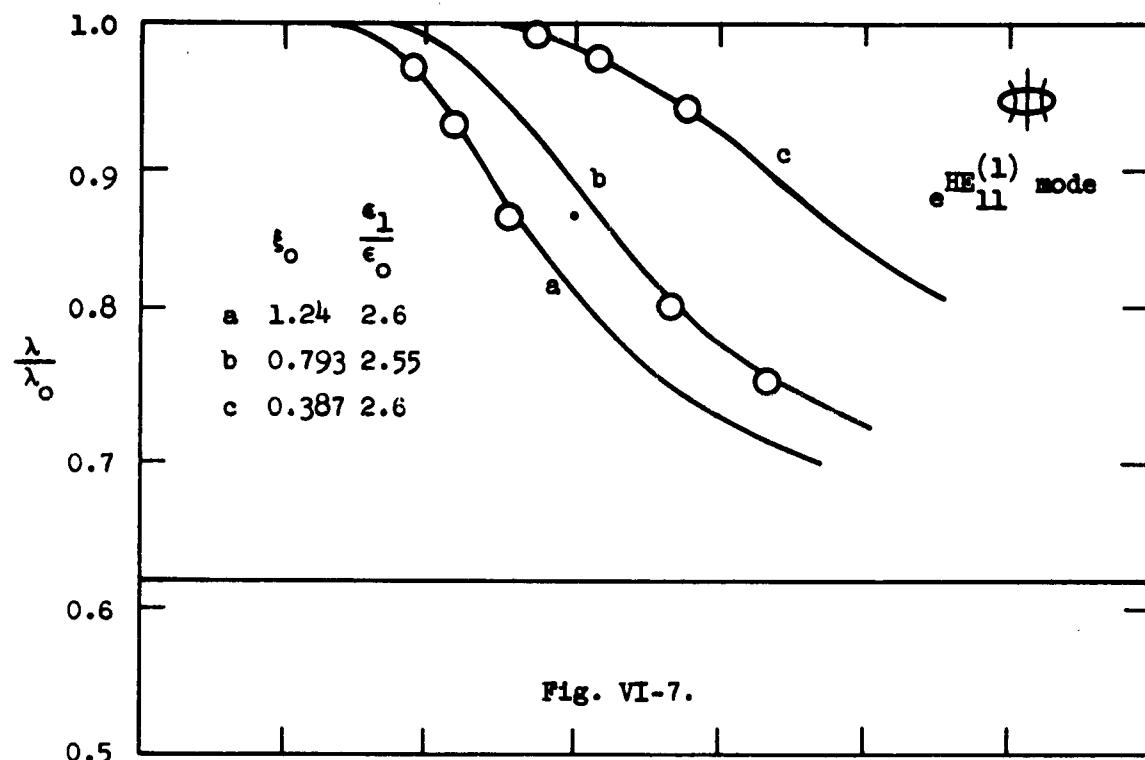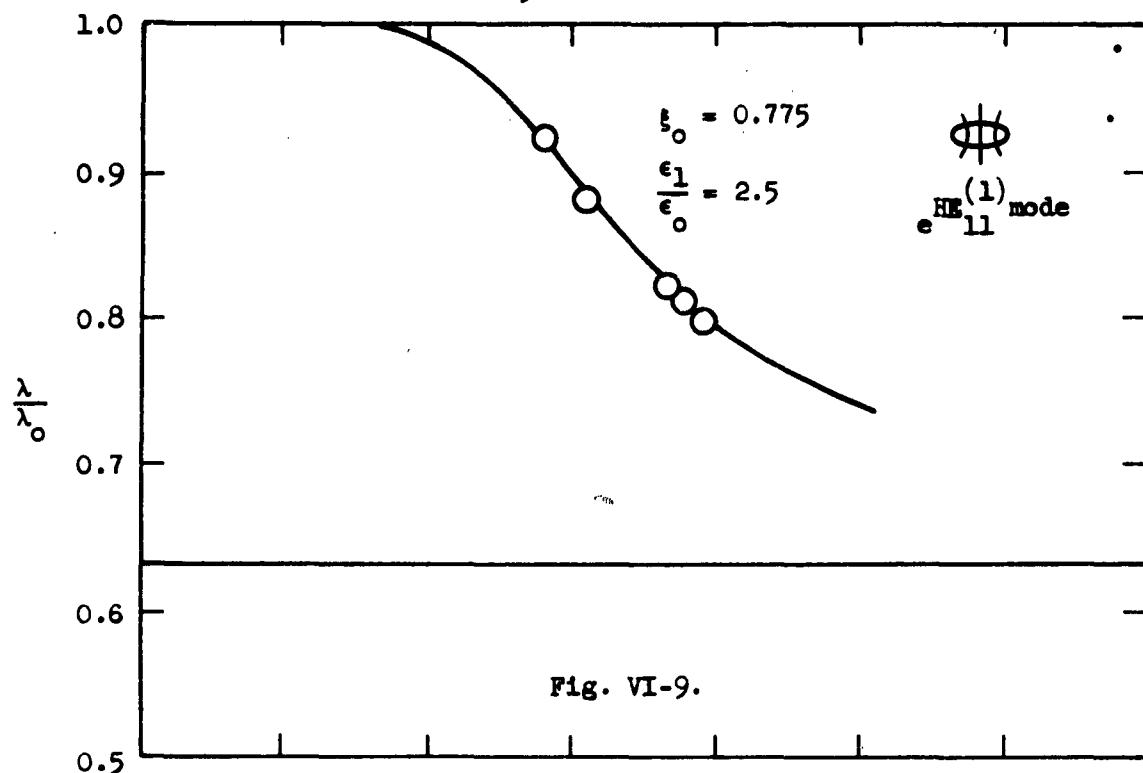
(Circles are experimental points)
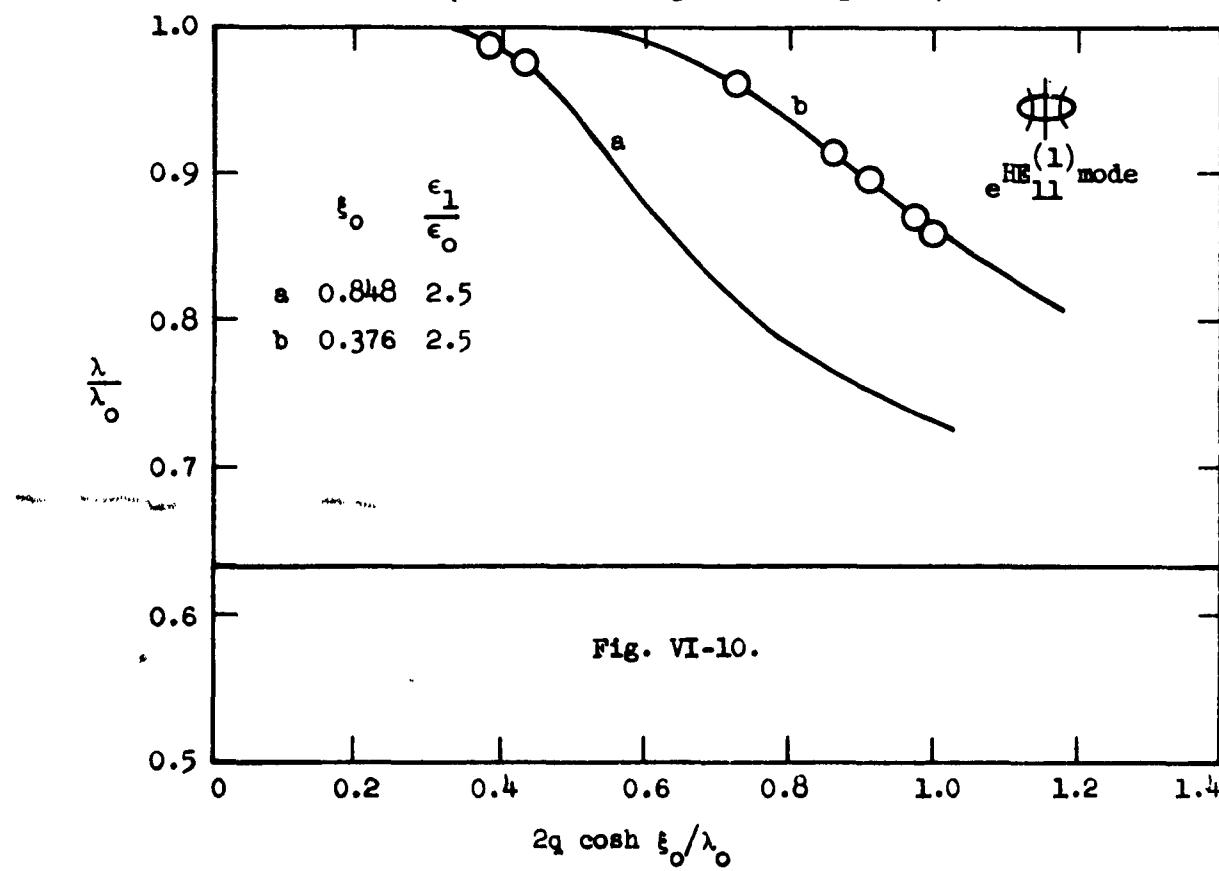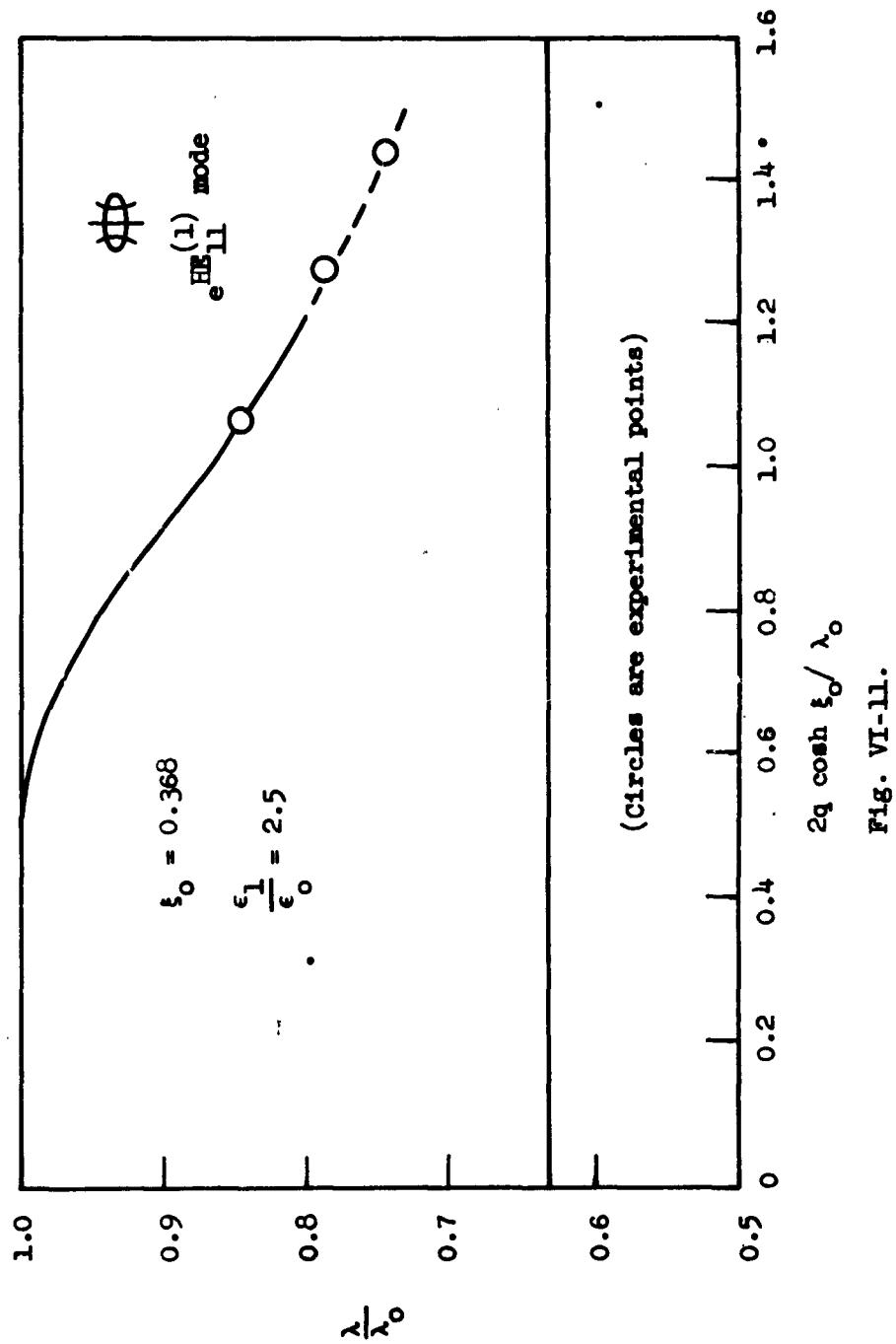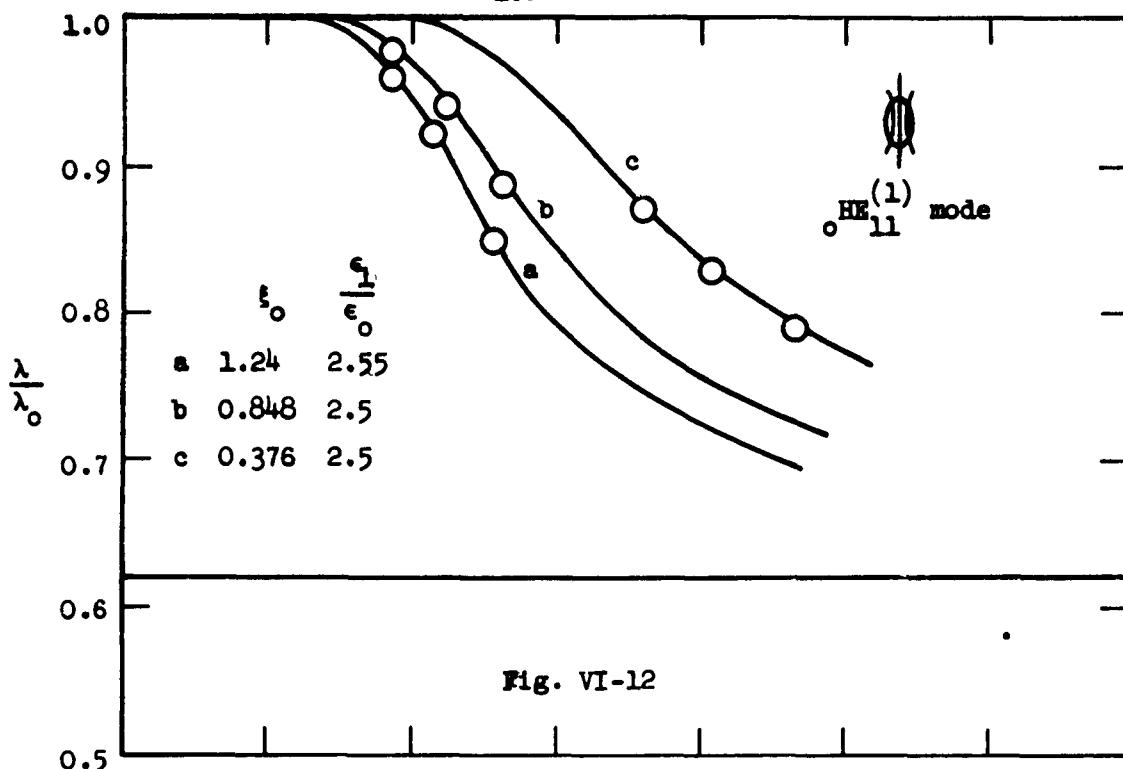
Fig. VI-11.

Fig. VI-12

(Circles are experimental points)

Fig. VI-13.

Fig. VI-14.

(Circles are experimental points)
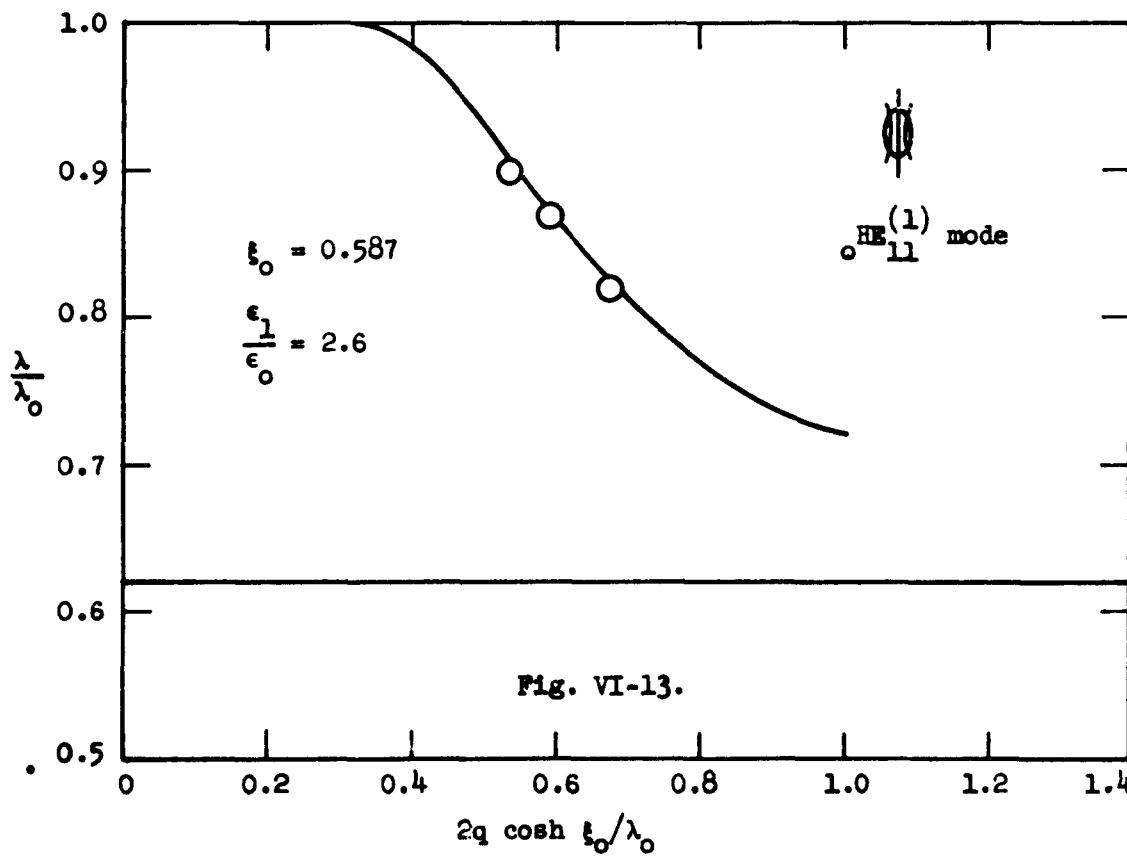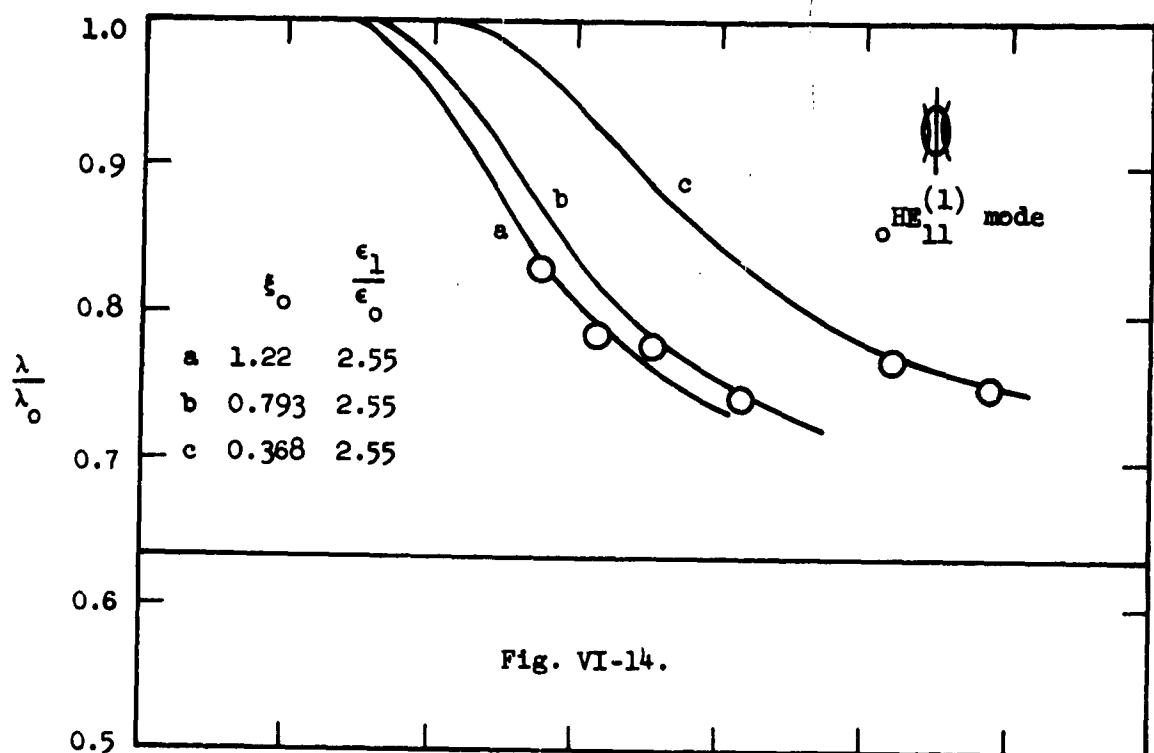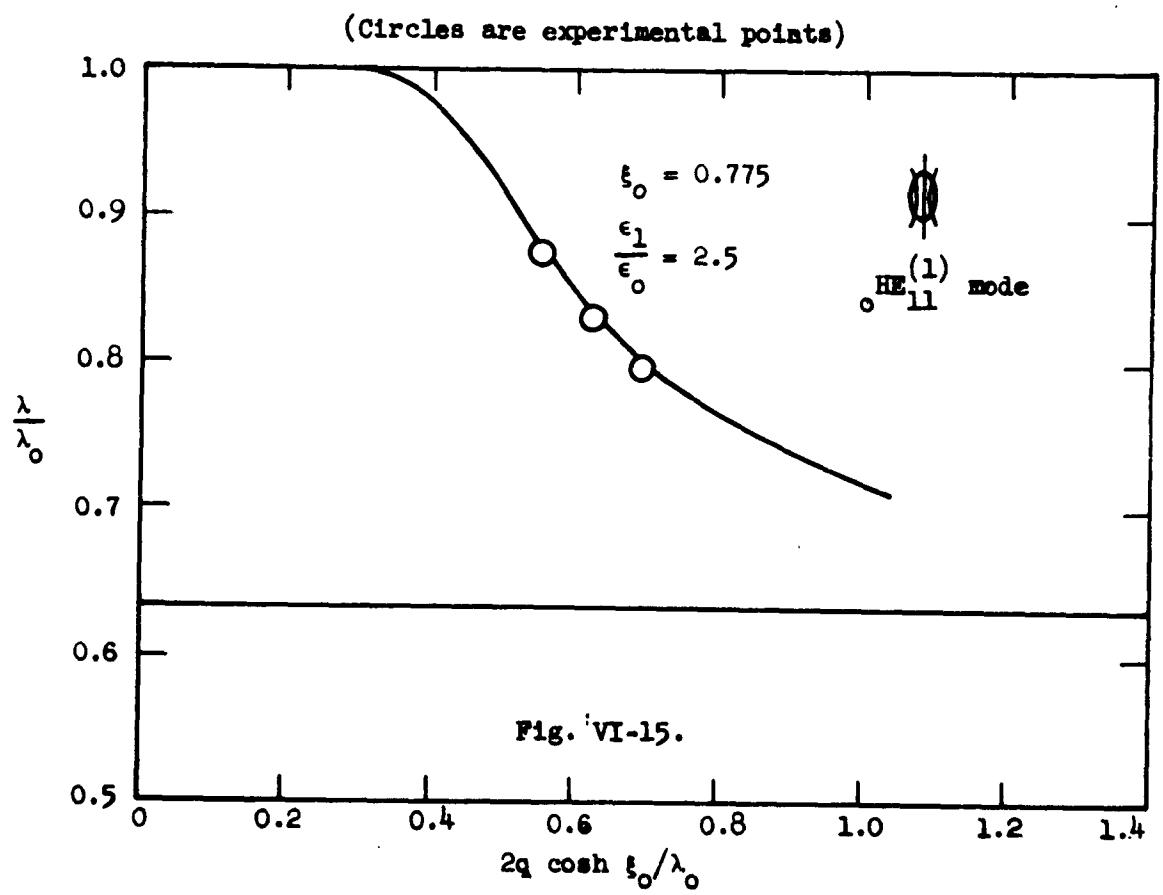

Fig. VI-15.

Mode of Operation	Size (2Ax2B)	ξ_o	$\dfrac{2q \cosh \xi_o}{\lambda_o}$	$\left(\dfrac{\lambda_g}{\lambda_o}\right)_{meas.}$	$\left(\dfrac{\lambda_g}{\lambda_o}\right)_{calc.}$	ϵ_o
$_e HE_{11}^{(1)}$	0.770"x0.645"	1.22	0.55	0.845	0.853	2.55
			0.63	0.80	0.804	
$_o HE_{11}^{(1)}$	0.770"x0.645"	1.22	0.555	0.83	0.833	2.55
			0.635	0.784	0.787	
$_e HE_{11}^{(1)}$	0.769"x0.505"	0.775	0.56	0.925	0.925	2.5
			0.785	0.80	0.802	
$_o HE_{11}^{(1)}$	0.769"x0.505"	0.775	0.55	0.875	0.882	2.5
			0.695	0.80	0.80	
$_e HE_{11}^{(1)}$	1.005"x0.361"	0.376	0.725	0.962	0.964	2.5
			1.00	0.862	0.862	
$_o HE_{11}^{(1)}$	1.005"x0.361"	0.376	0.72	0.87	0.873	2.5
			0.93	0.79	0.792	

It was found that the wavelength measurements were rather insensitive to small non-uniformity of the rods and to the variation of humidity and temperature in the laboratory. Incidentally, the above experiment also suggested a rather convenient way of measuring the dielectric constant of a certain low loss dielectric material.

B. The Field Distributions

In order to establish the degree of field purity an examination of the radial field decay at a fixed axial position was carried out. The decay of the axial electric field was measured since it can most easily be detected by a probe pointed in the axial direction. For maximum signal strength, the probe was aligned in the $\eta = \pi/2$ plane for the $_e HE_{11}^{(1)}$ mode and $\eta = 0$ for the $_o HE_{11}^{(1)}$ mode. The general method of measurement

has been outlined in section 6.2.

Experimental results, together with their theoretical results for the $_e\text{HE}_{11}^{(1)}$ mode are shown in Figures VI-16 through VI-18. Six different rods ranging from $\xi_o = \infty$ to $\xi_o = 0.376$ were used. It can be seen that the experimental results corresponded rather well with the analytical results. The largest differences were found among thin rods. This effect may be explained by the fact that for small values of NMA, a large percentage of energy was carried outside the dielectric rod, thus a small amount of curvature or sagging may have caused some errors in the field decay measurements. These measurements, together with the wavelength measurements verified the existence of the $_e\text{HE}_{11}^{(1)}$ mode along an elliptical dielectric rod.

Similar measurements were performed for the $_o\text{HE}_{11}^{(1)}$ mode. Four rods ranging from $\xi_o = \infty$ to $\xi_o = 0.376$ were used. Results are shown in Figures VI-19 through VI-20. Again, good agreement with theoretical results were observed. These measurements also confirmed the existence of the $_o\text{HE}_{11}^{(1)}$ mode.

The above discussion shows clearly the necessity of having a structure which may support the dielectric rod and at the same time will not interfere with the desired propagating mode. One of the best ideas, which was first proposed by D. D. King (20), is the use of the image plane. He took advantage of the symmetrical property of the HE_{11} mode and mounted a half-round dielectric rod on an image plane. It can be seen that his idea can very well be extended to the elliptical dielectric rod. This image plane can not only serve as a support without disturbing the fields, but also may serve as a polarization anchor.

Fig. VI-16.

Fig. VI-17.

Fig. VI-18.

Fig. VI-19.

Fig. VI-20.
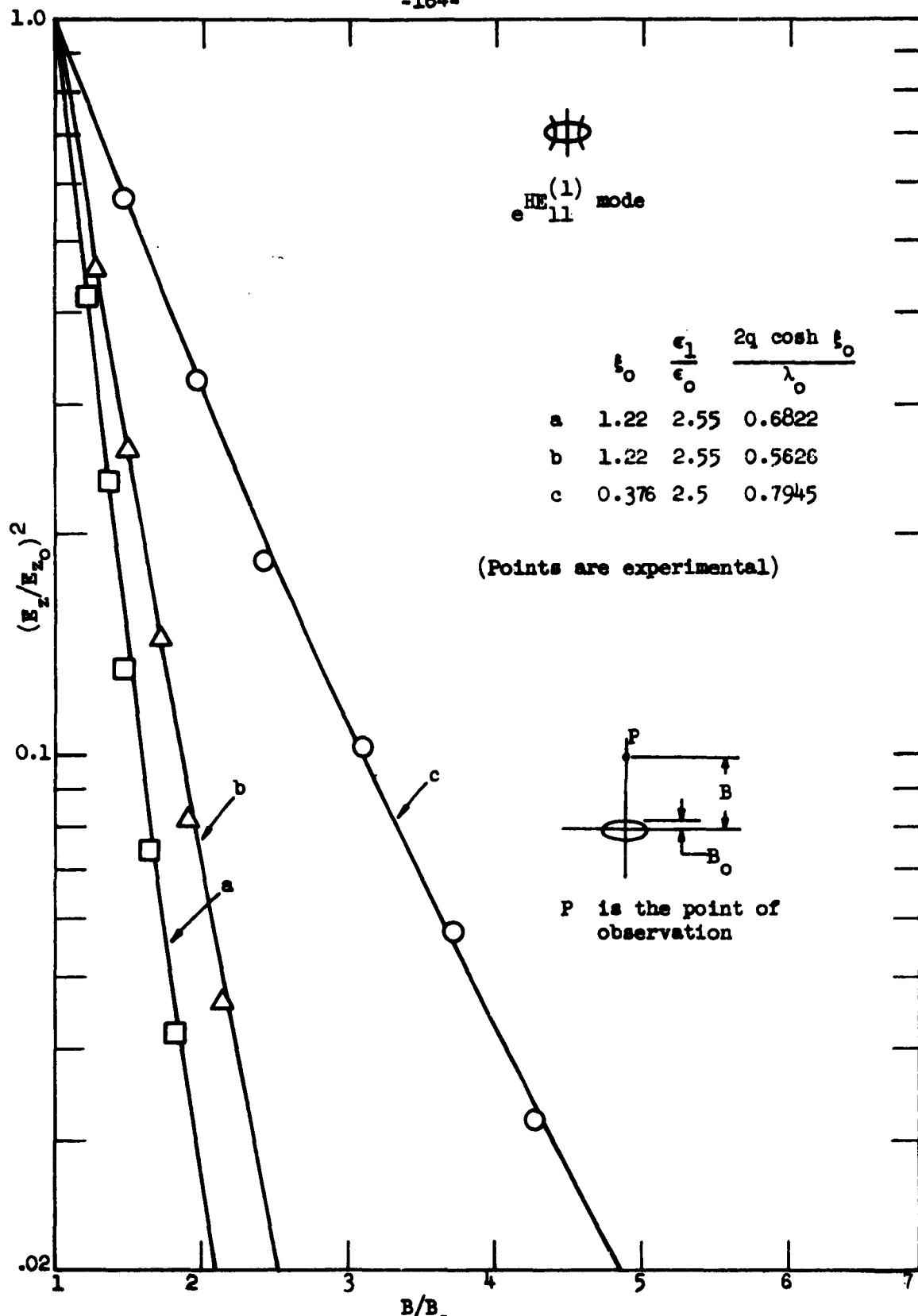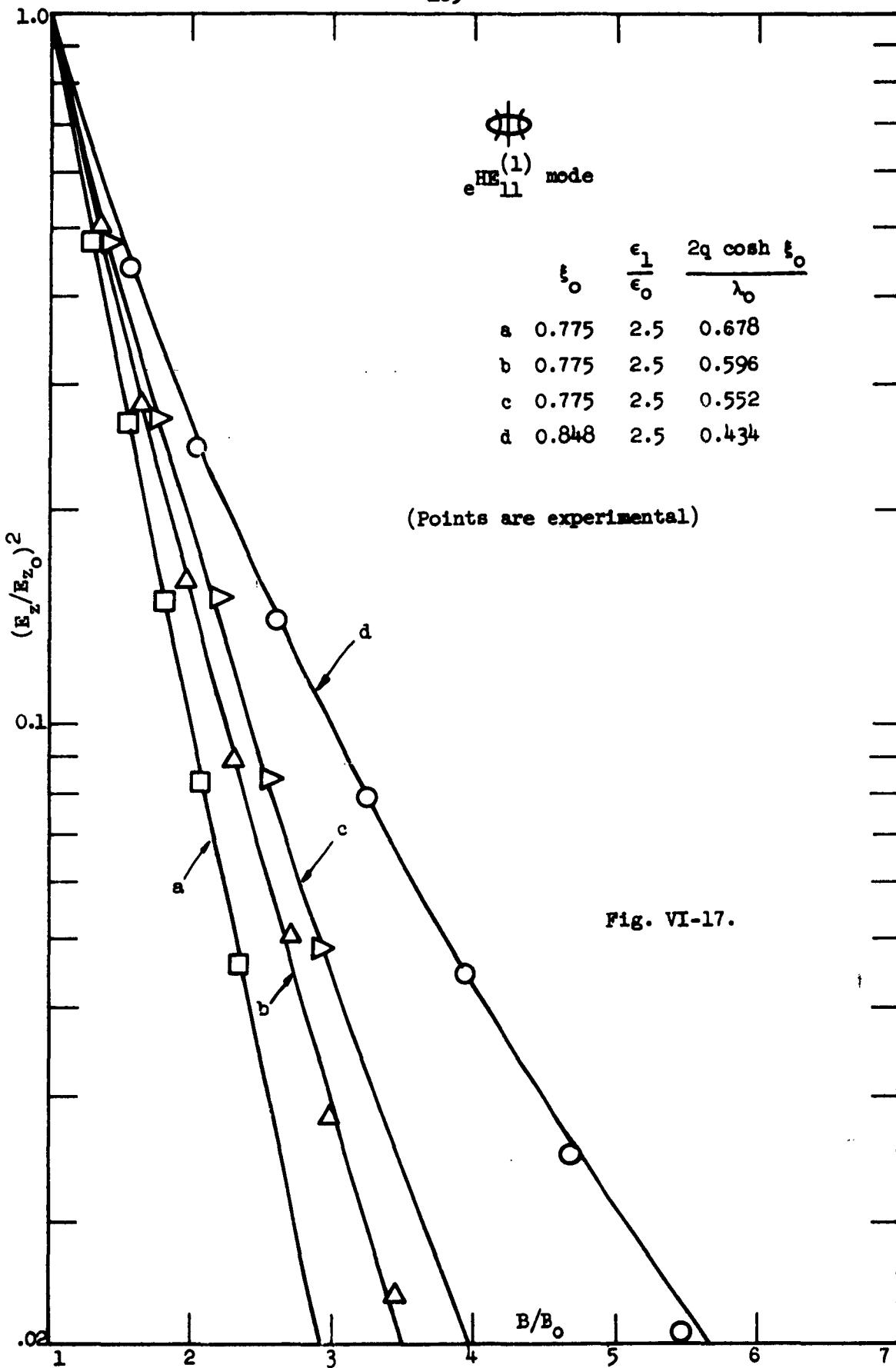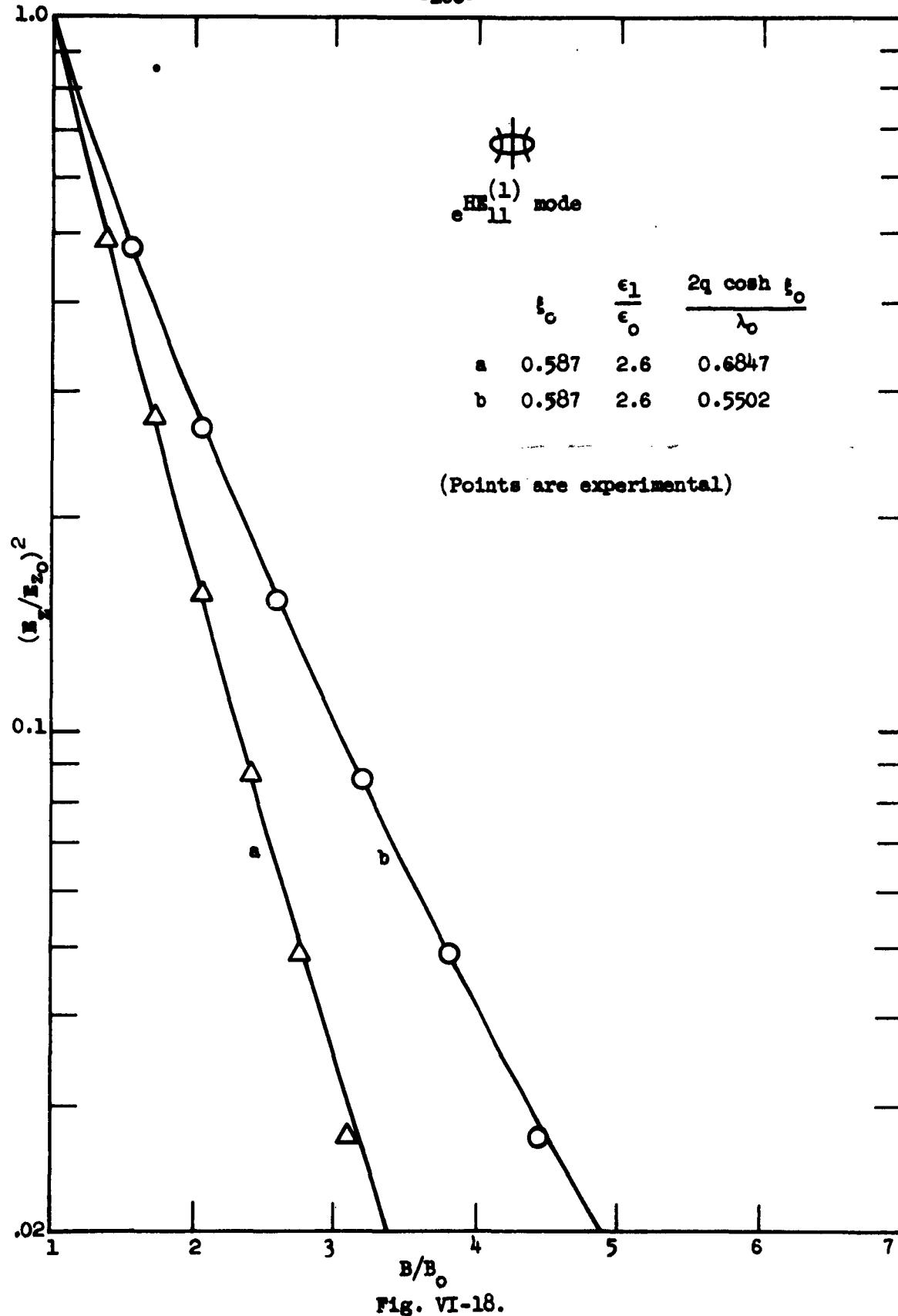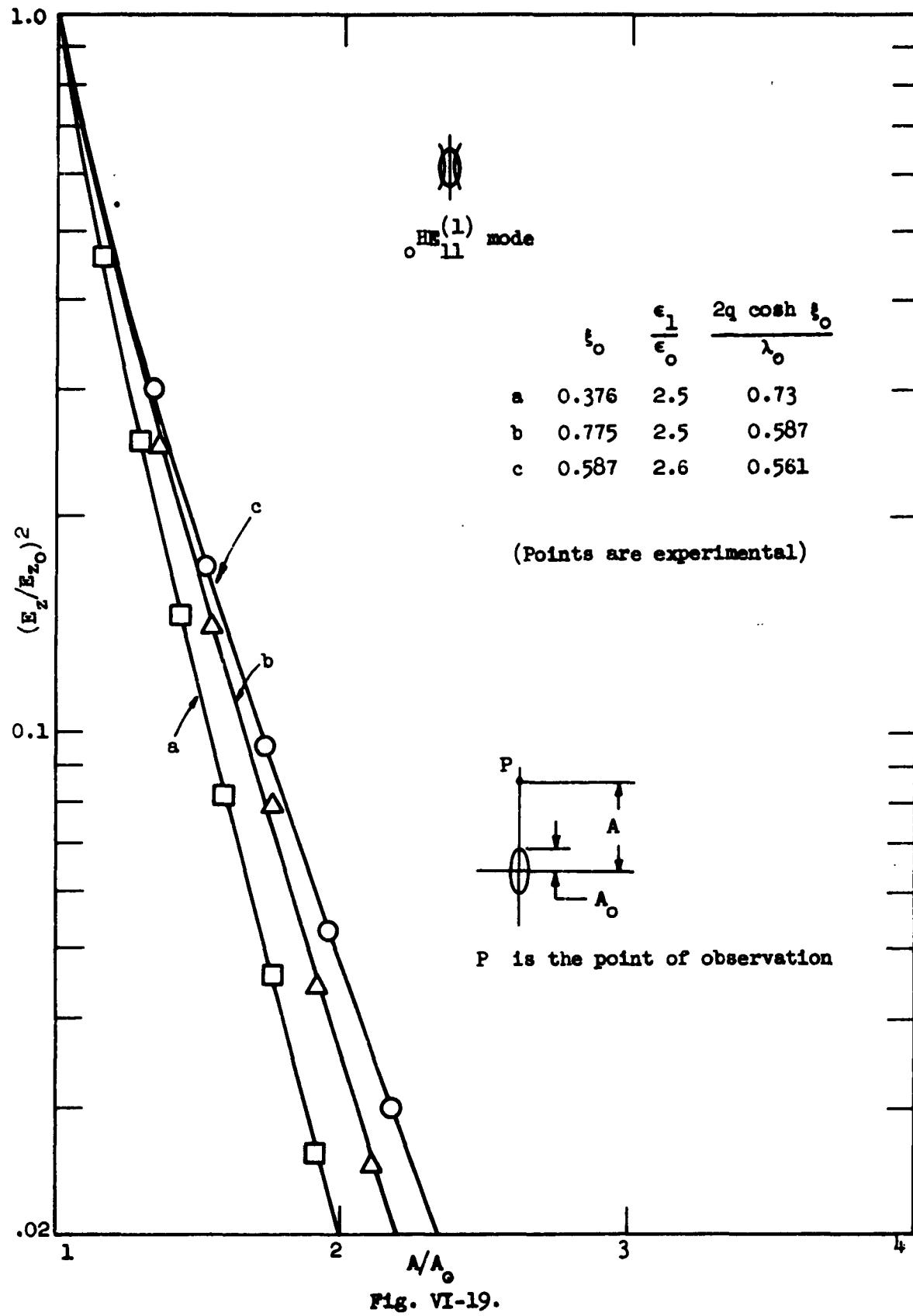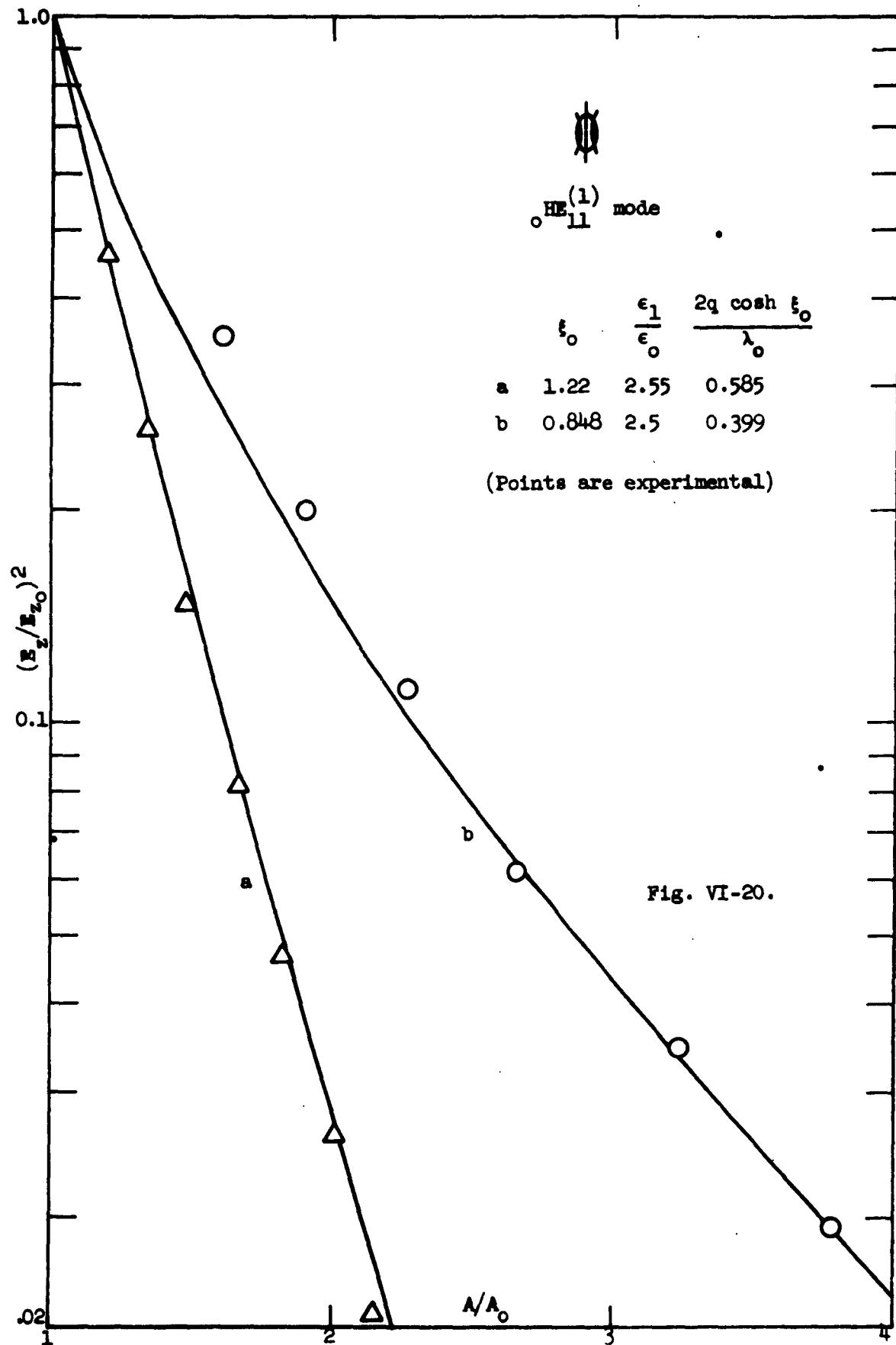
C. Attenuation Constants

Attenuation measurements were made by probe, using the standard standing wave technique (59). For each experimental point two measurements at two different locations were carried out in order that the loss due to the imperfections of the terminating reflecting plate could be eliminated, (See the footnote on p. 155). The percentage variations of the loss factor of these dielectric rods were found to be quite large. The loss factors for various rods were found to vary from $\tan\delta = 0.005$ to $\tan\delta = 0.003$. Both theoretical and experimental results for the $_e\mathrm{HE}_{11}^{(1)}$ and the $_o\mathrm{HE}_{11}^{(1)}$ waves are shown in Figures VI-21 through VI-27. In general, the agreement is quite good, and it is better at higher frequencies than at lower frequencies. One of the reasons for this is that at lower frequencies, more energy is distributed outside the rod; thus, more energy is radiated due to the slight curvature of this open guide. Furthermore, the disturbance of the field caused by the presence of the supporting threads and the probe is more pronounced at lower frequencies. Since the attenuation is lower at lower frequency, the standing wave ratio is higher and the percentage error in the measurements of this high standing wave ratio is therefore larger. Because the attenuation constant is a measure of the power loss as compared with the power transmitted, it is quite understandable that the above mentioned factors would affect the accuracy of our measurements more at lower frequencies. It is for this reason that the resonator method is superior for low attenuation measurements. At higher frequencies most of the energy is carried inside the guide; very little disturbance will result from the supporting threads, the probe, and the small curvatures of the rod. The accuracy

Fig. VI-21.

$\oint e^{HE_{11}^{(1)}}$ mode

(Points are experimental)

$\frac{\epsilon_D}{\epsilon_o} = 2.5$

Limit R = 0.633

	ξ_o	ϕ_d
a	0.775	0.003
b	0.368	0.0036

$2q \cosh \xi_o / \lambda_o$

Fig. VI-22.

(Points are experimental)

Fig. VI-23.

$\angle q \cosh \xi_o / \lambda_o$

Fig. VI-24.

(Points are experimental)

Fig. VI-25.

Fig. VI-26.

(Points are experimental)
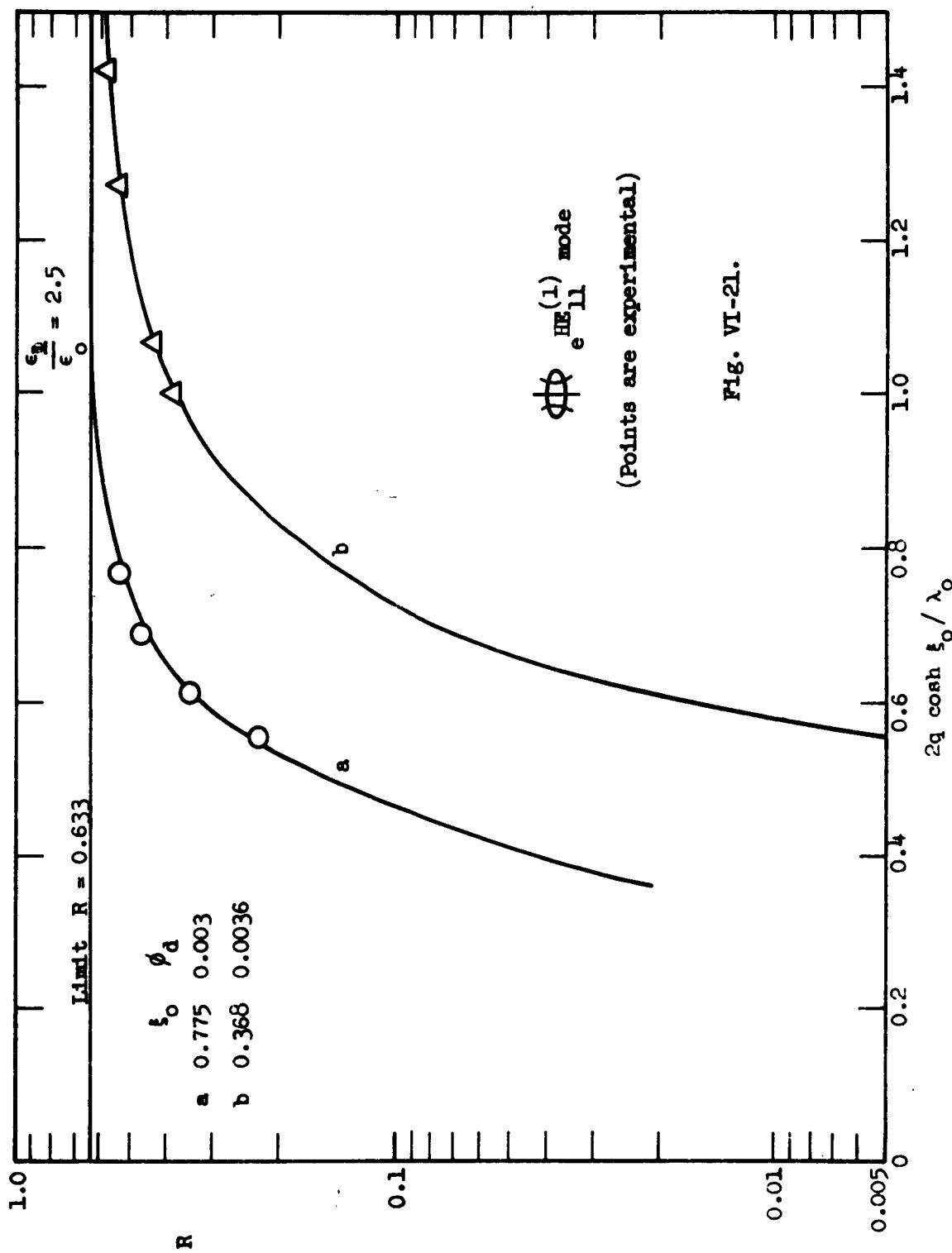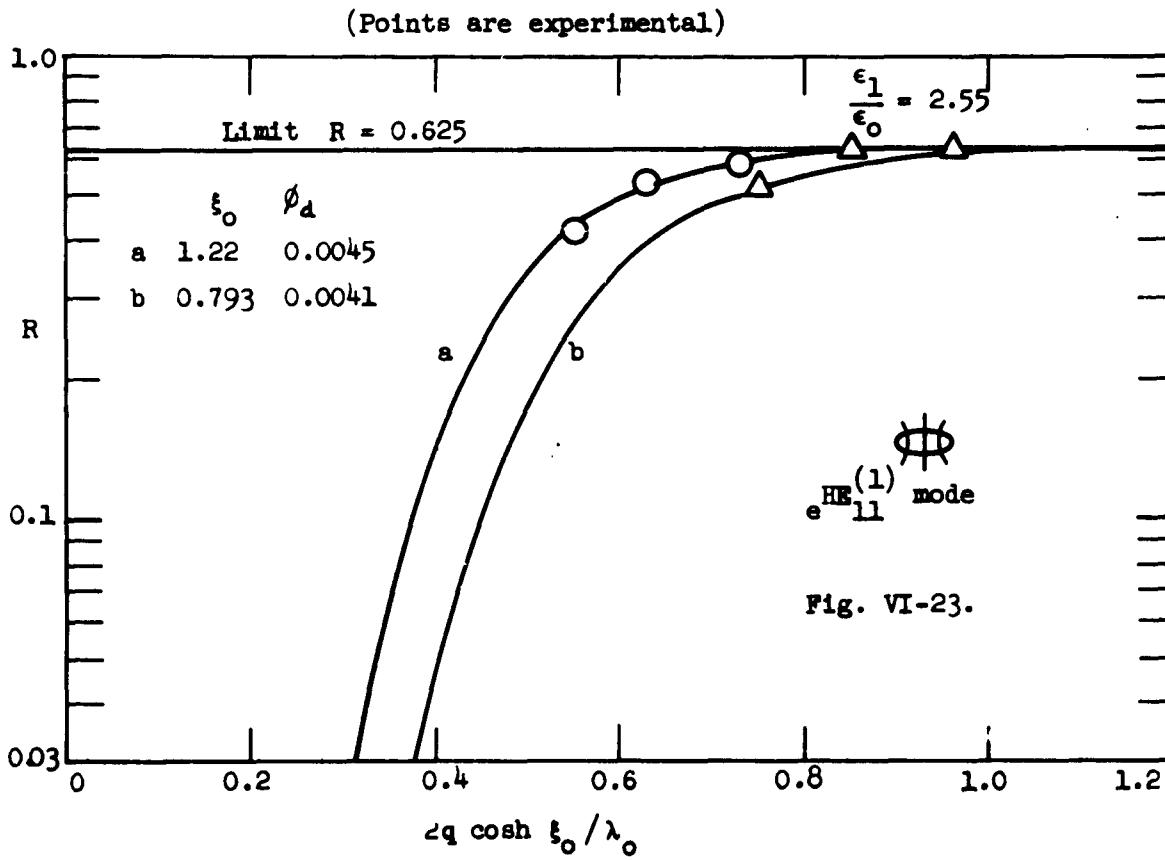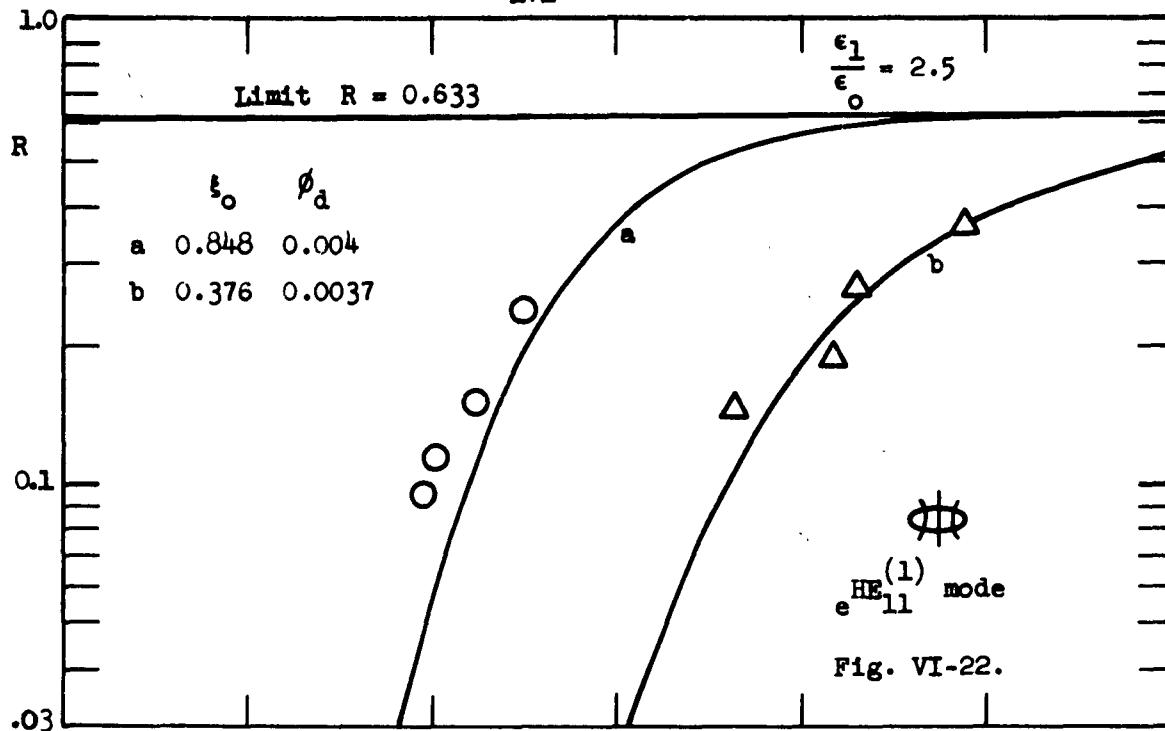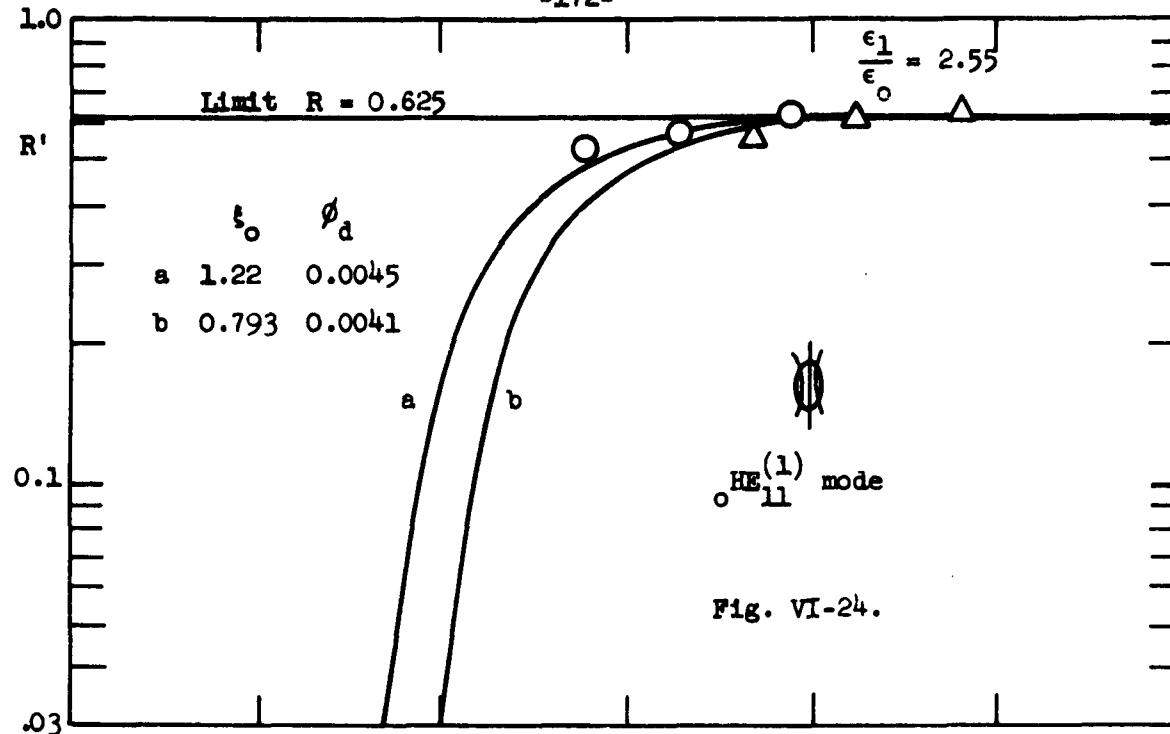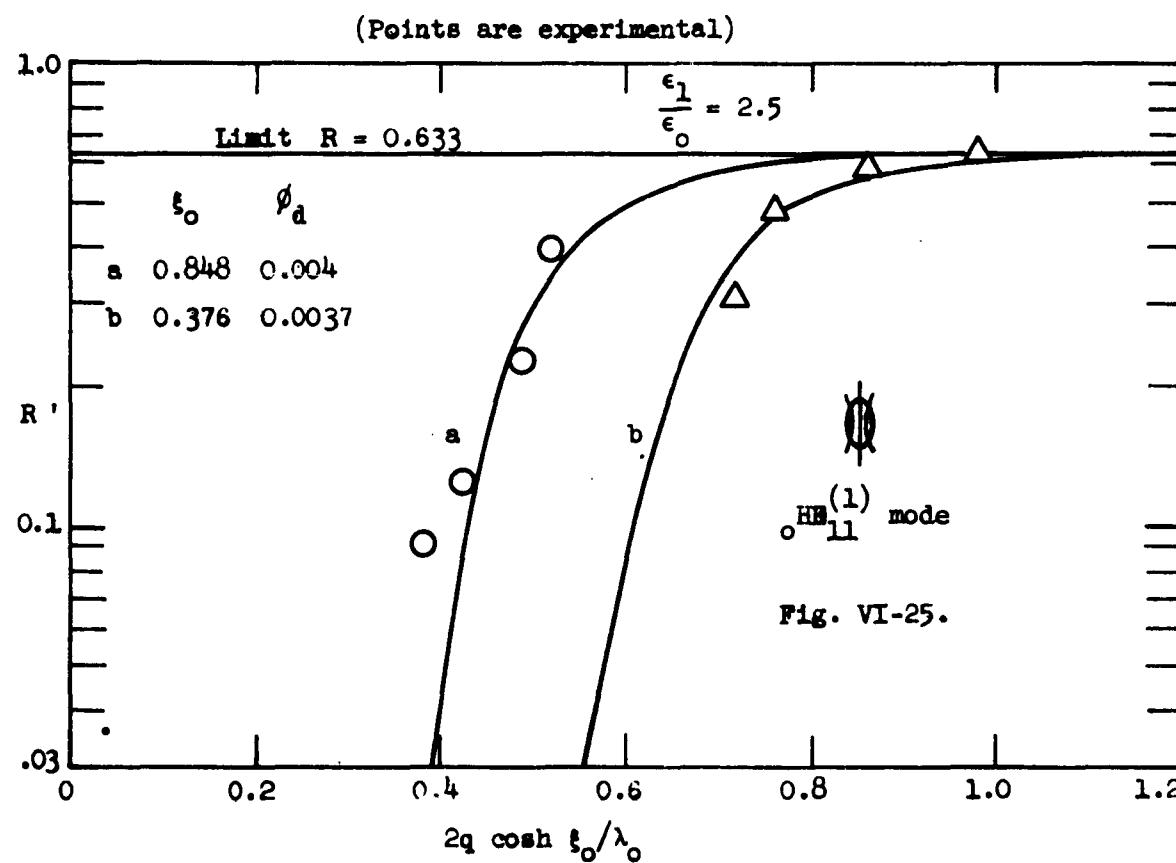
Fig. VI-27
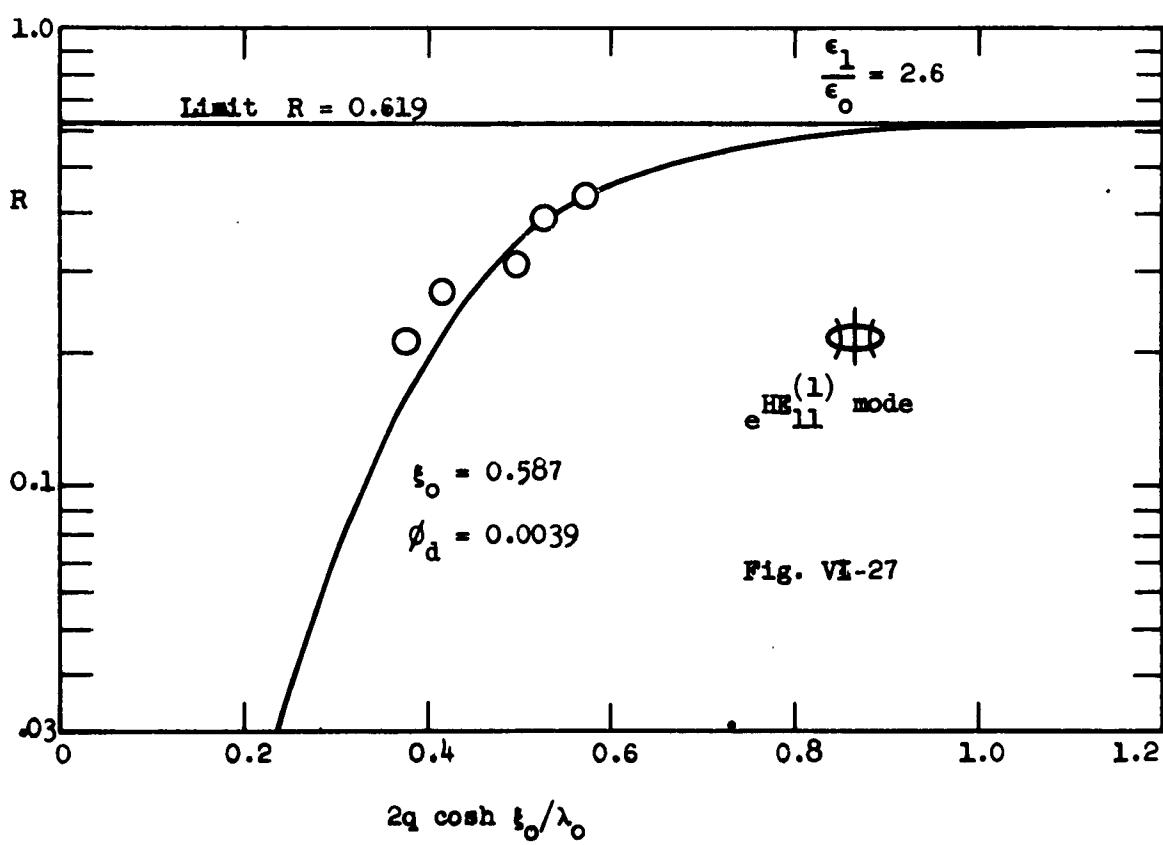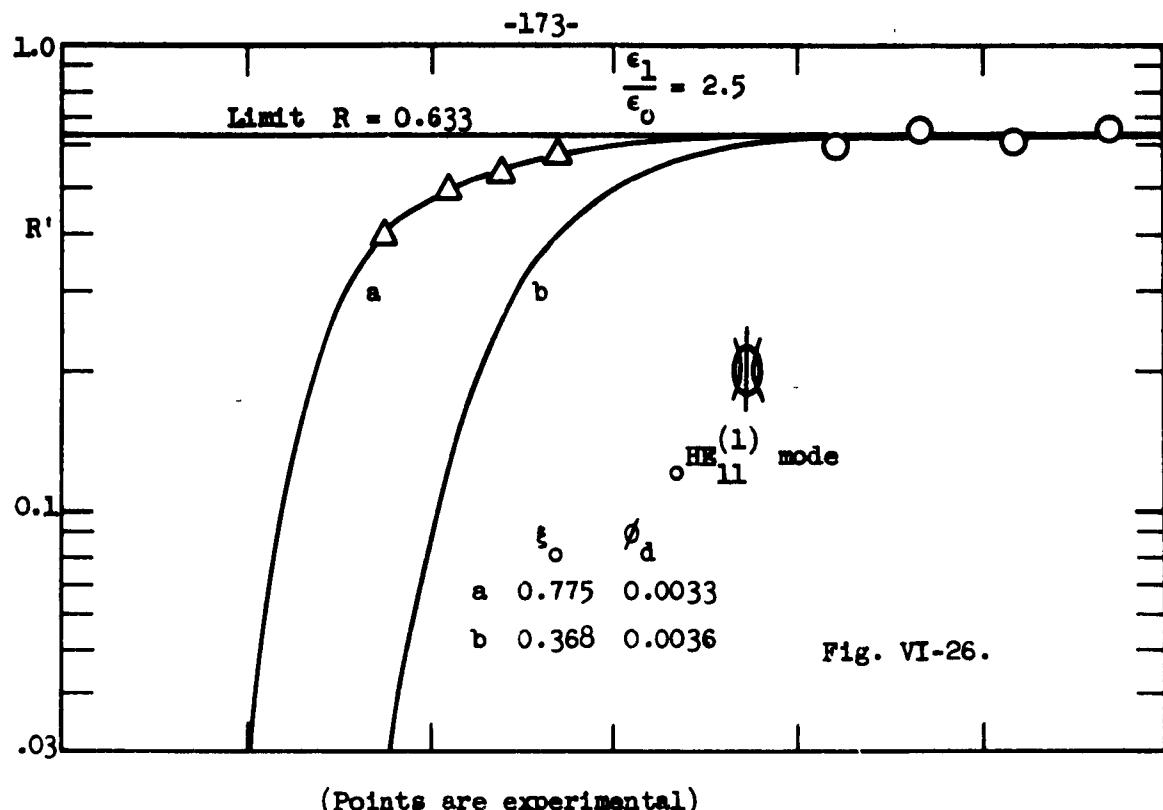
of the experimental measurements is thus greatly improved. Another source of error is probably due to the approximations used in computing the numerical results from the analytical equations. It was mentioned earlier in Chapter IV that as the elliptical cross sections become flatter, i.e., ξ_o gets smaller, more terms of the expansions are required to obtain more accurate numerical results. However, sufficiently close agreement between the analytical and experimental results is observed to warrant the verification of the theoretical predictions.

It is noted that a dielectric ribbon having the same cross sectional area as a circular dielectric rod and operating in the dominant $_e HE_{11}^{(1)}$ mode does indeed offer much less attenuation than the circular dielectric cylinder.

6.4 Conclusions

Special experimental apparatus was designed to measure the propagation characteristics of the two principal dominant modes, namely the $_e HE_{11}^{(1)}$ and the $_o HE_{11}^{(1)}$ modes. Despite the mentioned sources of experimental errors, measured results were found to be in good agreement with the calculated results. Particularly good agreement was observed in the guide wavelength category. The existence of these two dominant modes was verified.

It was noted experimentally that the next higher order mode occurs at a higher frequency for the flatter elliptical cross-section rod. Therefore, the flatter rod possessed not only a lower attenuation factor but also a wider bandwidth.

CHAPTER VII - SUMMARY AND CONCLUSIONS

The problem of electromagnetic wave propagation along an elliptical dielectric rod was considered. It was shown that, in general, no pure TE or TM wave might exist on such a waveguide except when the eccentricity of the rod was zero. In order to satisfy the boundary conditions, an infinite series of product terms of Mathieu and modified Mathieu functions were used to represent the field configurations in one of the two regions. The field components and the characteristic equations of four principal types of waves were obtained. They were classified as the $_e\text{HE}_{mn}^{(1)}$ mode, the $_e\text{HE}_{mn}^{(0)}$ mode, the $_o\text{HE}_{mn}^{(1)}$ mode, and the $_o\text{HE}_{mn}^{(0)}$ mode. These modes were degenerate and became the well known HE_{mn} mode when the eccentricity was zero. The modes with $m = 1$ and $n = 1$, called the dominant modes, possessed no cut-off frequency. The propagation characteristics of the dominant modes were considered in detail both analytically and experimentally. Extensive numerical computations on the properties of the guide wavelength, the rate of field decay, and the attenuation characteristics of the dominant modes were carried out.

Experiments were designed and performed using various sizes of elliptical lucite rod to verify the analytic results of the dominant modes. Measured data were compared with theoretical results and it was shown that very good agreement was obtained.

The Q of a dielectric cavity resonator operating in either one of the dominant modes was also computed. It was found that a very high Q cavity could be made using proper size dielectric strip.

It was demonstrated analytically and experimentally that a thin elliptical rod operating in the $_e\text{HE}_{11}^{(1)}$ mode typically had considerably

lower loss than did a circular rod, operating in the HE_{11} mode, having the same cross-sectional area.

Other advantages are listed below:

a. A flat elliptical dielectric rod has larger surface area, thus it would be easier to handle at very high frequencies, such as in the mm wavelength range.

b. The $_eHE_{11}^{(1)}$ mode possesses greater bandwidth, since the cut-off frequency of the next higher order mode is higher for flatter elliptical cross sections.

c. Depolarization effects are minimized because the guide wavelengths differ for the even and odd modes. It is known that internal strain, non-uniform dimensions, and bends of the circular rod cause the HE_{11} mode to change polarization.

d. A flat elliptical dielectric rod which may be approximated by a strip is easier to fabricate since wider dimensional tolerances are permitted. This is because the guide wavelength and the attenuation constant are slower varying functions of the dimensions for the strip than for the circular rod.

It should also be noted that the $_eHE_{11}^{(1)}$ mode can be launched as easily as the HE_{11} mode.

The advantages and disadvantages of using the dielectric tape line as a transmission line in comparison with the conventional metal tube waveguide (at frequencies above 50 kmc) are discussed below.

a. Keeping the spread of the field outside the dielectric tape within a reasonable distance from the surface of the dielectric guide, the loss factor of the $_eHE_{11}^{(1)}$ mode on a dielectric tape line can be made smaller than that of the dominant mode in a rectangular metal tube guide, but still somewhat larger than that of the TE_{01} mode in a circular metal tube guide.

    b. In order to avoid mode conversion the surface of the cir-
cular metal waveguide must meet very close tolerances.
These kind of tolerances are not required for the elliptical
dielectric rod; thus, it is easier to fabricate.

    c. Unlike the metal tube waveguide, the field of a dielectric
tape is not entirely confined within the strip. Consequently,
it can be subjected to interference due to nearby foreign
objects or foreign signals. The presence of curvature or
discontinuity of the strip will also cause energy loss by
radiation. It is rather difficult to support the dielectric
rod without disturbing the field. The use of image plane,
as proposed by King, as a supporting device appears to be
quite suitable.

The greatest attraction of a surface wave dielectric tape line as a
millimeter wave transmission line is in its simplicity of construction,
its low cost and ease of manufacture, and its flexibility.

The analytic method of solving this elliptical dielectric wave-
guide problem should prove applicable to others involving the use of
the elliptical coordinate system and the Mathieu functions. For
instance, one may apply this technique to the problemsof

    a. the propagation of electromagnetic waves along an ellip-
tical dielectric tube, or

    b. the surface wave propagation along an elliptical Sommer-
feld or Goubau wire, or

    c. the scattering of electromagnetic wave by an elliptical
dielectric cylinder.

Other analogous mechanical problems can also be solved in a similar
manner.

We did not consider the source-present problem. However, it is
emphasized here that it is not possible to express any arbitrary field

distribution in terms of the propagating modes alone for any open boundary problems. The problem with source present must then be formulated in terms of Green's function in the form of a contour integral. The residues at the poles of the integrand will give rise to modal type waves which are also called guided waves. The contribution of the integral around the branch cut will give rise to a radiated wave.

APPENDIX A

Mathematical Relations

Many of the formulas and expressions which are used throughout this report are given in the following sections for convenient reference. Those relationships which are considered well known are stated with only a reference to their origin. Others, which are considered not so well known are discussed in more detail. Some relations which are given here for the first time are derived.

A.1 Series Representations of Mathieu and Modified Mathieu Functions

The Mathieu differential equation may be written in the form

$$\frac{d^2\theta}{d\eta^2} + (c - 2\gamma^2\cos 2\eta)\theta = 0 \tag{A.1-1}$$

where γ^2 is a constant which may be positive or negative, and c is the separation constant or the characteristic number. The periodic solutions of A.1-1 which may be expanded in terms of trigonometric functions are given below (42,45):

For $\gamma^2 \geqq 0$,

$$ce_{2n}(\eta,\gamma^2) = \sum_{r=0}^{\infty} A_{2r}^{(2n)} \cos 2r\eta \tag{A.1-2}$$

$$ce_{2n+1}(\eta,\gamma^2) = \sum_{r=0}^{\infty} A_{2r+1}^{(2n+1)} \cos(2r+1)\eta \tag{A.1-3}$$

$$se_{2n+1}(\eta,\gamma^2) = \sum_{r=0}^{\infty} B_{2r+1}^{(2n+1)} \sin(2r+1)\eta \tag{A.1-4}$$

$$se_{2n+2}(\eta,\gamma^2) = \sum_{r=0}^{\infty} B_{2r+2}^{(2n+2)} \sin(2r+2)\eta \tag{A.1-5}$$

and for $\gamma^2 \leqq 0$,

$$ce^*_{2n}(\eta,|\gamma^2|) = \sum_{r=0}^{\infty} (-1)^{r+n} A^{(2n)}_{2r} \cos 2r\eta \qquad (A.1-6)$$

$$ce^*_{2n+1}(\eta,|\gamma^2|) = \sum_{r=0}^{\infty} (-1)^{r+n} B^{(2n+1)}_{2r+1} \cos(2r+1)\eta \qquad (A.1-7)$$

$$se^*_{2n+1}(\eta,|\gamma^2|) = \sum_{r=0}^{\infty} (-1)^{r+n} A^{(2n+1)}_{2r+1} \sin(2r+1)\eta \qquad (A.1-8)$$

$$se^*_{2n+2}(\eta,|\gamma^2|) = \sum_{r=0}^{\infty} (-1)^{r+n} B^{(2n+2)}_{2r+2} \sin(2r+2)\eta \qquad (A.1-9)$$

The expansion coefficients, $A^{(2n)}_{2r}$, $A^{(2n+1)}_{2r+1}$, $B^{(2n+1)}_{2r+1}$, and $B^{(2n+2)}_{2r+2}$ are functions of $|\gamma^2|$ and have been tabulated by NBS (49) for various values of $|\gamma^2|$ up to $|\gamma^2| = 25$.

The modified Mathieu differential equation may be written in the form

$$\frac{d^2R}{d\xi^2} - (c - 2\gamma^2 \cosh 2\xi)R = 0 \qquad (A.1-10)$$

where γ^2 is a constant which may be positive or negative and c is the separation constant or the characteristic number. The stable solutions of A.1-10 which correspond to the periodic solutions of A.1-1 can be expressed in terms of Bessel function product series. Comparing this with other ways of expressing the solutions of A.1-10, the Bessel function product series converge the fastest and therefore are best suited for computational purposes (45).

Let $u = |\gamma| e^{-\xi}$ and $v = |\gamma| e^{\xi}$; the set of stable solutions of A.1-10 with $\gamma^2 \geqslant 0$ is (45),

$$Ce_{2n}(\xi,\gamma^2) = \frac{p_{2n}}{A^{(2n)}_0} \sum_{r=0}^{\infty} (-1)^r A^{(2n)}_{2r} J_r(u) J_r(v) \qquad (A.1-11)$$

$$Ce_{2n+1}(\xi,\gamma^2) = \frac{p_{2n+1}}{A_1^{(2n+1)}} \sum_{r=0}^{\infty} (-1)^r A_{2r+1}^{(2n+1)} \left[J_r(u)J_{r+1}(v) + J_{r+1}(u)J_r(v) \right]$$

(A.1-12)

$$Se_{2n+1}(\xi,\gamma^2) = \frac{s_{2n+1}}{B_1^{(2n+1)}} \sum_{r=0}^{\infty} (-1)^r B_{2r+1}^{(2n+1)} \left[J_r(u)J_{r+1}(v) - J_{r+1}(u)J_r(v) \right]$$

(A.1-13)

$$Se_{2n+2}(\xi,\gamma^2) = \frac{s_{2n+2}}{B_2^{(2n+2)}} \sum_{r=0}^{\infty} (-1)^r B_{2r+2}^{(2n+2)} \left[J_r(u)J_{r+2}(v) - J_{r+2}(u)J_r(v) \right] \; .$$

(A.1-14)

And, the set of stable solutions of A.1-10 with $\gamma^2 \leq 0$ is (45),

$$Fek_{2n}(\xi,|\gamma^2|) = \frac{(-1)^n p_{2n}}{\pi A_0^{(2n)}} \sum_{r=0}^{\infty} A_{2r}^{(2n)} I_r(u) K_r(v)$$

(A.1-15)

$$Fek_{2n+1}(\xi,|\gamma^2|) = \frac{(-1)^n s_{2n+1}}{\pi B_1^{(2n+1)}} \sum_{r=0}^{\infty} B_{2r+1}^{(2n+1)} \left[I_r(u)K_{r+1}(v) - I_{r+1}(u)K_r(v) \right]$$

(A.1-16)

$$Gek_{2n+1}(\xi,|\gamma^2|) = \frac{(-1)^n p_{2n+1}}{\pi A_1^{(2n+1)}} \sum_{r=0}^{\infty} A_{2r+1}^{(2n+1)} \left[I_r(u)K_{r+1}(v) + I_{r+1}(u)K_r(v) \right]$$

(A.1-17)

$$Gek_{2n+2}(\xi,|\gamma^2|) = \frac{(-1)^{n+1} s_{2n+2}}{\pi B_2^{(2n+2)}} \sum_{r=0}^{\infty} B_{2r+2}^{(2n+2)} \left[I_r(u)K_{r+2}(v) - I_{r+2}(u)K_r(v) \right] \; .$$

(A.1-18)

The expansion coefficients $A_{2r}^{(2n)}$, $A_{2r+1}^{(2n+1)}$, $B_{2r+1}^{(2n+1)}$, $B_{2r+2}^{(2n+2)}$ and the connecting coefficients p_{2n}, p_{2n+1}, s_{2n+1}, s_{2n+2} are functions of $|\gamma^2|$ and have all been tabulated in a table prepared by NBS (49). The above series are absolutely and uniformly convergent. The analytic expressions for the connecting coefficients are

$$p_{2n} = ce_{2n}(0,\gamma^2) \, ce_{2n}(\tfrac{1}{2}\pi,\gamma^2) \Big/ A_0^{(2n)}$$

(A.1-19)

$$p_{2n+1} = ce_{2n+1}(0,\gamma^2) ce'_{2n+1}(\tfrac{1}{2}\pi, \gamma^2) \Big/ \gamma A_1^{(2n+1)}$$

(A.1-20)

$$s_{2n+1} = se'_{2n+1}(0,\gamma^2) \ se_{2n+1}(\tfrac{1}{2}\pi, \gamma^2) / \gamma \ B_1^{(2n+1)} \qquad (A.1-21)$$

$$s_{2n+2} = se'_{2n+2}(0,\gamma^2) se'_{2n+2}(\tfrac{1}{2}\pi,\gamma^2) / \gamma^2 B_2^{(2n+2)}. \qquad (A.1-22)$$

The prime signifies the derivative of the function with respect to η .

The normalizations introduced by Goldstein (60) will be used. They are

$$2\left[A_0^{(2n)}\right]^2 + \sum_{r=1}^{\infty} \left[A_{2r}^{(2n)}\right]^2 = 1 \qquad (A.1-23)$$

$$\sum_{r=0}^{\infty} \left[A_{2r+1}^{(2n+1)}\right]^2 = \sum_{r=0}^{\infty} \left[B_{2r+1}^{(2n+1)}\right]^2 = \sum_{r=0}^{\infty} \left[B_{2r+2}^{(2n+2)}\right]^2 = 1 \quad (A.1-24)$$

It is also defined that when $\gamma^2 = 0$

$$A_0^{(0)} = \frac{1}{\sqrt{2}} \ , \quad \left[A_{2r}^{2n}\right]^2 = \left[A_{2r+1}^{(2n+1)}\right]^2 = \left[B_{2r+1}^{(2n+1)}\right]^2 = \left[B_{2r+2}^{(2n+2)}\right]^2 = 1$$

$$\text{when} \quad r = n$$

$$= 0$$

$$\text{when} \quad r \neq n.$$

$$(A.1-25)$$

A.2 Approximate Expressions for the Modified Mathieu Functions Suitable for Small Values of $|\gamma^2|$

Mathieu (61) first derived the expressions for the expansion coefficients $A_{2r}^{(2n)}$, $A_{2r+1}^{(2n+1)}$, $B_{2r+1}^{(2n+1)}$, $B_{2r+2}^{(2n+2)}$ when $|\gamma^2|$ is small. They are

$$B_{m+2r}^{(m)} \approx A_{m+2r}^{(m)} \approx (-1)^r \ \frac{m!}{r!(m+r)!} \ (\tfrac{\gamma^2}{4})^r \ , \qquad (A.2-1)$$

$$(r \geq 0, \ m > 0)$$

$$\text{and} \quad B_{m-2r}^{(m)} \approx A_{m-2r}^{(m)} \approx \frac{(m-r-1)!}{r!(m-1)!} \ (\tfrac{\gamma^2}{4})^r \ , \qquad (A.2-2)$$

where $\approx$ means approximate equality.

a. Approximate Expressions for $\mathrm{Fek}_{2n+1}(\xi,|\gamma^2|)$ and $\mathrm{Gek}_{2n+1}(\xi,|\gamma^2|)$ when $|\gamma^2| \to 0$. The approximate expression for $\mathrm{Fek}_{2n+1}(\xi,|\gamma^2|)$ from A.1-16 is

$$\frac{\pi}{(-1)^n s_{2n+1}} \mathrm{Fek}_{2n+1}(\xi,|\gamma^2|) \approx \frac{1}{B_1^{(2n+1)}} \left\{ \cdots + B_{(2n+1)-2}^{(2n+1)} \right.$$

$$\times \left[I_{n-1}(u)K_n(v) - I_n(u)K_{n-1}(v) \right] + B_{2n+1}^{(2n+1)} \left[I_n(u)K_{n+1}(v) \right.$$

$$\left. - I_{n+1}(u)K_n(v) \right] + B_{(2n+1)+2}^{(2n+1)} \left[I_{n+1}(u)K_{n+2}(v) - I_{n+2}(u)K_{n+1}(v) \right] + \cdots \left. \right\}$$

$$(n \geq 1) \quad (A.2\text{-}3)$$

where

$$B_{2n-1}^{(2n+1)} \approx \frac{1}{2n} \frac{\gamma^2}{4} + O(\gamma^4) \tag{A.2-4}$$

$$B_{2n+1}^{(2n+1)} \approx 1 + O(\gamma^4) \tag{A.2-5}$$

and $\quad B_{2n+3}^{(2n+1)} \approx - \frac{1}{2(n+1)} \frac{\gamma^2}{4} + O(\gamma^4)$. $\tag{A.2-6}$

$O(\gamma^4)$ means that the next term in the expansion is of the order of γ^4. The value of $O(\gamma^4)$ in A.2-5 can easily be obtained from the normalization $\sum_{r=0}^{\infty} \left[B_{2r+1}^{(2n+1)} \right]^2 = 1$. Thus

$$B_{2n+1}^{(2n+1)} \approx 1 - \frac{\gamma^4}{128} \left[\frac{2n(n+1) + 1}{n^2(n+1)^2} \right] + O(\gamma^8) . \tag{A.2-7}$$

The following approximations for the modified Bessel functions (62) will be used, when u and v are small:

$$I_m(u) = \frac{u^m}{2^m m!}\left[1 + \frac{u^2}{2(2m+2)} + 0(u^4)\right] \quad , \tag{A.2-8}$$

and

$$K_m(v) = \frac{(m-1)!\, 2^{m-1}}{v^m} - \frac{2^{m-3}(m-2)!}{v^{m-2}} + 0\left(\frac{1}{v^{m-4}}\right) + (-1)^{m+1}\, I_m(v)\, \ln\left(\frac{e^\alpha v}{2}\right) \tag{A.2-9}$$

$$(m \geqq 1)$$

$$K_0(v) \approx - \ln\frac{v e^\alpha}{2} \tag{A.2-10}$$

where α is Euler's constant, $\alpha = 0.5772 \cdots$.

Substituting these expressions, A.2-4 and A.2-6 through A.2-10 into equation A.2-3 and remembering that $u = \gamma e^{-\xi}$, $v = \gamma e^\xi$, after considerable algebraic manipulations one obtains the approximate expression

$$\frac{\pi}{(-1)^n s_{2n+1}}\, Fek_{2n+1}(\xi,|\gamma^2|) = \frac{1}{B_1^{(2n+1)}}\left\{\left(\frac{1}{\gamma}\right)\left[e^{-(2n+1)\xi}\right]\right.$$
$$\left. - (\gamma)\left[\frac{e^{(-2n+1)\xi}}{8n(n+1)}\left((n+1) + 2e^{-2\xi} - ne^{-4\xi}\right)\right] + 0(\gamma^3) \right. \tag{A.2-11}$$

Putting the approximate expression for $B_1^{(2n+1)}$ into A.2-11, one finally arrives at the equation

$$\frac{\pi}{(-1)^n s_{2n+1}}\, Fek_{2n+1}(\xi,|\gamma^2|) = \frac{2^{2n}(2n)!}{\gamma^{2n+1} e^{(2n+1)\xi}}\left\{1 - \frac{\gamma^2 e^{2\xi}}{8n(n+1)}\left[(n+1)\right.\right.$$
$$\left.\left. + 2e^{-2\xi} - ne^{-4\xi}\right] + 0(\gamma^4)\right\} . \quad (n \geqq 1) \tag{A.2-12}$$

For the special case, $n = 0$

$$\frac{\pi}{s_1}\, Fek_1(\xi,|\gamma^2|) = \frac{1}{\gamma e^\xi} + \frac{\gamma e^\xi}{2} \ln\left(\frac{e^\alpha}{2}\gamma e^\xi\right)\left[1 - e^{-2\xi}\right] - \frac{\gamma e^{-3\xi}}{8} + 0(\gamma^3) . \tag{A.2-13}$$

The approximate expression for the $Gek_{2n+1}(\xi,|\gamma^2|)$ can be obtained in a similar manner. Carrying out the tedious algebraic steps, one arrives at the equation for $n \geq 1$

$$\frac{(-1)^n \pi}{p_{2n+1}} Gek_{2n+1}(\xi,|\gamma^2|) = \frac{2^{2n}(2n)!}{\gamma^{2n+1} e^{(2n+1)\xi}} \left\{ 1 - \frac{\gamma^2 e^{2\xi}}{8n(n+1)} \left[(n+1) - 2e^{-2\xi} - ne^{-4\xi} \right] + O(\gamma^4) \right\} \quad (A.2-14)$$

and for $n = 0$

$$\frac{\pi}{p_1} Gek_1(\xi,|\gamma^2|) = \frac{1}{\gamma e^\xi} + \frac{\gamma e^\xi}{2} n(\frac{e^\alpha}{2} \gamma e^\xi) \left[1 + e^{-2\xi} \right] - \frac{\gamma e^{-3\xi}}{8} + O(\gamma^3) . \quad (A.2-15)$$

b. Approximate Expressions for $Ce_{2n+1}(\xi,\gamma^2)$ **and** $Se_{2n+1}(\xi,\gamma^2)$ **as** $|\gamma^2| \to 0$. It is possible to expand $Ce_{2n+1}(\xi,\gamma^2)$ and $Se_{2n+1}(\xi,\gamma^2)$ in a series of Bessel functions (45). They are

$$Ce_{2n+1}(\xi,\gamma^2) = - \frac{ce'_{2n+1}(\frac{1}{2}\pi,\gamma^2)}{\gamma A_1^{(2n+1)}} \sum_{r=0}^\infty (-1)^r A_{2r+1}^{(2n+1)} J_{2r+1}(2\gamma \cosh \xi) \quad (A.2-16)$$

and

$$Se_{2n+1}(\xi,\gamma^2) = \frac{se'_{2n+1}(0,\gamma^2)}{\gamma B_1^{(2n+1)}} \sum_{r=0}^\infty B_{2r+1}^{(2n+1)} J_{2r+1}(2\gamma \sinh \xi) . \quad (A.2-17)$$

These series are absolutely and uniformly convergent (45). Substituting equations A.2-1 and A.2-2 and the small argument approximation of the Bessel function into equations A.2-16 and A.2-17, and keeping the first order approximation, we get

$$Ce_{2n+1}(\xi,\gamma^2) = - \frac{ce'_{2n+1}(\frac{1}{2}\pi,\gamma^2)}{\gamma A_1^{(2n+1)}} \left\{ \frac{\gamma^{2n+1}}{(2n)!} \sum_{r=0}^n (-1)^r \frac{(n+r)!}{(n-r)!} \frac{(\cosh \xi)^{2r+1}}{4^{n-r}(2r+1)!} + O(\gamma^{2n+3}) \right\} \quad (A.2-18)$$

$$(n \geq 0)$$

and

$$Se_{2n+1}(\xi,\gamma^2) = \frac{se'_{2n+1}(0,\gamma^2)}{\gamma \, B_1^{(2n+1)}} \left\{ \frac{\gamma^{2n+1}}{(2n)!} \sum_{r=0}^{n} (-1)^r \frac{(n+r)!}{(n-r)!} \frac{(\sinh \xi)^{2r+1}}{4^{n-r}(2r+1)} \right.$$

$$\left. + 0(\gamma^{2n+3}) \right\}, \quad (n \geq 0) \, . \quad \text{(A.2-19)}$$

c. **Approximate Expressions for** $\dfrac{Fek'_{2n+1}(\xi,|\gamma^2|)}{Fek_{2n+1}(\xi,|\gamma^2|)}$, $\dfrac{Gek'_{2n+1}(\xi,|\gamma^2|)}{Gek_{2n+1}(\xi,|\gamma^2|)}$,

$\dfrac{Ce'_{2n+1}(\xi,\gamma^2)}{Ce_{2n+1}(\xi,\gamma^2)}$ **and** $\dfrac{Se'_{2n+1}(\xi,\gamma^2)}{Se_{2n+1}(\xi,\gamma^2)}$ **as** $|\gamma^2| \to 0$.

Taking the derivative of equations A.2-12 through A.2-15 with respect to ξ , combining these derivatives with the required functions, and keeping only the second order term in the approximation, we arrive at the following expressions:

$$\frac{Fek'_{2n+1}(\xi,|\gamma^2|)}{Fek_{2n+1}(\xi,|\gamma^2|)} = -(2n+1) - \frac{\gamma^2 e^{2\xi}}{4n(n+1)} \left\{ (n+1) + ne^{-4\xi} \right\} + 0(\gamma^4) \, , \quad (n \geq 1)$$

$$\text{(A.2-20)}$$

$$\frac{Fek'_1(\xi,|\gamma^2|)}{Fek_1(\xi,|\gamma^2|)} = -1 + \frac{\gamma^2 e^{2\xi}}{2} \ln(\frac{e^\alpha}{2}\gamma e^\xi) \left[3 - 2e^{-2\xi} \right] + 0(\gamma^4) \, , \quad (n \geq 1)$$

$$\text{(A.2-21)}$$

$$\frac{Gek'_{2n+1}(\xi,|\gamma^2|)}{Gek_{2n+1}(\xi,|\gamma^2|)} = -(2n+1) - \frac{\gamma^2 e^{2\xi}}{4n(n+1)} \left\{ (n+1) + ne^{-4\xi} \right\} + 0(\gamma^4) \, , \quad (n \geq 1)$$

$$\text{(A.2-22)}$$

and

$$\frac{Gek'_1(\xi,|\gamma^2|)}{Gek_1(\xi,|\gamma^2|)} = -1 + \frac{\gamma^2 e^{2\xi}}{2} \ln(\frac{e^\alpha}{2}\gamma e^\xi) \left[3 + 2e^{-2\xi} \right] + 0(\gamma^4) \, , \quad (n \geq 1) \, .$$

$$\text{(A.2-23)}$$

Taking the derivative of equations A.2-18 and A.2-19 with respect to ξ , combining these derivatives with the required functions, and keeping only the first order term in the approximation, we arrive at the following

expressions:

$$\frac{Ce'_{2n+1}(\xi,\gamma^2)}{Ce_{2n+1}(\xi,\gamma^2)} = \tanh \xi \left\{ \frac{\sum\limits_{r=0}^{n} (-1)^r \frac{(n+r)!}{(n-r)!} \frac{(\cosh \xi)^{2r}}{4^{n-r}(2r)!}}{\sum\limits_{r=0}^{n} (-1)^r \frac{(n+r)!}{(n-r)!} \frac{(\cosh \xi)^{2r}}{4^{n-r}(2r+1)!}} \right\} + O(\gamma^2) ,$$

$$(n \geq 0) \quad (A.2\text{-}24)$$

$$\frac{Se'_{2n+1}(\xi,\gamma^2)}{Se_{2n+1}(\xi,\gamma^2)} = \coth \xi \left\{ \frac{\sum\limits_{r=0}^{n} (-1)^r \frac{(n+r)!}{(n-r)!} \frac{(\sinh \xi)^{2r}}{4^{n-r}(2r)!}}{\sum\limits_{r=0}^{\infty} (-1)^r \frac{(n+r)!}{(n-r)!} \frac{(\sinh \xi)^{2r}}{4^{n-r}(2r+1)!}} \right\} + O(\gamma^2) ,$$

$$(n \geq 0) \quad (A.2\text{-}25)$$

It should be noted that all the approximate expressions derived in this section reduce to the well known approximate expressions for the Bessel functions when the ellipse degenerates to a circle.

Similar approximate expressions for the even order modified Mathieu functions can be obtained in the same manner.

A.3 Degenerate Forms of Mathieu and Modified Mathieu Functions

When the ellipse tends to a circle, i.e., as the semifocal lengths q and ξ tend to zero and infinity respectively, such that

$$q \cosh \xi \approx q \sinh \xi \approx \frac{qe^\xi}{2} \to r ,$$

where r is the radial component of the circle, all $A_p^{(m)}$ and $B_p^{(m)}$ tend to zero except that $A_m^{(m)} = B_m^{(m)} \to 1$. Therefore the degenerate forms of the Mathieu functions are (45)

$$ce_m(\eta,\gamma^2) \to \cos m\eta \qquad (A.3\text{-}1)$$

$$se_m(\eta,\gamma^2) \to \sin m\eta \qquad (A.3\text{-}2)$$

with $m \geq 1$, and when $m = 0$

$$ce_0(\eta, \gamma^2) \to \frac{1}{\sqrt{2}} \qquad . \qquad (A.3\text{-}3)$$

The degenerate forms of the modified Mathieu functions are

$$Ce_{2n}(\xi, \gamma^2) \to (-1)^n \, p_{2n} J_{2n}(x \frac{r}{r_o}) \, , \qquad (A.3\text{-}4)$$

$$Ce_{2n+1}(\xi, \gamma^2) \to (-1)^n \, p_{2n+1} J_{2n+1}(x \frac{r}{r_o}) \, , \qquad (A.3\text{-}5)$$

$$Se_{2n+1}(\xi, \gamma^2) \to (-1)^n \, s_{2n+1} J_{2n+1}(x \frac{r}{r_o}) \, , \qquad (A.3\text{-}6)$$

$$Se_{2n+2}(\xi, \gamma^2) \to (-1)^{n+1} \, s_{2n+2} J_{2n+2}(x \frac{r}{r_o}) \, , \qquad (A.3\text{-}7)$$

$$Ce'_{2n}(\xi, \gamma^2) \to (-1)^n \, p_{2n}(x \frac{r}{r_o}) J'_{2n}(x \frac{r}{r_o}) \quad , \qquad (A.3\text{-}8)$$

$$Ce'_{2n+1}(\xi, \gamma^2) \to (-1)^n p_{2n+1}(x \frac{r}{r_o}) J'_{2n+1}(x \frac{r}{r_o}) \, , \qquad (A.3\text{-}9)$$

$$Se'_{2n+1}(\xi, \gamma^2) \to (-1)^n s_{2n+1}(x \frac{r}{r_o}) J'_{2n+1}(x \frac{r}{r_o}) \, , \qquad (A.3\text{-}10)$$

$$Se'_{2n+2}(\xi, \gamma^2) \to (-1)^{n+1} s_{2n+2}(x \frac{r}{r_o}) J'_{2n+2}(x \frac{r}{r_o}) \, , \qquad (A.3\text{-}11)$$

$$Fek_{2n}(\xi, \gamma^2) \to \frac{(-1)^n}{\pi} \, p_{2n} \, K_{2n}(y \frac{r}{r_o}) \, , \qquad (A.3\text{-}12)$$

$$Fek_{2n+1}(\xi, \gamma^2) \to \frac{(-1)^n}{\pi} \, s_{2n+1} K_{2n+1}(y \frac{r}{r_o}) \, , \qquad (A.3\text{-}13)$$

$$Gek_{2n+1}(\xi, \gamma^2) \to \frac{(-1)^n}{\pi} \, p_{2n+1} K_{2n+1}(y \frac{r}{r_o}) \, , \qquad (A.3\text{-}14)$$

$$Gek_{2n+2}(\xi, \gamma^2) \to \frac{(-1)^{n+1}}{\pi} \, s_{2n+2} K_{2n+2}(y \frac{r}{r_o}) \, , \qquad (A.3\text{-}15)$$

$$Fek'_{2n}(\xi, \gamma^2) \to \frac{(-1)^n}{\pi} \, p_{2n}(y \frac{r}{r_o}) \, K'_{2n}(y \frac{r}{r_o}) \, , \qquad (A.3\text{-}16)$$

$$Fek'_{2n+1}(\xi, \gamma^2) \to \frac{(-1)^n}{\pi} \, s_{2n+1} \, (y \frac{r}{r_o}) \, K'_{2n+1}(y \frac{r}{r_o}), \qquad (A.3\text{-}17)$$

$$\text{Gek}'_{2n+1}(\xi, \gamma^2) \to \frac{(-1)^n}{\pi} \, p_{2n+1} \, (y \, \frac{r}{r_o}) \, K'_{2n+1}(y \, \frac{r}{r_o}) \tag{A.3-18}$$

$$\text{Gek}'_{2n+2}(\xi, \gamma^2) \to \frac{(-1)^{n+1}}{\pi} \, s_{2n+2} \, (y \, \frac{r}{r_o}) \, K'_{2n+2}(y \, \frac{r}{r_o}) \tag{A.3-19}$$

where p_{2n}, p_{2n+1}, s_{2n+1}, s_{2n+2} are connecting factors which have been defined in section A.1, and $x^2 = k_1^2 r_o^2 - \beta^2 r_o^2$, $y^2 = \beta^2 r_o^2 - k_2^2 r_o^2$ in which r_o is the radius of the circle. The prime on the modified Mathieu function represents the derivative of the function with respect to ξ, while the prime on the Bessel or modified Bessel function represents the derivative of the function with respect to its argument.

A.4. Orthogonality Relations of Mathieu Functions

The orthogonality relations of Mathieu functions are (45)

a. For all γ^2's

$$\int_0^{2\pi} ce_m(\eta, \gamma^2) \, ce_p(\eta, \gamma^2) d\eta = 0 \qquad (m \neq p) \tag{A.4-1}$$

$$\int_0^{2\pi} se_m(\eta, \gamma^2) \, se_p(\eta, \gamma^2) d\eta = 0 \qquad (m \neq p) \tag{A.4-2}$$

$$\int_0^{2\pi} ce_m(\eta, \gamma^2) \, se_p(\eta, \gamma^2) d\eta = 0 \qquad \begin{matrix} (m \neq p \\ or \\ m = p) \end{matrix} \tag{A.4-3}$$

b. For $\gamma^2 \geq 0$

$$\int_0^{2\pi} ce_{2n}^2(\eta, \gamma^2) d\eta = 2\pi \left[A_o^{(2n)} \right]^2 + \pi \sum_{r=1}^{\infty} \left[A_{2r}^{(2n)} \right]^2 \tag{A.4-4}$$

$$\int_0^{2\pi} ce_{2n+1}^2(\eta, \gamma^2) d\eta = \pi \sum_{r=0}^{\infty} \left[A_{2r+1}^{(2n+1)} \right]^2 \tag{A.4-5}$$

$$\int_0^{2\pi} se^2_{2n+1}(\eta, r^2) d\eta = \pi \sum_{r=0}^{\infty} \left[B^{(2n+1)}_{2r+1} \right]^2 \qquad (A.4-6)$$

$$\int_0^{2\pi} se^2_{2n+2}(\eta, r^2) d\eta = \pi \sum_{r=0}^{\infty} \left[B^{(2n+2)}_{2r+2} \right]^2 \qquad (A.4-7)$$

c. For $r^2 \leq 0$

$$\int_0^{2\pi} ce^2_{2n}(\eta, |r^2|) d\eta = 2\pi \left[A^{(2n)}_0 \right]^2 + \pi \sum_{r=1}^{\infty} \left[A^{(2n)}_{2r} \right]^2 \qquad (A.4-8)$$

$$\int_0^{2\pi} ce^2_{2n+1}(\eta, |r^2|) d\eta = \pi \sum_{r=0}^{\infty} \left[B^{(2n+1)}_{2r+1} \right]^2 \qquad (A.4-9)$$

$$\int_0^{2\pi} se^2_{2n+1}(\eta, |r^2|) d\eta = \pi \sum_{r=0}^{\infty} \left[A^{(2n+1)}_{2r+1} \right]^2 \qquad (A.4-10)$$

$$\int_0^{2\pi} se^2_{2n+2}(\eta, |r^2|) d\eta = \pi \sum_{r=0}^{\infty} \left[B^{(2n+2)}_{2r+2} \right]^2 \qquad (A.4-11)$$

APPENDIX B

Tabulation of Integrals Involving Mathieu and Modified Mathieu Functions

Integrals resulting from the attenuation constant and Q factor calculations are tabulated in this appendix. Integrals are integrated analytically whenever possible, and the results are given. The integrals are divided into two categories; those involving the Mathieu functions are called the angle integrals since they correspond to the trigonometric integrals of the circular guide, and those involving the modified Mathieu functions are called the radial integrals since they correspond to the Bessel integrals of the circular guide.

B.1 Angle Integrals Involving Mathieu Functions

The definite integrals involving Mathieu functions can usually be integrated analytically. They are

$$I_1 = \int_0^{2\pi} ce_1'^2(\eta)d\eta = \pi \sum_{r=0}^{\infty} A_{2r+1}^{(1)2}(2r+1)^2$$

$$I_2 = \int_0^{2\pi} ce_1^2(\eta)d\eta = \pi \sum_{r=0}^{\infty} A_{2r+1}^{(1)2}$$

$$I_3 = \int_0^{2\pi} se_1^2(\eta)d\eta = \pi \sum_{r=0}^{\infty} B_{2r+1}^{(1)2}$$

$$I_4 = \int_0^{2\pi} se_1'^2(\eta)d\eta = \pi \sum_{r=0}^{\infty} B_{2r+1}^{(1)2}(2r+1)^2$$

$$I_5 = \int_0^{2\pi} ce_1'(\eta)se_1(\eta)d\eta = -\pi \sum_{r=0}^{\infty} A_{2r+1}^{(1)} B_{2r+1}^{(1)}(2r+1)$$

$$I_6 = \int_0^{2\pi} ce_1(\eta)se_1'(\eta)d\eta = -I_5$$

$$I_7 = \int_0^{2\pi} se_1^2(\eta)\,\cos 2\eta\,d\eta = \pi\left\{-\frac{1}{2}B_1^{(1)^2} + \sum_{r=0}^{\infty} B_{2r+1}^{(1)} B_{2r+3}^{(1)}\right\}$$

$$I_{7c} = \int_0^{2\pi} ce_1^2(\eta)\,\cos 2\eta\,d\eta$$

$$I_1' = \int_0^{2\pi} ce_1^{*'2}(\eta)\,d\eta = \pi\sum_{r=0}^{\infty} B_{2r+1}^{*(1)^2}(2r+1)^2$$

$$I_2' = \int_0^{2\pi} ce_1^{*2}(\eta)\,d\eta = \pi\sum_{r=0}^{\infty} B_{2r+1}^{*(1)^2}$$

$$I_3' = \int_0^{2\pi} ce_3^{*'2}(\eta)\,d\eta = \pi\sum_{r=0}^{\infty} B_{2r+1}^{*(3)^2}(2r+1)^2$$

$$I_4' = \int_0^{2\pi} ce_3^{*2}(\eta)\,d\eta = \pi\sum_{r=0}^{\infty} B_{2r+1}^{*(3)^2}$$

$$I_5' = \int_0^{2\pi} ce_1^{*'}(\eta)\,ce_3^{*'}(\eta)\,d\eta = -\pi\sum_{r=0}^{\infty} B_{2r+1}^{*(1)} B_{2r+1}^{*(3)}(2r+1)^2$$

$$I_6' = \int_0^{2\pi} ce_1^*(\eta)\,ce_3^*(\eta)\,d\eta = -\pi\sum_{r=0}^{\infty} B_{2r+1}^{*(1)} B_{2r+1}^{*(3)}$$

$$I_7' = \int_0^{2\pi} se_1^{'*2}(\eta)\,d\eta = \pi\sum_{r=0}^{\infty} A_{2r+1}^{*(1)^2}(2r+1)^2$$

$$I_8' = \int_0^{2\pi} se_1^{*2}(\eta)\,d\eta = \pi\sum_{r=0}^{\infty} A_{2r+1}^{*(1)^2}$$

$$I_9' = \int_0^{2\pi} se_3^{'*2}(\eta)\,d\eta = \pi\sum_{r=0}^{\infty} A_{2r+1}^{*(3)^2}(2r+1)^2$$

$$I_{10}' = \int_0^{2\pi} se_3^{*2}(\eta)\,d\eta = \pi\sum_{r=0}^{\infty} A_{2r+1}^{*(3)^2}$$

$$I'_{11} = \int_0^{2\pi} se_1^{*'}(\eta)\ se_3^*(\eta)d\eta = -\pi \sum_{r=0}^{\infty} A_{2r+1}^{*(1)}\ A_{2r+1}^{*(3)}(2r+1)^2$$

$$I'_{12} = \int_0^{2\pi} se_1^*(\eta)\ se_3^*(\eta)d\eta = -\pi \sum_{r=0}^{\infty} A_{2r+1}^{*(1)}\ A_{2r+1}^{*(3)}$$

$$I'_{13} = \int_0^{2\pi} ce_1^*(\eta)\ se_1^*(\eta)d\eta = -\pi \sum_{r=0}^{\infty} A_{2r+1}^{*(1)}\ B_{2r+1}^{*(1)}(2r+1)$$

$$I'_{14} = \int_0^{2\pi} ce_1^*(\eta)\ se_1^*(\eta)d\eta = -I'_{13}$$

$$I'_{15} = \int_0^{2\pi} ce_3^{*'}(\eta)\ se_1^*(\eta)d\eta = \pi \sum_{r=0}^{\infty} B_{2r+1}^{*(3)}\ A_{2r+1}^{*(1)}(2r+1)$$

$$I'_{16} = \int_0^{2\pi} se_1^{*'}(\eta)\ ce_3^*(\eta)d\eta = -I'_{15}$$

$$I'_{17} = \int_0^{2\pi} ce_1^{*'}(\eta)\ se_3^*(\eta)d\eta = \pi \sum_{r=0}^{\infty} B_{2r+1}^{*(1)}\ A_{2r+1}^{*(3)}(2r+1)$$

$$I'_{18} = \int_0^{2\pi} ce_1^*(\eta)\ se_3^{*'}(\eta)d\eta = -I'_{17}$$

$$I'_{19} = \int_0^{2\pi} ce_3^{*'}(\eta)\ se_3^*(\eta)d\eta = -\pi \sum_{r=0}^{\infty} A_{2r+1}^{*(3)}\ B_{2r+1}^{*(3)}(2r+1)$$

$$I'_{20} = \int_0^{2\pi} ce_3^*(\eta)\ se_3^{'*}(\eta)d\eta = -I'_{19}$$

$$I_a = \int_0^{2\pi} se_1^{*2}(\eta)\cos 2\eta\, d\eta = -\pi\left[\frac{1}{2}A_1^{*(1)2} + \sum_{r=0}^{\infty} A_{2r+1}^{*(1)}\ A_{2r+3}^{*(1)}\right]$$

$$I_b = \int_0^{2\pi} se_3^{*2}(\eta)\cos 2\eta\, d\eta = -\pi\left[\frac{1}{2}A_1^{*(3)2} + \sum_{r=0}^{\infty} A_{2r+1}^{*(3)}\ A_{2r+3}^{*(3)}\right]$$

$$I_c = \int_0^{2\pi} se_1^*(\eta) se_3^*(\eta) \cos 2\eta \, d\eta = \frac{\pi}{2}\left[A_1^{*(1)} A_1^{*(3)} + \sum_{r=0}^{\infty} (A_{2r+1}^{*(1)} A_{2r+3}^{*(3)} + A_{2r+1}^{*(3)} A_{2r+3}^{*(1)}) \right]$$

$$I_a' = \int_0^{2\pi} ce_1^{*2}(\eta) \cos 2\eta \, d\eta = \pi\left[\frac{1}{2} B_1^{*(1)^2} - \sum_{r=0}^{\infty} B_{2r+1}^{*(1)} B_{2r+3}^{*(1)} \right]$$

$$I_b' = \int_0^{2\pi} ce_3^{*2}(\eta) \cos 2\eta \, d\eta = \pi\left[\frac{1}{2} B_1^{*(3)^2} - \sum_{r=0}^{\infty} B_{2r+1}^{*(3)} B_{2r+1}^{*(3)} \right]$$

$$I_c' = \int_0^{2\pi} ce_3^*(\eta) ce_1^*(\eta) \cos 2\eta \, d\eta = -\frac{\pi}{2}\left[B_1^{*(1)} B_1^{*(3)} + \sum_{r=0}^{\infty} (B_{2r+1}^{*(1)} B_{2r+3}^{*(3)} + B_{2r+1}^{*(3)} B_{2r+3}^{*(1)}) \right].$$

The prime signifies the derivative of the function with respect to η. The * indicates that the argument γ^2 of the Mathieu functions or the expansion coefficients is $(\beta^2 - k_0^2) q^2 \cosh^2 \xi_0 / 4$.

B.2 Radial Integrals Involving Modified Mathieu Functions

All these radial integrals are integrated numerically by Simpson's Rule (50). The normalized dimensionless variables

$$z_1 = \frac{xe^{\xi}}{2 \cosh \xi_0} \quad , \quad z_2 = \frac{ye^{\xi}}{2 \cosh \xi_0}$$

where $x^2 = q^2 \cosh^2 \xi_0 (k_1^2 - \beta^2)$ and $y^2 = q^2 \cosh^2 \xi_0 (\beta^2 - k_0^2)$ are used. As the ellipse approaches a circle, $z_1 \to x \frac{r}{r_0}$ and $z_2 = y \frac{r}{r_0}$. The limits of integration instead of being from 0 to ξ_0 and ξ_0 to ∞ will be from $\frac{x}{2 \cosh \xi_0}$ to $\frac{xe^{\xi_0}}{2 \cosh \xi_0}$ and $\frac{ye^{\xi_0}}{2 \cosh \xi_0}$ to ∞ respectively. Assuming

$$a_1 = \frac{x}{2 \cosh \xi_0} \quad , \quad a_2 = \frac{xe^{\xi_0}}{2 \cosh \xi_0} \quad , \quad b_1 = \frac{ye^{\xi_0}}{2 \cosh \xi_0} \quad \text{and} \quad b_2 = \infty \quad ,$$

we have the following radial integrals

$$I_8 = \int_{a_1}^{a_2} Ce_1^2(z_1) \frac{dz_1}{z_1}$$

$$I_9 = \int_{a_1}^{a_2} Ce_1'^2(z_1) z_1 dz_1$$

$$I_{10} = \int_{a_1}^{a_2} Se_1'^2(z_1) z_1 dz_1$$

$$I_{11} = \int_{a_1}^{a_2} Se_1^2(z_1) \frac{dz_1}{z_1}$$

$$I_{12} = \int_{a_1}^{a_2} Ce_1(z_1) Se_1'(z_1) dz_1$$

$$I_{13} = \int_{a_1}^{a_2} Ce_1'(z_1) Se_1(z_1) dz_1$$

$$I_{14_N} = \int_{a_1}^{a_2} Se_1^2(z_1) \left[\frac{4 \cosh^2 \xi_o z_1^2 - x^2}{4 \cosh^2 \xi_o z_1 x} \right] \frac{dz_1}{z_1}$$

$$I_{14_{NN}} = \int_{a_1}^{a_2} Ce_1^2(z_1) \left[\frac{4 \cosh^2 \xi_o z_1^2 - x^2}{4 \cosh^2 \xi_o z_1 x} \right] \frac{dz_1}{z_1}$$

$$I_{21}' = \int_{b_1}^{b_2} Fek_1^2(z_2) \frac{dz_2}{z_2}$$

$$I_{22}' = \int_{b_1}^{b_2} Fek_1'^2(z_2) z_2 dz_2$$

$$I_{23}' = \int_{b_1}^{b_2} Fek_3^2(z_2) \frac{dz_2}{z_2}$$

$$I'_{24} = \int_{b_1}^{b_2} Fek'^2_3(z_2) z_2 dz_2$$

$$I'_{25} = \int_{b_1}^{b_2} Fek_1(z_2)\, Fek_3(z_2)\, \frac{dz_2}{z_2}$$

$$I'_{26} = \int_{b_1}^{b_2} Fek'_1(z_2)\, Fek'_3(z_2)\, \frac{dz_2}{z_2}$$

$$I'_{27} = \int_{b_I}^{b_2} Gek^2_1(z_2)\, \frac{dz_2}{z_2}$$

$$I'_{28} = \int_{b_1}^{b_2} Gek'^2_1(z_2) z_2 dz_2$$

$$I'_{29} = \int_{b_1}^{b_2} Gek^2_3(z_2)\, \frac{dz_2}{z_2}$$

$$I'_{30} = \int_{b_1}^{b_2} Gek'^2_3(z_2) z_2 dz_2$$

$$I'_{31} = \int_{b_1}^{b_2} Gek_1(z_2)\, Gek_3(z_2)\, \frac{dz_2}{z_2}$$

$$I'_{32} = \int_{b_1}^{b_2} Gek'_1(z_2)\, Gek'_3(z_2) z_2 dz_2$$

$$I'_{33} = \int_{b_1}^{b_2} Fek_1(z_2)\, Gek'_1(z_2) dz_2$$

$$I'_{34} = \int_{b_1}^{b_2} Fek'_1(z_2)\ Gek_1(z_2)dz_2$$

$$I'_{35} = \int_{b_1}^{b_2} Fek_3(z_2)\ Gek'_1(z_2)dz_2$$

$$I'_{36} = \int_{b_1}^{b_2} Fek'_3(z_2)\ Gek_1(z_2)dz_2$$

$$I'_{37} = \int_{b_1}^{b_2} Fek_1(z_2)\ Gek'_3(z_2)dz_2$$

$$I'_{38} = \int_{b_1}^{b_2} Fek'_1(z_2)\ Gek_3(z_2)dz_2$$

$$I'_{39} = \int_{b_1}^{b_2} Fek_3(z_2)\ Gek'_3(z_2)dz_2$$

$$I'_{40} = \int_{b_1}^{b_2} Fek'_3(z_2)\ Gek_3(z_2)dz_2$$

$$I'_{41} = \int_{b_1}^{b_2} Gek_1^2(z_2) \left[\frac{4\ \cosh^2\xi_o\ z_2^2 - y^2}{4\ \cosh^2\xi_o\ z_2 y} \right] \frac{dz_2}{z_2}$$

$$I'_{42} = \int_{b_1}^{b_2} Gek_3^2(z_2) \left[\frac{4\ \cosh^2\xi_o\ z_2^2 - y^2}{4\ \cosh^2\xi_o\ z_2 y} \right] \frac{dz_2}{z_2}$$

$$I'_{43} = \int_{b_1}^{b_2} Gek_1(z_2)\ Gek_3(z_2) \left[\frac{4\ \cosh^2\xi_o\ z_2^2 - y^2}{4\ \cosh^2\xi_o\ z_2 y} \right] \frac{dz_2}{z_2}$$

$$I'_{44} = \int_{b_1}^{b_2} Fek_1^2(z_2) \left[\frac{4\ \cosh^2\xi_o\ z_2^2 - y^2}{4\ \cosh^2\xi_o\ z_2 y} \right] \frac{dz_2}{z_2}$$

$$I'_{45} = \int_{b_1}^{b_2} Fek_3^2(z_2) \left[\frac{4 \cosh^2\xi_o \, z_2^2 - y^2}{4 \cosh^2\xi_o \, z_2 y} \right] \frac{dz_2}{z_2}$$

$$I'_{46} = \int_{b_1}^{b_2} Fek_1(z_2) \, Fek_3(z_2) \left[\frac{4 \cosh^2\xi_o \, z_2^2 - y^2}{4 \cosh^2\xi_o \, z_2 y} \right] \frac{dz_2}{z_2} \, .$$

The prime on the modified Mathieu function indicates the derivative of
the function with respect to its argument.

BIBLIOGRAPHY AND REFERENCES

1. Sommerfeld, A., "Uber die Fortplanzung Elektrodynamischer Wellen langes eines Drahtes", Ann. Physik und Chemie, 67, 233, (1899).

2. Hondros, D., and Debye, P., "Electromagnetische Wellen in dielektrischen Drahtes", Ann. der Physik 32, 465 (1910).

3. Hondros, D., "Electromagnetische Wellen in Drahtes", Ann. der Physik 30, 905, (1909).

4. Goubau, G., "Surface waves and their application to transmission lines", J. Appl. Phys., 21, 119 (1950).

5. Harms, F., "Electromagnetic Waves on a wire with a cylindrical insulating sheath", Ann.der Physik 23, 44 (1907).

6. Barlow, H.E.M.and Karbowiak, A.E., "An investigation of the characteristics of cylindrical surface waves", Proc. IEE 100, pt.III, 321, (1953).

7. Scheibe, E.H., King, B.G., and Van Zeeland, D.L., "Loss measurements of surface wave transmission lines", J.Appl.Phys.25, 790 (1954).

8. Roberts, T.E., "Theory of the single-wire transmission line", J.Appl. Phys.24, 57 (1954).

9. Kiely, D.G., "Experiments with single-wire transmission line at 3 cm. wavelength", J.Brit.IRE 13, 194 (1953).

10. Zahn, H., "Detection of Electromagnetic waves along dielectric wires" Ann. der Physik 49, 907 (1916).

11. Ruter, H. and Schriever, O., "Electromagnetische Wellen an dielektrischen Drahten", Schriften des Naturalwissenschaftlichen vereines fur Schleswig-Holstein 16, 2 (1915).

12. Schriever, O., "Electromagnetic waves in dielectric conductors", Ann. der Physik 63, 645 (1920).

13. Carson, J.R., Mead, S.P., and Schelkunoff, S.A., "Hyperfrequency waveguides--mathematical theory", Bell Sys. Tech. J. 15, 310 (1936).

14. Southworth, G.C., "Hyperfrequency waveguides--general considerations and experimental results", Bell Sys. Tech. J. 15, 284 (1936).

15. Borgnis, F.E. and Papas, C.H., "Electromagnetic waveguides", Encyclopedia of Physics, Vol.16, Springer-Verlag, Berlin (1958).

16. Mallach, "Dielectrische Richtstrahler", Bericht des V.I.f.s., (1943).

17. Wegener, G.F., "Ausbreitungsgeschwindigkeit, Wellenwiderstand und Dampfung elektromagnetischer Wellen an dielektrischen Zylindern", Dissertation, Air Material Command Microfilm ZWB/FB/RE/2018, R8117F831.

18. Elsasser, W.M., "Attenuation in a dielectric circular rod", J. Appl. Phys., 20, 1193 (1949).

19. Chandler, C.H., "An investigation of dielectric rod as waveguides", J. Appl. Phys. 20, 1188 (1949).

20. King, D.D., "Dielectric image line", J. Appl. Phys. 23, 699 (1952).

21. King, D.D., and Schlesinger, S.P., "Losses in dielectric image lines", IRE Trans. on Microwave Theory and Technique, MTT-5, 31, (1957).

22. Zachoval, L., "Electromagnetic wave propagation along cylindrical dielectric tube", Rozpravy ces Akademie II, 47, No. 34 (1933).

23. Liska, J., "Experiments on the propagation of electromagnetic wave along a dielectric tube", Casopis pro Pestovani Matematiky a Fysiky 63, 69 (1934).

24. Astrahan, M.M., "Dielectric tube waveguide", Dissertation, North-western University, Illinois (1949).

25. Unger, H.G., "Dielectric tubes as waveguides", Arch. elek Übertragang 8, 241 (1954).

26. Becker, R.C., and Coleman, P.D., "The dielectric tube resonator: a device for the generation and measurement of mm and sub-mm waves", MRI Symposium proceedings, Vol.IX, 191 (1959).

27. Karbowiak, A.E., "The elliptic surface wave", Brit. J. Appl. Phys.5, 328 (1954).

28. King, M.J. and Wiltse, J.C., "Surface wave propagation on a dielectric rod of elliptic cross section", Scientific Report No.1, Electronic Communications Inc., St. Petersburg, Florida, August 1960.

29. Roe, G.M., "The Theory of Acoustic and Electromagnetic Wave Guides and Cavity Resonators", PhD Thesis, University of Minnesota, March 1947.

30. Sommerfeld, A., "An oscillating dipole above a finitely conducting plane", Ann. der Physik 28, 665 (1909).

31. Stratton, J.A., "Electromagnetic Theory", McGraw Hill Book Company, Inc., New York (1941).

32. Whitmer, R.M., "Fields in non-metallic waveguides", Proc. IRE 36, 1105 (1948).

33. Tai, C.T., "Effect of a grounded slab on radiation from a line source" J. Appl. Phys. 22, 405 (1951).

34. Brick, D.B., "The radiation of a Hertzian dipole over a grounded conductor", Proc. IEE 102, Part C, 104 (1955).

35. Wait, J.R., "Excitation of surface waves on conducting, stratified, dielectric coated and corrugated surfaces", J. Research Natl. Bur. Standards 59, 365 (1957).

36. Cullen, A.L., "The excitation of plane surface waves", Proc. IEE 101 Part IV, 225 (1954).

37. Brown, J., "Some Theoretical Results for Surface Wave Launchers", paper presented at URSI Symposium, Toronto, Canada (1959).

38. Armand, N.A., "The propagation of surface electromagnetic waves along a many-wire system", J. Tech. Phys. USSR.

39. Marcuse, D., "Investigation of the energy exchange and the field distribution for parallel surface-wave transmission lines", Arch. elek. übertragung 10, 117 (1956).

40. Snitzer, E., "Proposed fiber cavities for optical masers", J. Appl. Phys. 32, 36, 1961.

41. Davidson, C.F., and Simmonds, J.C., "Cylindrical Cavity Resonators", Wireless Eng. 21, 420 (1944).

42. Meixner, J., and Schafke, F.W., "Mathieu-Funktionen und Spharoid-Funktionen", Berlin-Gottingen-Heidelberg (1954).

43. Ince, E.L., "A proof of the impossibility of the coexistence of two Mathieu functions", Cambridge Phil. Soc. Proc. 21, 117 (1922).

44. Ince, E.L., "Ordinary Differential Equations", Chapter X, London, Longmans (1927).

45. McLachlan, N.W., "Theory and Application of Mathieu Functions", University Press, Oxford (1951).

46. Borgnis, F. and Papas, C.H., "Randwertprobleme der Mikrowellen-physik", Springer-Verlag, Berlin (1955).

47. Kantorovich, L.V., and Krylov, V.I., "Approximate Methods of Higher Analysis", Interscience Publishers Inc., New York (1958) (English Translation).

48. Ince, E.L., "Characteristic Numbers of Mathieu's Equation", Roy. Soc. Edin. Proc. 46, 26 (1925); 46, 316 (1926); 47, 294 (1927).

49. National Bureau of Standards, "Tables Relating to Mathieu Functions" Columbia Univ. Press, New York (1951).

50. Kunz, K. S., "Numerical Analysis", McGraw Hill Book Company, New York (1957).

51. Kornhauser, E.T., "On the discrete spectrum for dielectric rods of arbitrary cross section", Research Report AF4561/3, Division of Eng., Brown University, March 1959.

52. Collin, R.E., "Field Theory of Guided Waves", McGraw-Hill Book Co., New York, 1960.

53. Richtmyer, R.D., "Dielectric Resonators", J. Appl. Phys. 10, 391, (1939).

54. Beam, R.E. et al, "Final Report on Investigations of Multi-Mode Propagation in Waveguides and Microwave Optics", Microwave Lab., Northwester University, Evanston, Ill. (1950).

55. Barlow, H.M. and Cullen, A.L., "Microwave Measurements", Constable and Company, Ltd., London (1950).

56. Schelkunoff, S.A., "The Impedance Concept and its Application to Problems of Reflection, Refraction, Shielding and Power Absorption", Bell Sys. Tech. J. 17, 17 (1938).

57. Private communication with Prof. Roy Gould, California Institute of Technology, Pasadena, California.

58. Roberts, S. and von Hipple, A., "A new method for measuring dielectric constant and loss in the range of contimeter waves", J. Appl. Phys. 17, 610 (1946).

59. Montgomery, C.G., "Technique of Microwave Measurements", McGraw-Hill Book Company, New York (1947).

60. Goldstein, S., "Mathieu Functions", Trans. Cambridge Phil. Soc. $\underline{23}$, 303 (1927).

61. Mathieu, É., "Mémoire sur le mouvement vibratoire d'une membrane de forme elliptique", Jour. de Math. Pures et Appl. $\underline{13}$, 137 (1868).

62. Smythe, W.R., "Static and Dynamic Electricity" McGraw-Hill Book Co, New York (1950).

63. Von Hippel, A. ed, "Dielectric Materials and Applications", J.Wiley and Sons, Inc., New York, New York (1954).

DISTRIBUTION OF REPORT NO. 27

AF18(600)-1113

Commander   3
AF Office of Scientific Research
ATTN: SRPP
Washington 25, D. C.

Commander   2
AF Office of Scientific Research
ATTN: SRGL
Washington 25, D. C.

Commander   1
AF Cambridge Research Laboratories
ATTN: CRRELA
L. G. Hanscom Field
Bedford, Massachusetts

Aeronautical Research Laboratories   1
ATTN: Technical Library
Building 450
Wright-Patterson Air Force Base
Ohio

A.S.T.I.A.   10
ATTN: TIPCR
Arlington Hall Station
Arlington 12, Virginia

Director, Naval Research Lab.   1
ATTN: Technical Information Officer
Washington 25, D. C.

Chief of Research and Development   1
ATTN: Scientific Information Branch
Department of the Army
Washington 25, D. C.

U.S. Atomic Energy Commission   1
Technical Information Extension
P.O. Box 62
Oak Ridge, Tennessee

National Bureau of Stds. Library   1
Room 203, Northwest Building
Washington 25, D. C.

National Aeronautics and Space Adm.   3
Washington 25, D. C.

Rand Corporation   1
1700 Main Street
Santa Monica, California

Dr. R. W. P. King   1
Harvard University
Cambridge, Massachusetts

Director   1
Research Lab. of Electronics
Massachusetts Inst. of Tech.
Cambridge 39, Massachusetts

Stanford Electronics Lab   1
Document Library
Stanford University
Stanford, California

Professor E. Weber   1
Microwave Research Laboratory
Polytechnic Inst. of Brooklyn
Brooklyn, New York

Head, GE Microwave Laboratory   1
601 California Avenue
Palo Alto, California

Professor T. E. Tice   1
Dept. of Electrical Eng.
Ohio State University
Columbus 10, Ohio

General Electric Company   1
Missile and Ordnance Systems
3198 Chestnut Street
Philadelphia 4, Pennsylvania
ATTN: Library Manager

Professor W. G. Shepherd
Dept. of Electrical Eng.
University of Minnesota
Minneapolis, Minnesota

Professor John Hoffman   1
Dept. of Electrical Eng.
University of Illinois
Champaign, Illinois

Technical Library   1
Research and Development Labs
Hughes Aircraft Company
Culver City, California

Dr. R. E. Hutter, Chief Eng.   1
Sylvania Electric Products
P.O. Box 997
Mountain View, California

Professor P. Kusch   1
Radiation Laboratory
Columbia University
New York, New York

Distribution of Reports, AF18(600)-1113

Dr. D. W. Healy
Electrical Engineering Dept.
Syracuse University Res.Inst.
Syracuse 10, New York   1

U. of Southern California
Electrical Engineering Dept.
Los Angeles 7, California
ATTN: Z. Kaprielian   1

Stanford University
Microwave Research Laboratory
Stanford, California
ATTN: M. Chodorow   1

University of Minnesota
Electrical Engineering Dept.
Minneapolis 14, Minnesota
ATTN: H. Oskam   1

Northeastern University
Physics Department
Boston, Massachusetts
ATTN: G. Lanza   1

University of New Hampshire
Department of Physics
Durham, New Hampshire
ATTN: L. Mower   1

Rutgers University
Microwave Laboratory
New Brunswick, New Jersey
ATTN: M. Sirkis   1

NYU Inst.of Mathematical Sciences
25 Waverly Place
New York 3, New York
ATTN: M. Kline   1

Oxford University
Oxford, ENGLAND
ATTN: H. Motz   1

University of Illinois
Dept. of Electrical Engineering
Urbana, Illinois
ATTN: P. Coleman   1

Stevens Inst. of Technology
Physics Department
Hoboken, New Jersey
ATTN: W. Bostick   1

University of California
Electronics Research Laboratory
Berkeley 4, California
ATTN: J. Whinnery   1

Office of Naval Research
346 Broadway
New York 12, New York
Attn: I. Rowe   1

Brooklyn Polytechnic Institute
Microwave Research Institute
55 Johnson Street
Brooklyn 1, New York
ATTN: N. Marcuvitz   1

Dr. Glenn H. Keitel
Advanced Programs Section
Philco Corporation
3875 Fabian Way
Palo Alto, California   1

Office of Naval Research,London
Navy 100, Box 39, FPO
New York, New York   5

National Bureau of Standards
Boulder Laboratories
Boulder, Colorado
Attn: James R. Wait

Dr. R. C. Hansen
Space Technology Laboratories
Box 95001
Los Angeles 45, California   1

Dr. Donald E. Kerr
John Hopkins University
Department of Physics
Baltimore 18, Maryland   1